# Redox Biology of Infection and Consequent Disease

Special Issue Editor in Chief: Maria Isaguliants
Guest Editors: Birke Bartosch and Alexander Ivanov

Redox Biology of Infection and Consequent Disease

Redox Biology of Infection and Consequent Disease

Special Issue Editor in Chief: Maria Isaguliants
Guest Editors: Birke Bartosch and Alexander Ivanov

Chief Editor

Jeannette Vasquez-Vivar, USA

Editorial Board

Contents

Editorial

Redox Biology of Infection and Consequent Disease

Maria G. Isaguliants [1,2,3,4] **Birke Bartosch** [5,6] **and Alexander V. Ivanov** [7]

[1]*Riga Stradins University, LV-1007 Riga, Latvia*
[2]*Department of Microbiology, Tumor and Cell Biology, Karolinska Institutet, 17177 Stockholm, Sweden*
[3]*N.F. Gamaleja Research Center of Epidemiology and Microbiology, 123098 Moscow, Russia*
[4]*Chumakov Federal Scientific Center for Research and Development of Immune-and-Biological Products of Russian Academy of Sciences, 108819 Moscow, Russia*
[5]*Cancer Research Center Lyon, INSERM U1052 and CNRS 5286, Lyon University, 69003 Lyon, France*
[6]*DevWeCan Laboratories of Excellence Network (Labex), France*
[7]*Center for Precision Genome Editing and Genetic Technologies for Biomedicine, Engelhardt Institute of Molecular Biology, Vavilov str, 32, 119991 Moscow, Russia*

Correspondence should be addressed to Maria G. Isaguliants; maria.issagouliantis@rsu.lv
and Alexander V. Ivanov; aivanov@yandex.ru

Bacteria, viruses, and parasites are the etiological agents that trigger various diseases referred to as communicable. According to WHO statistics, they are responsible for 16% of deaths worldwide. Many of these agents cause severe morbidities already during the initial infection but can also persist in their host and cause long-term inflammation; fibrosis; and cardiovascular, neurodegenerative, and autoimmune diseases. Extensive research over the last two decades demonstrated that many of these chronic infections are associated with elevated production of reactive oxygen species (ROS) and reactive nitrogen species (RNS). Enhanced ROS/RNS production has been implicated in numerous pathologies such as fibrosis, cirrhosis, metabolic dysfunction, lung tissue injury, and epithelial barrier dysfunction, which in turn often increase the susceptibility to secondary infections and/or trigger cancer. Redox biology significantly advanced our understanding of these pathologies. Furthermore, tremendous progress has been achieved in understanding how ROS/RNS affect signaling pathways. However, still too little is known about the mechanisms by which pathogens manipulate oxidative/nitrosative stress reaction(s) of the host. With this in mind, we invited original research and review articles on redox biology of infections and associated pathologies, as well as studies that mechanistically explore

redox biology that in the future may be applicable to infection studies.

Infectious agents induce oxidative/nitrosative stress by different mechanisms. Amongst the host or pathogen enzymes which produce ROS/RNS and are induced or activated in the process of infection, particular attention in the past was drawn to the electron transport chain of mitochondria and NADPH oxidases. Other ROS-producing systems, mentioned in our review on hepatitis B and C viruses [1], remained largely ignored. To fill this gap, a comprehensive review of A. V. Snezhkina et al. presents a thorough summary of the activities of a (broad) panel of ROS-generating enzymes and pathways. They also discuss influence of glycolysis and adjacent metabolic pathways on the redox status of cells, as they affect NADPH/NADP and NADH/NAD ratio and, thus, may change the overall redox balance.

Extensive data have accumulated on the redox biology of viral infections, including viral hepatitis B and C, human immunodeficiency virus (HIV-1), influenza viruses, herpes-, respiratory syncytial, rhino-, corona-, and papillomaviruses. Particularly well studied is the redox biology of hepatitis C virus. During last two decades, numerous papers reported how HCV triggers oxidative stress, how it affects the antioxidant defense systems of the host cell, and what virus-

associated pathologies develop due to continuous production of ROS. As reviewed by Z. Zhang et al., most of the HCV proteins are capable of inducing oxidative stress, including core, E1, E2, NS3, NS4B, and NS5A. Of these, core stands as a key inducer of calcium perturbations and ROS production, which in turn regulate the viral replication cycle by molecular mechanisms that remain largely unknown. M. K. Kukhanova et al. present exciting novel concepts to fill this gap. They have demonstrated that the RNA-dependent RNA polymerase encoded by HCV undergoes S-glutathionylation and that this modification affects enzymatic activity of the protein. Thus, M. K. Kukhanova et al. showed that this protein is a bona fide "redox switch" with activity/functions regulated through redox-dependent posttranslational modifications of cysteine residues (such as S-glutathionylation, nitration, and oxidation to sulfenic, sulfinic, and sulfonic acids) [2].

Zika and dengue viruses belong to the same family as HCV, the Flaviviridae. The redox biology of these pathogens is much less studied, despite association of these viruses with severe human diseases. In a comprehensive review, Z. Zhang et al. carefully discuss the current state of the art for different members of Flaviviridae family and for the whole Flavivirus genus. Many of these viruses cause cell damage by generating ROS and changing redox homeostasis. In turn, ROS facilitate viral replication in variable ways, depending on the cell type and involved virus, but in general, both flaviviruses and alphaviruses use oxidative stress produced during infection to temporally control genome RNA capping and genome replication. According to Z. Zhang et al., viruses vary in their ability to induce ROS but share a common pathway to defend the infected cell against oxidative stress which involves nuclear factor erythroid 2 p45-related factor 2 (Nrf2), a master transcriptional factor regulating a panel of antioxidant and cellular defense genes in response to oxidative stress.

Hepatitis B virus (HBV) of Hepadnaviridae family is another pathogen which, similar to HCV, causes liver disease characterized by chronic liver inflammation, fibrosis, cirrhosis, and eventually liver cancer. Noteworthily, there are currently no approved drugs, which can cure this infection. Many attempts were made to unveil the impact of HBV on the redox status of infected hepatocytes. Not surprisingly, several independent groups revealed that overexpression of single individual HBV proteins promotes production of ROS and pointed to mitochondria and endoplasmic reticulum as their most likely source. HBV core and surface antigens (HBc and HBs) were claimed responsible for induction of ER stress as well as the event(s) occurring during accumulation of the misfolded proteins, a process closely linked to the production of ROS. No specific mechanisms for these events have yet been proposed. In this issue, M. Mehmankhah et al., albeit not studying this process directly, presented a model of HBs structure and, based on this model, performed an in silico search for small molecular weight ligands that block HBV infection. This research on HBs folding will lead to the elucidation of mechanisms behind the accumulation of misfolded HBs and resultant oxidative stress. As the efflux of Ca^{2+} ions from ER to mitochondria and mitochondrial dysfunction are the direct consequences of ER stress, this study will aid our understanding of the molecular/structural basis of HBV's influence on ROS production and calcium homeostasis.

Main bulk of data in the viral redox biology concerns human pathogens while the knowledge on their animal counterparts remains obscure. In this special issue, X. Fu et al. studied the status of the Nrf2/ARE pathway in cells infected with Bovine herpesvirus type 1 (BoHV-1) that is a significant cofactor for bovine respiratory disease complex, the most important inflammatory disease in cattle. They demonstrated that BoHV-1 infection in cell culture induces overproduction of ROS and depletion of Nrf2 and its downstream targets heme oxygenase-1 and NAD(P)H quinone oxidoreductase-1 proteins. BoHV-1 inhibited the Nrf2 signaling pathway by complicated mechanisms including promoting Nrf2 degradation, relocalization of nuclear Nrf2, and inhibition of Nrf2 acetylation. This may account for or at least contribute to the pathogenicity of this infection in cattle.

Tissue inflammation and regeneration processes induced in multiple chronic microbial infections evolve over long periods of time in the context of a strongly oxidative microenvironment leading to mutations in many cellular signaling cascades that drive cell growth and proliferation. This makes oxidative stress a driving force of the infection-induced or infection-associated neoplastic transformation [1]. The best studied oncogenic viruses are human papillomaviruses (HPV), associated with anal, cervical, oropharyngeal, and penile cancer; hepatitis B and C viruses (HBV and HCV), associated with liver cancer; and Epstein-Barr virus, associated with Burkitt's lymphoma, Hodgkin's disease, and nasopharyngeal carcinoma. The oncogenic potential of HIV has for a long time been thought to be due to the virus-mediated immune suppression. However, HIV-infected people were also found to be at an increased risk of "non-AIDS-defining" malignancies not directly linked to immune suppression but associated with other viral infections. Their incidence has been increasing despite successful antiretroviral therapy. The mechanism behind this phenomenon is unclear. E. Bayurova et al. obtained daughter clones of murine mammary gland adenocarcinoma 4T1luc2 cells expressing variants of consensus HIV-1 reverse transcriptase (RT) and found that expression of these RT variants in 4T1luc2 cells leads to increased production of ROS, lipid peroxidation, enhanced cell motility in the wound healing assay, and upregulation of expression of Vimentin and Twist. Importantly, when implanted into syngeneic BALB/C mice, 4T1luc2 cells expressing HIV-1 RT demonstrated enhanced rate of tumor growth and increased metastatic activity. This study establishes links between the expression of HIV-1 RT, production of ROS, induction of EMT, and enhanced propagation of RT-expressing tumor cells. E. Bayurova et al. proposed this scenario as one of the mechanisms of HIV-induced/enhanced carcinogenesis not associated with immune suppression. This study reinforces the earlier findings on the mechanisms of HIV-1-induced production of ROS and effect of ROS on HIV-1 replication [3].

In their review, A. V. Snezhkina et al. described the molecular basis underlying carcinogenesis. They have listed positive effects of ROS, including activation of apoptotic

pathways and aiding anticancer treatments, but also described ROS-mediated mechanisms of carcinogenesis, including DNA damage, leading to the accumulation of mutations and genome instability, as well as reprogramming of cell metabolism and signaling. Which properties of HIV-1 RT are responsible for the induction of ROS, if not the enzymatic activities, remained unknown. E. Bayurova et al. refer to a review of cellular interactions of HIV-1 RT, listing factors which directly or indirectly bind to RT and regulate reverse transcription but at the same time are involved in the maintenance of the redox balance of the cell, the latter possibly affected by their interaction with RT [4].

Bacterial infections traditionally have not been considered to be a major cause of cancer. Recently, however, it has been reported that microbiota can promote carcinogenesis by inducing oxidative stress, genotoxicity, host immune response disturbance, and chronic inflammation. A vivid example is carcinogenesis induced by infection with *Helicobacter pylori* infection [4]. There is also increasing data on the role for oxidative stress in salmonellosis, tuberculosis, and pseudomonas infections. In this context, the search for bioactive substances capable to modulate excessive ROS production in the host represents a new direction in the development of new antimicrobial and, potentially, anticancer drugs. Schiff bases (SBs) are chemical compounds displaying a significant pharmacological potential. In this issue, C. C. Login et al. presented a new thiazolyl-triazole SB with antibacterial activity against *L. monocytogenes* and *P. aeruginosa*, being two times more active than ciprofloxacin. Antibacterial activity on the Gram-negative bacilli was attributed to the decrease of the bacterial NO synthase level and formation of complexes with metals located in the active center of certain bacterial enzymes. Importantly, this new compound showed radical scavenging activity, attributable to the presence of –SH group. The effect of SB on oxidative stress tested in cell culture revealed a decrease in the lipid peroxidation and the protein level of enzymes COX2 and an iNOS involved in the modulation of oxidative stress and inflammatory response.

Positive effects of antioxidants were also recorded in another study presented in this issue by E. K. Fetisova et al., who assessed the therapeutic effect of the mitochondria-targeted antioxidant SkQ1 on a culture model of Multiple Sclerosis (MS). MS is a heterogeneous autoimmune disease of unknown etiology characterized by inflammation, demyelination, and axonal degeneration affecting both the white and grey matter of the CNS. Events leading to the activation of immune cells in MS are mostly unknown; however, damage to the nerve tissue by MS lesions resembles those observed in infectious leprosy [5]. The main cause of the nerve damage was suggested to be nitrozooxidative stress [6]. With this in mind, E. K. Fetisova et al. studied the effect of mitochondria-targeted antioxidant SkQ1 in an *in vitro* model of MS, primary oligodendrocyte culture of the cerebellum, challenged with lipopolysaccharide (LPS). SkQ1 accumulated in the mitochondria of microglial cells and in oligodendrocytes, restoring their capacity to produce myelin, initially blocked by LPS. These results implicate that mitochondria-targeted antioxidants could be promising components of a combined therapy for MS and related neurological disorders, including bacterial infections of the nervous tissues, as an alternative therapy for the cases where immunomodulating disease-modifying therapy is not available or not possible. The latter relates to immunosuppressed individuals, who are at an increased risk of treatment complications due to polyoma- and herpesvirus infections [7]. In contrast to immunomodulatory drugs, mitochondria-targeted antioxidants do not cause any signs of immunosuppression and would not cause such complications.

Emerging evidence indicates that certain parasites such as the blood fluke *Schistosoma haematobium* and small liver flukes *Opisthorchis viverrini* and *Clonorchis sinensis* can also serve as causative agents of malignancies such as bladder cancer caused by schistosomes and cholangiocarcinoma by liver flukes. Recent studies revealed that the generation of ROS and RNS associated with oxidative stress plays a crucial role in the development of systemic complications caused by malaria [8]. In this journal issue, D. M. S. Pereira et al. revealed that another manifestation of *P. falciparum* pathogenicity associated with oxidative stress, namely, cerebral malaria, is mediated through the ROS-dependent functions of housekeeping transient receptor potential (TRP) channels. Cerebral malaria is a clinical syndrome of a severe form of the disease characterized by neurological complications (coma and convulsions) associated with brain inflammation [9]. Several mechanisms were found to contribute to cerebral malaria including alterations in nitric oxide availability, unbalanced oxidative stress responses, and brain inflammation [10]. TRP channels are nonselective cationic channels, distributed in a diverse range of tissues, with local expression in the free terminals of nociceptive nerve fibers and skin [11], involved in the direct detection of stimuli associated with senses and maintenance of ionic homeostasis [12]. TRPV1 plays an important role in the physiology of the digestive system, cardiovascular system, and respiratory system, as well as the development of various pathologies through evoking an inflammatory response [13, 14]. D. M. S. Pereira et al. for the first time demonstrated that mice infected with *P. berghei* exhibited lower levels of expression of TRPV1 than noninfected controls. In the absence of TRPV1 expression, infection with *P. berghei* did not progress to cerebral malaria. The majority of the infected mice remained protected against the development of any disease symptoms and signals apart from blood parasitaemia. Similar protection was provided by treatment with the TRPV1 antagonist SB366791. This study underpinned the molecular mechanisms linking parasite infection with regulation of production of ROS [15] by the host, each and both affecting host cell machinery.

TRPV1 is linked with both the process of inflammation and of calcium signaling and thus may contribute to cancer progression [16]. This creates an association between a decrease in expression of TRPV1 as a factor of selection predisposing to survival from the cerebral malaria and at the same time increasing risk(s) of acquisition of cancer. A similar association was noted for Duffy Antigen Receptor for Chemokines expressed by red blood cells [17]. Whether these "malaria-cancer" associations actually translate into increased risks of induction cancer, specifically of Burkitt

lymphomas, in individuals infected with malaria [18] remains to be elucidated. Even with this inclarity, the main message of this special issue remains: oxidative stress caused by infections, especially chronic infections, directly or indirectly potentiates neoplastic transformation.

Conflicts of Interest

The editors declare that they have no conflicts of interest regarding the publication of this special issue.

Acknowledgments

Maria G. Isaguliants
Birke Bartosch
Alexander V. Ivanov

References

[1] A. V. Ivanov, V. T. Valuev-Elliston, D. A. Tyurina et al., "Oxidative stress, a trigger of hepatitis C and B virus-induced liver carcinogenesis," *Oncotarget*, vol. 8, no. 3, pp. 3895–3932, 2017.

[2] H. Sies, "Oxidative stress: a concept in redox biology and medicine," *Redox Biology*, vol. 4, pp. 180–183, 2015.

[3] A. V. Ivanov, V. T. Valuev-Elliston, O. N. Ivanova et al., "Oxidative stress during HIV infection: mechanisms and consequences," *Oxidative Medicine and Cellular Longevity*, vol. 2016, Article ID 8910396, 18 pages, 2016.

[4] M. A. Lichtman, "A bacterial cause of cancer: an historical essay," *The Oncologist*, vol. 22, no. 5, pp. 542–548, 2017.

[5] T. Masaki, J. Qu, J. Cholewa-Waclaw, K. Burr, R. Raaum, and A. Rambukkana, "Reprogramming adult Schwann cells to stem cell-like cells by leprosy bacilli promotes dissemination of infection," *Cell*, vol. 152, no. 1-2, pp. 51–67, 2013.

[6] T. R. Schalcher, J. L. F. Vieira, C. G. Salgado, R. . S. Borges, and M. C. Monteiro, "Antioxidant factors, nitric oxide levels, and cellular damage in leprosy patients," *Revista da Sociedade Brasileira de Medicina Tropical*, vol. 46, no. 5, pp. 645–649, 2013.

[7] L. Ivanova, D. Tsaneva, Z. Stoykova, and T. Kostadinova, "Viral diseases in transplant and Immunocompromised patients," in *Immunopathology and Immunomodulation*, K. Metodiev, Ed., pp. 885–1124, IntechOpen, London, 2015.

[8] S. Percario, D. R. Moreira, B. A. Gomes et al., "Oxidative stress in malaria," *International Journal of Molecular Sciences*, vol. 13, no. 12, pp. 16346–16372, 2012.

[9] H. J. Shikani, B. D. Freeman, M. P. Lisanti, L. M. Weiss, H. B. Tanowitz, and M. S. Desruisseaux, "Cerebral malaria: we have come a long way," *The American Journal of Pathology*, vol. 181, no. 5, pp. 1484–1492, 2012.

[10] N. Narsaria, C. Mohanty, B. K. Das, S. P. Mishra, and R. Prasad, "Oxidative stress in children with severe malaria," *Journal of Tropical Pediatrics*, vol. 58, no. 2, pp. 147–150, 2012.

[11] C. Kunert-Keil, F. Bisping, J. Krüger, and H. Brinkmeier, "Tissue-specific expression of TRP channel genes in the mouse and its variation in three different mouse strains," *BMC Genomics*, vol. 7, no. 1, article 1471-2164-7-159, p. 159, 2006.

[12] I. S. Ramsey, M. Delling, and D. E. Clapham, "An introduction to TRP channels," *Annual Review of Physiology*, vol. 68, pp. 619–647, 2006.

[13] W. L. Kong, Y. Y. Peng, and B. W. Peng, "Modulation of neuroinflammation: role and therapeutic potential of TRPV1 in the neuro-immune axis," *Brain, Behavior, and Immunity*, vol. 64, pp. 354–366, 2017.

[14] Q. Du, Q. Liao, C. Chen, X. Yang, R. Xie, and J. Xu, "The role of transient receptor potential vanilloid 1 in common diseases of the digestive tract and the cardiovascular and respiratory system," *Frontiers in Physiology*, vol. 10, 2019.

[15] A. C. Gupta, S. Mohanty, A. Saxena, A. K. Maurya, and D. U. Bawankule, "Plumbagin, a vitamin K3 analogue ameliorate malaria pathogenesis by inhibiting oxidative stress and inflammation," *Inflammopharmacology*, vol. 26, no. 4, pp. 983–991, 2018.

[16] J. K. Bujak, D. Kosmala, I. M. Szopa, K. Majchrzak, and P. Bednarczyk, "Inflammation, cancer and immunity-implication of TRPV1 channel," *Frontiers in Oncology*, vol. 9, 2019.

[17] A. V. Nordor, D. Bellet, and G. H. Siwo, "Cancer–malaria: hidden connections," *Royal Society Open Biology*, vol. 8, no. 10, 2018.

[18] E. M. Molyneux, R. Rochford, B. Griffin et al., "Burkitt's lymphoma," *Lancet*, vol. 379, no. 9822, pp. 1234–1244, 2012.

Research Article

HIV-1 Reverse Transcriptase Promotes Tumor Growth and Metastasis Formation via ROS-Dependent Upregulation of Twist

Ekaterina Bayurova [1,2] **Juris Jansons,**[3,4] **Dace Skrastina,**[3,4] **Olga Smirnova** [5]
Dzeina Mezale,[3] **Anastasia Kostyusheva,**[6] **Dmitry Kostyushev,**[6] **Stefan Petkov,**[7]
Philip Podschwadt,[7] **Vladimir Valuev-Elliston** [5] **Sviataslau Sasinovich,**[7] **Sergey Korolev** [8]
Per Warholm,[9] **Anastasia Latanova** [1,5] **Elizaveta Starodubova** [1,5] **Amir Tukhvatulin** [1]
Oleg Latyshev,[1] **Renat Selimov,**[10] **Pavel Metalnikov,**[10] **Alexander Komarov,**[10]
Olga Ivanova [5] **Tatiana Gorodnicheva,**[11] **Sergey Kochetkov** [5] **Marina Gottikh,**[8]
Ilze Strumfa,[3] **Alexander Ivanov** [5] **Ilya Gordeychuk,**[1,2,12] **and Maria Isaguliants** [1,2,3,7]

[1]*NF Gamaleya Research Center of Epidemiology and Microbiology, Moscow, Russia*
[2]*Chumakov Federal Scientific Center for Research and Development of Immune-and-Biological Products of Russian Academy of Sciences, Moscow, Russia*
[3]*Department of Pathology, Riga Stradins University, Riga, Latvia*
[4]*Latvian Biomedical Research and Study Centre, Riga, Latvia*
[5]*Engelhardt Institute of Molecular Biology, Russian Academy of Sciences, Moscow, Russia*
[6]*National Medical Research Center for Tuberculosis and Infectious Diseases, Moscow, Russia*
[7]*Department of Microbiology, Tumor and Cell Biology, Karolinska Institutet, Stockholm, Sweden*
[8]*Chemistry Department and Belozersky Institute of Physico-Chemical Biology, Lomonosov Moscow State University, Moscow, Russia*
[9]*Science for Life Laboratory, Stockholm University, Stockholm, Sweden*
[10]*Russian State Center for Quality and Standardization of Veterinary Drugs and Feed (VGNKI), Moscow, Russia*
[11]*Evrogen, Moscow, Russia*
[12]*Sechenov First Moscow State Medical University, Moscow, Russia*

Correspondence should be addressed to Ekaterina Bayurova; ekaterinapankova48135@gmail.com
and Maria Isaguliants; maria.issagouliantis@rsu.lv

HIV-induced immune suppression results in the high prevalence of HIV/AIDS-associated malignancies including Kaposi sarcoma, non-Hodgkin lymphoma, and cervical cancer. HIV-infected people are also at an increased risk of "non-AIDS-defining" malignancies not directly linked to immune suppression but associated with viral infections. Their incidence is increasing despite successful antiretroviral therapy. The mechanism behind this phenomenon remains unclear. Here, we obtained daughter clones of murine mammary gland adenocarcinoma 4T1luc2 cells expressing consensus reverse transcriptase of HIV-1 subtype A FSU_A strain (RT_A) with and without primary mutations of drug resistance. In *in vitro* tests, mutations of resistance to nucleoside inhibitors K65R/M184V reduced the polymerase, and to nonnucleoside inhibitors K103N/G190S, the RNase H activities of RT_A. Expression of these RT_A variants in 4T1luc2 cells led to increased production of the reactive oxygen species (ROS), lipid peroxidation, enhanced cell motility in the wound healing assay, and upregulation of expression of *Vimentin* and *Twist*. These properties, particularly, the expression of *Twist*, correlated with the levels of expression RT_A and/or the production of ROS. When implanted into syngeneic BALB/C mice, 4T1luc2 cells expressing nonmutated RT_A demonstrated

enhanced rate of tumor growth and increased metastatic activity, dependent on the level of expression of RT_A and *Twist*. No enhancement was observed for the clones expressing mutated RT_A variants. Plausible mechanisms are discussed involving differential interactions of mutated and nonmutated RTs with its cellular partners involved in the regulation of ROS. This study establishes links between the expression of HIV-1 RT, production of ROS, induction of EMT, and enhanced propagation of RT-expressing tumor cells. Such scenario can be proposed as one of the mechanisms of HIV-induced/enhanced carcinogenesis not associated with immune suppression.

1. Introduction

HIV-induced depletion of CD4$^+$ T-helper cells determines high prevalence of HIV/AIDS-associated malignancies, including Kaposi sarcoma, non-Hodgkin lymphoma, and cervical cancer. In the era of antiretroviral therapy (ART), their rates have sharply declined but still remain elevated many fold compared to the general population. HIV-infected people also have increased risks for the forms of cancer not directly associated with the immune suppression, such as lung cancer, liver cancer caused by infections with hepatitis B and hepatitis C viruses, and anogenital and oropharyngeal cancer associated with human papillomavirus (HPV) infections [1]. Multiple studies reported significant increases in their rates [2–5].

The exact mechanisms of HIV-induced carcinogenesis under the successful ART are not known; however, a series of studies show the direct role of HIV, or rather of HIV proteins, in cancer progression. HIV-1 matrix protein p17 promotes B-cell growth in non-Hodgkin lymphoma by modifying intracellular signaling and promoting genomic instability leading to cell transformation; this occurs also in HIV transgenic mice [6, 7]. Furthermore, p17 generates a prolymphangiogenic microenvironment predisposing the lymph nodes to lymphoma growth and metastasis [8], increasing the aggressiveness of human triple-negative breast cancer cells [9]. HIV-1 Nef promotes angiogenesis and tumorigenesis, synergizing with Kaposi's sarcoma (KS) KSHV oncoprotein K1 [10, 11]. Mechanistically, Nef inhibits the apoptotic function of p53; it decreases the half-life of p53 and interferes with p53 DNA binding activity and transcriptional activation [12]. HIV-1 glycoprotein gp120 stimulates glycolysis [13]. Increased glycolysis, also known as the Warburg effect, is a well-known feature of the majority of tumors that supports unconstrained proliferation and invasion of tumor cells [14, 15]. Indeed, gp120 has been shown to promote proliferation, migration, and survival of tumor cells when expressed on the viral particles, on the surface of infected cells, or as a virus-free soluble protein [13, 16]. Expression of HIV-1 Tat has been associated with the development of B-cell lymphomas [17, 18] and colorectal [19] and HPV-associated cancers [20]. Tat inhibits epithelial cytodifferentiation, blocks apoptosis, increases cell migration/motility, and accelerates tumor formation [19]. In tumor cells, it induces a significant reduction in the expression of cell cycle inhibitors of transcription and an increase in the levels of proliferation markers [21] and stimulates growth of tumor cells [22]. Thus, both structural and regulatory HIV-1 proteins demonstrate direct carcinogenic effects and/or promote the effects of known carcinogens.

Exposure of the oral keratinocytes from HIV-negative individuals to individual HIV proteins (Tat and gp120) alone or in the virions induces epithelial mesenchymal transition (EMT). Furthermore, introduction of Tat into the human uterine cervical carcinoma cells causes an upregulation of expression of HPV oncoprotein E6 with concomitant decrease in the levels of p53 [23]. Keratinocytes affected by HIV proteins (but not the unexposed ones) can then be transformed by HPV-16 DNA, exhibiting loss of cell adhesion and increased proliferation and migration/mobility critical for the progression of neoplastic processes [24]. This led to the suggestion that the promotion of EMT in the urogenital mucosa driven by HIV proteins could be one of the mechanisms by which HIV-1 enhance the carcinogenic effect of HPV oncoproteins [24].

Interestingly, a panel of HIV proteins, including ones mentioned above, has been shown to induce the production of reactive oxygen species (ROS) [18, 25–27]. ROS as such are weak carcinogens, but strong tumor promoters [28]; chronic overproduction of ROS leads to the spontaneous tumor formation [29], indicating that the induction of ROS might underlie the direct carcinogenicity of HIV-1.

We have previously found that the transient expression of HIV-1 reverse transcriptase (RT) in the mammalian cells induces the production of ROS, oxidative stress, and oxidative stress response [26, 27]. The biological implications of these findings (except for a negative effect of ROS production on the cellular immunogenicity of RT following DNA immunization) remained unknown. Here, we have explored the effects of RT-induced ROS production on the growth and motility/migration of tumor cells *in vitro* and *in vivo* on the model of murine mammary gland adenocarcinoma 4T1luc2 cells made to express a panel of HIV-1 RT variants. We found that stable expression of RT leads to an increase in the production of ROS above the already high levels observed in the parental tumor cells. RT-expressing cells exhibit enhanced migration (motility) and a shift to a mesenchymal phenotype, concomitant with an increased expression of the transcription factors Twist and Snail, which coordinate EMT. In syngeneic immunocompetent mice, these properties of RT-expressing cells lead to the enhanced tumor growth and increased metastatic activity. We found the above features to correlate with the expression of RT and/or the production of ROS. Analysis of the complex events induced by the expression of a single HIV-1 protein, the reverse transcriptase, advances our understanding of the possible mechanism(s) of HIV-driven carcinogenesis unrelated to immune suppression.

2. Materials and Methods

2.1. Design of the Consensus RT of HIV-1 Subtype A FSU-A Strain. The full-length sequences of the reverse transcriptase (RT) of the variants of HIV-1 subtype A FSU_A strain isolated from the treatment-naïve patients on the territory of the former Soviet Union were selected from the HIV sequence database (http://www.hiv.lanl.gov/content/index) and Stanford Drug Resistance database ($n = 44$) (Suppl. Fig 1). The following sequences were used, designated by HIV subtype, country of collection, year of collection, and GenBank accession number of HIV isolate: A1.GE.1999. 99GEMZ011.DQ207944; A1.KZ.2002.02KZKAR300435.EF5 89042; A1.KZ.2002.02KZPAV300480.EF589043; A1.KZ.200 2.02KZPAV300497.EF589039; A1.KZ.2002.02KZPAV3005 02.EF589044; A1.KZ.2002.02KZYUZ300413.EF589040; A1. KZ.2002.02KZYUZ300425.EF589041; A1.RU.2000.RU0005 1.EF545108; A1.RU.2002.RU01029.JQ292892; A1.RU.2003. 03RU20_06_13.AY500393; A1.RU.2005.RU_560_1125_JA. JQ292895; A1.RU.2006.RU_915_1016.JQ292896; A1.RU.20 06.RU_915_1035.JQ292897; A1.RU.2006.RU_915_1038.JQ2 92898; A1.RU.2006.RU_915_1041.JQ292899; A1.RU.2006. RU_SP_B_049.JQ292900; A1.RU.2007.Irkutsk_5.JQ292891; A1.RU.2008.DEMA108RU003.KF716491; A1.RU.2008.DE-MA108RU004.KF716492; A1.RU.2008.PokA1Ru.FJ864679; A1.RU.2008.RUA001.JQ292893; A1.RU.2008.RUA007.JQ2 92894; A1.RU.2010.10RU6617.JX500696; A1.RU.2010.10R-U6792.JX500695; A1.RU.2011.11RU6950.JX500694; A1.UA. 2000.98UA0116.AF413987; A1.UA.2001.01UADN121.DQ8 23358; A1.UA.2001.01UADN139.DQ823357; A1.UA.2001.0 1UAKV254.DQ823361; A1.UA.2001.01UAOD10.DQ82336 5; A1.UA.2001.01UAOD35.DQ823366; A1.UA.2001.01UA OD89.DQ823367; A1.UA.2001.01UAPol293.DQ823359; A 1.UA.2001.01UAPol294.DQ823356; A1.UA.2001.01UAPol3 03.DQ823360; A1.UZ.2002.02UZ0659.AY829209; A1.UZ.20 02.02UZ0663.AY829210; A1.UZ.2002.02UZ0667.AY829211; A1.UZ.2002.02UZ0672.AY829212; A1.UZ.2002.02UZ652.A Y829203; A1.UZ.2002.02UZ694.AY829205; A1.UZ.2002.02 UZ698.AY829206; A1.UZ.2002.02UZ740.AY829208; A1.B Y.2013.KT983615.

Sequences were aligned using Multiple Sequence Comparison by Log-Expectation (MUSCLE; http://www.ebi.ac .uk/Tools/msa/muscle/), and consensus sequence was generated with Geneious 8.1.2 software (Biomatters Ltd., Auckland, New Zealand, https://www.geneious.com/academic/). Amino acids in variable positions of the consensus sequences were chosen with the help of covariance networks obtained by squaring the difference between the number of observed and expected amino acid pairs and normalizing this difference by the number of entries (excluding gaps) in each column (the observed minus expected squared method, OMES) using custom written scripts kindly provided by Prof. J. Tavis and Dr. M. Donlin from St. Louis Medical School, USA [30]. A humanized synthetic gene encoding the corresponding amino acid sequence was designed using the web service utility at http://genomes.urv.es/OPTIMIZER [31] and the online customer portal at http://www .invitrogen.com. To ensure adequate protein expression, the expression-optimized gene was provided with an AAT-ATG-GGA sequence fused to its $5'$-end. This resulted in the extension of the N-terminal region of RT with additional amino acids Met-Gly. The resulting mRNA was checked for the absence of undesirable folding (UNAFold at http://mfold.rna.albany.edu/ and OPTIMIZER at http://genomes.urv.es/OPTIMIZER/). The coding sequence for the consensus HIV-1 RT_A (RT_A) was synthesized by Evrogen (Moscow, Russia).

2.2. Cloning of RT_A Gene for Prokaryotic Expression and Generation of Plasmids Expressing RT_A Variants. RT_A-encoding DNA was cloned into the plasmid p6HRT-prot (a gift from Dr. S. Le Grice, NCI-Frederick, Frederick, MD) in substitution for the sequence encoding the wild-type p66/p51 heterodimeric RT of HIV-1 HXB2 strain. Plasmid p6HRT-prot had two restriction sites for BamHI endonuclease at the $5'$-end of the polynucleotide sequence encoding RT of HIV-1 HXB2 (RT_B), one of them was deleted by site-directed mutagenesis. RT_A encoding sequence was cloned between the remaining $5'$-BamHI and $3'$-SalI restriction sites, generating p6HRT_A encoding the consensus RT of HIV-1 FSU_A1 strain with the N-terminal hexahistidine tag. Mutations M184V and K65R conferring resistance to nucleoside RT inhibitors (NRTI) and K103N and G190S conferring resistance to nonnucleoside RT inhibitors (NNRTI) were introduced into p6HRT_A by site-directed mutagenesis (Evrogen) generating plasmids p6HRT_An (65/184) and p6HRT_Ann (103/190), respectively.

2.3. Reverse Transcriptase Expression and Purification. Heterodimeric p66/p51 RT_A variants were expressed in M-15 (pREP4) E. coli cells (Qiagen, Hilden, Germany) transformed by the plasmids p6HRT_A, p6HRT_An (65/184), and p6HRT_Ann (103/190) and purified as was described previously [32]. In brief, cells harboring the expression vector were grown overnight in 5 mL of LB medium supplemented with 10 g/L glucose, 150 mg/L ampicillin (A150), and 50 mg/L kanamycin (K15) at 37°C. After the overnight culture, cells were harvested by centrifugation, the pellet was resuspended in 300 mL of the fresh medium supplemented with A150 and K50, and cells were grown at 37°C up to OD_{600} 0.5. At this point, isopropyl-β-D-thiogalactopyranoside (IPTG) was added to a final concentration of 1 mM, and cells were grown for additional 5 h and then harvested by centrifugation at 4000g at 4°C for 30 min. The cell pellet was resuspended on ice in 15 mL of buffer A (25 mM Tris-HCl, pH 7.9, 500 mM NaCl, 10% (v/v) glycerol, 5 mM β-mercaptoethanol) with 1% (v/v) Triton X-100 supplemented with protease inhibitors phenylmethylsulfonyl fluoride (PMSF, 1 mM) and Protease Inhibitor Cocktail for expression of hexahistidine-tagged proteins (Sigma, Darmstadt, Germany). The suspension was lysed by sonication on ice and pelleted at 8000g for 30 min. The clarified lysate was applied onto a 2 mL Ni-NTA-agarose column (Novagen, Darmstadt, Germany). The column was successively washed with buffer A containing 10, 30, and 40 mM imidazole (10 column volumes each); protein was eluted by the same buffer containing 200 mM imidazole. Fractions (0.7 mL each) were analyzed by the Bradford protein assay [33]. The target fractions were pooled,

dialyzed against buffer B (25 mM Tris-HCl (pH 7.5), 300 mM NaCl, 10% (v/v) glycerol, 5 mM DTT, and 10 mM $MgCl_2$) for 2 hours at 4°C, then dialyzed against buffer C (25 mM Tris-HCl (pH 7.5), 300 mM NaCl, 50% (v/v) glycerol, 5 mM DTT, and 10 mM $MgCl_2$) for 12 hours at 4°C, aliquoted, and stored at −20°C.

2.4. *Polymerase Activity Assays.* The RT assays using activated DNA (Amersham, Buckinghamshire, UK) were performed as follows: the standard reaction mixture (20 μL) contained 0.75 μg of activated DNA, 0.02–0.05 μg RT, 3 μM dATP, 30 μM of dCTP, dGTP, and dTTP, 1 μCi [α-^{32}P] dATP in a Tris-HCl buffer (50 mM, pH 7.5) supplemented with 10 mM $MgCl_2$, and 0.2 M KCl. The reaction mixtures were incubated for 12 minutes at 37°C and applied onto Whatman 3MM filters with 0.5 M EDTA solution to stop the reaction. After drying on air, the filters were washed twice with 10% trichloroacetic acid, then twice with 5% trichloroacetic acid, once with ethanol, and dried on air. The radioactivity was measured by the Cherenkov method [34] in a Tri-Carb 2810 TR scintillation counter (PerkinElmer, Franklin Lakes, NJ, USA).

Kinetic parameters of the DNA-dependent DNA polymerase reaction included the Michaelis constant (K_M) determined as the substrate concentration at half of the maximal velocity and maximal reaction velocity (V_{max}) determined as the velocity, which cannot be further increased by the increase of the substrate concentration. Kinetic parameters were determined by the standard methods using RT variants in concentrations corresponding to 17 nM of RT of HIV-1 HXB2 strain (RT_B), expressed and purified as described previously [32]. 20 μL of the reaction mixture contained dATP in varying concentrations (0.05, 0.07, 0.11, 0.25, 0.5, and 1.5 μM); other components of the reaction mixture and reaction conditions were as described above. K_M to dATP and V_{max} were calculated using Sigma Plot 8.0 software (Systat Software Inc., London, UK).

2.5. *RNase H Activity Assay.* RNase H activity of HIV-1 RTs was tested by using 6.7 mmol of 18-ribo-Fl/18-deoxy duplex formed by 18-mer oligoribonucleotide 18-ribo-Fl 5′-r(GAUCUGAGCCUGGGAGCU)-fluorescein-3′ and 18-mer oligodeoxyribonucleotide 5′-d(AGCTCCCAGGCTCAGAUC)-3′. RNA/DNA duplex was added to the reaction mixtures consisting of 15 μL of 50 mM Tris-HCl pH 8.0 containing 60 mM KCl, 10 mM $MgCl_2$, and various concentrations of RT_A variants or RT_B (5, 20, 100, and 400 nM) and incubated for 15 min at 37°C. The reaction was stopped by adding 80 μL of a solution containing 7 mM EDTA, 0.375 M sodium acetate, 10 mM Tris-HCl, pH 8.0, and 0.125 mg/mL glycogen. The mixture was extracted by phenol/chloroform, and RNA/DNA fragments were precipitated with ethanol. The reaction products were separated by electrophoresis in a 20% polyacrylamide/7 M urea gel. Gel images were recorded using a phosphoimager and then quantified using Quantity One 4.6.6. (Bio-Rad, USA). In order to determine the specific RNase H activity of the recombinant RT, 100 μL reaction mixtures containing 100 μM RNA/DNA duplex, 50 mM Tris-HCl pH 8.0,

10 mM $MgCl_2$, 60 mM KCl and RTs in variable concentrations (20, 40, and 80 nM) were incubated at 37°C and aliquots of 15 μL were removed after 1, 1.5, 2.5, 3.5, 5.5, and 15 minutes and quenched with 80 μL of stop solution (1 mM CH_3COONa, 200 mM glycogen, and 200 mM EDTA). RNA/DNA fragments were precipitated with ethanol at 0°C and analyzed by electrophoresis in a 20% polyacrylamide/7 M urea gel. The specific activities of enzymes as dependence of the initial velocities of RNase H reaction on the concentration of the enzyme were calculated as described previously [35, 36]. Kinetic parameters of the ribonuclease reaction were determined by standard methods using RT variants in different concentrations conferred to their specific activities: 40 nM of RT_B variant, 45.6 nM of RT_A, 41.6 nM of RT_An variant, and 56.8 nM of RT_Ann variant. 10 μL of the reaction mixture composed of RT and RNA/DNA duplex in varying concentrations (100, 110, 125, 150, 200, 250, 500, 1000, and 2500 nM) dissolved in the buffer containing 50 mM Tris-HCl (pH 8.0), 10 mM $MgCl_2$, and 60 mM KCl was incubated at 37°C for 3 minutes and then analyzed as described above. K_M and V_{max} parameters were calculated using Sigma Plot 8.0 software (Systat Software Inc., London, UK).

2.6. *Preparation of Lentiviral Vectors Encoding RT Variants.* Coding sequences for RT_A, RT_An, and RT_Ann were recloned from p6HRT_A, p6HRT_An (65/184), and p6HRT_Ann (103/190) into the lentiviral vector pRRLSIN.cPPT.PGK (Addgene plasmid #12252; a gift from D. Trono) generating a set of lentiviral vectors pLV-RT_A, pLV-RT_An, or pLV-RT_Ann (Suppl. Figure 2). Lentiviral particles were produced by transient transfection of 293T cells as described elsewhere [37] and concentrated 10-fold with Amicon Ultra-15 100K centrifuge concentrators (Merck-Millipore, Darmstadt, Germany). Infectious titers of the lentiviral particles were determined on HT1080 cells by quantitative real-time PCR [37] using standard samples of HT-1080 DNA with a known number of viral genome copies.

2.7. *Lentiviral Transduction of 4T1luc2 Cells and Isolation of Clones Expressing RT_A Variants.* Lentivirus preparations were used to transduce murine mammary gland adenocarcinoma cells expressing firefly luciferase 4T1luc2 (PerkinElmer). Transduction of 4T1luc2 cells was performed with the multiplicity of lentiviral infection of 1, 5, and 20 of transducing units per cell for nonmutated and 1 and 10 for mutated RT_A variants. The resulting cell lines were cloned to single cells by limiting dilution in 96-well plates generating monoclonal populations of 4T1luc2 derivative clones. All 4T1luc2 derivatives were cultured in the full RPMI-1640 medium with 10% FBS and 100 mg/mL penicillin/streptomycin mix at 37°C in 5% CO_2 and split every 2-3 days.

The presence of the sequences encoding RT_A variants in the genome of 4T1luc2 derivative clones was confirmed by PCR with a pair of primers specific for the lentivector backbone and flanking the RT insert (Suppl. Table 1, Suppl. Figure 2).

Doubling time of the derivative clones was estimated as described previously [38, 39].

2.8. Confirmation of RT Expression by RT-PCR and Western Blotting.

RNA was isolated using TRI reagent (Sigma, Darmstadt, Germany) according to the manufacturer protocol and reverse transcribed using MINT reverse transcription kit (Evrogen). Presence of RT mRNA was confirmed using conventional PCR with primers, specific to RT and HPRT1 (hypoxanthine-guanine phosphoribosyltransferase) (Suppl. Table 1); PCR products were resolved by agarose electrophoresis.

Expression of RT_A variants was analyzed by Western blot of cell lysates performed as described previously [40]. The exact amount of each RT variant produced per cell was calculated using protein calibration curve built using recombinant RT, resolved by PAGE and Western blotting using polyclonal anti-RT antibodies. These antibodies are equally effective in the detection of different RT variants [41]. Signals from the bands containing known amount of recombinant RT were quantified by ImageJ software (http://rsb.info.nih.gov/ij) and used to build a calibration curve. Using this curve, we assessed the amount of RT in the aliquots of cell lysates loaded onto the gel, and by dividing this value by the number of cells used to prepare the lysate, we determined the levels of RT expression per cell for each derivative clone. In all further assays of the activities of RT_A variants, we assessed their effect in a known number of cells, calculated the effect per cell, and then normalized the effect per cell to the amount of RT variant produced by this cell.

2.9. Assessment of the Production of Reactive Oxygen Species (ROS).

Production of ROS was registered with $2',7'$-dichlorodihydrofluoresceine diacetate (DCFH2-DA) as described previously [42, 43]. Cells treated with oxidants tert-butylhydroquinone (tBHQ) (Sigma, Darmstadt, Germany) and H_2O_2 at $100\,\mu M$ concentrations were used as positive controls of ROS induction. Antioxidants N-acetyl cysteine (NAC) in concentration 5 mM were used as a general inhibitor of ROS production, [44], and tocopherol (both from Sigma, Darmstadt, Germany) in concentration $1\,\mu M$, as the inhibitor of lipid peroxidation [45].

2.10. Analysis of Lipid Peroxidation.

The level of malondialdehyde (MDA) in the cells was determined using high-performance liquid chromatography with mass-spectrometric detection. A $50\,\mu L$ aliquot of cell suspension containing known number of cells was supplemented with $250\,\mu L$ of 1% sulfuric acid. The mixture was shaken vigorously for 1 min by hand, then vortexed for 2 min to disrupt the cells, and supplemented with $300\,\mu L$ of 1.3 mM DNPH (Acros Organics, New Jersey, USA). The mixture was kept in a dark place at the ambient temperature for 40 min to derivatize MDA. After the completion of the reaction, the mixture was neutralized by adding $20\,\mu L$ of 4 M NaOH. The sample was centrifuged at 10000g for 15 min at 4°C, and the supernatant was collected and transferred into an HPLC vial. Samples, $5\,\mu L$ each, were injected into an HPLC system with $150*2$ mm Pursuit

XRs $5\,\mu$m C18 column (Agilent, Santa Clara, USA). The analysis was carried out in the gradient mode using 0.5% formic acid solution as phase A and 0.5% formic acid solution in methanol as phase B. MDA-DNPH signal was recorded by 6500 QTRAP mass-spectrometer (Sciex, Framingham, USA) using three MRM channels: 235 > 159 (quantifier), 235 > 189, and 235 > 143 (qualifiers). The linear calibration curve was set by the acid hydrolysis of tetramethoxypropane (Cell Biolabs, San Diego, USA) in 1% sulfuric acid using five standard points (10–200 pmol/mL). NIH3T3 cells served as a negative and serial dilutions of a solution containing known concentrations of MDA (MyBioSource, Vancouver, Canada) as positive controls. The MDA quantity was calculated per cell and normalized to the amount of RT variant produced by this cell (calculated as described above).

2.11. Wound Healing Assay.

Cells were harvested in 24-well cell culture plates to obtain absolutely confluent monolayer in standard medium or in the medium with 5 mM N-acetyl cysteine. A cross-shaped wound was scratched at the center of each well with a $200\,\mu L$ sterile tip. Wells were photographed at 0, 13, and 18 hours using a light microscope (Leica, Wetzlar, Germany). Borders of the gaps were marked using the Adobe Photoshop CC software (Adobe, San Jose, CA, USA). Distances between the edges were measured using the ImageJ software.

2.12. Isolation of Nucleic Acids, Reverse Transcription, and Semiquantitative PCR.

Cell culture medium was discarded; cells were detached using 0.25% Trypsin with EDTA before lysis in AmpliSens Riboprep lysis buffer (CRIE, Moscow, Russia). Nucleic acids were isolated using AmpliSens Riboprep kit (CRIE, Moscow, Russia) according to the manufacturer's instructions and reverse transcribed using AmpliSens Reverta-FL (CRIE, Moscow, Russia). Gene-specific PCRs were performed on a RotorGene 6000 (Qiagen, Hilden, Germany) cycler using primers specific to E-cadherin, N-cadherin, Vimentin, Twist, and Snail genes (Suppl. Table 1) and SYBR Green (Thermo Fisher Scientific, Waltham, MA USA). Levels of mRNAs were measured relative to HPRT1 mRNA used as a reference. Relative gene expression levels were calculated using the ddCt method [46].

2.13. Assessment of Tumorigenicity of 4T1luc2 Derivative Clones.

Animal experiments were performed in the animal facilities of the NF Gamaleya Research Center of Epidemiology and Microbiology (GRCEM), Ministry of Health of the Russian Federation (Moscow, Russia) and of the Latvian Biomedical Research and Study Centre (Riga, Latvia). The experiments were carried in compliance with the bioethical principles adopted by the European Convention for the Protection of Vertebrate Animals Used for Experimental and Other Scientific Purposes (Strasbourg, 1986). Experimental procedures were approved by the ethical committee of the GRCEM (protocol N10, March 14, 2017) and by the Latvian Animal Protection Ethics Committee of the Latvian Food and Veterinary Service (permit no. 99 from April 4, 2018). Eight-week-old BALB/c mice from "Pushchino" breeding

facility of the Institute of Bioorganic Chemistry RAS (Push-chino, Russia) or Laboratory Animal Center University of Tartu (Tartu, Estonia) were housed under a 12 h/12 h light-dark cycle with *ad libitum* access to water and food. Mice were marked with earmarking and housed in groups of three to five animals per cage. During all interventions, mice were anesthetized with the 1 L/min flow of air containing 4% iso-flurane at the induction and 2.5% at the maintenance stage, administered through the facial masks.

The capacity of the derivative cell lines to form tumors and metastases was tested by ectopic implantation into 8-week-old female BALB/c mice. Prior to injection, 4T1luc2 and derivative clones grown in the selective medium were detached, sedimented, washed with serum-free RPMI-1640, stained for viability with Trypan Blue dye (Life Technologies, Carlsbad, CA), then counted in a hemocytometer, and ali-quoted 10^4, 2×10^4, and 4×10^4 cells in $50\,\mu L$ of RPMI-1640 in sterile test tubes. Aliquots were injected with a 25G needle mounted on an insulin syringe (B Braun, Germany) subcutaneously into two sites, to the right and to the left of the base of the tail. Tumor size was assessed by morphomet-ric measurements done at regular intervals using calipers; tumor volume was calculated using the standard formula for xenograft volume [47, 48]: $V = xy^2/2$. Tumor growth was also assessed by bioluminescent imaging (BLI) on Spectrum CT (PerkinElmer, Waltham, MA, USA) following the procedures recommended by PerkinElmer and described by us earlier [27]. Monitoring of bioluminescence was done directly after the implantation, then on days 1, 2, 4, and 6 and then every 2-3 days until the tumor volume of the first mouse in the experiment reached the volume of 1 cm^3 which was set as the experimental endpoint. Mice were weighed at each monitoring point. At the experimental endpoint, nor-mally on days 18 to 21 after the implantation, mice were humanely euthanized and organs were collected. All experi-ments were done in two independent runs, 1st on five and 2nd time on three mice per cell line and cell dose.

2.14. In Vivo Bioluminescence Imaging.

Detailed procedure of *in vivo* imaging was described earlier [27]. In brief, freshly prepared solution of XenoLight D-luciferin potassium salt (PerkinElmer, Waltham, MA, USA) was administered into mice in the amount of 150 mg/kg based on their actual weight. The substrate was diluted in $200\,\mu L$ PBS and injected intraperitoneally. After 10 min, mice were anesthetized as described above. The area of the skin over the tumor in the radius of 1.5 cm was shaved and depilated using a depilating cream for sensitive skin. After that, mice were transferred into the In Vivo Imaging System (IVIS; IVIS Spectrum CT, PerkinElmer) with the continuous flow of 1 L per min of air containing 4.0% isoflurane at the initiation and 2.5% at the maintenance stages. IVIS was set to automatic exposure time (60 sec at early stages, reduced to 2 to 10 sec at late stages of tumor growth). Images were captured, and total photon flux from the regions of interest (ROI) of the same area was ana-lyzed using Living Image 4.5 Software® (PerkinElmer). After the completion of monitoring, mice were transferred back to their cages with close placement to reduce the risk of hypothermia.

2.15. Experimental Endpoint and Collection of Mouse Organs for Rapid Ex Vivo Assessment of the Formation of Metastases.

At the experimental endpoint, mice were anaesthetized as described above. Freshly prepared solution of XenoLight D-luciferin potassium salt (PerkinElmer) in PBS was injected into mice intraperitoneally in an amount of 150 mg/kg based on the actual weight. Ten minutes later, mice were euthanized by cervical dislocation by a skilled animal handler. The fur and skin of the mice were disin-fected with 70% ethanol. After that, tumors, spleen, liver, and lungs, affected by the distant metastasis in the 4T1 tumor model [49, 50], were dissected with surgical scis-sors. Tumors and organs were transferred into the wells of a 24-well tissue culture test plate (Wallac, Turku, Fin-land) containing 2 mL RPMI-1640 medium. *Ex vivo* biolu-minescent imaging of tumors and organs was performed as described for *in vivo* imaging. Thereafter, tumors and all organs, except for spleens, were transferred to 5 mL of 4% formaldehyde solution in PBS, incubated for 24 to 48 h at +6°C, then washed five times with PBS, and used to prepare FFPE blocks, according to the standard proto-col [51].

2.16. Preparation of Splenocytes and Analysis of Their Immune Reactivity.

Spleens were washed from luciferin with PBS, transferred into the Petri dishes containing 3 mL RPMI, and grinded with a syringe plunger, and single-cell spleno-cyte cultures were prepared as described earlier [52]. Popula-tion of white blood cells in the splenocyte samples was analyzed on a FACSAria II cytometer (BD Biosciences, USA). Data were exported as FCS3.0 files with the use of FACSuite software and analyzed using FlowJo X.07 program (FlowJo LLC, Ashland, USA). General lymphocyte and gran-ulocyte areas were defined on forward scatter (FSC) versus side scatter (SSC) plot. Remaining splenocytes were tested for the capacity to proliferate in response to stimulation with synthetic peptides. Cytokine production by stimulated cells was assessed using IFN-γ/IL-2 Fluorospot Kits (Mabtech, Nacka Strand, Sweden) following the procedures described earlier [52]. In brief, single-cell cultures 2.5×10^5 splenocytes per well in the duplicate wells were stimulated for 18 h with a peptide representing the region between aa 145 and 168 of RT_A QYNVLPQGWKGSPSIFQSSMTKIL, which we have shown to contain a cluster of CD4$^+$ and CD8$^+$ T cell epitopes recognized by CD4$^+$ and CD8$^+$ T cells of BALB/c mice (S Pet-kov, M Isaguliants, unpublished data) and a peptide GFQSMYTFV derived from firefly luciferase (both peptides from Synpeptide Co. LTD, Shanghai, China). Peptides were dissolved in PBS and used at the final concentration of $10\,\mu g/mL$. Unrelated peptides and medium alone served as negative and mitogen Concanavalin A ($5\,\mu g/mL$) as a positive control. The stimuli were diluted in the complete culture media consisting of RPMI supplemented with 5% FBS, 100 U/mL penicillin, $100\,\mu g/mL$ streptomycin, and 0.3 mg/mL glutamine (Gibco, Thermo Fisher, Waltham, MA, USA). After 20 h incubation, plates were processed fol-lowing the protocol provided by the manufacturer and read on ImmunoSpot CTL S5 UV Analyzer (Cellular Technology Limited (CTL), Cleveland, USA) to assess the number of

splenocytes producing IFN-γ and IL-2 (cytokine-producing cells; SFCs) per well. The number of cytokine-producing cells was recalculated per 10^6 splenocytes.

2.17. Tumor Histology and Ex Vivo Assessment of the Metastases. FFPE blocks were prepared from the formalin-fixed tumor tissues and murine lungs and livers and sectioned on cryostat microtome according to the standard protocols (https://www.protocolsonline.com/histology/sample-preparation/paraffin-processing-of-tissue/). Sections mounted on slides were dewaxed, rehydrated, stained with Mayer's hematoxylin solution, then washed, rinsed, and counterstained with eosin Y solution, after that, dehydrated, washed with absolute alcohol, and covered with cover slips for microscopic evaluation. Histological evaluation was based on the standard parameters such as acinar formation, nuclear size, and pleomorphism and mitotic activity [51]. Grade of the tumors was calculated according to [53]. The slides were examined by light microscopy (Leica DM500, Wetzlar, Germany). Formalin-fixed, Paraplast-embedded liver tissues were used to diagnose and evaluate the formation of metastases. For each mouse, the area of tumor metastases was quantified in 25 high-power (×400) microscope fields of hematoxylin-eosin-stained slides by computer-assisted morphometry using specialized NIS-Elements software (Nikon, Tokyo, Japan). Total DNA was isolated from five freshly prepared sections using Allprep DNA/RNA FFPE Kit (Qiagen). The presence of the sequences encoding RT_A variants was confirmed by PCR using a pair of primers, one specific for the lentivector backbone and the other to RT coding sequence (Suppl. Table 1).

2.18. Statistics. Statistical analysis was performed using STATISTICA AXA 10.0 (StatSoft Inc., OK, USA). Nonparametric statistics were chosen as appropriate for sample sizes < 100 entries. Continuous but not normally distributed variables, such as enzymatic parameters, the normalized levels of gene expression, the total photon flux, tumor volume, number and size of the metastases, and the number of cytokine-producing cells (SFCs), were compared in groups using Dunn's test for pairwise multiple comparisons of the ranked data as the post hoc test following Kruskal-Wallis test and pairwise by Mann-Whitney U test or Fisher LSD tests. Data grouped by two variables were analyzed using ordinary two-way ANOVA with the correction for multiple comparison. Correlation analysis was done using Spearman Rank Correlation test. R in Spearman test represented the regular Pearson product-moment correlation coefficient (Pearson r) in terms of the proportion of variability accounted for computed from the ranks. Spearman R assumed that the variables under consideration were measured on at least an ordinal (rank order) scale with the individual observations (cases) ranked into two ordered series. Multiple regression analysis was done by first building and then analyzing the correlation matrix; all calculations involved in the actual multiple regression analysis were performed in double precision. Matrix inversion was accomplished via sweeping. The regression weights, residual sums of squares, tolerances, and partial correlations were calculated as part of the sweeping operation. The F value (Regression Mean Square/Residual Mean Square), t (df), and resulting p value were used as an overall F test of the relationship between the dependent variable and the set in independent variables. F value associated with the multiple R and the t values associated with the regression coefficients were calculated using standard built-in formulas (STATISTICA AXA 10.0). Parametrical statistical analysis was performed using IBM SPSSv23 software including descriptive assessment as detection of mean values and standard deviation (SD). For all types of analysis, p values < 0.05 were considered significant.

3. Results

3.1. Design of the Consensus RT of HIV-1 Subtype A FSU_A Strain and Its Variants with Compromised Polymerase and RNase H Activities. We have earlier found that transient expression of RT of HIV-1 clade B strains in eukaryotic cells induces oxidative stress [26, 27]. Here, we aimed to determine if this is a general property of HIV-1 RTs, whether or not it depends on the enzymatic activities of RT, and what are the *in vitro* and *in vivo* implications of the induction of oxidative stress for RT-expressing cells. To resolve these questions, we designed a consensus RT of a different clade, namely, HIV-1 clade A FSU_A strain and a panel of its variants with compromised polymerase and RNase H activities.

Amino acid sequences of RTs of HIV-1 FSU_A isolates from the treatment-naïve patients without known drug resistance mutations were selected from HIV-1 sequence database and HIV Drug Resistance database ($n = 44$). The majority of sequences dated 1999 and 2012 were from the Russian Federation (41%) and the rest from other countries of the former Soviet Union: Ukraine (23%), Uzbekistan (18%), Kazakhstan (14%), and Belarus and Georgia (2% each) (Suppl. Figure 1). In concordance with the earlier observations [54], we observed very low average amino acid diversity of RT amino acid sequences, which allowed us to build a reliable consensus sequence of HIV-1 FSU_A RT (RT_A) (Figure 1).

On the basis of this consensus, we designed mutant RT variants with compromised activities of polymerase and RNase H. This was achieved by the insertion of biologically relevant primary mutations of drug resistance to nucleoside (NRTI) and nonnucleoside (NNRTI) inhibitors characteristic to FSU_A isolates: mutations of resistance to NRTI are known to reduce the polymerase, and to NNRTI, both the polymerase and RNase activities of the enzyme [55]. The most frequent mutation of resistance to NRTI worldwide is M184V/I, followed by K65R/N, L74V/I, Y115F, and Q151M, and the most prevalent for FSU_A is M184V, followed by K65R/N [56–58]. These mutations diminish the polymerase activity of RT [59]. The most frequent primary mutation of resistance to NNRTI worldwide is G190S (http://hivdb.stanford.edu/DR/NNRTIResiNote.html). It is also the most frequent mutation of resistance to NNRTI in patients infected with HIV-1 FSU_A [58, 60]. It is present either alone or in combination with other mutations, such as K103N, and is never detected in HIV-1 patients naïve to

```
!Domain=Data;
#RT_A                      PISPIETVPV TLKPGMDGPK VKQWPLTEEK IKALIDICKE MEKEGKISKI GPENPYNTPV FVIKKKDSTK WRKLVDFREL   [ 80]
#RT_An                     .......... .......... .......... .......... .......... .......... ....R..... ..........   [ 80]
#RT_Ann                    .......... .......... .......... .......... .......... .......... .......... ..........   [ 80]
#K03455.1_HIV-1_subtype_B_(HXB2)  .......... K......... .......... ....VE..T. .......... .......... .A........ ..........   [ 80]

#RT_A                      NKRTQDFWEV QLGIPHPAGL KKKKSVTVLD VGDAYFSVPL DESFRKYTAF TIPSINNETP GIRYQYNVLP QGWKGSPSIF   [160]
#RT_An                     .......... .......... .......... .......... .......... .......... .......... ..........   [160]
#RT_Ann                    .......... .......... ..N....... .......... .......... .......... .......... ..........   [160]
#K03455.1_HIV-1_subtype_B_(HXB2)  .......... .......... .......... .......... ..D....... .......... .......... ......A..   [160]

#RT_A                      QSSMTKILEP FRLKNPEIVI YQYMDDLYVG SDLEIGQHRT KIEELRAHLL SWGFTTPDKK HQKEPPFLWM GYELHPDKWT   [240]
#RT_An                     .......... .......... ...V...... .......... .......... .......... .......... ..........   [240]
#RT_Ann                    .......... .......... .........S .......... .......... .......... .......... ..........   [240]
#K03455.1_HIV-1_subtype_B_(HXB2)  .......... ..KQ..D... .......... .......... .......... .....Q... R..L...... ..........   [240]

#RT_A                      VQPIMLPDKD SWTVNDIQKL VGKLNWASQI YPGIKVRQLC KLLRGAKALT DIVTLTEEAE LELAENREIL KEPVHGVYYD   [320]
#RT_An                     .......... .......... .......... .......... .......... .......... .......... ..........   [320]
#RT_Ann                    .......... .......... .......... .......... .......... .......... .......... ..........   [320]
#K03455.1_HIV-1_subtype_B_(HXB2)  ....V..E.. .......... .......... .......... .......... ...T..... EVIP...... ..........   [320]

#RT_A                      PSKDLVAEIQ KQGQDQWTYQ IYQEPFKNLK TGKYAKKGSA HTNDVKQLTA VVQKVATESI IIWGKTPKFR LPIQKETWEA   [400]
#RT_An                     .......... .......... .......... .......... .......... .......... .......... ..........   [400]
#RT_Ann                    .......... .......... .......... .......... .......... .......... .......... ..........   [400]
#K03455.1_HIV-1_subtype_B_(HXB2)  .....I.... ....G..... .......... .....RMRG. .........E A...IT.... V........K .........T   [400]

#RT_A                      WWMEYWQATW IPEWEFVNTP PLVKLWYQLE KEPIVGAETF YVDGAANRET KIGKAGYVTD RGRQKVVPLT ETTNQKTELH   [480]
#RT_An                     .......... .......... .......... .......... .......... .......... .......... ..........   [480]
#RT_Ann                    .......... .......... .......... .......... .......... .......... .......... ..........   [480]
#K03455.1_HIV-1_subtype_B_(HXB2)  ..T....... .......... .......... .......... .......... .L........N .......T.. D........Q   [480]

#RT_A                      AIHLALQDSG SEVNIVTDSQ YALGIIQAQP DRSESEIVNK IIEKLIEKER VYLSWVPAHK GIGGNEQVDK LVSNGIRRVL   [560]
#RT_An                     .......... .......... .......... .......... .......... .......... .......... ..........   [560]
#RT_Ann                    .......... .......... .......... .......... .......... .......... .......... ..........   [560]
#K03455.1_HIV-1_subtype_B_(HXB2)  ..Y....... L......... .......... .Q....L..Q ...Q..K..K ...A...... .......... ...A...K..   [560]
```

FIGURE 1: Alignment of the amino acid sequences of the consensus HIV-1 reverse transcriptase and its drug resistance variants designed in the study. "RT_A," consensus of amino acid sequences ($n = 44$) of HIV-1 subtype A FSU_A strain isolated between 1999 and 2012, with amino acids in variable positions chosen using OMES-based covariance network. "RT_An," RT_A variant with introduced mutations of resistance to NRTI K65R and M184V; "RT_Ann," RT_A variant with introduced mutations of resistance to NNRTI K103N and G190S; "K03455.1 HIV-1 subtype B (HXB2)," reference sequence of HIV-1 subtype B RT used for position numbering [63].

treatment with NNRTIs. G190S and K103N have little effect on RT-driven polymerization but selectively slow down RNase H cleavage and delay initiation of DNA synthesis, resulting in a significant reduction of viral replication competence [61, 62]. Based on this, we designed RT_A with M184V and K65R/N (RT_An) and RT_A with K103N and G190S (RT_Ann) which we predicted to have reduced polymerase and RNase H activities, respectively.

Synthetic DNA encoding consensus RT_A optimized for eukaryotic expression was cloned into the prokaryotic expression vector p6HRT to generate plasmid p6HRT_A for prokaryotic expression of RT_A. Mutations M184V/K65R or K103N/G190S were introduced into p6HRT_A by site-directed mutagenesis, yielding plasmids for prokaryotic expression of RT_An and RT_Ann, respectively, to purify respective proteins and determine their enzymatic activities.

3.2. Prokaryotic Expression of HIV Clade A RTs and Assessment of Their Enzymatic Activity. Prokaryotic expression vectors p6HRT_A encoding RT_A, p6HRT_An (65/184) encoding RT_An, and p6HRT_Ann (103/190) encoding RT_Ann were used to transform *E. coli*. RT_A, RT_An, and RT_Ann proteins which were purified using Ni-NTA-agarose chromatography and assessed for their polymerase and RNase H activities.

The polymerase activity was assessed using a template-primer complex represented by a nicked double-stranded DNA duplex ("activated DNA"). All three RT_A variants were highly active and exhibited similar level of activity with Michaelis constant (K_M) of approximately 0.4μM and maximum velocity (V_{max}) ranging from 4 to 7.5μM/sec∗mg, comparable to RT of HIV-1 clade B HXB2 strain (Table 1). Consensus RT_A had higher V_{max} than RT of HIV-1 HXB2. As expected, NRTI resistance mutations led to a decrease of the polymerization rate compared to V_{max} of the parental RT_A ($p = 0.005$) and of NNRTI-resistant RT_Ann ($p = 0.006$; Table 1). Thus, as predicted, mutations of resistance to NRTI reduced, and to NNRTI, had no effect on polymerization rate.

Next, we assessed RNase H activity of RT_A variants using as substrate the RNA/DNA heteroduplex consisting of 18 nt DNA strand and 18 nt fluorescein-labeled RNA. All RT variants were enzymatically active even at concentrations as low as 5 nM (Suppl. Figure 3). At 5 nM concentration, RT_A variants were less active than RT_B, but at higher enzyme concentrations (100 and 400 nM), their RNase H activities were similar (Suppl. Figure 3). All three RT_A variants had lower specific activity compared to HXB2 RT (Suppl. Figure 3, Table 1). As expected, the consensus RT_A and RT_An had similar specific RNase H activities, whereas RT_Ann exhibited only 60% of the activity of the consensus RT_A (Table 1). Further, we determined K_M and V_{max} of the RNase H reaction. All RT_A variants had lower V_{max} of the cleavage of RNA/DNA heteroduplex than RT of HIV-1 HXB2 ($p < 0.05$ for all pairwise comparisons; Fisher LSD test) with RT_Ann exhibiting somewhat lower V_{max} than RT_A ($p = 0.09$; Table 1). Thus, as predicted, mutations of resistance to NRTI had no effect, and to NNRTI, reduced the activity of RNase H. Thus, we generated two RT_A

TABLE 1: Kinetic parameters of the polymerase and RNase H activity of the variants of consensus RT of HIV-1 clade A FSU_A compared to RT of HIV-1 clade B HXB2 strain.

HIV-1 RT variants	Polymerase activity*		RNase H activity*	
	K_M (nM)	V_{max}/mg RT (μM/sec∗mg)	K_M (nM)	V_{max}/mg RT (μM/sec∗mg)
Wild-type RT of subtype B HXB2 strain (RT_B)	390 ± 95	4.0 ± 0.88	430 ± 60	21 ± 5
Consensus RT of subtype A (RT_A)	340 ± 100	7.5 ± 0.97 >RT_B ($p = 0.01$)**	470 ± 110	13 ± 4 <RT_B ($p = 0.014$)
Consensus RT of subtype A with primary mutations of resistance to nucleoside inhibitors K65R and M184 (RT_An)	320 ± 95	4.4 ± 0.18 <RT_A ($p = 0.0055$) <RT_Ann ($p = 0.005$)	400 ± 100	14 ± 2 <RT_B ($p = 0.034$)
Consensus RT of subtype A with primary mutations of resistance to nonnucleoside inhibitors K103N and G190S (RT_Ann)	400 ± 77	6.1 ± 0.5 >RT_B ($p = 0.02$) >RT_An ($p = 0.005$)	360 ± 60	8 ± 1 <RT_B ($p = 0.0005$) ≤RT_A ($p = 0.09$)

*Results presented as mean ± SD in triplicate tests. **Significance of difference assessed by Fisher LSD test.

TABLE 2: Clones of 4T1luc2 expressing consensus RT of HIV-1 clade A FSU_A strain (RT_A) and its variants with primary mutations of resistance to NRTI (RT_An) and NNRTI (RT_Ann), obtained by lentiviral transduction of 4T1luc2 cells at different multiplicities of infection (MOI).

Enzyme	Polymerization V_{max}*, relative to RT_A**	RNase H activity V_{max}*, relative to RT_A**	Lentivirus	MOI	Derivative clone
RT-A	100%	100%	LV-RT-A	1	4T1luc2_RT-1.3
			LV-RT-A	5	4T1luc2_RT-5.3
			LV-RT-A	20	4T1luc2_RT-20.1
RT-An	59%	107%	LV-RT-An	1	4T1luc2_RT-An-1.4
			LV-RT-An	10	4T1luc2_RT-An-10.1
RT-Ann	81%	62%	LV-RT-Ann	1	4T1luc2_RT-Ann-1.5
			LV-RT-Ann	10	4T1luc2_RT-Ann-10.2

*V_{max} for polymerase and RNase H activities according to Table 1. **Mean V_{max} for the given RT_A variant divided by mean V_{max} for RT_A, in %.

variants with deficiencies in each of the enzymatic activities, to further relate them to the ability of these enzymes to induce oxidative stress.

3.3. Derivatives of 4T1luc2 Cell Line Stably Expressing RT Variants. To assess the capacity of RT_A variants to generate oxidative stress and relate this to their tumorigenic potential, we generated RT-expressing derivatives of murine mammary gland adenocarcinoma 4T1 cells which form solid tumors with a high metastatic potential in BALB/c mice [64, 65]. Stable expression of luciferase reporter (Luc) in the daughter cell line 4T1luc2 (PerkinElmer, Franklin Lakes, NJ, USA) allows *in vivo* monitoring of tumor growth and metastasis formation. As we have previously shown, Luc expression induces an anti-Luc response that limits the metastatic potential of 4T1luc2 compared to the parental 4T1 cells [49]. Here, we have conducted the experiments to see if expression of RT_A variants would induce oxidative stress and through this modify the tumorigenic and metastatic potential of 4T1luc2 cells *in vitro* and *in vivo*.

Nucleotide sequences encoding RT_A, RT_An, and RT_Ann were recloned into the lentiviral vector under the control of the human phosphoglycerate kinase promoter, generating derivative vectors pLV-RT-A, pLV-RT-An, and pLV-RT-Ann, further used to transduce 4T1luc2 cells. Through this, we generated seven daughter clones of 4T1luc2 with genomic insertions of 2000 nt fragments encoding RT_A, RT_An, and RT_Ann (confirmed by sequencing) (Table 2).

All derivative clones were shown to express proteins with the expected molecular mass of 66 kDa, corresponding to the nonprocessed form of HIV-1 reverse transcriptase, specifically recognized by anti-RT antibodies (Figure 2(a)). We also detected minor amounts of the protein with molecular mass of 51 kDa corresponding to the processed form of HIV-1 RT, resulting from the cleavage of p66 by cellular proteases [66]. RT p66 forms homodimers [67], which predominate over the heterodimeric p51/p66 form (as was previously shown for RT-expressing HeLa cells [52]).

We assessed the levels of expression of RT_A variants and defined the amount of protein expressed by each of the derivative clones per one cell (Figure 2(a); see Materials and Methods for description). RT_A was expressed in the amount of 40 to 200 fg; RT_An, 6 to 10 fg; and RT_Ann, 3 to 4 fg per cell (Figure 2(b)). The level of expression of RT_A variants correlated with the multiplicity of infection (MOI) used to generate the respective clone (clones generated at higher MOI exhibited higher levels of RT expression) (Figure 2). The level of expression of RT_A, even at the lowest MOI, was higher than the level of expression of the mutated RT_A variants (Figure 2(b)).

(a)

(b)
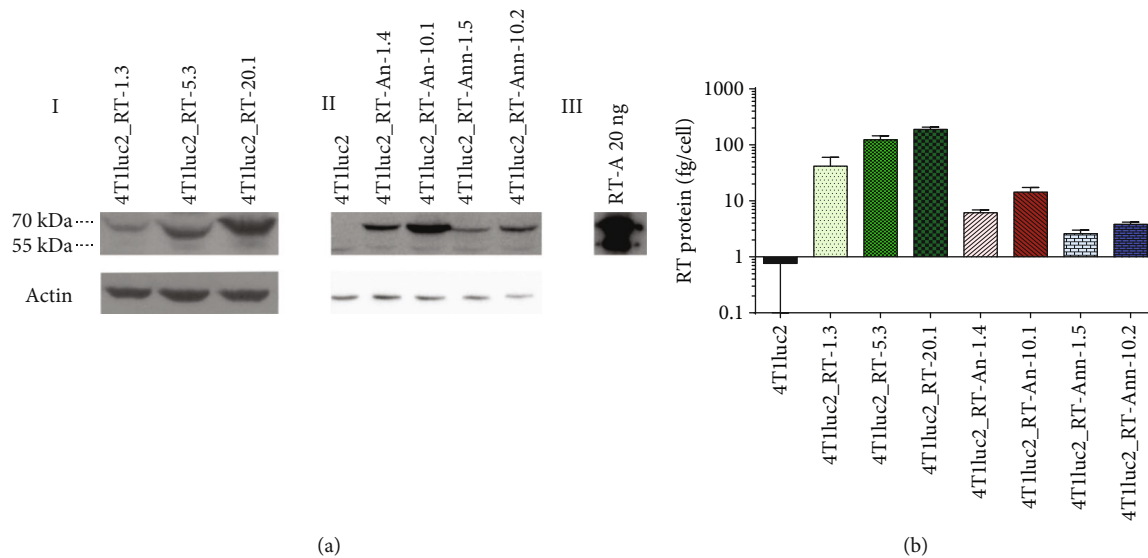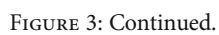
FIGURE 2: Expression of reverse transcriptase (RT) by 4T1luc2-derived cell lines carrying genomic inserts of sequences encoding variants of the consensus HIV-1 FSU_A RT. (a) Western blot analysis of lysates of derivative 4T1luc2 clones (Table 2) stained with rabbit polyclonal anti-RT antibodies [68] (I and II upper panels), and anti-actin monoclonal antibodies (I and II lower panels), recombinant RT_A as positive control (III). The parental 4T1luc2 cell line was used as a reference. Polyclonal anti-RT antibodies weakly bind to reverse transcriptase expressed by the lentivirus used to generate the parental 4T1luc2 cell line (II). Position of the weight mass marker is shown on the left. (b) Quantification of RT_A expression using ImageJ software. Signal in the lane corresponding to a given derivative clone was quantified using calibration curve built with the help of recombinant RT_A. Total amount of the expressed RT_A variant was divided by the number of cells used to make the lysate (see Materials and Methods for description). Data represent the results (mean ± SD) from three independent experiments.

3.4. RT_A-Expressing 4T1luc2 Cells Produce High Levels of Reactive Oxygen Species (ROS). Cancer cells produce elevated levels of ROS due to high metabolic activity; modified cellular signaling; peroxisomal activity; mitochondrial dysfunction; activation of oncogenes; increased enzymatic activity of oxidases, cyclooxygenases, lipoxygenases, and thymidine phosphorylases; and ROS-mediated signaling supporting cancer survival, angiogenesis, and progression [69]. Therefore, we expected the parental 4T1luc2 cells to release increased levels of ROS and inquired if expression of RT_A variants could additionally increase ROS production and if the levels of ROS depend on the dose and nature of the expressed RT variants.

Levels of ROS production in 4T1luc2 derivative clones were assessed with the help of the sensor fluorescent dye 2′,7′-dichlorodihydrofluoresceine diacetate (DCFH2-DA). DCFH2-DA reacts with various types of ROS yielding a fluorescent product which allows to assess the general redox status of cells [70]. Early after seeding, the parental 4T1luc2 cell line demonstrated increased total levels of ROS per cell compared to immortal murine cells (line NIH3T3; Figure 3(a)). Levels of ROS in cell lines expressing RT_A variants exceeded the level in the parental cell line by nearly 100% (Figure 3(a)). Treatment with tocopherol which prevents peroxide oxidation, or NAC which neutralizes free radicals, decreased the levels of ROS to the levels observed in the parental 4T1luc2 cells (Figure 3(a)). The effect of expression of RT_A variants on 4T1luc2 cells was comparable to that of oxidants H_2O_2 or tBHQ (Suppl. Fig. 4A). Interestingly, addition of H_2O_2 or tBHQ to RT_A-expressing 4T1luc2 cells

induced no further increase in ROS production, while antioxidant treatment reduced ROS production to basal levels (Suppl. Fig. 4A). After two weeks of culturing, all 4T1luc2 daughter clones reduced the levels of ROS production but still produced more ROS per cell than the immortal NIH3T3 cells (Figure 3(b)). Levels of ROS exhibited by RT-expressing clones tended to correlate with the level of RT expression per cell ($R = 0.53$; $p = 0.05$, Spearman ranking test). Thus, stable expression of RT_A variants led to an increase in ROS production over the already high levels characteristic to murine adenocarcinoma cells. Interestingly, during prolonged cell culture, some of the cell lines were able to quench it, at least partially (Figure 3(b)).

We wanted to see if longitudinal ROS production was related to the level of RT expression and/or to the nature of RT_A variant. For this, we normalized the levels of ROS in expressing cells after two weeks in culture to the average amount of RT_A variant per cell produced by this cell line (Figure 3(c)). We found that cells expressing nonmutated RT_A were able to significantly quench ROS production; quenching was less efficient in cells expressing RT_An and inefficient on cells expressing RT_Ann ($p < 0.05$; Figure 3(c)). High levels of ROS in a cell maintained over a long period of time were translated into increased levels of lipid peroxidation (expressed as relative levels of MDA per fg of RT; Figure 3(d)). Levels of MDA were highly correlated to the levels of ROS ($R = 0.83$; $p = 0.0008$). Production of MDA was reduced by treatment of cells with antioxidants (Suppl. Figure 4B). Thus, constitutive expression of RT_A variants caused an increase in the production of ROS over

(a)

(b)

(c)

Figure 3: Continued.

(d)
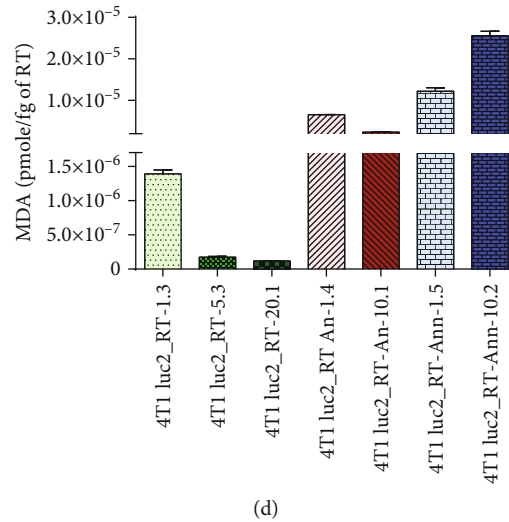
Figure 3: Derivatives of 4T1luc2 cells expressing variants of consensus HIV-1 FSU_A reverse transcriptase (Table 2) exhibit increased levels of ROS production (a–c) and lipid peroxidation (d). ROS production was measured using fluorescent dye DCFH2-DA and normalized to the signal generated by DAPI staining. Total levels of ROS per cell on day 6 of cell culture; production of ROS is quenched by treatment with antioxidants tocopherol ($1\,\mu$M) and NAC (5 mM); red asterisk indicates significant differences between 4T1luc2_RT-Ann-1.5 and other RT-expressing variants ($p < 0.05$) (a). Total levels of ROS production per cell on day 14 of cell culture relative to the levels exhibited by the parental 4T1luc2 cells (b). ROS levels on day 14 of cell culture normalized to the amount of RT_A variant (in fg) produced by one cell (c). Level of lipid peroxidation on day 14 of cell culture assessed as the concentration of MDA in the lysate of a single cell normalized to the amount of RT_A variant (in fg) produced by one cell (d). Values represent mean ± SD from two independent assays run in duplicates. ns: not significant; $^*p < 0.05$; $^{**}p < 0.01$; $^{***}p < 0.001$; $^{****}p < 0.0001$ (Kruskal-Wallis, followed by Mann-Whitney tests or ordinary one-way ANOVA followed by unpaired t-test).

the levels characteristic to the parental adenocarcinoma cells, resulting, on the long term, in increased levels of lipid peroxidation. Interestingly, however, this effect was minimal for cells expressing high levels of nonmutated RT_A (Figure 3(d)).

3.5. RT_A-Expressing 4T1luc2 Cells Exhibit High Motility in the Wound Healing Assay. Next, we assessed if expression of RT_A variants influences the motility of 4T1luc2 cells in the wound healing assay. All derivative clones had similar doubling time of 13 to 15 hours. Considering this, cells grown on plates were assessed for the capacity to heal the gap within 14 hours.

After the scratch (Suppl. Figure 5A-H, panels 1, 2), we observed a difference between the parental 4T1luc2 cell line and derivative clones in the closure of the wound during the first 14 hours (a tendency for 4T1luc2_RT-20.1, 4T1luc2_RT-An-1.4, and 4T1luc2_RT-An-10.1 and significant difference for 4T1luc2_RT-Ann-10.2; Figure 4(a); $p < 0.05$). Overall, the derivative clones healed larger areas than the parental 4T1luc2 clone, with a higher speed of wound healing (Figures 4(b) and 4(d)). We also tested if the derivative clones were capable of continued growth after passing the doubling time (with a short distance left to cover between the edges of the healing wound). For this, we measured wound healing 18 hours after the scratch (Suppl. Figure 5A-H; panels 1, 3). Interestingly, while the parental cell line and clones expressing nonmutated RT_A nearly stopped growing ($p > 0.05$ in all pairwise comparisons; RT_ 1.3, 5.3, and 20.1 behaved similarly to the parental 4T1luc2

cells; Figure 4(c)), cells of four clones expressing mutant RT_ As continued to move towards each other, albeit with a different speed (Figure 4(e)). We noticed that cells of these clones were moving both as a monolayer (epithelial phenotype) and as single cells (mesenchymal phenotype) (exemplified by Suppl. Figure 5H3).

Thus, the expression of RT_A variants led to an enhanced capacity of the derivative 4T1luc2 clones to heal the wound. The rates of cell migration during the first 14 hours after the scratch (Figure 4(d)) directly correlated to the total level of ROS produced per cell in longitudinal culture (Figure 3(b); $R = 0.775$, $p < 0.024$, Spearman test) but not to the level of RT expression.

3.6. RT_A-Expressing 4T1luc2 Cells Express Increased Levels of Factors Associated with the Epithelial Mesenchymal Transition (EMT). Acceleration of growth at the late stages of wound healing and appearance of "jumping" cells may indicate a change in the cell phenotype. This stimulated us to investigate the expression in these cells of the factors associated with epithelial/mesenchymal transition (EMT). Expression of the basic factors indicative of the epithelial or mesenchymal cell phenotype, *E-cadherin* as characteristic of the epithelial and *N-cadherin*, *Vimentin*, and transcription factors *Twist* and *Snail* as characteristic of the mesenchymal cell phenotype [71, 72], was assessed by the levels of respective mRNAs normalized to that in the parental 4T1luc2 cells. The assessment was done at days 3 and 14 of cell culture. All markers demonstrated stable levels of expression, except for *Vimentin*, expression of which significantly increased with
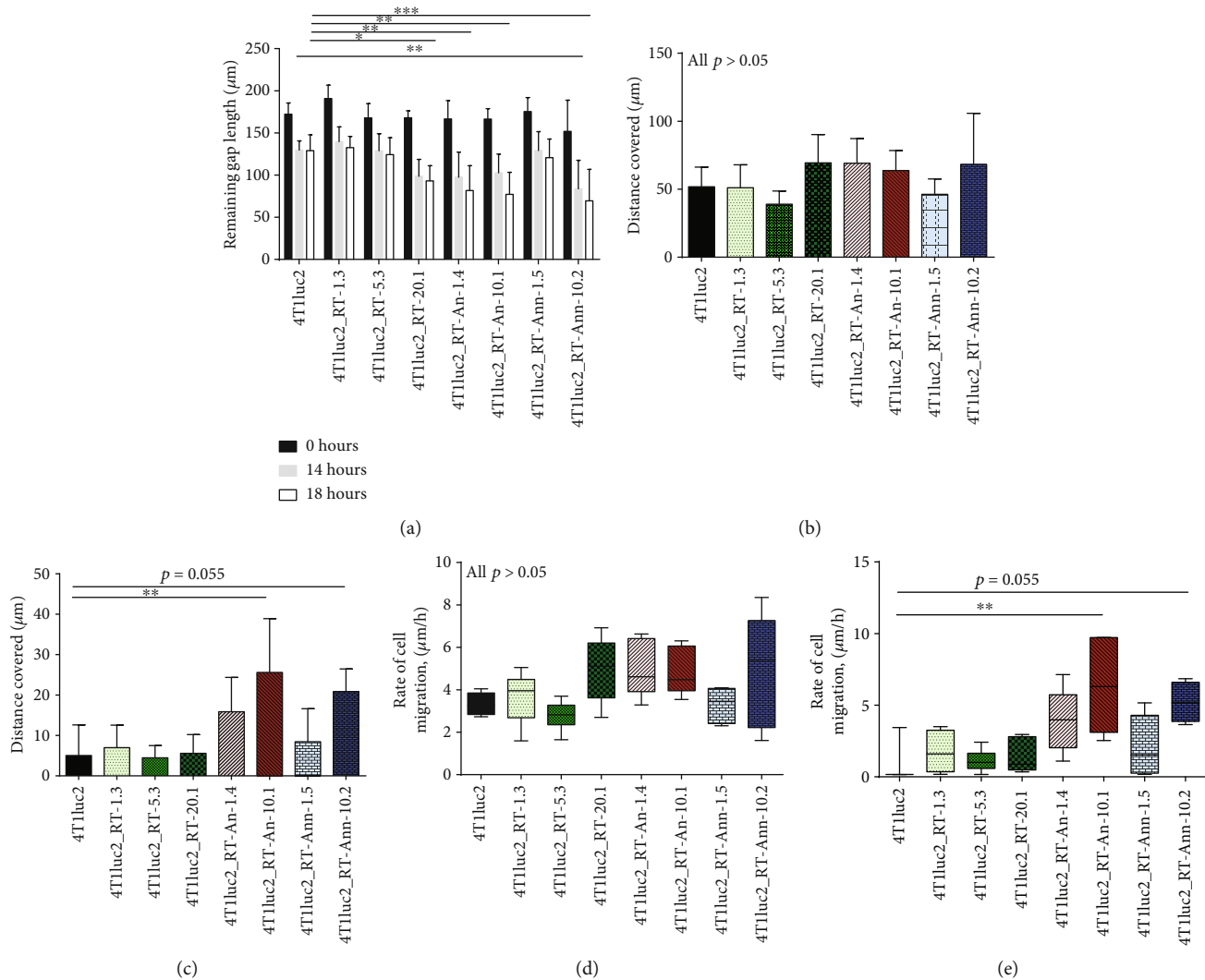
Figure 4: Performance of the derivatives of 4T1luc2 cells expressing variants of consensus HIV-1 FSU_A reverse transcriptase (Table 2) in the wound healing assay. (a) The length of the gap (wound) in μm, at the time of the scratch and 14 and 18 hours later. (b) Distance covered by the cells during the first 14 hours after the scratch, calculated as a difference in the length of the gap at the time of the scratch and after 14 hours. (c) Distance covered by the cells in the interval between 14 and 18 hours after the scratch. (d) Speed of cell migration during the first 14 hours after the scratch, calculated as the covered distance divided by 14 h. (e) Speed of cell migration in the interval between 14 and 18 hours after the scratch. The length of the gap (distance covered by the cells) was calculated based on the light microscopy images using ImageJ software. All values are expressed as mean ± SD from five independent experiment runs. ns: not significant; $^{*}p < 0.05$; $^{**}p < 0.01$; $^{***}p < 0.001$; $^{****}p < 0.0001$.

time in all cell lines ($p < 0.0001$). This demonstrated that in their phenotype all clones expressing RT_A variants were similar to the parental cells but during long culture (14 days equivalent to 24 doubling times) acquired more pronounced mesenchymal features (Figure 5, Suppl. Table 2).

We have further assessed if expression of EMT markers after 3 and 14 days in culture correlated with the levels of expression of RT_A variants (Suppl. Table 2). None of the parameters showed any correlation with the level of expression of RT_A variants (*E-cadherin*: $R = -0.3$, $p = 0.5$; *N-cadherin*: $R = 0.21$, $p = 0.7$; *Vimentin*: $R = 0.4$, $p = 0.4$; *Snail*: $R = 0.2$, $p = 0.7$, Spearman test), except for *Twist*; the latter reached high significance by day 14 ($R = 0.9$, $p = 0.002$) (Figure 6; Suppl. Figure 6). Levels of Twist expression on day 14 showed a weak tendency to correlate

to the levels of ROS ($R = 0.71$, $p = 0.13$; Spearman test). We confirmed ROS dependence of the upregulation of expression of *Twist* by treating cells with the antioxidant NAC. NAC treatment resulted in a complete disappearance of the correlation between the levels of RT expression and observed relative levels of *Twist* mRNA (Suppl. Fig. 6).

Twist expression correlated with the levels of expression of *Snail* ($R = 0.78$, $p = 0.02$) and *N-cadherin* ($R = 0.8$, $p = 0.016$) and tended to correlate with expression of *Vimentin* ($p = 0.11$) (all on day 14 of culture) (Suppl. Fig. 7). Importantly, early expression of *N-cadherin* and late expression on *Vimentin* highly correlated with the production of ROS ($p = 0.02$, Suppl. Figure 8). This pointed at the interconnection between oxidative stress and induction of factors associated with EMT: *N-cadherin*, *Vimentin*, and
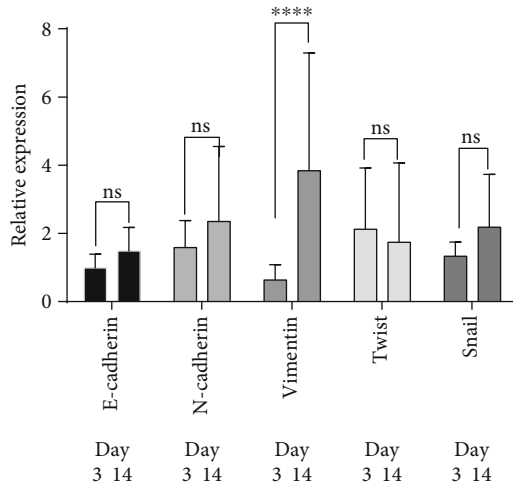
FIGURE 5: Relative expression levels of EMT markers in the derivatives of 4T1luc2 cells expressing variants of consensus HIV-1 FSU_A reverse transcriptase (Table 2) after 3 and 14 days in culture. Expression level was normalized to *HPRT1* expression and calculated as fold change compared to the parental 4T1luc2 line. Results are presented as mean ± SD from two independent assays run in duplicates. ns: not significant; ****$p < 0.0001$ by the ordinary two-way ANOVA.

Twist. Interestingly, relative levels of *Twist* expression on day 14 together with the levels of ROS and the level of RT expression reliably predicted the speed of migration of RT-expressing cells in the wound healing assay (multiple regression analysis, Suppl. Table 3). The dependence of the motility on the level of expression of RT was the least significant, but still important for the prediction. Thus, stable expression of RT_A variants led to a shift towards mesenchymal phenotype with enhanced expression of *Twist*, which governs the late stages of epithelial mesenchymal transition, which we have shown to depend on the production of ROS.

3.7. Tumorigenicity of 4T1luc2 Derivative Clones Expressing Variants of RT_A. Finally, we performed an *in vivo* study of tumorigenic and metastatic potential of RT_A-expressing clones by implanting them into the syngeneic BALB/c mice; parental 4T1luc2 cells served as control. All RT_A-expressing derivative clones formed solid tumors within 6 to 7 days after ectopic implantation. Starting from day 3 and up to the experimental endpoint, tumors formed by cells expressing nonmutated RT_A were significantly larger than tumors formed by the parental cell line, whereas tumors formed by 4T1luc2 cells expressing mutant RT_As did not differ in size from those formed by 4T1luc2 cells (Figures 7(a) and 7(e)). Furthermore, tumors exhibited different growth rates (Figures 7(b) and 7(c)). Clones expressing RT_A demonstrated higher *in vivo* growth at the exponential phase (Figures 7(c) and 7(d)) and also by the experimental endpoint (Figure 7(e)). The *in vivo* growth characteristics of 4T1luc2 clones expressing mutant RT_As did not differ from those of the parental cells (Figures 7(a)–7(f)).

The size of the tumors generated by a given clone, as assessed by an increase in the total photon flux from day 1 to day 18, strongly correlated with the *in vitro* properties of the inducing cell line, namely, the level of late expression of *Twist* in an *in vitro* assay and the level of RT expression (Figures 8(a) and 8(b); $R = 0.73$ and $R = 0.76$ correspondingly, both $p < 0.05$, Spearman test). Tumor volume in the morphometric assay (Figure 7(f)) tended to correlate with the late expression of *Twist* ($R = 0.74$, $p = 0.05$) and strongly correlated with the increase in expression of *Twist* between days 3 and 14 of an *in vitro* culture of the respective tumor-inducing cells ($R = 0.96$, $p = 0.0001$; Figure 8(c)).

At the experimental endpoint, tumors were excised, fixed, paraffin embedded, sectioned, H&E stained, and examined by an experienced oncopathologist. All tumors were high grade (G3) poorly differentiated adenocarcinomas with increased cellular and nuclear atypia, stromal desmoplasia, and frequent necrotic areas, multifocal for tumors formed by the parental and RT_A-expressing 4T1luc2 cells or central for tumors formed by 4T1luc2 cells expressing mutant RT_As (Figures 9(a)–9(h)). Analysis of DNA isolated from the sections confirmed presence of inserts corresponding to the coding sequences of RT_A variants.

3.8. Metastatic Potential of 4T1luc2 Derivative Clones Expressing Variants of RT_A. Next, we inquired if constitutive expression of HIV-1 RT variants could influence the metastatic activity of 4T1luc2 cells, in terms of the number of distant metastases and/or their organ distribution. We compared the metastatic activity of 4Tluc2 clones expressing RT_A with that of two clones expressing relatively high levels of mutant RT_A variants, 4T1luc2_RT-An-10.1 and 4T1luc2_RT-Ann-10.2. Organs (lungs, liver, and spleen) of mice bearing respective tumors were excised and immediately after assessed for the presence of luciferase-expressing cells by *ex vivo* bioluminescent imaging. Earlier, by injecting mice with known numbers of 4Tluc2 cells, we have established a direct correlation between the total photon flux from the injected tissue and the number of injected luciferase-expressing 4T1luc2 cells [73]. The total flux from the organs of mice bearing tumors expressing RT_A significantly exceeded the total flux from the organs of mice bearing tumors formed by the parental 4T1luc2 cells. This was especially pronounced for lungs and livers of mice implanted with cell lines expressing high levels of nonmutated RT_A (4Tluc2-RT-5.3 and 4Tluc2-RT-20.1; Figures 10(a) and 10(b)) indicating that these mice had significantly more luciferase-expressing cells in these organs than mice with tumors formed by the parental cell line.

This approach did not allow to establish the actual number of metastases, as they could have been formed by different numbers of cells (from as few as 3 to as many as 10000 [74]). To characterize the formation of metastases, we performed histochemical screening of the selected organs.

Earlier, we have shown that the expression of luciferase by 4T1 cells compromise the capacity of these cells to form metastases in distant organs, specifically in the liver [49]. Based on these observations, we have chosen to assess the actual number of metastases formed by the derivatives of

(a)

(b)
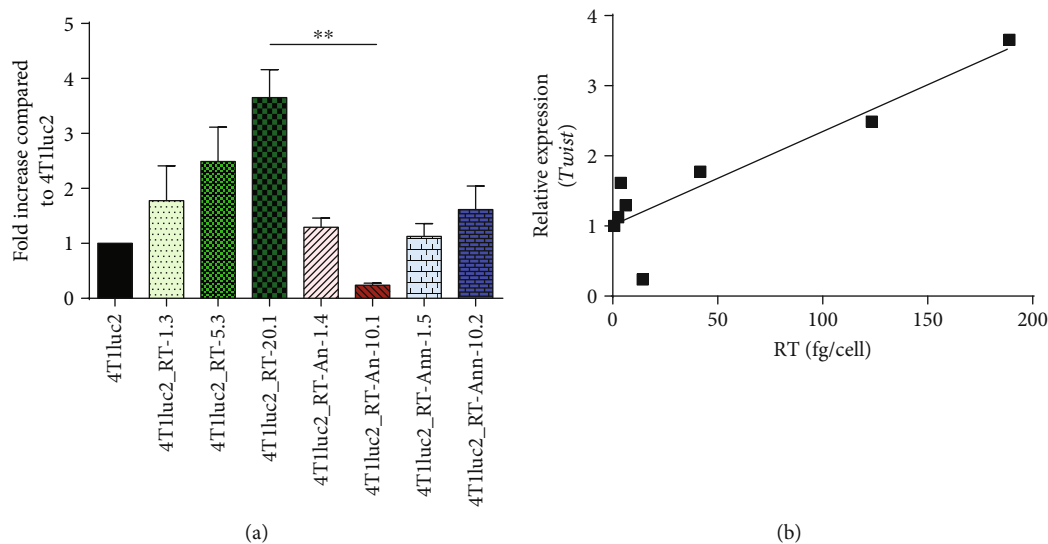
FIGURE 6: Relative levels of expression of *Twist* by the derivatives of 4T1luc2 cells expressing variants of consensus HIV-1 FSU_A reverse transcriptase (Table 2) after 14 days in culture (a) and correlation of the relative expression of *Twist* with the levels of expression of RT_A variants (b). Expression level of *Twist* was normalized to the expression of *HPRT1* and calculated as fold change compared to the levels exhibited by the parental 4T1luc2 cells. Values are presented as mean ± SD from the assay run in triplicates. The amount of RT_A variant produced per cell and expression of *Twist* at day 14 were correlated using Spearman ranking test ($R = 0.9$, $p = 0.002$); $^{**}p < 0.01$.

4Tluc2 cells in the liver as a sensitive indicator of possible deficiencies in the metastatic activity. The assessment of H&E-stained liver sections revealed that mice implanted with 4T1luc2 cells expressing RT_A had significantly more metastases in the liver than mice implanted with the parental 4Tluc2 cells or 4Tluc2 derivatives expressing mutant RT_As (Figures 11(a)–11(g)).

The metastases formed by 4T1luc2 expressing RT_A variants did not differ in size (Figure 11(h)); however, on the average, their size was larger than the size of metastasis formed by the parental 4T1luc2 cells (Figure 11(i)). The number of metastases formed by derivative 4Tluc2 clones tended to correlate with their capacity to express *Twist* (Figure 11(j); $R = 0.83$, $p = 0.06$) and RT_A protein (per cell) (Figure 11(k); $R = 0.9$, $p = 0.08$); statistical significance was not reached due to a small sample size. No correlations were observed between the number of metastases detected by the histochemical assay and any of the *in vitro* characteristics of the clones other than *Twist* (such as the levels of production of ROS, MDA, the parameters of the wound healing assay, or the expression of EMT factors; all $p > 0.1$). Thus, expression of HIV-1 RT, particularly of the nonmutated RT_A variant, led to an increase in the metastatic activity of 4T1luc2 cells expressing the respective RT_A variant, compared to the parental cells, with the increase proportional to the expression of RT and induction of expression of *Twist*.

3.9. Mice Bearing Tumors Formed by the Derivatives of 4T1luc2 Cells Expressing RT_A Exhibit Splenomegaly with Granulocyte Infiltration into the Spleen and No Cellular Response to a Mitogen. Initial examination revealed that all mice bearing 4Tluc2-derived tumors developed splenomegaly, especially pronounced in mice bearing tumors expressing RT_A (Figure 12(a); normal spleen weight in healthy naïve 12-week BALB/c mice is 80 ± 10 mg). The weight of the

spleen increased proportionally to the level of RT_A expression by the clone (not significant due to a small number of observations).

Further, we prepared single splenocyte cultures and assessed the proportion of leukocyte subpopulations in the spleens by flow cytometry. Analysis revealed a reduced number of lymphocytes and gross overrepresentation of granulocytes (Figure 12(b)), supporting the earlier findings in mice bearing 4T1 tumors [75, 76]. Due to this disproportion, splenocyte cell cultures of mice bearing RT_A-expressing tumors exhibited low proliferative response to the mitogen Concanavalin A (ConA) (given as number of IFN-γ-producing cells per 10^6 splenocytes): 100 ± 50 for subclones expressing nonmutated and 1100 ± 600 for subclones expressing mutated RT_As. In mice implanted with 4T1luc2, the number of IFN-γ-producing cells per 10^6 splenocytes was 400 ± 200, and in healthy mice of similar age, over 3000 IFN-γ-producing cells per 10^6 splenocytes. We have also stimulated splenocytes with a peptide, which we have earlier shown to contain a cluster of CD4$^+$ and CD8$^+$ T cell epitopes of RT [52, 77], to see if any of them formed an immune response against RT_A as a foreign antigen. No responses were detected in any of the groups (less than 50 IFN-γ-producing cells per 10^6 splenocytes). Thus, expression of HIV-1 RT by 4T1luc2 tumors induced a systemic pathological effect manifested by splenomegaly, disproportion of leukocyte populations in the murine spleen, and anergy, which was more pronounced in mice implanted with RT_A-expressing 4T1luc2 than in those implanted with the parental 4Tluc2 cells.

4. Discussion

Our first findings of enhanced ROS production by eukaryotic cells expressing RT of HIV-1 were made for RT of an HIV-1 clade B HXB2 strain [26, 27]. Here, we inquired if this is a

(a)

(b)

(c)

(d)

(e)

(f)
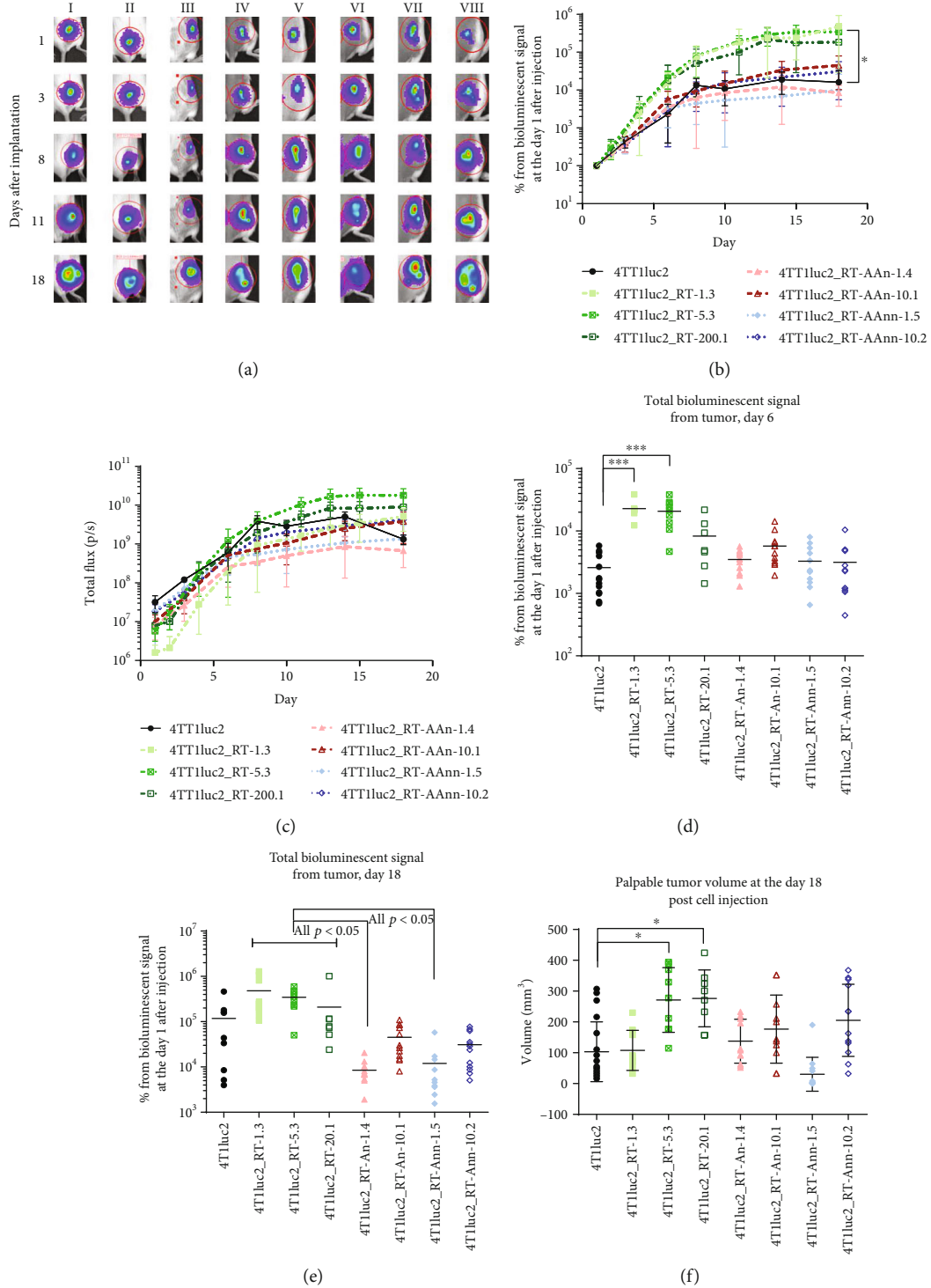
Figure 7: Formation of solid tumors by the derivative clones of 4T1luc2 expressing variants of HIV-1 FSU_A reverse transcriptase (RT_A) after ectopic implantation into BALB/c mice. *In vivo* bioluminescent images showing growth of representative tumors formed by clones 4T1luc2_RT-1.3 (I), 4T1luc2_RT-5.3 (II), 4T1luc2_RT-20.1 (III), 4T1luc2_RT-An-1.4 (IV), 4T1luc2_RT-An-10.1 (V), 4T1luc2_RT-Ann-1.5 (VI), 4T1luc2_RT-Ann-10.2 (VII), and parental cells 4T1luc2 (VIII); red circles show the regions of interest (ROI) from which the total luminescent signal was collected (a). Growth of tumors assessed as the average total photon flux from the sites of injection encircled by ROI (b), the average percent change in the total photon flux compared to the photon flux from the site obtained on day 1 (c), the total photon flux from each of the injections sites on days 6 (d) and 18 (e) as percent of that on day 1, and palpable tumor size at the experimental endpoint (f). All group values represent the mean ± SD. After day 3, 4T1luc2_RT-1.3 and 4T1luc2_RT-5.3 derivative clones demonstrated significantly higher total photon flux, and 4T1luc2_RT-20.1 tended to have higher photon flux ($p = 0.1$) than the parental 4T1luc2 cells. $^*p < 0.05$, $^{**}p < 0.005$, $^{***}p < 0.0005$, and $^{****}p < 0.0001$, Kruskal-Wallis, followed by Mann-Whitney tests.

(a)

(b)

(c)
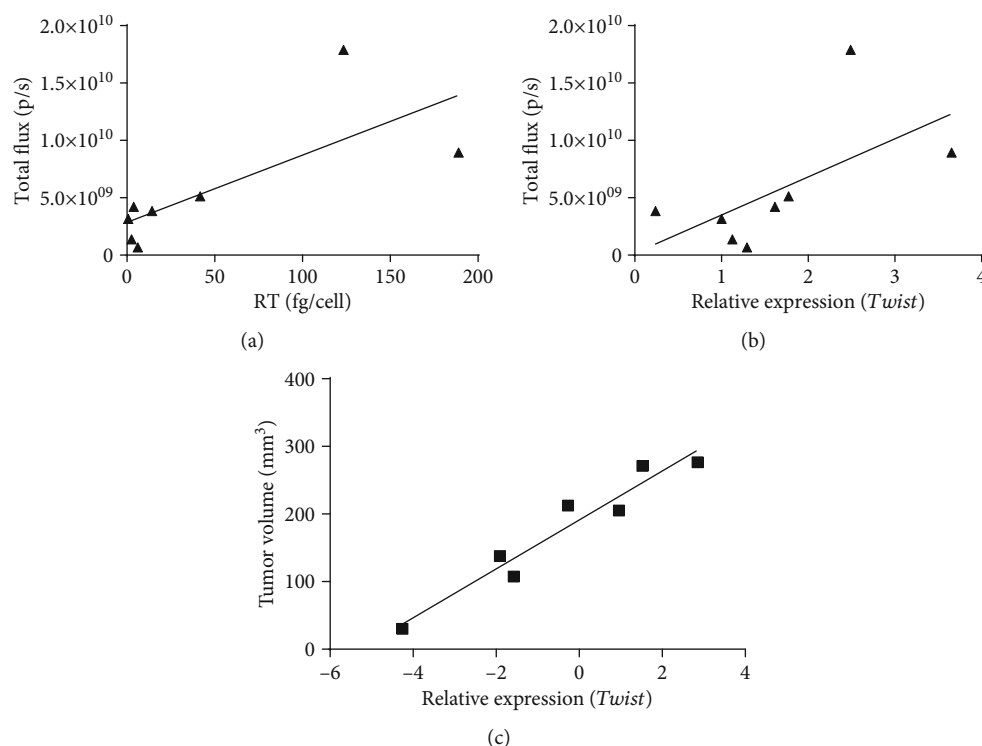
FIGURE 8: Correlations (Spearman correlation test) between the tumor sizes represented by the total photon flux from tumor on day 18 and the levels of expression of RT_A variant per cell ($R = 0.76$, $p < 0.05$) (a); the levels of expression of Twist (normalized against the expression of HPRT1 and represented as fold increase compared to that of the parental 4T1luc2 cells) ($R = 0.74$, $p < 0.05$) (b); and palpable tumor volume on day 18 and change in the levels of expression of Twist from day 3 to day 14 in % ($R = 0.96$, $p = 0.0001$) (c).

general property of HIV-1 reverse transcriptases and if this property is linked to the enzymatic activity of the protein. We designed the consensus RT of HIV-1 clade A FSU_A strain (RT_A) and two RT_A variants with primary mutations of resistance to NRTI (K65R and M184V; RT_An) and NNRTI (K103N and G190S; RT_Ann) [60, 78]. NRTI resistance mutations reduce the efficacy of tRNA-primed (-)ssDNA synthesis resulting in a diminished enzyme processivity [36, 79]. NNRTI resistance mutations affect RNase H activity and DNA synthesis from tRNALys [61, 80]. By introducing these mutations, we expected to generate RT_A variants with reduced respective activities to further test how this would affect the capacity of the enzyme to induce ROS. As expected, the consensus RT_A was enzymatically active, RT-An (K65R/M184 V) was compromised in the polymerase, and RT_Ann (K103N/G190S), in the RNase H activities.

We started with the study of the effects of these RTs on an epithelial cell line. Epithelial cells appear to be grossly affected by HIV-1. Deposition of HIV-1 in the intact oropharyngeal [81], anal/rectal [82], cervicovaginal and foreskin/penile [81, 83–85], airway [86], and gastric epithelial cells [87] promotes systemic infection of CD4$^+$ T lymphocytes, Langerhans/dendritic cells, and macrophages both *in vivo* and *ex vivo* [83, 84, 88–92]. This "contamination" creates proinflammatory environment characterized by the production of inflammatory mediators such as IL-6 and TNF-α and

impairment of cell adhesion [86, 87, 90, 93]. With this in mind, we selected a cell line of epithelial origin, namely, murine mammary gland adenocarcinoma 4T1 cells syngeneic to BALB/c mice, to further evaluate the effect of RT expression on the properties of these cells *in vitro* (induction of ROS, cell phenotype, and motility) and *in vivo* (tumor growth and metastasis formation).

All variants of RT_A induced production of ROS over the already high levels exhibited by the parental 4T1luc2 cells. This supported our earlier findings for clade B RT, as ROS were induced by a panel of RT_Bs including multidrug-resistant and inactivated variants [26, 27]. The effect was long lasting in cell lines expressing low levels of RT_An and RT_Ann and subsided with time in cells overexpressing RT_A (see clones 4T1luc2_RT-5.3 and 4T1luc2_RT-20.1; Figure 3). High levels of ROS persisting over a long period of time were translated into increased levels of lipid peroxidation. Cells expressing nonmutated RT_A were able to diminish ("quench") ROS production and prevent lipid peroxidation. "Quenching" was inefficient in cells expressing mutated RT_A variants with compromised enzymatic activities.

ROS orchestrated cell migration. The rates of cell migration directly correlated with the normalized levels of ROS produced in a prolonged cell culture (day 13; $R = 0.9048$, $p < 0.01$, Spearman test). Further, we observed a change in the pattern of cell migration in the wound healing
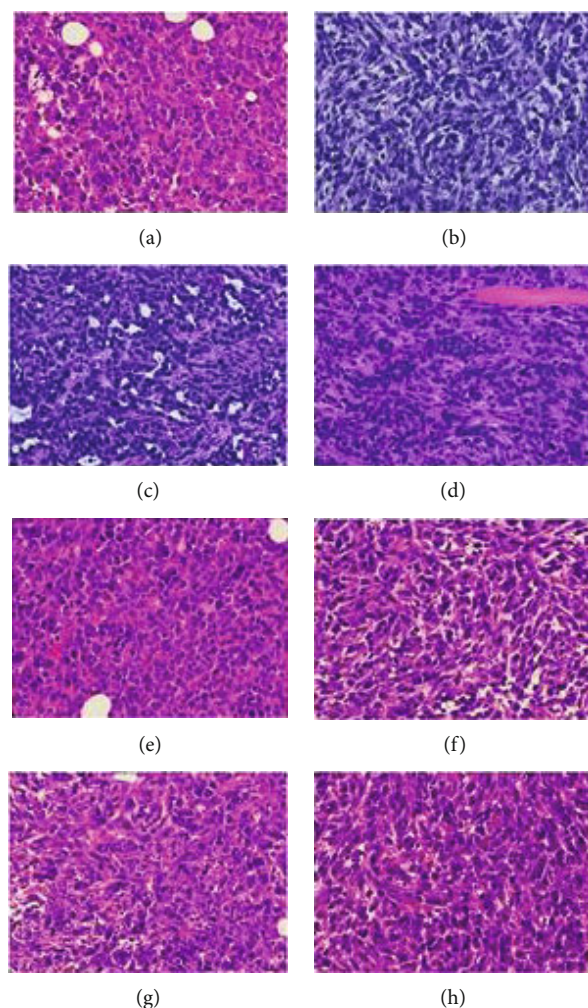
Figure 9: Histochemical characterization of the solid tumors formed by the parental 4T1luc2 cells (a) and their derivatives expressing variants of HIV-1 FSU_A reverse transcriptase (RT_A) after ectopic implantation into BALB/c mice: 4T1luc2_RT-1.3 (b), 4T1luc2_RT-5.3 (c), 4T1luc2_RT-20.1 (d), 4T1luc2_RT-An-1.4 (e), 4T1luc2_RT-An-10.1 (f); 4T1luc2_RT-Ann-1.5 (g), 4T1luc2_RT-Ann-10.2 (h). H&E staining: magnification ×400.

assay, namely, clones expressing mutated "nonquenching" RT variants demonstrated steady growth with little or no contact inhibition even when cells were in close proximity (after 14 hours of culture). Cell motility could have been accelerated by ROS or ROS-induced soluble mediators released by cells residing at the edges of the wound. Indeed, it has been shown that ROS production elicits rapid ion fluxes to the cytosol and triggers the response in the adjacent cells opening them to a slow entry of extracellular ROS through aquaporins. This terminates ROS signaling in the current cell and amplifies it in the neighboring cells [94, 95]. One such soluble mediator could be H_2O_2 with the life of 1 ms which can cover the distances of hundreds of micrometers [96]. In support of this assumption, H_2O_2 at low levels is known to promote adhesion, migration, and wound healing in epithelial cells [97].

ROS play essential role in the EMT process in cancer cells by regulating extracellular matrix remodeling, cytoskeleton remodeling, cell-cell junctions, and cell mobility [98, 99]. Recent study has shown that ROS induce EMT by activating

Snail expression, which then represses the expression of E-cadherin, a classical marker of the epithelial phenotype [100]. Several independent studies demonstrated that EMT can be induced by direct contact of epithelial cells with HIV proteins [24, 86, 101, 102]. To see if this is the case for 4T1luc2 cells expressing RT, we monitored them for the expression of *E-cadherin*, mesenchymal cell phenotype markers *N-cadherin* and *Vimentin*, and of two transcription factors, heavily involved in EMT, *Twist* and *Snail* [71, 98]. We compared the relative levels of expression of these EMT markers and checked if their expression was correlated with the expression of RT_A variants. Analysis revealed that at the late stages of cell culture (14 days or >20 doubling times) cell lines characterized by high levels of RT expression had proportionally increased expression of *Twist*. This was a fascinating finding considering the results of a recent study demonstrating functional linkage between *Twist* factors and ROS [103]. Based on this study, one can assume that in 4T1luc2 cells stably expressing HIV-1 RT, RT induces the production of ROS, which in its turn, directly or through

(a)

(b)

(c)
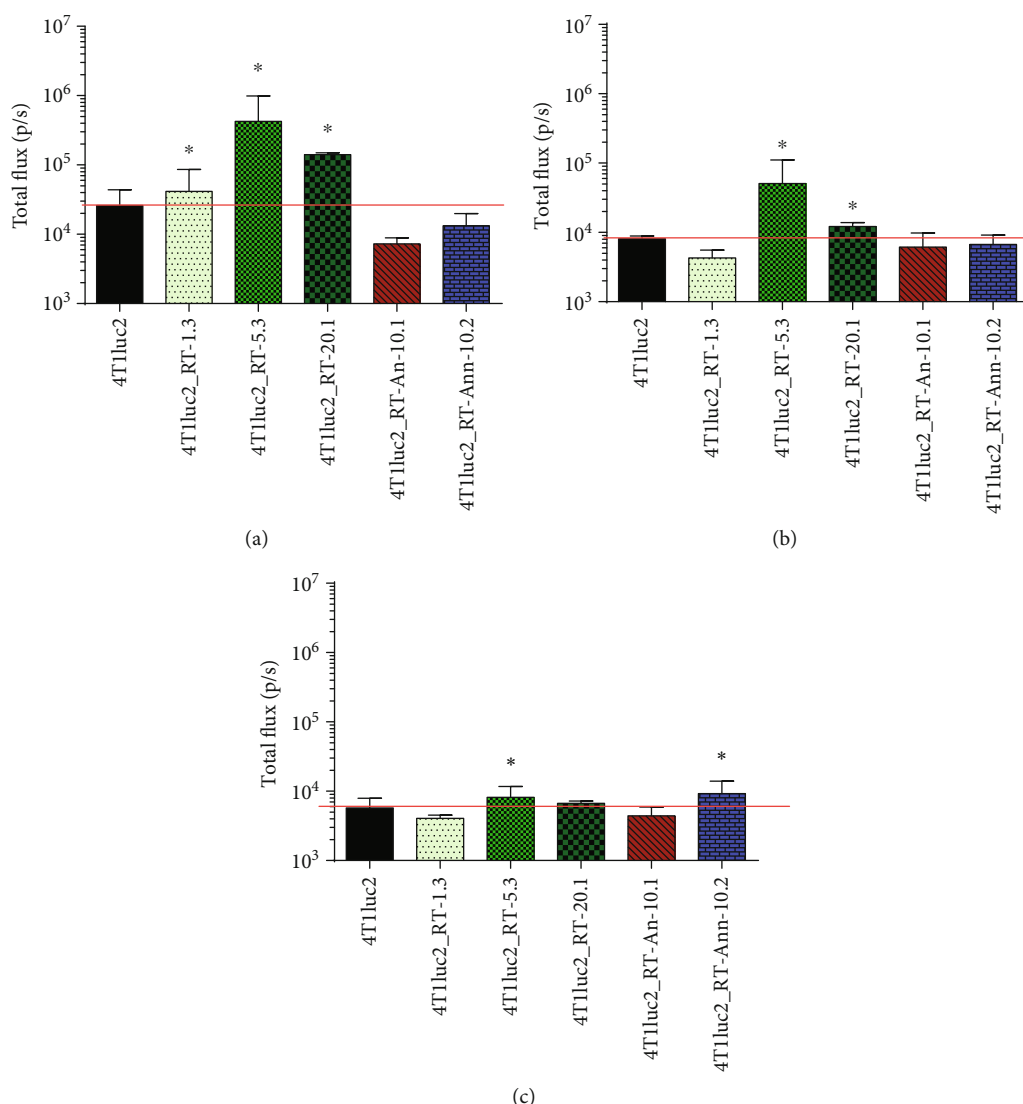
FIGURE 10: Localization of luciferase-expressing cells in the organs of mice implanted with 4Tluc2 and derivative clones expressing variants of HIV-1 FSU_A reverse transcriptase (RT_A) after ectopic implantation into BALB/c mice as assessed by *ex vivo* bioluminescent imaging of the lungs (a), liver (b), and spleen (c). The values represent the mean total flux (p/s) ± SD ($n = 3$). *Significant difference from the value exhibited by the respective organ in 4Tluc2-implanted mice ($p < 0.05$; Mann-Whitney test).

mediators, upregulates the expression of *Twist* switching on the antioxidant activities of the latter. This would explain the low normalized levels of ROS (per fg of RT per cell) in 4T1luc2 daughter clones expressing high levels of nonmutated RT_A and high levels of *Twist* as a result of a "positive feedback loop": overexpressed RT_A induces high total levels of ROS production and activates Twist, which, in its turn, suppresses the production of ROS. This would explain highly significant dependence of *Twist* expression on the level of RT expression, but not on the levels of ROS.

Twist occupies a key position in the EMT cascade in tumor cells, regulating the expression of a large number of genes, including *Nrf-2* [104] and *Snail* [105]. The RT/ROS-dependent induction of *Twist* described here gives additional mechanistic explanation to our earlier findings of the RT-induced upregulation of expression of Nrf-2 [26] and of *Snail* observed in this study. Overexpression of *Twist* may promote

the migration of 4T1luc2 cells, as it has been previously shown, specifically in cancer cells [106, 107]. Indeed, we were able to reliably predict the motility of RT_A-expressing 4Tl cells using three parameters: the level of RT expression, expression of *Twist* on day 14, and relative levels of ROS production.

Finally, we undertook the *in vivo* study of tumorigenic and metastatic potential of RT-expressing cells compared to the parental 4T1luc2 cell line. All RT-expressing clones formed solid tumors and metastases in multiple organs. The tumors formed by 4T1luc2 clones expressing nonmutated RT_A were significantly larger than tumors formed by the parental cells or cells expressing mutant RT_A variants. Tumor size correlated with late expression of *Twist* in the *in vitro* tests and could be predicted based on the properties of implanted cells, such as the level of expression of RT and relative expression of *Twist*.

(a)

(b)

(c)

(d)

(e)

(f)

(g)

(h)
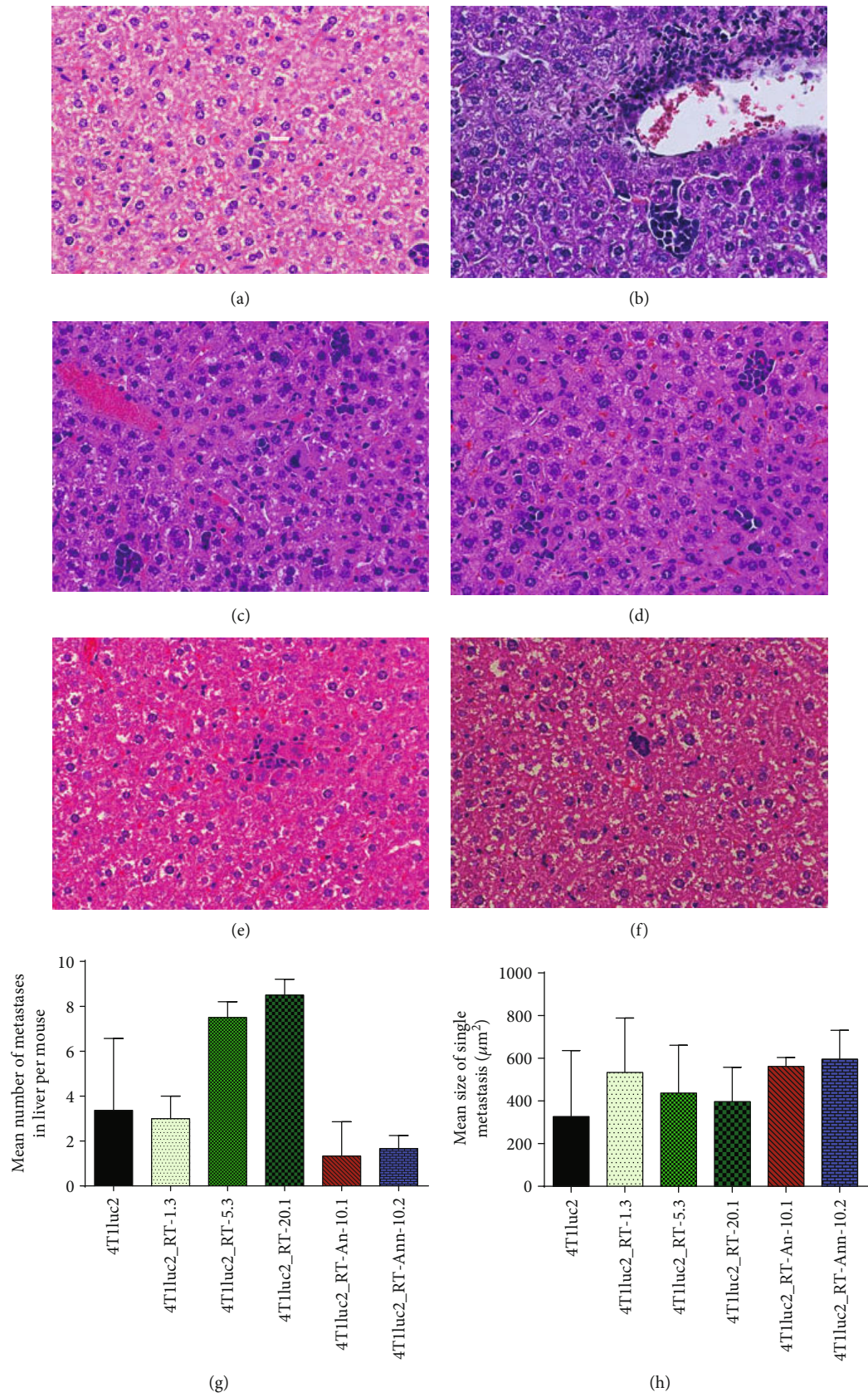
Figure 11: Continued.

(i)

(j)

(k)
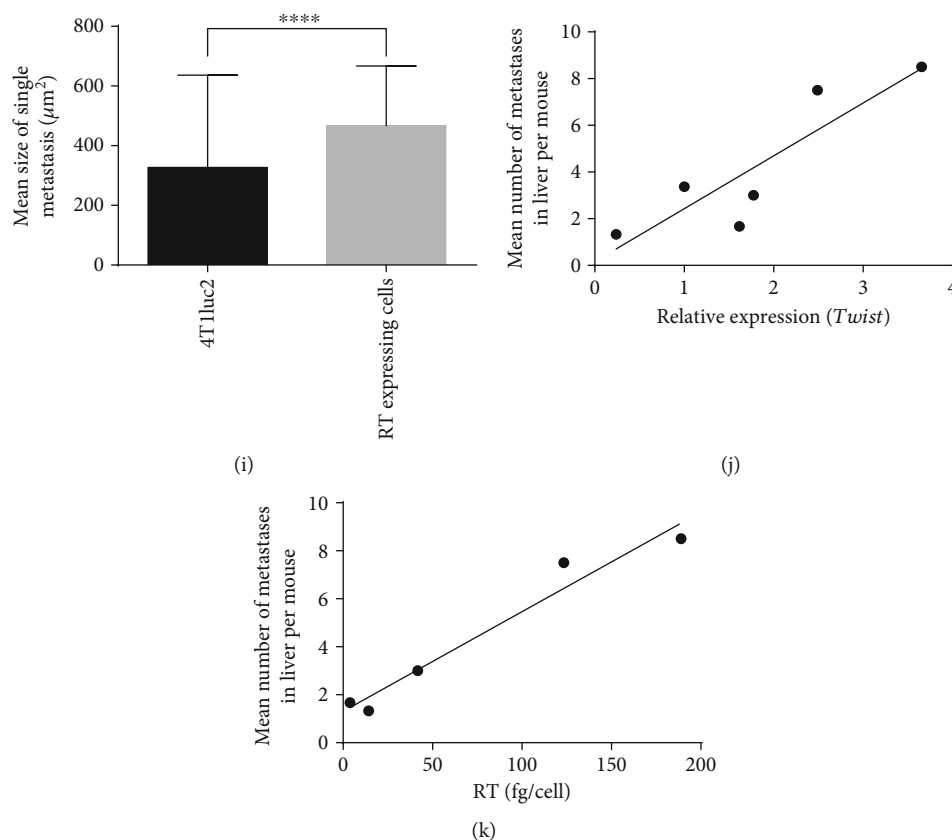
FIGURE 11: Histochemical characterization of the formation of metastases in the livers of BALB/c mice ectopically implanted with 4Tluc2 and derivative clones expressing variants of HIV-1 FSU_A reverse transcriptase (RT_A). H&E staining of liver sections of mice injected with 4T1luc2 and its RT-expressing subclones (×400): 4T1luc2 (a), 4T1luc2_RT-1.3 (b), 4T1luc2_RT-5.3 (c), 4T1luc2_RT-20.1 (d), 4T1luc2_RT-An-10.1 (e), 4T1luc2_RT-Ann-10.2 (f). Mean number (g) and size (h) of metastases. Mean size of liver metastasis formed by all RT_A-expressing clones compared to the parental 4Tluc2 cells (i). Correlations between the mean numbers of metastases in a mouse liver assessed by histochemical staining and the levels of expression by the respective 4T1luc2 clone of Twist (day 14 of cell culture) (j) and of RT_A variant per cell (k). Ten high-power fields per mouse ($n = 3$) were screened to assess the number of metastasis; their size was evaluated using NIS-Elements software (Nikon, Tokyo, Japan), both values were represented as mean ± SD. Expression level of Twist was normalized to the expression level of HPRT1 and represented as fold change compared to the level in the parental 4T1luc2 cells. Comparisons were done using the Mann-Whitney test, and correlations, using the Spearman correlation test. $^{*}p < 0.05$, $^{**}p < 0.005$, $^{***}p < 0.0005$, and $^{****}p < 0.0001$.

Mice harboring RT_A-expressing tumors had pronounced splenomegaly marked by infiltration of granulocytes, characteristic to the 4T1 tumor model [76]. Recent studies reported the accumulation in the tumor-bearing animals, most notably in the spleen, of immature myeloid-derived suppressor cells, neutrophils, and granulocyte-macrophage progenitor-derived splenic monocytes ($CD11b^{+}Gr-1^{+}$). These overlapping cell populations express immunosuppressive enzymes such as arginase 1 and inducible nitric oxide synthase (NOS2), produce ROS, suppress antitumor T cell activity in vivo, and inhibit T cell proliferation/IFN-γ production in coculture experiments [108]. These observations support our findings of the suppressed response of splenocytes of tumor-bearing mice to a mitogen as well as the absence of immune recognition of RT_A as foreign protein. Another nonexcluding explanation of these findings would be the properties of 4T1 cells, which release soluble mediators (detectable in conditioned media of cultured cells)

inhibiting INF-γ production, which could also occur in the murine spleens infiltrated by the metastatic cells [109].

As the result, mice bearing 4T1luc2 tumors expressing nonmutated RT_A demonstrated complete loss of immune control of tumor growth (which may have otherwise led to the rejection of tumors [110]) and wide dissemination of metastatic luciferase-expressing cells in multiple organs, compared to that in mice bearing tumors formed by the parental 4T1luc2 cells [110]. Interestingly, mice with 4T1luc2 tumors expressing nonmutated RT_A had significantly more Luc-expressing cells in the lungs, spleen, and liver than mice implanted with cells expressing mutant RT_As. Thus, the expression of RT_A, but not of the mutated RT_A variants, "rescued" the metastatic potential of 4T1luc2 cells. This data was confirmed by the histochemical evaluation of the number of metastasis in the liver. The number of metastatic cells detected in the livers of mice bearing tumors formed by RT_A-expressing 4T1luc2 cells was

(a)

(b)
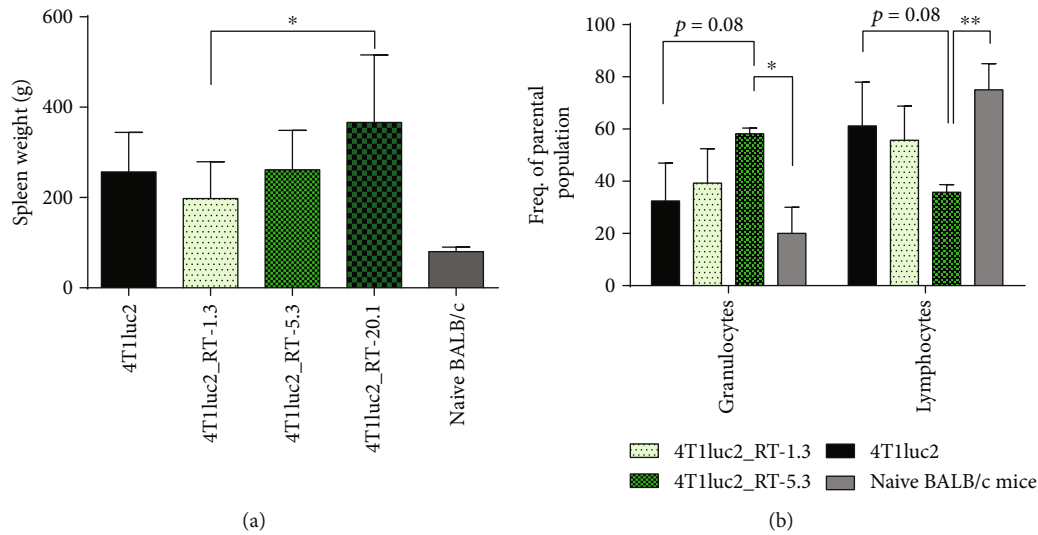
FIGURE 12: BALB/c mice ectopically implanted with 4Tluc2 and derivative clones expressing HIV-1 FSU_A reverse transcriptase (RT_A) have grossly enlarged spleens (a) and a disproportion in the leukocyte subpopulations in the spleen (b). Spleen weight, in mg (a) and proportion of leukocytes in the spleen (b) of BALB/C implanted with given 4T1luc2 derivative clones ($n = 3$-9) was assessed at the experimental end-point, and represent mean ± SD. Data from naïve BALB/c mice ($n = 3$-5) is given for comparison. $^*p < 0.05$; $^{**}p < 0.005$ (two-way ANOVA test).

significantly higher than that in mice implanted with tumor cells expressing mutated RT_As or the parental cells. The number of metastasis significantly correlated to the propensity of the inducing cells to express *Twist* in the *in vitro* assay. No correlations were observed of the number of metastatic cells (by BLI or by histology) with any other cell line parameter of the ones assessed in this study. Earlier, we had observed that 4Tluc2 cell line is impaired in the capacity to form metastases in organs and tissues other than the lungs (such as liver, brain, or bones); we attributed this property to the induction of immune response against luciferase which can clear metastatic cells expressing the reporter [49]. Here, we demonstrate that expression of nonmutated RT_A (but not of RT_An or RT_Ann) restores the metastatic potential of 4T1luc2 cells to the level of the initial 4T1 adenocarcinoma cells, possibly by increasing the level of immune suppression.

Altogether, our data on ROS induction, lipid peroxidation, cell motility, upregulation of transcription of EMT factors, specifically of *Twist*, tumor growth, and metastatic potential of 4T1luc2 cells expressing HIV-1 RT indicate that RT_A variants had differential effects on the expressing cells. Although mutated RT_A variants induced the production of ROS, they seemed to be compromised in other properties associated with malignancy, starting from inability to efficiently induce the expression of *Twist*. Thus, the *in vitro* and *in vivo* properties of RT_A-expressing cell lines were not clustered according to the upkeep of their individual enzymatic activities, either polymerase (RT_A and RT_Ann have intact polymerase activity) or RNase H (RT_A and RT_An have intact RNase H activity). In contrast, according to their properties, RT_A-expressing 4T1luc2 variants could be clustered into highly malignant clones overexpressing nonmutated RT_A and clones expressing low levels of RT_An and RT_Ann, nondistinguishable from the parental cells. In this context, it is important to mention that drug resis-

tance mutations in RT target it to processing by the proteasome [41]. Mutations may be important not because of their effect on the enzymatic activity of the protein but as determinants of protein availability, localization, and intracellular partnerships.

Which properties of HIV-1 RT are responsible for the induction of ROS, if not the enzymatic activities, remains unknown. A review done by Warren et al. described cellular interactions of HIV-1 RT, listing factors which directly or indirectly bind to RT and regulate the reverse transcription [111]. The spectrum of RT partners included APOBEC3G, DNA Topoisomerase I, components of the Sin3a complex, GErmin2, a number of IN-binding proteins including IN1. Two of these partners are of specific interest: HuR (also referred to as ELAVL1, HuA, or MelG) and the kinase anchor protein 121 (also referred to as AKAP1 or AKAP149 as human homologue). HuR is an ubiquitously expressed 326 amino acid protein with nucleocytoplasmic shuttling capabilities. Overexpression of HuR in cancer cells has been associated with poor prognosis and resistance to therapy. Absence of HuR is signified by the defective mitochondrial metabolism resulting in production of the large amounts of ROS and increased DNA damage [112, 113]. AKAP121 is an essential regulator of the mitochondrial respiration. Displacement of AKAP121 with an inactive analog results in the mitochondrial dysfunction manifested by the increased production of ROS [114]. Both HuR and AKAP121 are involved in the mitochondrial metabolism, their interaction with HIV-1 RT may imply their mitochondrial colocalization. Interestingly, regions of RT interacting with HuR and AKAP1 were both mapped to the RNase H domain of RT [115]. We find it reasonable to hypothesize that increased levels of ROS production observed in several RT-expressing eukaryotic cell lines tested by us previously and in RT-expressing 4T1luc2 cells tested here might be a consequence

of direct interaction of HIV RT with HuR and/or AKAP121, which disturb their functions. Interference of RTs with HuR and/or AKAP121 functions would induce the production of ROS, which in its turn, would activate *Twist*, and start the cascade of EMT-related events, resulting in the enhancement of oncogenic and metastatic potential of RT-expressing tumor cells.

As we have shown earlier, drug-resistant HIV-1 RTs are proteolytically unstable with degradation governed by the proteasome. The half-life of the protein decreases from approximately 20 h for the wild-type RT to <2 hours for the multidrug-resistant enzyme forms [40, 41]. Both HuR [116] and AKAP1 [117] are degraded by the proteasome. One can speculate that binding of HuR and/or AKA121 to the mutated RT variants can target them to an enhanced proteasomal degradation. This way to deplete the pool of regulatory proteins is widely used by tumorigenic viruses, for example, E6 protein of HPV [118] or LT antigen of SV40 [119]. Reduced intracellular levels of HuR and/or AKA121 in 4Tluc2 cells expressing mutated RT_A variants would lead to overproduction of ROS beyond the levels controlled by Twist. Another explanation of overproduction of ROS in cells expressing mutant RT_As would be their aberrant capacity to induce Twist, which implies direct (not purely ROS mediated) involvement of HIV-1 RT in the regulation of Twist expression. The actual mechanism of the RT-induced production of ROS with possible involvement of HuR, AKAP 1, and/or other protein partners remains to be investigated.

In conclusion, the capacity to induce ROS appears to be a general property of HIV-1 reverse transcriptase; however, only the wild-type enzyme can efficiently induce activation of *Twist* to hamper oxidative stress. This property is responsible for the enhancement of tumorigenic and metastatic potential of RT-expressing cells. Our study casts light on one of the mechanisms of the direct potentiation of tumorigenesis by HIV resulting from the prooxidative activity of HIV-1 proteins. RT-mediated induction of ROS is of great interest also in the context of HIV-1 infection, as ROS are known to promote HIV-1 replication [120].

Data Availability

All data used to support the findings of this study are included within the article and the supplementary information file(s). Data not shown in the article used to support the findings of this study are available from the corresponding authors upon request.

Conflicts of Interest

The authors declare no conflict of interests.

Acknowledgments

Supplementary Materials

Supplementary Table 1: table of primers. Primers used for confirmation of RT expression in 4T1luc2 derivatives and for relative quantification of epithelial to mesenchymal transition markers. Supplementary Table 2: table of semiquantitative PCR values. Relative expression levels of EMT markers in 4T1luc2 subclones expressing RT. Raw data used for correlation analysis and analysis of antioxidant treatment effect. Supplementary Table 3: table of statistical characteristics of multiple regression analysis of in vitro migration rate in wound healing assay. Statistical model of prediction of 4T1luc2 subclone migration in vitro in wound healing assay during 14 hours after the scratch was made based on different parameters, such as RT protein level, relative level of Twist expression, and migration in wound healing test during 14-18 hours after the scratch was made. Prediction was made by multiple regression analysis. Supplementary Figure 1: geographic and temporal distribution of RT amino acid sequences. Geographic origins and year of sample collection of the full-length sequences of reverse transcriptase (RT) of HIV-1 subtype A FSU_A strain used for the design of the amino acid consensus AFSUp66 ($n = 44$). Sequences were isolated from treatment-naïve patients free of known drug resistance mutations selected from HIV-1 sequence database and HIV Drug Resistance database. Supplementary Figure 2: schematic representation of lentiviral vector pRRLSIN.cPPT.PGK used for transduction of 4T1luc2 cell line with the polynucleotide sequences encoding the consensus RT_A with or without drug resistance mutations. Lentiviral transduction resulted in seven 4T1luc2 derivative clones expressing different levels of three RT variants. Supplementary Figure 3: RNase H activity of consensus RT_A variants with and without drug resistance mutations. Graphs demonstrate RNase activity of RT_A variants, firstly as products of RNase H cleavage of the substrate after analysis by PAGE and secondly concentration dependence of RNase H activity of the variants of consensus RT of clade A FSU_A strain with and without drug resistance mutations. The respective kinetic parameters are described in the main text. Supplementary Figure 4: graphs comparing the levels of ROS in 4T1luc2 cells expressing RT_A, parental 4T1luc2 cells, and immortal NIH3T3 cell line. Increased level of produced ROS by 4T1luc2 derivative clones expressing RT compared to the parental cells, measured as an increase of relative intensity of DCFH2-DA/DAPI fluorescent signal. Cells treated with H_2O_2 or *tert*-butylhydroquinone (tBHQ) were used as positive control, and cells treated with antioxidants tocopherol and N-acetyl-L-cysteine (NAC) as negative control. Increased level of ROS production in the parental 4T1luc2 resulted in increased basal level of lipid peroxidation, measured by MDA level in cell lysates, as compared to the immortal NIH3T3 cell line known to produce low

levels of ROS. Supplementary Figure 5: wound healing assay. Panels represent light microscopy images of the gap area at 0, 14, and 18 hours after making the scratch. Timeline was settled to measure the migration rate before and after doubling time (approx. 14 hours). Original .tif files of high resolution are available at the following link https://drive.google.com/drive/folders/1a4VbLzFYeny9LDf5iTxyhSmSanIesLl1?usp=sharing. Supplementary Figure 6: graphs showing that expression of Twist on day 14, but not on day 3 of cell culture, correlates to the level of expression of RT. Treatment of cells with antioxidant N-acetyl-L-cysteine (NAC) leads to the loss of correlation between expression of RT and Twist on day 14, demonstrating that induction of expression of Twist depends on the production of ROS. Graphs are supplemented with r, r^2, and p values of the Spearman correlation test. Supplementary Figure 7: graphs showing correlation between the levels of expression of Twist and other EMT markers. On day 14 of cell culture, level of expression of Twist correlated with the levels of expression of EMT markers N-cadherin, Vimentin, and Snail, but not with the expression of E-cadherin. Textbox in the figure shows correlation values (r, r^2, and p) measured by the Spearman correlation test. Supplementary Figure 8: graphs showing correlation between the levels of ROS and the levels of expression of EMT markers N-cadherin on day 3 and Vimentin on day 14 of cell culture. ROS levels are presented either per cell or relative to the levels exhibited by the parental 4T1luc2 cells. Textbox in the figure shows correlation values (r, r^2, and p) measured by the Spearman correlation test. *(Supplementary Materials)*

References

[1] M. S. Shiels and E. A. Engels, "Evolving epidemiology of HIV-associated malignancies," *Current Opinion in HIV and AIDS*, vol. 12, no. 1, pp. 6–11, 2017.

[2] E. A. Engels, M. V. Brock, J. Chen, C. M. Hooker, M. Gillison, and R. D. Moore, "Elevated incidence of lung cancer among HIV-infected individuals," *Journal of Clinical Oncology*, vol. 24, no. 9, pp. 1383–1388, 2006.

[3] M. Herida, M. Mary-Krause, R. Kaphan et al., "Incidence of non–AIDS-defining cancers before and during the highly active antiretroviral therapy era in a cohort of human immunodeficiency virus–infected patients," *Journal of Clinical Oncology*, vol. 21, no. 18, pp. 3447–3453, 2003.

[4] C. Piketty, H. Selinger-Leneman, S. Grabar et al., "Marked increase in the incidence of invasive anal cancer among HIV-infected patients despite treatment with combination antiretroviral therapy," *AIDS*, vol. 22, no. 10, pp. 1203–1211, 2008.

[5] M. J. Silverberg, C. Chao, W. A. Leyden et al., "HIV infection, immunodeficiency, viral replication, and the risk of cancer," *Cancer Epidemiology, Biomarkers & Prevention*, vol. 20, no. 12, pp. 2551–2559, 2011.

[6] R. Dolcetti, C. Giagulli, W. He et al., "Role of HIV-1 matrix protein p17 variants in lymphoma pathogenesis," *Proceedings of the National Academy of Sciences of the United States of America*, vol. 112, no. 46, pp. 14331–14336, 2015.

[7] V. A. Carroll, M. K. Lafferty, L. Marchionni, J. L. Bryant, R. C. Gallo, and A. Garzino-Demo, "Expression of HIV-1 matrix protein p17 and association with B-cell lymphoma in HIV-1 transgenic mice," *Proceedings of the National Academy of Sciences of the United States of America*, vol. 113, no. 46, pp. 13168–13173, 2016.

[8] F. Caccuri, C. Rueckert, C. Giagulli et al., "HIV-1 matrix protein p17 promotes lymphangiogenesis and activates the endothelin-1/endothelin B receptor axis," *Arteriosclerosis, Thrombosis, and Vascular Biology*, vol. 34, no. 4, pp. 846–856, 2014.

[9] F. Caccuri, F. Giordano, I. Barone et al., "HIV-1 matrix protein p17 and its variants promote human triple negative breast cancer cell aggressiveness," *Infectious Agents and Cancer*, vol. 12, no. 1, p. 49, 2017.

[10] X. Zhu, Y. Guo, S. Yao et al., "Synergy between Kaposi's sarcoma-associated herpesvirus (KSHV) vIL-6 and HIV-1 Nef protein in promotion of angiogenesis and oncogenesis: role of the AKT signaling pathway," *Oncogene*, vol. 33, no. 15, pp. 1986–1996, 2014.

[11] M. Xue, S. Yao, M. Hu et al., "HIV-1 Nef and KSHV oncogene K1 synergistically promote angiogenesis by inducing cellular miR-718 to regulate the PTEN/AKT/mTOR signaling pathway," *Nucleic Acids Research*, vol. 42, no. 15, pp. 9862–9879, 2014.

[12] A. L. Greenway, D. McPhee, K. Allen et al., "Human immunodeficiency virus type 1 Nef binds to tumor suppressor p53 and protects cells against p53-mediated apoptosis," *Journal of Virology*, vol. 76, no. 6, pp. 2692–2702, 2002.

[13] G. Valentin-Guillama, S. López, Y. V. Kucheryavykh et al., "HIV-1 envelope protein gp120 promotes proliferation and the activation of glycolysis in glioma cell," *Cancers*, vol. 10, no. 9, p. 301, 2018.

[14] O. Warburg, "On the origin of cancer cells," *Science*, vol. 123, no. 3191, pp. 309–314, 1956.

[15] R. A. Gatenby and R. J. Gillies, "Why do cancers have high aerobic glycolysis?," *Nature Reviews Cancer*, vol. 4, no. 11, pp. 891–899, 2004.

[16] P. Mazzuca, A. Caruso, and F. Caccuri, "HIV-1 infection, microenvironment and endothelial cell dysfunction," *The New Microbiologica*, vol. 39, no. 3, pp. 163–173, 2016.

[17] R. K. Kundu, F. Sangiorgi, L. Y. Wu et al., "Expression of the human immunodeficiency virus-Tat gene in lymphoid tissues of transgenic mice is associated with B-cell lymphoma," *Blood*, vol. 94, no. 1, pp. 275–282, 1999.

[18] R. El-Amine, D. Germini, V. V. Zakharova et al., "HIV-1 Tat protein induces DNA damage in human peripheral blood B-lymphocytes via mitochondrial ROS production," *Redox Biology*, vol. 15, pp. 97–108, 2018.

[19] D. Huynh, E. Vincan, T. Mantamadiotis, D. Purcell, C. K. Chan, and R. Ramsay, "Oncogenic properties of HIV-Tat in colorectal cancer cells," *Current HIV Research*, vol. 5, no. 4, pp. 403–409, 2007.

[20] R. H. Kim, J. M. Yochim, M. K. Kang, K. H. Shin, R. Christensen, and N. H. Park, "HIV-1 Tat enhances replicative potential of human oral keratinocytes harboring HPV-16 genome," *International Journal of Oncology*, vol. 33, no. 4, pp. 777–782, 2008.

[21] J. Nyagol, E. Leucci, A. Onnis et al., "The effects of HIV-1 Tat protein on cell cycle during cervical carcinogenesis," *Cancer Biology & Therapy*, vol. 5, no. 6, pp. 684–690, 2006.

[22] K. Mani, S. Sandgren, J. Lilja et al., "HIV-Tat protein transduction domain specifically attenuates growth of polyamine

deprived tumor cells," *Molecular Cancer Therapeutics*, vol. 6, no. 2, pp. 782–788, 2007.

[23] G. Barillari, C. Palladino, I. Bacigalupo, P. Leone, M. Falchi, and B. Ensoli, "Entrance of the Tat protein of HIV-1 into human uterine cervical carcinoma cells causes upregulation of HPV-E6 expression and a decrease in p53 protein levels," *Oncology Letters*, vol. 12, no. 4, pp. 2389–2394, 2016.

[24] S. M. Tugizov, R. Herrera, P. Veluppillai, D. Greenspan, and J. M. Palefsky, "46. HIV-induced epithelial–mesenchymal transition in mucosal epithelium facilitates HPV paracellular penetration," *Sexual Health*, vol. 10, no. 6, pp. 592–592, 2013.

[25] G. Nunnari, J. A. Smith, and R. Daniel, "HIV-1 Tat and AIDS-associated cancer: targeting the cellular anti-cancer barrier?," *Journal of Experimental & Clinical Cancer Research*, vol. 27, no. 1, p. 3, 2008.

[26] M. Isaguliants, O. Smirnova, A. V. Ivanov et al., "Oxidative stress induced by HIV-1 reverse transcriptase modulates the enzyme's performance in gene immunization," *Human Vaccines & Immunotherapeutics*, vol. 9, no. 10, pp. 2111–2119, 2013.

[27] A. Latanova, S. Petkov, Y. Kuzmenko et al., "Fusion to Flaviviral Leader Peptide Targets HIV-1 Reverse Transcriptase for Secretion and Reduces Its Enzymatic Activity and Ability to Induce Oxidative Stress but Has No Major Effects on Its Immunogenic Performance in DNA- Immunized Mice," *Journal of Immunology Research*, vol. 2017, Article ID 7407136, 16 pages, 2017.

[28] P. A. Cerutti, "Prooxidant states and tumor promotion," *Science*, vol. 227, no. 4685, pp. 375–381, 1985.

[29] V. M. Factor, D. Laskowska, M. R. Jensen, J. T. Woitach, N. C. Popescu, and S. S. Thorgeirsson, "Vitamin E reduces chromosomal damage and inhibits hepatic tumor formation in a transgenic mouse model," *Proceedings of the National Academy of Sciences of the United States of America*, vol. 97, no. 5, pp. 2196–2201, 2000.

[30] R. Aurora, M. J. Donlin, N. A. Cannon, and J. E. Tavis, "Genome-wide hepatitis C virus amino acid covariance networks can predict response to antiviral therapy in humans," *The Journal of Clinical Investigation*, vol. 119, no. 1, pp. 225–236, 2009.

[31] P. Puigbo, E. Guzman, A. Romeu, and S. Garcia-Vallve, "OPTIMIZER: a web server for optimizing the codon usage of DNA sequences," *Nucleic Acids Research*, vol. 35, no. Web Server, pp. W126–W131, 2007.

[32] R. S. Fletcher, G. Holleschak, E. Nagy et al., "Single-step purification of recombinant wild-type and mutant HIV-1 reverse transcriptase," *Protein Expression and Purification*, vol. 7, no. 1, pp. 27–32, 1996.

[33] M. M. Bradford, "A rapid and sensitive method for the quantitation of microgram quantities of protein utilizing the principle of protein-dye binding," *Analytical Biochemistry*, vol. 72, no. 1-2, pp. 248–254, 1976.

[34] K. Rengan, "Cerenkov counting technique for beta particles: advantages and limitations," *Journal of Chemical Education*, vol. 60, no. 8, p. 682, 1983.

[35] M. D. Miller, P. D. Lamy, M. D. Fuller et al., "Human immunodeficiency virus type 1 reverse transcriptase expressing the K70E mutation exhibits a decrease in specific activity and processivity," *Molecular Pharmacology*, vol. 54, no. 2, pp. 291–297, 1998.

[36] H.-T. Xu, J. L. Martinez-Cajas, M. L. Ntemgwa et al., "Effects of the K65R and K65R/M184V reverse transcriptase mutations in subtype C HIV on enzyme function and drug resistance," *Retrovirology*, vol. 6, no. 1, p. 14, 2009.

[37] M. Giry-Laterrière, E. Verhoeyen, and P. Salmon, "Lentiviral vectors," *Methods in Molecular Biology*, vol. 737, pp. 183–209, 2011.

[38] C. S. Weiler and S. Chisholm, "Phased cell division in natural populations of marine dinoflagellates from shipboard cultures," *Journal of Experimental Marine Biology and Ecology*, vol. 25, no. 3, pp. 239–247, 1976.

[39] F. Comes, A. Matrone, P. Lastella et al., "A novel cell type-specific role of p38 α in the control of autophagy and cell death in colorectal cancer cells," *Cell Death and Differentiation*, vol. 14, no. 4, pp. 693–702, 2007.

[40] E. S. Starodubova, A. Boberg, M. Litvina et al., "HIV-1 reverse transcriptase artificially targeted for proteasomal degradation induces a mixed Th1/Th2-type immune response," *Vaccine*, vol. 26, no. 40, pp. 5170–5176, 2008.

[41] M. G. Isaguliants, S. V. Belikov, E. S. Starodubova et al., "Mutations conferring drug resistance affect eukaryotic expression of HIV type 1 reverse transcriptase," *AIDS Research and Human Retroviruses*, vol. 20, no. 2, pp. 191–201, 2004.

[42] A. V. Ivanov, O. A. Smirnova, O. N. Ivanova, O. V. Masalova, S. N. Kochetkov, and M. G. Isaguliants, "Hepatitis C virus proteins activate NRF2/ARE pathway by distinct ROS-dependent and independent mechanisms in HUH7 cells," *PLoS One*, vol. 6, no. 9, p. e24957, 2011.

[43] A. Ivanov, O. A. Smirnova, I. Y. Petrushanko et al., "HCV core protein uses multiple mechanisms to induce oxidative stress in human hepatoma Huh7 cells," *Viruses*, vol. 7, no. 6, pp. 2745–2770, 2015.

[44] O. N. Ivanova, A. V. Snezhkina, G. S. Krasnov et al., "Activation of polyamine catabolism by N1,N11-Diethylnorspermine in hepatic HepaRG cells induces dedifferentiation and mesenchymal-like phenotype," *Cell*, vol. 7, no. 12, p. 275, 2018.

[45] C. Brault, P. Lévy, S. Duponchel et al., "Glutathione peroxidase 4 is reversibly induced by HCV to control lipid peroxidation and to increase virion infectivity," *Gut*, vol. 65, no. 1, pp. 144–154, 2016.

[46] J. D. Zhang, M. Ruschhaupt, and R. Biczok, *ddCt method for qRT–PCR data analysis*, 2010.

[47] M. M. Tomayko and C. P. Reynolds, "Determination of subcutaneous tumor size in athymic (nude) mice," *Cancer Chemotherapy and Pharmacology*, vol. 24, no. 3, pp. 148–154, 1989.

[48] D. M. Euhus, C. Hudd, M. LaRegina, and F. E. Johnson, "Tumor measurement in the nude mouse," *Journal of Surgical Oncology*, vol. 31, no. 4, pp. 229–234, 1986.

[49] V. P. Baklaushev, A. Kilpeläinen, S. Petkov et al., "Luciferase expression allows bioluminescence imaging but imposes limitations on the orthotopic mouse (4T1) model of breast cancer," *Scientific Reports*, vol. 7, no. 1, p. 7715, 2017.

[50] B. A. Pulaski and S. Ostrand-Rosenberg, "Mouse 4T1 breast tumor model," *Current protocols in immunology*, vol. 39, no. 1, pp. 20.2. 1–20.2. 16, 2000.

[51] A. Āboliņš, A. Vanags, G. Trofimovičs, E. Miklaševičs, J. Gardovskis, and I. Štrumfa, "Molecular subtype shift in breast cancer upon trastuzumab treatment: a case report," *Polish Journal of Pathology*, vol. 62, no. 1, pp. 65–68, 2011.

[52] A. A. Latanova, S. Petkov, A. Kilpelainen et al., "Codon optimization and improved delivery/immunization regimen enhance the immune response against wild-type and drug-resistant HIV-1 reverse transcriptase, preserving its Th2-polarity," *Scientific Reports*, vol. 8, no. 1, p. 8078, 2018.

[53] C. W. Elston and I. O. Ellis, "Pathological prognostic factors in breast cancer. I. The value of histological grade in breast cancer: experience from a large study with long-term follow-up," *Histopathology*, vol. 19, no. 5, pp. 403–410, 1991.

[54] G. Li, S. Piampongsant, N. R. Faria et al., "An integrated map of HIV genome-wide variation from a population perspective," *Retrovirology*, vol. 12, no. 1, p. 18, 2015.

[55] J. Martinez-Picado and M. A. Martinez, "HIV-1 reverse transcriptase inhibitor resistance mutations and fitness: a view from the clinic and ex vivo," *Virus Research*, vol. 134, no. 1-2, pp. 104–123, 2008.

[56] E. V. de Parga, A. Rakhmanova, L. Pérez-Álvarez et al., "Analysis of drug resistance-associated mutations in treatment-naïve individuals infected with different genetic forms of HIV-1 circulating in countries of the former Soviet Union," *Journal of Medical Virology*, vol. 77, no. 3, pp. 337–344, 2005.

[57] O. A. Rumyantseva, I. A. Olkhovskiy, M. A. Malysheva et al., "Epidemiological networks and drug resistance of HIV type 1 in Krasnoyarsk region, Russia," *AIDS Research and Human Retroviruses*, vol. 25, no. 9, pp. 931–936, 2009.

[58] Е. В. Казеннова, И. А. Лаповок, А. В. Лебедев et al., "Анализ резистентности ВИЧ в Приволжском федеральном округе Российской Федерации," *ВИЧ-инфекция и иммуносупрессии*, vol. 7, no. 3, pp. 56–66, 2015.

[59] J. Weber, B. Chakraborty, J. Weberova, M. D. Miller, and M. E. Quiñones-Mateu, "Diminished replicative fitness of primary human immunodeficiency virus type 1 isolates harboring the K65R mutation," *Journal of Clinical Microbiology*, vol. 43, no. 3, pp. 1395–1400, 2005.

[60] A. N. Kolomeets, V. Varghese, P. Lemey, M. R. Bobkova, and R. W. Shafer, "A uniquely prevalent nonnucleoside reverse transcriptase inhibitor resistance mutation in Russian subtype A HIV-1 viruses," *AIDS*, vol. 28, no. 17, pp. F1–F8, 2014.

[61] J. Wang, C. Dykes, R. A. Domaoal, C. E. Koval, R. A. Bambara, and L. M. Demeter, "The HIV-1 reverse transcriptase mutants G190S and G190A, which confer resistance to non-nucleoside reverse transcriptase inhibitors, demonstrate reductions in RNase H activity and DNA synthesis from tRNA$^{Lys, 3}$ that correlate with reductions in replication efficiency," *Virology*, vol. 348, no. 2, pp. 462–474, 2006.

[62] J. Wang, R. A. Bambara, L. M. Demeter, and C. Dykes, "Reduced fitness in cell culture of HIV-1 with nonnucleoside reverse transcriptase inhibitor-resistant mutations correlates with relative levels of reverse transcriptase content and RNase H activity in virions," *Journal of Virology*, vol. 84, no. 18, pp. 9377–9389, 2010.

[63] L. Ratner, W. Haseltine, R. Patarca et al., "Complete nucleotide sequence of the AIDS virus, HTLV-III," *Nature*, vol. 313, no. 6000, pp. 277–284, 1985.

[64] A. Fantozzi and G. Christofori, "Mouse models of breast cancer metastasis," *Breast Cancer Research*, vol. 8, no. 4, p. 212, 2006.

[65] G. H. Heppner, F. R. Miller, and P. M. Shekhar, "Nontransgenic models of breast cancer," *Breast Cancer Research*, vol. 2, no. 5, pp. 331–334, 2000.

[66] E. Freed and M. Martin, "Human immunodeficiency viruses: replication," *Fields virology*, vol. 2, pp. 1502–1560, 2013.

[67] S. K. Sharma, N. Fan, and D. B. Evans, "Human immunodeficiency virus type 1 (HIV-1) recombinant reverse transcriptase: asymmetry in p66 subunits of the p66/p66 homodimer," *FEBS Letters*, vol. 343, no. 2, pp. 125–130, 1994.

[68] M. G. Isaguliants, S. O. Gudima, O. V. Ivanova et al., "Immunogenic properties of reverse transcriptase of HIV type 1 assessed by DNA and protein immunization of rabbits," *AIDS Research and Human Retroviruses*, vol. 16, no. 13, pp. 1269–1280, 2000.

[69] S. Kumari, A. K. Badana, M. M. G, S. G, and R. R. Malla, "Reactive oxygen species: a key constituent in cancer survival," *Biomarker Insights*, vol. 13, article 1177271918755391, 2018.

[70] B. Kalyanaraman, V. Darley-Usmar, K. J. Davies et al., "Measuring reactive oxygen and nitrogen species with fluorescent probes: challenges and limitations," *Free Radical Biology and Medicine*, vol. 52, no. 1, pp. 1–6, 2012.

[71] S. Lamouille, J. Xu, and R. Derynck, "Molecular mechanisms of epithelial–mesenchymal transition," *Nature Reviews Molecular Cell Biology*, vol. 15, no. 3, pp. 178–196, 2014.

[72] F. M. Davis, I. Azimi, R. A. Faville et al., "Induction of epithelial-mesenchymal transition (EMT) in breast cancer cells is calcium signal dependent," *Oncogene*, vol. 33, no. 18, pp. 2307–2316, 2014.

[73] M. Abakumov, A. Kilpeläinen, S. Petkov et al., "Evaluation of cyclic luciferin as a substrate for luminescence measurements in in vitro and in vivo applications," *Biochemical and Biophysical Research Communications*, vol. 513, no. 3, pp. 535–539, 2019.

[74] E. Hammond, R. Brandt, and K. Dredge, "PG545, a heparan sulfate mimetic, reduces heparanase expression in vivo, blocks spontaneous metastases and enhances overall survival in the 4T1 breast carcinoma model," *PLoS One*, vol. 7, no. 12, article e52175, 2012.

[75] S. Tabaries, V. Ouellet, B. E. Hsu et al., "Granulocytic immune infiltrates are essential for the efficient formation of breast cancer liver metastases," *Breast Cancer Research*, vol. 17, no. 1, p. 45, 2015.

[76] K. W. Hunter Jr., "Murine mammary carcinoma 4T1 induces a leukemoid reaction with splenomegaly: association with tumor-derived growth factors," *Experimental and Molecular Pathology*, vol. 82, no. 1, pp. 12–24, 2007.

[77] S. Petkov, E. Starodubova, A. Latanova et al., "DNA immunization site determines the level of gene expression and the magnitude, but not the type of the induced immune response," *PLoS One*, vol. 13, no. 6, article e0197902, 2018.

[78] M. Bobkova, "Current status of HIV-1 diversity and drug resistance monitoring in the former USSR," *AIDS Reviews*, vol. 15, no. 4, pp. 204–212, 2013.

[79] S. Garforth, C. Lwatula, and V. Prasad, "The lysine 65 residue in HIV-1 reverse transcriptase function and in nucleoside analog drug resistance," *Viruses*, vol. 6, no. 10, pp. 4080–4094, 2014.

[80] P. Gerondelis, R. H. Archer, C. Palaniappan et al., "The P236L delavirdine-resistant human immunodeficiency virus type 1 mutant is replication defective and demonstrates alterations in both RNA $5'$-end- and DNA $3'$-end-directed RNase H activities," *Journal of Virology*, vol. 73, no. 7, pp. 5803–5813, 1999.

[81] S. V. Joag, I. Adany, Z. Li et al., "Animal model of mucosally transmitted human immunodeficiency virus type 1 disease: intravaginal and oral deposition of simian/human immunodeficiency virus in macaques results in systemic infection, elimination of CD4+ T cells, and AIDS," *Journal of Virology*, vol. 71, no. 5, pp. 4016–4023, 1997.

[82] M. L. Bosch, A. Schmidt, M. B. Agy, L. E. Kimball, and W. R. Morton, "Infection of Macaca nemestrina neonates with HIV-1 via different routes of inoculation," *AIDS*, vol. 11, no. 13, pp. 1555–1563, 1997.

[83] A. M. Carias, S. McCoombe, M. McRaven et al., "Defining the interaction of HIV-1 with the mucosal barriers of the female reproductive tract," *Journal of Virology*, vol. 87, no. 21, pp. 11388–11400, 2013.

[84] T.-H. Dinh, K. P. Delaney, A. Goga et al., "Impact of maternal HIV seroconversion during pregnancy on early mother to child transmission of HIV (MTCT) measured at 4-8 weeks postpartum in South Africa 2011-2012: a national population-based evaluation," *PLoS One*, vol. 10, no. 5, article e0125525, 2015.

[85] M. GIRARD, J. MAHONEY, Q. WEI et al., "Genital infection of female chimpanzees with human immunodeficiency virus type 1," *AIDS Research and Human Retroviruses*, vol. 14, no. 15, pp. 1357–1367, 1998.

[86] K. A. Brune, F. Ferreira, P. Mandke et al., "HIV impairs lung epithelial integrity and enters the epithelium to promote chronic lung inflammation," *PLoS One*, vol. 11, no. 3, article e0149679, 2016.

[87] R. Liu, L. Huang, J. Li et al., "HIV infection in gastric epithelial cells," *The Journal of Infectious Diseases*, vol. 208, no. 8, pp. 1221–1230, 2013.

[88] Y. Ganor, Z. Zhou, D. Tudor et al., "Within 1 h, HIV-1 uses viral synapses to enter efficiently the inner, but not outer, foreskin mucosa and engages Langerhans-T cell conjugates," *Mucosal Immunology*, vol. 3, no. 5, pp. 506–522, 2010.

[89] F. Hladik, P. Sakchalathorn, L. Ballweber et al., "Initial events in establishing vaginal entry and infection by human immunodeficiency virus type-1," *Immunity*, vol. 26, no. 2, pp. 257–270, 2007.

[90] D. Maher, X. Wu, T. Schacker, J. Horbul, and P. Southern, "HIV binding, penetration, and primary infection in human cervicovaginal tissue," *Proceedings of the National Academy of Sciences*, vol. 102, no. 32, pp. 11504–11509, 2005.

[91] Z. Zhou, N. Barry de Longchamps, A. Schmitt et al., "HIV-1 efficient entry in inner foreskin is mediated by elevated CCL5/RANTES that recruits T cells and fuels conjugate formation with Langerhans cells," *PLoS Pathogens*, vol. 7, no. 6, article e1002100, 2011.

[92] E. Stoddard, H. Ni, G. Cannon et al., "gp340 promotes transcytosis of human immunodeficiency virus type 1 in genital tract-derived cell lines and primary endocervical tissue," *Journal of Virology*, vol. 83, no. 17, pp. 8596–8603, 2009.

[93] A. M. Micsenyi, C. Zony, R. A. Alvarez, N. D. Durham, B. K. Chen, and M. E. Klotman, "Postintegration HIV-1 infection of cervical epithelial cells mediates contact-dependent productive infection of T cells," *The Journal of Infectious Diseases*, vol. 208, no. 11, pp. 1756–1767, 2013.

[94] S. Gilroy, M. Białasek, N. Suzuki et al., "ROS, calcium, and electric signals: key mediators of rapid systemic signaling in plants," *Plant Physiology*, vol. 171, no. 3, pp. 1606–1615, 2016.

[95] R. Mittler, S. Vanderauwera, N. Suzuki et al., "ROS signaling: the new wave?," *Trends in Plant Science*, vol. 16, no. 6, pp. 300–309, 2011.

[96] P. Niethammer, C. Grabher, A. T. Look, and T. J. Mitchison, "A tissue-scale gradient of hydrogen peroxide mediates rapid wound detection in zebrafish," *Nature*, vol. 459, no. 7249, pp. 996–999, 2009.

[97] Q. Pan, W. Y. Qiu, Y. N. Huo, Y. F. Yao, and M. F. Lou, "Low levels of hydrogen peroxide stimulate corneal epithelial cell adhesion, migration, and wound healing," *Investigative Ophthalmology & Visual Science*, vol. 52, no. 3, pp. 1723–1734, 2011.

[98] E. Giannoni, M. Parri, and P. Chiarugi, "EMT and oxidative stress: a bidirectional interplay affecting tumor malignancy," *Antioxidants & Redox Signaling*, vol. 16, no. 11, pp. 1248–1263, 2012.

[99] J. Jiang, K. Wang, Y. Chen, H. Chen, E. C. Nice, and C. Huang, "Redox regulation in tumor cell epithelial-mesenchymal transition: molecular basis and therapeutic strategy," *Signal Transduction and Targeted Therapy*, vol. 2, no. 1, article 17036, 2017.

[100] S. Y. Lee, M. K. Ju, H. M. Jeon et al., "Reactive oxygen species induce epithelial-mesenchymal transition, glycolytic switch, and mitochondrial repression through the Dlx-2/Snail signaling pathways in MCF-7 cells," *Molecular Medicine Reports*, vol. 20, no. 3, pp. 2339–2346, 2019.

[101] A. Yadav, S. Vallabu, D. Kumar et al., "HIVAN phenotype: consequence of epithelial mesenchymal transdifferentiation," *American Journal of Physiology-Renal Physiology*, vol. 298, no. 3, pp. F734–F744, 2009.

[102] L. T. Wang, S. N. Wang, S. S. Chiou et al., "TIP60-dependent acetylation of the SPZ1-TWIST complex promotes epithelial-mesenchymal transition and metastasis in liver cancer," *Oncogene*, vol. 38, no. 4, pp. 518–532, 2019.

[103] N. Floc'h, J. Kolodziejski, L. Akkari et al., "Modulation of oxidative stress by twist oncoproteins," *PLoS One*, vol. 8, no. 8, article e72490, 2013.

[104] C. Del Vecchio, Y. Feng, E. S. Sokol et al., "De-Differentiation Confers Multidrug Resistance Via Noncanonical PERK-Nrf2 Signaling," vol. 12, no. 9, Article ID e1001945, 2014.

[105] H. Zheng and Y. Kang, "Multilayer control of the EMT master regulators," *Oncogene*, vol. 33, no. 14, pp. 1755–1763, 2014.

[106] N. Matsuo, H. Shiraha, T. Fujikawa et al., "Twist expression promotes migration and invasion in hepatocellular carcinoma," *BMC Cancer*, vol. 9, no. 1, p. 240, 2009.

[107] S. Ansieau, A. P. Morel, G. Hinkal, J. Bastid, and A. Puisieux, "TWISTing an embryonic transcription factor into an oncoprotein," *Oncogene*, vol. 29, no. 22, pp. 3173–3184, 2010.

[108] V. Bronte and M. J. Pittet, "The spleen in local and systemic regulation of immunity," *Immunity*, vol. 39, no. 5, pp. 806–818, 2013.

[109] A. Kano, "Tumor cell secretion of soluble factor(s) for specific immunosuppression," *Scientific Reports*, vol. 5, no. 1, p. 8913, 2015.

[110] C. P. Day, J. Carter, Z. W. Ohler et al., ""Glowing head" mice: a genetic tool enabling reliable preclinical image-based evaluation of cancers in immunocompetent allografts," *PLoS One*, vol. 9, no. 11, article e109956, 2014.

[111] K. Warren, D. Warrilow, L. Meredith, and D. Harrich, "Reverse transcriptase and cellular factors: regulators of

HIV-1 reverse transcription," *Viruses*, vol. 1, no. 3, pp. 873–894, 2009.

[112] M. Mehta, K. Basalingappa, J. N. Griffith et al., "HuR silencing elicits oxidative stress and DNA damage and sensitizes human triple-negative breast cancer cells to radiotherapy," *Oncotarget*, vol. 7, no. 40, pp. 64820–64835, 2016.

[113] M. D. Diaz-Muñoz, S. E. Bell, K. Fairfax et al., "The RNA-binding protein HuR is essential for the B cell antibody response," *Nature Immunology*, vol. 16, no. 4, pp. 415–425, 2015.

[114] A. Czachor, A. Failla, R. Lockey, and N. Kolliputi, "Pivotal role of AKAP121 in mitochondrial physiology," *American Journal of Physiology-Cell Physiology*, vol. 310, no. 8, pp. C625–C628, 2016.

[115] J. Lemay, P. Maidou-Peindara, T. Bader et al., "HuR interacts with human immunodeficiency virus type 1 reverse transcriptase, and modulates reverse transcription in infected cells," *Retrovirology*, vol. 5, no. 1, p. 47, 2008.

[116] I. Grammatikakis, K. Abdelmohsen, and M. Gorospe, "Post-translational control of HuR function," *Wiley Interdisciplinary Reviews: RNA*, vol. 8, no. 1, p. e1372, 2017.

[117] A. Carlucci, L. Lignitto, and A. Feliciello, "Control of mitochondria dynamics and oxidative metabolism by cAMP, AKAPs and the proteasome," *Trends in Cell Biology*, vol. 18, no. 12, pp. 604–613, 2008.

[118] K. Munger, M. Scheffner, J. M. Huibregtse, and P. M. Howley, "Interactions of HPV E6 and E7 oncoproteins with tumour suppressor gene products," *Cancer Surveys*, vol. 12, pp. 197–217, 1992.

[119] D. Ahuja, M. T. Saenz-Robles, and J. M. Pipas, "SV40 large T antigen targets multiple cellular pathways to elicit cellular transformation," *Oncogene*, vol. 24, no. 52, pp. 7729–7745, 2005.

[120] A. V. Ivanov, V. T. Valuev-Elliston, O. N. Ivanova et al., "Oxidative stress during HIV infection: mechanisms and consequences," *Oxidative Medicine and Cellular Longevity*, vol. 2016, Article ID 8910396, 18 pages, 2016.

Research Article

A Novel Thiazolyl Schiff Base: Antibacterial and Antifungal Effects and *In Vitro* Oxidative Stress Modulation on Human Endothelial Cells

Cristian Cezar Login [iD],[1] **Ioana Bâldea** [iD],[1] **Brîndușa Tiperciuc** [iD],[2] **Daniela Benedec** [iD],[3] **Dan Cristian Vodnar** [iD],[4] **Nicoleta Decea** [iD],[1] and **Șoimița Suciu**[1]

[1]*Department of Physiology, Iuliu Hațieganu University of Medicine and Pharmacy, 1 Clinicilor Street, 400006 Cluj-Napoca, Romania*
[2]*Department of Pharmaceutical Chemistry, Iuliu Hațieganu University of Medicine and Pharmacy, 41 Victor Babeș Street, 400012 Cluj-Napoca, Romania*
[3]*Department of Pharmacognosy, Iuliu Hațieganu University of Medicine and Pharmacy, 12 Ion Creangă Street, 400010 Cluj-Napoca, Romania*
[4]*Department of Food Science, University of Agricultural Sciences and Veterinary Medicine, 3-5 Mănăștur Street, 400372 Cluj-Napoca, Romania*

Correspondence should be addressed to Ioana Bâldea; baldeaioana@gmail.com and Brîndușa Tiperciuc; brandu32@yahoo.com

Received 5 April 2019; Revised 13 July 2019; Accepted 5 September 2019; Published 10 October 2019

Guest Editor: Birke Bartosch
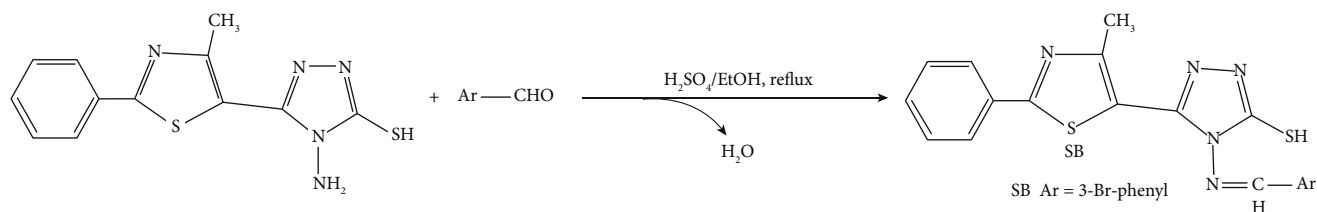
Schiff bases (SBs) are chemical compounds displaying a significant pharmacological potential. They are able to modulate the activity of many enzymes involved in metabolism and are found among antibacterial, antifungal, anti-inflammatory, antioxidant, and antiproliferative drugs. A new thiazolyl-triazole SB was obtained and characterized by elemental and spectral analysis. The antibacterial and antifungal ability of the SB was evaluated against Gram-positive and Gram-negative bacteria and against three *Candida* strains. SB showed good antibacterial activity against *L. monocytogenes* and *P. aeruginosa*; it was two times more active than ciprofloxacin. Anti-*Candida* activity was twofold higher compared with that of fluconazole. The effect of the SB on cell viability was evaluated by colorimetric measurement on cell cultures exposed to various SB concentrations. The ability of the SB to modulate oxidative stress was assessed by measuring MDA, TNF-α, SOD1, COX2, and NOS2 levels *in vitro*, using human endothelial cell cultures exposed to a glucose-enriched medium. SB did not change the morphology of the cells. Experimental findings indicate that the newly synthetized Schiff base has antibacterial activity, especially on the Gram-negative *P. aeruginosa*, and antifungal activity. SB also showed antioxidant and anti-inflammatory activities.

1. Introduction

Aerobic organisms have antioxidant defense systems against reactive oxygen species- (ROS-) induced damage produced in various stress conditions. ROS are also involved in the innate immune system and have an important role in the inflammatory response; they attract cells, by chemotaxis, to the inflammation site. Nitric oxide (NO) is another important intracellular and intercellular signaling molecule involved in the regulation of multiple physiological and pathophysiological mechanisms. It acts as a biological modulator.

NO is able to regulate vascular tone and can function as a host defense effector. Also, it can act as a cytotoxic agent in inflammatory disorders. NO synthase (NOS) enzyme family catalyzes NO production. Inhibition of inducible NOS (iNOS) might be beneficial in the course of treatment of certain inflammatory diseases [1]. The reactions between NO and ROS, such as superoxide radicals ($O_2^{·-}$), lead to the production of a potent prooxidant radical (peroxynitrite), thus inducing endothelial and mitochondrial dysfunction. The major cellular defense against peroxide and peroxynitrite radicals are the superoxide dismutases (SODs) that catalyzes

Scheme 1: Synthesis of the Schiff base (SB).

the transformation of peroxide radicals into hydrogen peroxide (H_2O_2), which is further transformed by catalase into water and molecular oxygen. Also, SODs play an important role in preventing peroxynitrite formation [2]. All isoforms have in their catalytic site a transition metal, such as copper and manganese [3].

Recent studies showed that exogenous NO, produced by bacterial NOS, protects Gram-positive and Gram-negative bacteria (*Pseudomonas aeruginosa*, *Staphylococcus aureus*, etc.) against oxidative stress and increases bacterial resistance to a broad spectrum of antibiotics [4]. Fungal resistance to antimycotic treatment is one of the consequences of the emergence of resistant strains, but more and more, in the last years, fungal resistance is due to the capacity of fungal strains to form biofilms, which are considered critical in invasive fungal infections, associated with high mortality. Certain studies showed that only a few antimycotics are effective against fungal biofilms. All of them have the capacity to induce ROS formation in fungal biofilm cells [5]. In this context, finding bioactive substances capable to reduce NO synthesis in bacteria or able to induce ROS synthesis in fungal biofilms could represent new directions in the development of new antimicrobial drugs. Thiazoles, triazoles, and their derivatives are found among antibacterial and anti-inflammatory drugs [6–9].

Schiff bases (SBs) are chemical structures that have a significant pharmacological potential. SBs contain an azomethine group obtained through the condensation of primary amines with carbonyl compounds [10]. The pharmacophore potential of this group is due to their ability to form complex compounds with bivalent and trivalent metals located in the active center of numerous enzymes involved in metabolic reactions. The relationship between a chemical structure and biological activity (SAR) underlines the importance of the azomethine group for the synthesis of new compounds with antibacterial, antifungal, and even antitumor activities [11–13].

Multiple studies showed the ability of SBs to act as antiproliferative and antitumoral agents [14–16]. The azomethine pharmacophore is used in developing new bioactive molecules [17]. The discovery of selective cytotoxic drugs influenced oncological therapy. However, completely satisfactory answers for metastasis onset have not yet been found. Due to the increased prevalence of neoplasia and to the existence of various cellular tumor lines resistant to cytotoxic therapy, the research of new active agents is justified [18, 19].

The current study is aimed at testing a newly synthetized heterocyclic SB in terms of antimicrobial activity against Gram-positive and Gram-negative bacteria and antifungal effects against *Candida* strains [20, 21], as well as to evaluate the biocompatibility of the SB *in vitro* on human endothelial cells and the ability of this SB to modulate oxidative stress, by assessing enzymes involved in cellular antioxidant defense.

2. Materials and Methods

2.1. Synthesis of the Schiff Base. All reagents and solvents used were purchased from Sigma-Aldrich and were used without further purification. The starting compound was previously reported and was synthesized by us according to methodologies described in the literature [21].

The synthesis of Schiff base (SB) 4-(3-bromobenzylideneamino)-5-(4-methyl-2-phenylthiazol-5-yl)-4H-1,2,4-triazole-3-thiol was made using a general procedure (Scheme 1) [21]. 2 mmol (0.578 g) of 4-amino-5-(4-methyl-2-phenylthiazol-5-yl)-4H-1,2,4-triazole-3-thiol was suspended in 10 mL of absolute ethanol. The resulting suspension was added with an alcoholic solution of 2 mmol of 3-bromobenzaldehyde in 5 mL of absolute ethanol and 2-3 drops of concentrated H_2SO_4, as a catalyst. The reaction mixture was refluxed for 6 h. The obtained precipitate was filtered hot and washed with absolute ethanol, and then, it was dried and recrystallized from dimethyl sulfoxide (DMSO).

2.2. In Vitro Antibacterial and Antifungal Screening

2.2.1. Preparation of Sample Solution. SB was dissolved in DMSO, at a final concentration of 100 μg/mL. Sample solution was stored at 4°C [22, 23].

2.2.2. Inhibition Zone Diameter Measurements. Antimicrobial activity was tested *in vitro* using the agar disk diffusion method through the measurement of the inhibition zone diameters. Agar plates were inoculated with a standardized inoculum of the test microorganisms: two Gram-negative bacterial strains—*Salmonella enteritidis* ATCC 14028 and *Escherichia coli* ATCC 25922, two Gram-positive bacterial strains—*Listeria monocytogenes* ATCC 19115 and *Staphylococcus aureus* ATCC 49444, and a fungal strain—*Candida albicans* ATCC 10231. Petri plates with Mueller Hinton Agar (20.0 mL) were used for all bacterial tests. Mueller-Hinton medium supplemented with 2% glucose (providing adequate growth of yeasts) and 0.5 g/L methylene blue (providing a better definition of the inhibition zone diameter) was used for antifungal testing. Each paper disk was impregnated with 10 μL of solution (100 μg compound/disk). The filter paper disks were placed on Petri dishes previously seeded "in layer" with the tested bacterial strain inoculums. Then, Petri dishes were maintained at room temperature to ensure the equal

diffusion of the compound in the medium, and afterwards, the dishes were incubated at 37°C for 24 hours. Inhibition zones were measured after 24 hours of incubation. Assessment of the antimicrobial effect was realized by measuring the diameter of the growth inhibition zone. Ciprofloxacin (10 μg/well) and fluconazole (25 μg/well) were used as standard antibacterial and antifungal drugs. DMSO was used for comparison, as a negative control, for all experiments, and it did not inhibit the growth of microorganisms (diameter = 6 mm). The clear halos with a diameter larger than 10 mm were considered positive results [22, 23]. Tests were performed in triplicate, and values are presented as the average value ± standard deviation.

2.2.3. Determination of Minimum Inhibitory Concentrations (MICs), Minimum Bactericidal Concentrations (MBCs), and Minimum Fungicidal Concentrations (MFCs).

Minimum inhibitory concentrations (MICs), minimum bactericidal concentrations (MBCs), and minimum fungicidal concentrations (MFCs) were determined by an agar dilution method. Strains of microorganisms used were as follows: *Salmonella enteritidis* ATCC 14028, *Escherichia coli* ATCC 25922, *Listeria monocytogenes* ATCC 19115, *Staphylococcus aureus* ATCC 49444, *Candida albicans* ATCC 10231, *Candida albicans* (ATCC 18804), and *Candida krusei* (ATCC 6258) [22–26]. For the experiment, 100 μL nutrient broths were placed in a 96-well plate, and sample solution at high concentration (100 μg/mL) was added into the first rows of the microplates. 10 μL of culture suspensions was inoculated into all the wells. The plates were incubated at 37°C for 16-24 hours (48 hours for fungi). The reference drugs, ciprofloxacin and fluconazole, were used in the same concentrations.

2.3. Determination of Antioxidant Activity by DPPH (2,2-Diphenyl-1-picrylhydrazyl) Bleaching Assay.

The DPPH antioxidant activity assay was done as previously described, with minor modification. SB was dissolved in DMSO (1 mg/mL). DPPH• radical was dissolved in methanol (0.25 mM). Equal volumes (1.0 mL) of methanolic DPPH solution and sample solution (or standard) in methanol at different concentrations have been used. The mixtures were incubated for 30 min at 40°C in a thermostatic bath; absorbance was measured at 517 nm. The percent DPPH scavenging ability was calculated as follows: DPPH scavenging ability = $(A_{control} - A_{sample})/A_{control} \times 100$, where $A_{control}$ is the absorbance of DPPH radical and methanol (containing all reagents, except the sample) and A_{sample} is the absorbance of the mixture of DPPH radical and sample. A curve of % DPPH scavenging ability versus concentration was plotted, and IC_{50} values were calculated. The IC_{50} value is the sample concentration required to scavenge 50% of DPPH free radicals. The lesser the IC_{50} value, the stronger the antioxidant capacity. Thus, if $IC_{50} \leq 50$ μg/mL, the sample shows a high antioxidant capacity; if 50 μg/mL $< IC_{50} \leq 200$ μg/mL, the sample has a moderate antioxidant capacity; if $IC_{50} > 200$ μg/mL, the sample has poor or no activity. BHT (butylated hydroxytoluene) and trolox (6-hydroxy-2,5,7,8-tetramethylchroman-2-carboxylic acid) were used as positive controls [20, 27–30].

2.4. Assessment of the Ability of the SB to Modulate Inflammatory Response and Oxidative Stress on Cell Cultures

2.4.1. Cell Source.
Human umbilical vein endothelial cells (HUVECs, Promocell, Hamburg, Germany) were used. The cells were grown in RPMI medium supplemented with 5% fetal calf serum, 50 μg/mL gentamycin, and 5 ng/mL amphotericin (Biochrom Ag, Berlin, Germany). Cell cultures in the 13rd to 15th passages were used. SB was diluted in DMSO (Biochrom Ag, Berlin, Germany) to obtain a stock solution of 1 mg/mL. The stock solution was used to make further dilutions in complete cell growth medium, immediately prior to the experiments. The final DMSO concentration was lower than 0.05%, a nontoxic concentration for the cells [31].

2.4.2. Cell Viability Testing.
Cells cultured at a density of 10^4/well on ELISA 96-well plaques (TPP, Switzerland) were settled for 24 hours, then exposed to different concentrations of the substance ranging from 0.001 to 200 μg/mL. Viability was measured by the colorimetric measurement of a colored compound—formazan, generated by viable cells using the CellTiter 96® AQueous Non-Radioactive Cell Proliferation Assay (Promega Corporation, Madison, USA). Readings were done at 540 nm, using an ELISA plate reader (Tecan, Mannedorf, Austria). Results were presented as OD_{540}. All experiments were performed in triplicate. Untreated cultures were used as controls [32].

2.4.3. Experimental Design.
Four groups were made: (1) control cells treated only with medium, (2) cells exposed to a high-glucose (4.5 g/L) medium, (3) cells treated with SB 0.001 μg/mL, and (4) cells concomitantly exposed to high glucose and SB (0.001 μg/mL). All groups were treated for 24 hours. Afterwards, cells were used for the assessment of cytoskeleton modifications—phalloidin staining (fluorescence microscopy), oxidative stress (Western blot measurement of SOD1, COX2, and inducible NOS2 and spectrophotometric measurement of MDA), and inflammation (ELISA measurement of TNF-α).

2.4.4. Cell Lysis.
The cell lysates used in the following experiments were prepared as previously described [33]. Protein concentrations were determined by the Bradford method, according to the manufacturer's specifications (Bio-Rad, Hercules, California, USA) and using bovine serum albumin as standard. For all assays, the lysates were corrected by total protein concentration.

2.4.5. Oxidative Stress and Inflammation Assessment.
Quantification of malondialdehyde (MDA) a marker for the peroxidation of membrane lipids was performed by spectrophotometry, as previously described [34]. All reagents were purchased from Sigma-Aldrich. Data were expressed as nM/mg protein [35]. Following viability testing and following the assessment of the MDA level, cells used in further experiments were treated with a concentration of 0.001 μg/mL.

TNF-α ELISA Immunoassay kit from R&D Systems, Inc. (Minneapolis, USA) was used. Cell supernatants were treated according to the manufacturer's instructions; readings were done at 450 nm with correction wavelength set at 540 nm, using an ELISA plate reader (Tecan) [33].

Lysates (20 μg protein/lane) were separated by electrophoresis on SDS PAGE gels and transferred to polyvinylidene difluoride membranes, using a Bio-Rad Miniprotean system (Bio-Rad). Blots were blocked and then incubated with antibodies against superoxide dismutase 1 (SOD1), cyclooxygenase 2 (COX2), and inducible nitric oxide synthase 2 (NOS2), then further washed and incubated with corresponding secondary peroxidase-linked antibodies. All antibodies were acquired from Santa Cruz Biotechnology. Proteins were detected using Supersignal West Femto Chemiluminescent substrate (Thermo Fisher Scientific, Rockford IL, USA) and a Gel Doc Imaging system equipped with a XRS camera and Quantity One analysis software (Bio-Rad). Glyceraldehyde 3-phosphate dehydrogenase (GAPDH, Trevigen Biotechnology, Gaithersburg, MD (Maryland), USA) was used as a protein loading control.

Phalloidin-FITC 50 μg/mL (Sigma-Aldrich, St. Louis, MO, USA) a marker for actin myofilaments (green) was used, according to the manufacturer's instructions. Cells were seeded in chamber slides at a density of 5×10^4/chamber, allowed to settle for 24 hours, and then exposed to high glucose and SB as described above. Treated cells were then stained with phalloidin-FITC. Images of cells were documented at a magnification of 20x, using an inverted microscope Olympus BX40 equipped with an Olympus CKX-RFA fluorescent lamp and an E330 camera (Olympus, Hamburg, Germany).

2.5. Statistical Analysis. The statistical significance of the differences between the control group and the treated groups was assessed with the nonparametric Kruskal-Wallis test for multiple groups, followed by a post hoc analysis using the Conover test. Correlation coefficients between parameters have been calculated using Spearman's correlation coefficient for ranks (rho). Statistical tests were performed using Med-Calc version 18.11.3 and GraphPad Prism Software version 8.0.2. The results were considered statistical significant at $p < 0.05$.

3. Results

3.1. Chemical Characterization of the SB. The SB structure was confirmed by elemental analysis and on the basis of its mass spectrum (MS), infrared spectrum (IR), and nuclear magnetic resonance (^{1}H NMR and ^{13}C NMR) spectra [21].

4-(3-Bromobenzylideneamino)-5-(4-methyl-2-phenylthiazol-5-yl)-4H-1,2,4-triazole-3-thiol. Yield 80.3% (0.366 g); m.p. 268-270°C; light yellow powder; Anal. Calcd for $C_{19}H_{14}BrN_5S_2$ (456.38): C, 49.89; H, 3.06; N, 15.33; S, 14.02; Found: C, 50.1; H, 3.07; N, 15.33; S, 14.07; IR (ATR, cm^{-1}): 3104 (ν NH$_{triazole}$), 1618 (ν -N=CH-), 1274 (ν C=S); 1055 (ν C-Br); ^{1}H NMR (500 MHz, DMSO-d_6, δ/ppm): 14.18 (s, 1H, NH), 9.52 (s, 1H, -N=CH-), 7.97–8.06

TABLE 1: Inhibition zone diameters on tested microorganisms.

Samples	Diameter of the inhibition zone (mm)				
	SA	LM	EC	ST	CA
Schiff base	14	14	14	18	18
Ciprofloxacin	28	18	27	22	—
Fluconazole	—	—	—	—	25

SA: *Staphylococcus aureus*; LM: *Listeria monocytogenes*; EC: *Escherichia coli*; ST: *Salmonella typhimurium*; CA: *Candida albicans*.

(d, 2H, ArH), 7.92 (s, 1H, ArH), 7.77 (d, 1H, ArH), 7.59 (d, 1H, ArH), 7.47-7.54 (m, 4H, ArH), 2.41 (s, 3H, CH$_3$); ^{13}C NMR (125 MHz, DMSO-d_6, δ/ppm): 170.12 (C=S), 159.15 (C), 157.66 (CH=N), 153.81 (C), 151.07 (C), 143.96 (C), 135.16 (C), 134.51 (C), 131.21 (CH), 130.93 (2CH), 130.29 (CH), 129.29 (2CH), 128.94 (CH), 128.68 (C), 127.36 (CH), 127.14 (CH), 15.92 (CH$_3$); MS (EI, 70 eV) m/z (%): 457 (M + 1).

3.2. Antimicrobial Activity. Results obtained by measuring the diameters of growth inhibition zones of the tested microorganisms, compared to ciprofloxacin and fluconazole, used as standard reference drugs, are presented in Table 1.

MIC, MBC, and MFC values of the new compound are presented in Tables 2 and 3. The results showed that MIC values ranged from 1.95 (*Listeria monocytogenes*) to 62.5 μg/mL, MBC values were between 3.9 and 125 μg/mL, and MFC scores ranged between 62.5 and 125 μg/mL.

3.3. In Vitro Antioxidant Capacity. The antioxidant capacity of the SB was determined by the DPPH bleaching method, and BHT and trolox were used as positive controls. The results are displayed in Table 4. The new compound showed a very low IC$_{50}$ value (16.10 μg/mL), similar to that of BHT (16.39 μg/mL).

3.4. Cell Viability. SB did not lead to significant changes in HUVEC viability for doses lower than 0.1 μg/mL (Figure 1). Higher concentrations led to a dose-dependent viability decrease, compared with control.

3.5. Assessment of the Ability of the SB to Modulate Inflammatory Response and Oxidative Stress on HUVECs. Lipid peroxidation level (MDA), the ability to modulate inflammatory response (TNF-α, COX2), and the activity of enzymes involved in the prooxidant/antioxidant equilibrium (SOD1, NOS2) were appreciated. The ability of the SB to modulate oxidative stress was tested *in vitro* on HUVECs, using a glucose-enriched medium [36–38]. A SB concentration of 0.001 μg/mL was used for all experiments.

The effect of the newly synthetized compound on lipid peroxidation (MDA level) was assessed. SB administration decreased the MDA level compared with both control and glucose-enriched medium, thus reducing the lipid peroxidation in endothelial cells (Figure 2).

The TNF-α level was quantified through ELISA for the same SB concentration (Figure 3). Glucose-enriched medium slightly increased the TNF-α level. SB also increased the TNF-α level both alone and in combination with glucose.

TABLE 2: Minimum inhibitory concentrations (MIC).

| Samples | Minimum inhibitory concentration (MIC (μg/mL)) | | | | | |
	SA	LM	PA	ST	CA (ATCC 10231)	CA (ATCC 18804)
Schiff base	31.25	1.95	1.95	62.5	62.5	31.25
Ciprofloxacin	1.95	3.9	3.9	0.97	—	—
Fluconazole	—	—	—	—	62.5	62.5

SA: Staphylococcus aureus; LM: Listeria monocytogenes; PA: Pseudomonas aeruginosa; ST: Salmonella typhimurium; CA: Candida albicans.

TABLE 3: Minimum bactericidal (MBC) and minimum fungicidal concentrations (MFC).

| Samples | MBC (μg/mL) | | | | MFC (μg/mL) | | |
	SA	LM	PA	ST	CA (ATCC 10231)	CA (ATCC 18804)	CK (ATCC 6258)
Schiff base	62.5	3.9	3.9	125	125	62.5	62.5
Ciprofloxacin	3.9	7.8	7.8	1.95	—	—	—
Fluconazole	—	—	—	—	125	125	125

SA: Staphylococcus aureus; LM: Listeria monocytogenes; PA: Pseudomonas aeruginosa; ST: Salmonella typhimurium; CA: Candida albicans; CK: Candida krusei.

TABLE 4: Antioxidant capacity using the DPPH method.

Samples	IC_{50} (μg/mL)
Schiff base	16.10 ± 1.2
BHT	16.39 ± 0.9
Trolox	11.98 ± 0.4

The same SB concentration (0.001 μg/mL) was used to further test its effect on the protein level of the enzymes involved in the oxidant/antioxidant equilibrium and in the inflammatory response (SOD1, NOS2, and COX2).

An inflammatory marker (COX2) and antioxidant enzyme (constitutive SOD1 and inducible NOS2) expression was quantified by Western Blot (Figure 4).

COX2, an inflammatory marker, significantly decreased after both glucose and SB treatments, compared to control. Combined exposure (SB+G) strongly decreased the protein level of COX2 (Figure 4(b)). This finding is consistent with MDA levels and may be due to the antioxidant effect of the SB in this experimental setting. Interestingly, it is not consistent with TNF-α, a fact which might be explained by a different mechanism than oxidative stress that triggers an increase of TNF-α. Exposure to glucose-enriched medium significantly decreased SOD1. SB slightly decreased SOD1 activity compared with the control group, but SOD1 activity was maintained at a significantly higher level, compared with glucose ($p < 0.05$). Combination (SB+G) treatment significantly decreased SOD1 compared with both glucose and control (Figure 4(c)). Exposure to glucose increased significantly NOS2. The SB drastically decreased the NOS2 level compared with both the control and glucose groups (Figure 4(d)).

Correlation analysis, using Spearman's coefficient for rank correlation (Table 5), revealed statistically significant positive correlations between MDA and enzyme (COX2, SOD1, and NOS2) levels. On the other hand, the TNF-α level negatively correlates with both MDA and all enzymes measured.

Cell morphology does not seem to be affected by exposure to the Schiff base compared to control. When exposed to high-glucose concentration, cells had a tendency to conglomerate and to form multilayered spherical bodies, with alteration of the actin filament disposition. The aspect of the cells receiving combination treatment was similar to those of controls (Figure 5).

4. Discussion

The structure of the Schiff base was established by elemental analysis and on the basis of its mass spectrum (MS), infrared spectrum (IR), and nuclear magnetic resonance (^{1}H-NMR and ^{13}C-NMR) spectra. The results of the C, H, N, S quantitative elemental analysis were in agreement with the calculated values, within ±0.4% of the theoretical values. The spectral data confirmed the formation of the SB. The recorded mass spectrum revealed the correct molecular ion peak ($M + 1$), as suggested by the molecular formula. The absence of the NH_2 asymmetric and symmetric stretching vibrations at 3281 cm^{-1} and 3186 cm^{-1}, and the presence of N=CH stretch absorption bands at 1618 cm^{-1} in the IR spectrum of the final compound provided strong evidences for the formation of the SB. The ^{1}H-NMR spectrum of the starting compound was recorded a signal characteristic for the amino protons, as a singlet, at 5.73 ppm. The absence of this signal from the ^{1}H-NMR spectrum of the newly synthesized compound and the presence of a singlet characteristic to the N=CH proton at 9.52 ppm further confirmed the condensation between the 4-amino-5-(4-methyl-2-phenylthiazol-5-yl)-4H-1,2,4-triazole-3-thiol and the 3-bromo-phenyl-carbaldehyde. The ^{13}C-NMR spectrum of the newly synthesized compound was consistent with the proposed structure.

The aim of the present study was to evaluate the antibacterial and antifungal activity of a new SB as well as its ability to modulate oxidative stress.

The new thiazolyl SB exerted moderate to good antibacterial activity against tested strains (Tables 1–3). The inhibition of bacterial growth was more pronounced in Gram-negative bacteria, especially in Pseudomonas aeruginosa strain, where
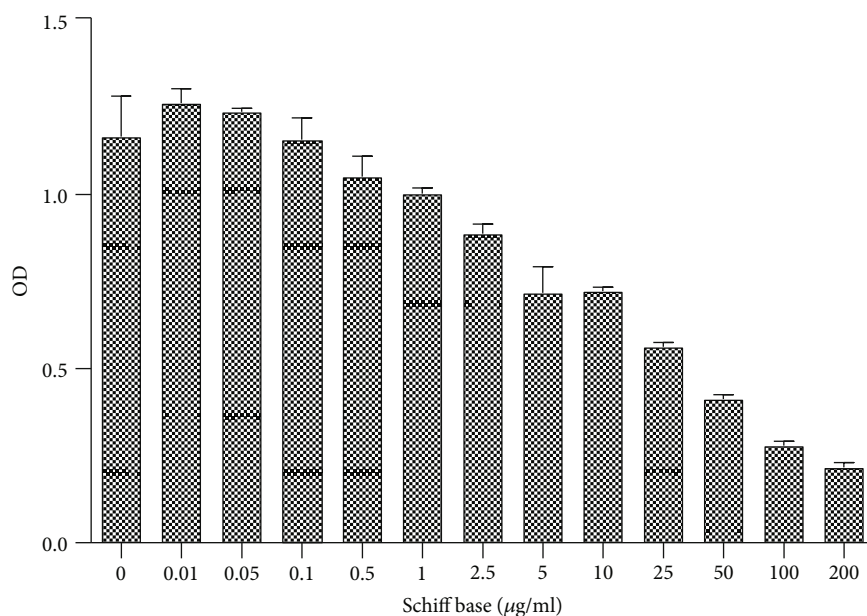
FIGURE 1: Cell viability testing. Schiff base (SB) was tested for multiple concentrations (0.01-200 μg/mL). Cell viability is presented as OD 540 nm (mean values ± standard deviation at 540 nm, $n = 3$).
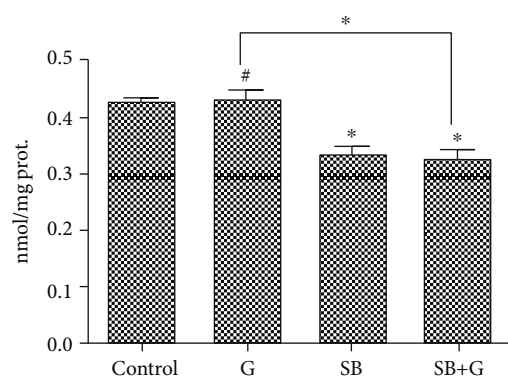
FIGURE 2: Lipid peroxidation levels (MDA) in endothelial cells exposed to medium (control), glucose (G), Schiff base (SB), and combination treatment (SB+G). Each bar represents the mean ± standard deviation ($n = 3$). #Not significant. *$p < 0.05$.
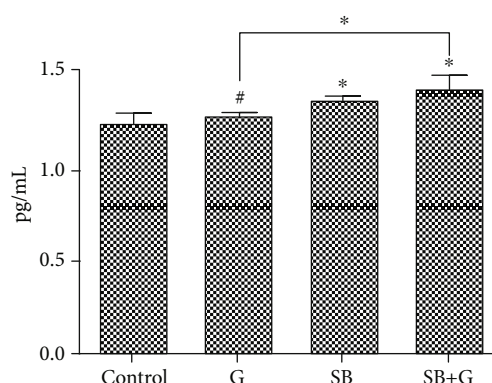
FIGURE 3: TNF-α levels in endothelial cells exposed to medium (control), glucose (G), Schiff base (SB), and combination treatment (SB+G). Each bar represents the mean ± standard deviation ($n = 3$). #Not significant. *$p < 0.05$.

the SB showed better activity compared with ciprofloxacin, used as the reference drug. Regarding antifungal activity, the compound showed a better anti-*Candida* effect than fluconazole, used as the reference drug. Previous studies showed that SBs have the ability to modulate oxidative stress [17, 39]. This ability can be exploited in order to use them as antibacterial drugs and/or as potential oxidative stress modulators in medicine. The SB was tested on endothelial cells exposed to a glucose-enriched environment.

High-carbohydrate intake, impaired glucose tolerance, and diabetes mellitus lead to hyperglycemia and chronic inflammatory status. Endothelial lesions are often involved in the pathology of these conditions [40]. During inflammatory episodes, such as response to injury, nitric oxide (NO) is released in order to modulate vascular tone. Since glycocalyx

plays an important role in transducing the fluid stress to the cytoskeleton of the endothelial cells, vasodilator substance production is stimulated [40–42]. High-glucose concentration increases oxidative stress and influences the structure of the cytoskeleton. Exposure to high-glucose hyperosmolar medium induces, using an AQP1-dependent mechanism, remodeling of the F-actin and cytoskeleton [43]. Our results are consistent with these findings (Figure 5). A high-glucose level led to mitochondrial dysfunction and increased production of ROS [44, 45].

A glucose-enriched environment also triggers the release of proinflammatory cytokines, such as tumor necrosis factor alpha (TNF-α), by the cells involved in immune reactions [46, 47], along with other proinflammatory molecules, such as CRP, interleukin 6, intercellular adhesion molecule 1, and VCAM-1. In diabetic patients, TNF-α was related with

(a)

(b)

(c)

(d)
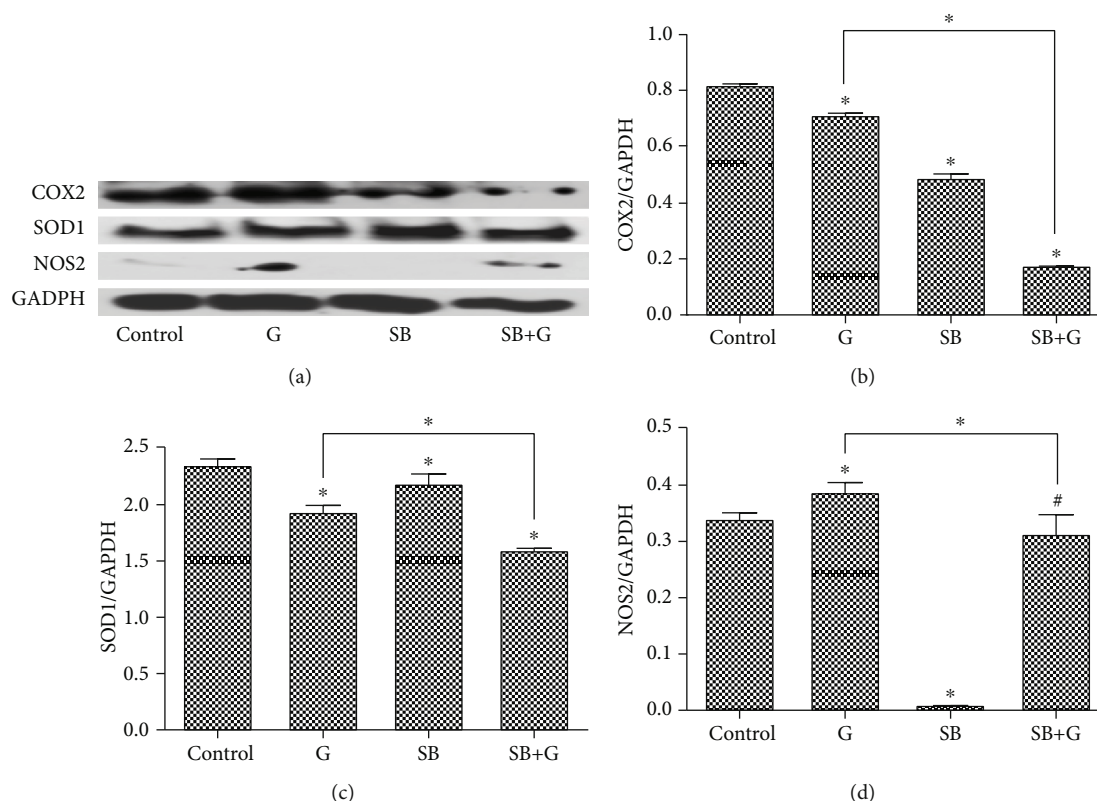
FIGURE 4: Protein levels of COX2, SOD1, and NOS2 in endothelial cells exposed to medium (control), glucose (G), Schiff base (SB), and combination treatment (SB+G). Comparative Western blot images showing expressions of COX2, SOD1, and NOS2 in HUVECs (b, c, d). Image analysis of Western blot bands (a) was performed by densitometry; results were normalized to GAPDH. Each bar represents the mean ± standard deviation ($n = 3$). #Not significant. *$p < 0.05$.

an atherogenic profile and with vascular complications [48]. A similar effect was obtained in our study, where higher levels of TNF-α were observed after hyperglycemia exposure. This effect was also seen after SB treatment and was augmented by the combined SB and high-glucose concentration. However, TNF-α production was negatively correlated with MDA and antioxidant enzymes (Table 5). This suggests that the increased TNF-α was not produced through enhanced oxidative stress, but through a different mechanism. Its clarification requires further studies. Since TNF-α acts as a promoter of leucocyte adhesion to the endothelium, the SB might be beneficial as antimicrobial, local immune response, and oxidative status modulator in the treatment of infectious diseases.

The results obtained by the DPPH study showed that the SB exhibited antioxidant activity. The low IC$_{50}$ value, similar to the positive control (BHT), reflects a strong antioxidant activity *in vitro*. The new compound showed radical scavenging activity according to the DPPH method, the presence of the -SH group being probably responsible of the radical scavenging activity [49–51]. The effect of the SB on the oxidative stress was also tested *in vitro* on cell cultures (HUVECs), by assessing the MDA level, a marker of lipid peroxidation and the expression of two enzymes involved in the oxidative equilibrium (SOD1 and NOS2). The results showed that, at the tested concentration (0.001 μg/mL), SB decreased lipid peroxidation (MDA) and the protein level of certain enzymes

TABLE 5: Spearman's coefficient of rank correlation (rho) between the oxidative stress and inflammation markers in HUVECs.

	MDA	TNF-α	COX2	SOD1	NOS2
MDA	1.00	-0.776**	0.699*	0.462	0.595*
TNF-α		1.00	-0.818**	-0.566	-0.455
COX2			1.00	0.755**	0.431
SOD1				1.00	-0.144
NOS2					1.00

*$p < 0.05$, **$p < 0.01$.

involved in the modulation of oxidative stress and inflammatory response (COX2 and NOS2). These changes are consistent with the DPPH result and suggest an anti-inflammatory effect of the tested SB, mostly by interfering with the prooxidant mediators.

The ability of the SB, in low concentrations, to decrease lipid peroxidation, might be explained by its capacity to form complexes with the bivalent and trivalent metal ions located in the active center of the enzymes involved in the onset of the oxidative stress or in the scavenging of the prooxidant molecules [52–57]. The antioxidant effect on the human cells (Figures 2 and 4) is also consistent with the absence of morphological changes of the cells observed in the present study (Figure 5).

(a)

(b)
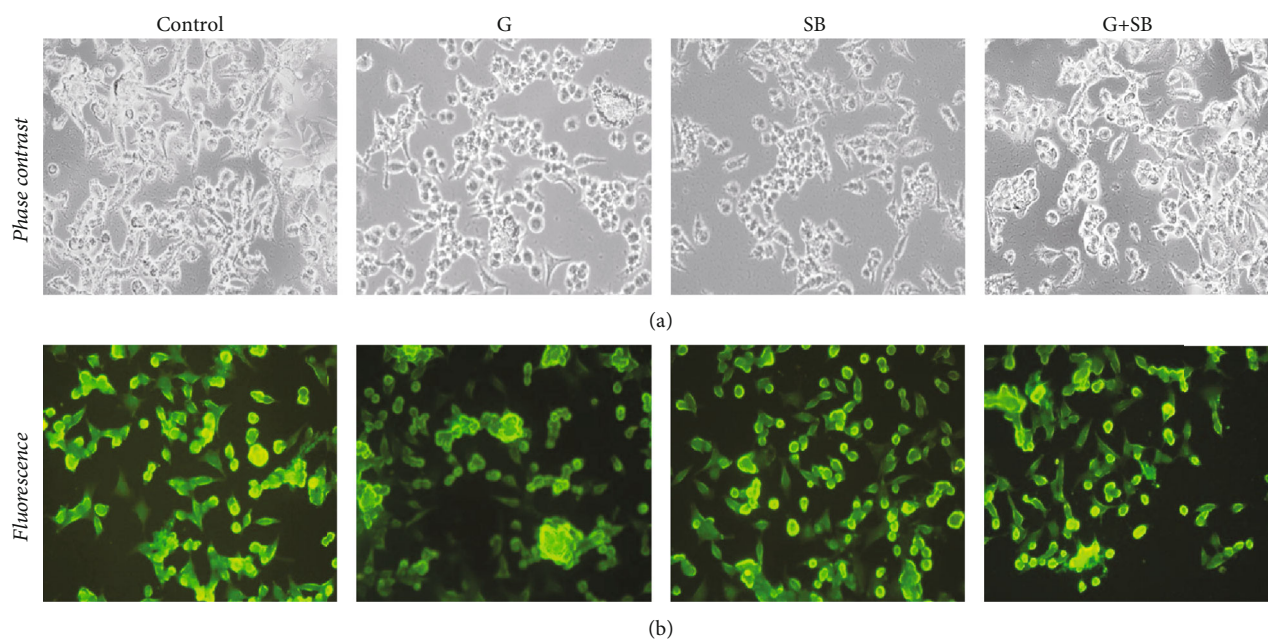
FIGURE 5: Images of HUVECs treated with medium (control), glucose (G), Schiff base (SB), and combination treatment (SB+G), stained with phalloidin-FITC; the same microscopic field is presented as phase contrast images (a) and fluorescence images (b) for comparison (pictures taken through an Olympus BX inverted microscope, original magnification 20x).

Considering antibacterial activity, especially against *Pseudomonas aeruginosa*, the decrease of the NOS2 protein level in HUVECs after SB exposure, it might be possible that the synthesis of NO by bacteria could also be reduced. One of the many proposed roles of NO in bacteria is to help protect the bacteria from host cell antibiotic-induced oxidative stress; therefore, the inhibition of bacterial nitric oxide synthase has been identified as a promising antibacterial strategy, especially for resistant bacteria [58].

Nitric oxide synthase (NOS) inhibitor NO-donating drugs were reported to inhibit IL-1β production, modulate PGE$_2$ production, and protect against apoptosis in human endothelial cells and human monocytes [59]. In type 2 diabetes, hyperglycemia stimulates endothelial cell migration in the retina, leading to retina neoangiogenesis and visual impairment by CXC receptor-4 stimulation and activation of the PI3K/Akt/eNOS signaling pathway. Therefore, SB modulation of the NOS2 might be beneficial for the endothelial dysfunction in hyperglycemia [60, 61].

Recent studies showed that the antibacterial and antifungal activity in general and antibiofilm activity of some newly identified classes seem to correlate with their ability to induce ROS synthesis [5]. The SB showed an anti-*Candida* effect, with a twofold increased activity compared with the consecrated antifungal fluconazole (Tables 2 and 3). Also, the results showed that SB reduced the SOD1 level and increased the activity of the proinflammatory cytokine (TNF-α). The antifungal effect could also be explained by the ability of the tested SB to form complexes between the azomethine group and the metal from the active center of the enzymes and also by its capacity to induce ROS production, similar with some antifungal azoles (e.g., miconazole) [5].

Additional studies are needed in order to clarify the effect of such compounds as SB and their role as adjuvant antioxidant, antimicrobial, and local immune response modulators (TNF-α) in the treatment of infectious diseases.

5. Conclusions

The new Schiff base exhibited antibacterial effects on both Gram-positive and Gram-negative bacteria, as well as antifungal activity against *Candida albicans*. The results of the present study show that the new SB plays a role in the prooxidant/antioxidant equilibrium. In the tested dose, SB does not change endothelial cell morphology, has an antioxidant effect, as demonstrated by the DPPH test, decreased lipid peroxidation (MDA), and decreased the inducible NOS2 level. Therefore, it can be considered a potential candidate with promising antioxidant properties that may be used as an adjuvant therapy in diseases caused by excessive free radical production. The decrease in COX2 and NOS2 levels also might suggest an anti-inflammatory action. A possible mechanism for the antibacterial activity on Gram-negative bacilli could include the decrease of the bacterial NOS level and the formation of complexes with metals located in the active center of certain bacterial enzymes. Also, the SB might potentially act as an antifungal agent, through ROS production in fungal biofilm cells. Its clarification requires further studies.

Data Availability

The data used to support the findings of this study are included within the article.

Conflicts of Interest

The authors declare that there is no conflict of interest regarding the publication of this paper.

Authors' Contributions

Cristian Cezar Login, Şoimiţa Suciu, Ioana Bâldea, and Brînduşa Tiperciuc conceived and planned the experimental design. Brînduşa Tiperciuc performed the chemical synthesis and the characterization of the compounds. Dan Cristian Vodnar performed the antibacterial and antifungal investigation. Daniela Benedec performed the *in vitro* assessment of the antioxidant activity. Ioana Bâldea performed the *in vitro* testing on cell cultures. Nicoleta Decea performed the biochemical assessment of some oxidative stress markers. Cristian Cezar Login and Ioana Bâldea performed the statistical analysis. Cristian Cezar Login, Ioana Bâldea, Brînduşa Tiperciuc, Daniela Benedec, and Şoimiţa Suciu analyzed the data and wrote the paper. Cristian Cezar Login, Brînduşa Tiperciuc, Ioana Bâldea, and Daniela Benedec equally contributed to this work.

Acknowledgments

References

[1] F. Aktan, "iNOS-mediated nitric oxide production and its regulation," *Life Sciences*, vol. 75, no. 6, pp. 639–653, 2004.

[2] W. Droge, "Free radicals in the physiological control of cell function," *Physiological Reviews*, vol. 82, no. 1, pp. 47–95, 2002.

[3] T. Fukai and M. Ushio-Fukai, "Superoxide dismutases: role in redox signaling, vascular function, and diseases," *Antioxidants & Redox Signaling*, vol. 15, no. 6, pp. 1583–1606, 2011.

[4] B. D. McCollister, M. Hoffman, M. Husain, and A. Vázquez-Torres, "Nitric oxide protects bacteria from aminoglycosides by blocking the energy-dependent phases of drug uptake," *Antimicrobial Agents and Chemotherapy*, vol. 55, no. 5, pp. 2189–2196, 2011.

[5] N. Delattin, B. P. Cammue, and K. Thevissen, "Reactive oxygen species-inducing antifungal agents and their activity against fungal biofilms," *Future Medicinal Chemistry*, vol. 6, no. 1, pp. 77–90, 2014.

[6] L. Balanean, C. Braicu, I. Berindan-Neagoe et al., "Synthesis of novel 2-metylamino-4-substituted-1,3-thiazoles with antiproliferative activity," *Revista de Chimie-Bucharest*, vol. 65, pp. 1413–1417, 2014.

[7] R. Tamaian, A. Moţ, R. Silaghi-Dumitrescu et al., "Study of the relationships between the structure, lipophilicity and biological activity of some thiazolyl-carbonyl-thiosemicarbazides and thiazolyl-azoles," *Molecules*, vol. 20, no. 12, pp. 22188–22201, 2015.

[8] Y. Ünver, K. Sancak, F. Çelik et al., "New thiophene-1,2,4-triazole-5(3)-ones: highly bioactive thiosemicarbazides, structures of Schiff bases and triazole-thiols," *European Journal of Medicinal Chemistry*, vol. 84, pp. 639–650, 2014.

[9] G. Y. Nagesh, K. Mahendra Raj, and B. H. M. Mruthyunjayaswamy, "Synthesis, characterization, thermal study and biological evaluation of Cu(II), Co(II), Ni(II) and Zn(II) complexes of Schiff base ligand containing thiazole moiety," *Journal of Molecular Structure*, vol. 1079, pp. 423–432, 2015.

[10] E. M. Zayed and M. A. Zayed, "Synthesis of novel Schiff's bases of highly potential biological activities and their structure investigation," *Spectrochimica Acta. Part A, Molecular and Biomolecular Spectroscopy*, vol. 143, pp. 81–90, 2015.

[11] K. P. Rakesh, H. M. Manukumar, and D. C. Gowda, "Schiff's bases of quinazolinone derivatives: synthesis and SAR studies of a novel series of potential anti-inflammatory and antioxidants," *Bioorganic & Medicinal Chemistry Letters*, vol. 25, no. 5, pp. 1072–1077, 2015.

[12] N. Parmar, S. Teraiya, R. Patel, H. Barad, H. Jajda, and V. Thakkar, "Synthesis, antimicrobial and antioxidant activities of some 5-pyrazolone based Schiff bases," *Journal of Saudi Chemical Society*, vol. 19, no. 1, pp. 36–41, 2015.

[13] M. Yıldız, Ö. Karpuz, C. T. Zeyrek et al., "Synthesis, biological activity, DNA binding and anion sensors, molecular structure and quantum chemical studies of a novel bidentate Schiff base derived from 3,5-bis(triflouromethyl)aniline and salicylaldehyde," *Journal of Molecular Structure*, vol. 1094, pp. 148–160, 2015.

[14] N. El-wakiel, M. El-keiy, and M. Gaber, "Synthesis, spectral, antitumor, antioxidant and antimicrobial studies on Cu(II), Ni(II) and Co(II) complexes of 4-[(1H-benzoimidazol-2-ylimino)-methyl]-benzene-1,3-diol," *Spectrochimica Acta. Part A, Molecular and Biomolecular Spectroscopy*, vol. 147, pp. 117–123, 2015.

[15] S. A. Al-Harbi, M. S. Bashandy, H. M. Al-Saidi, A. A. A. Emara, and T. A. A. Mousa, "Synthesis, spectroscopic properties, molecular docking, anti-colon cancer and anti-microbial studies of some novel metal complexes for 2-amino-4-phenylthiazole derivative," *Spectrochimica Acta. Part A, Molecular and Biomolecular Spectroscopy*, vol. 145, pp. 425–439, 2015.

[16] R. Selwin Joseyphus, C. Shiju, J. Joseph, C. Justin Dhanaraj, and D. Arish, "Synthesis and characterization of metal complexes of Schiff base ligand derived from imidazole-2-carboxaldehyde and 4-aminoantipyrine," *Spectrochimica Acta. Part A, Molecular and Biomolecular Spectroscopy*, vol. 133, pp. 149–155, 2014.

[17] N. Turan, M. F. Topçu, Z. Ergin et al., "Pro-oxidant and antiproliferative effects of the 1,3,4-thiadiazole-based Schiff base and its metal complexes," *Drug and Chemical Toxicology*, vol. 34, no. 4, pp. 369–378, 2011.

[18] S. Gupta, A. Roy, and B. S. Dwarakanath, "Metabolic cooperation and competition in the tumor microenvironment: implications for therapy," *Frontiers in Oncology*, vol. 7, p. 68, 2017.

[19] K. Zhao, D. Li, W. Xu et al., "Targeted hydroxyethyl starch prodrug for inhibiting the growth and metastasis of prostate cancer," *Biomaterials*, vol. 116, pp. 82–94, 2017.

[20] C. Nastasă, B. Tiperciuc, M. Duma, D. Benedec, and O. Oniga, "New hydrazones bearing thiazole scaffold: synthesis, characterization, antimicrobial, and antioxidant investigation," *Molecules*, vol. 20, no. 9, pp. 17325–17338, 2015.

[21] A. Stana, A. Enache, D. Vodnar et al., "New thiazolyl-triazole Schiff bases: synthesis and evaluation of the anti-Candida potential," *Molecules*, vol. 21, no. 11, p. 1595, 2016.

[22] C. Nastasă, D. Vodnar, I. Ionuţ et al., "Antibacterial evaluation and virtual screening of new thiazolyl-triazole Schiff bases as

potential DNA-gyrase inhibitors," *International Journal of Molecular Sciences*, vol. 19, no. 1, p. 222, 2018.

[23] A. Stana, D. Vodnar, R. Tamaian et al., "Design, synthesis and antifungal activity evaluation of new thiazolin-4-ones as potential lanosterol 14α-demethylase inhibitors," *International Journal of Molecular Sciences*, vol. 18, no. 1, p. 177, 2017.

[24] M. A. Hassan, A. M. Omer, E. Abbas, W. M. A. Baset, and T. M. Tamer, "Preparation, physicochemical characterization and antimicrobial activities of novel two phenolic chitosan Schiff base derivatives," *Scientific Reports*, vol. 8, no. 1, p. 11416, 2018.

[25] M. Krátký, M. Dzurková, J. Janoušek et al., "Sulfadiazine salicylaldehyde-based Schiff bases: synthesis, antimicrobial activity and cytotoxicity," *Molecules*, vol. 22, no. 9, p. 1573, 2017.

[26] C. T. Zeyrek, B. Boyacioğlu, M. Yıldız et al., "Synthesis, characterization, and evaluation of (E)-methyl 2-((2-oxonaphthalen-1(2H)-ylidene)methylamino)acetate as a biological agent and an anion sensor," *Bioorganic & Medicinal Chemistry*, vol. 24, no. 21, pp. 5592–5601, 2016.

[27] Y. Ünver, S. Deniz, F. Çelik, Z. Akar, M. Küçük, and K. Sancak, "Synthesis of new 1,2,4-triazole compounds containing Schiff and Mannich bases (morpholine) with antioxidant and antimicrobial activities," *Journal of Enzyme Inhibition and Medicinal Chemistry*, vol. 31, no. sup3, pp. 89–95, 2016.

[28] W. Yehye, N. Abdul Rahman, O. Saad et al., "Rational design and synthesis of new, high efficiency, multipotent Schiff base-1,2,4-triazole antioxidants bearing butylated hydroxytoluene moieties," *Molecules*, vol. 21, no. 7, p. 847, 2016.

[29] E. S. Lima, A. C. S. Pinto, K. L. Nogueira et al., "Stability and antioxidant activity of semi-synthetic derivatives of 4-nerolidylcatechol," *Molecules*, vol. 18, no. 1, pp. 178–189, 2013.

[30] D. Benedec, L. Vlase, I. Oniga et al., "Polyphenolic composition, antioxidant and antibacterial activities for two Romanian subspecies of Achillea distans Waldst. et Kit. ex Willd," *Molecules*, vol. 18, no. 8, pp. 8725–8739, 2013.

[31] I. Baldea, G. E. Costin, Y. Shellman et al., "Biphasic pro-melanogenic and pro-apoptotic effects of all-trans-retinoic acid (ATRA) on human melanocytes: time-course study," *Journal of Dermatological Science*, vol. 72, no. 2, pp. 168–176, 2013.

[32] I. Baldea, D. E. Olteanu, P. Bolfa et al., "Efficiency of photodynamic therapy on WM35 melanoma with synthetic porphyrins: role of chemical structure, intracellular targeting and antioxidant defense," *Journal of Photochemistry and Photobiology. B*, vol. 151, pp. 142–152, 2015.

[33] D. Tudor, I. Nenu, G. A. Filip et al., "Combined regimen of photodynamic therapy mediated by Gallium phthalocyanine chloride and metformin enhances anti-melanoma efficacy," *PLoS One*, vol. 12, no. 3, p. e0173241, 2017.

[34] M. L. Hu, "[41] Measurement of protein thiol groups and glutathione in plasma," *Methods in Enzymology*, vol. 233, pp. 380–385, 1994.

[35] A. Filip, D. Daicoviciu, S. Clichici, T. Mocan, A. Muresan, and I. D. Postescu, "Photoprotective effects of two natural products on ultraviolet B-induced oxidative stress and apoptosis in SKH-1 mouse skin," *Journal of Medicinal Food*, vol. 14, no. 7-8, pp. 761–766, 2011.

[36] J. Shen, M. Liu, J. Xu, B. Sun, H. Xu, and W. Zhang, "ARL15 overexpression attenuates high glucose-induced impairment of insulin signaling and oxidative stress in human umbilical

[37] R. Chibber, P. A. Molinatti, and E. M. Kohner, "Intracellular protein glycation in cultured retinal capillary pericytes and endothelial cells exposed to high-glucose concentration," *Cellular and Molecular Biology (Noisy-le-Grand, France)*, vol. 45, no. 1, pp. 47–57, 1999.

[38] R. J. Esper, J. O. Vilariño, R. A. Machado, and A. Paragano, "Endothelial dysfunction in normal and abnormal glucose metabolism," *Advances in Cardiology*, vol. 45, pp. 17–43, 2008.

[39] J. Joseph and G. B. Janaki, "Copper complexes bearing 2-aminobenzothiazole derivatives as potential antioxidant: synthesis, characterization," *Journal of Photochemistry and Photobiology. B*, vol. 162, pp. 86–92, 2016.

[40] N. W. Hansen, A. J. Hansen, and A. Sams, "The endothelial border to health: mechanistic evidence of the hyperglycemic culprit of inflammatory disease acceleration," *IUBMB Life*, vol. 69, no. 3, pp. 148–161, 2017.

[41] J. A. Florian, J. R. Kosky, K. Ainslie, Z. Pang, R. O. Dull, and J. M. Tarbell, "Heparan sulfate proteoglycan is a mechanosensor on endothelial cells," *Circulation Research*, vol. 93, no. 10, pp. e136–e142, 2003.

[42] S. Mochizuki, H. Vink, O. Hiramatsu et al., "Role of hyaluronic acid glycosaminoglycans in shear-induced endothelium-derived nitric oxide release," *American Journal of Physiology. Heart and Circulatory Physiology*, vol. 285, no. 2, pp. H722–H726, 2003.

[43] R. Madonna, Y. J. Geng, H. Shelat, P. Ferdinandy, and R. de Caterina, "High glucose-induced hyperosmolarity impacts proliferation, cytoskeleton remodeling and migration of human induced pluripotent stem cells via aquaporin-1," *Biochimica et Biophysica Acta*, vol. 1842, no. 11, pp. 2266–2275, 2014.

[44] W. Zhu, Y. Yuan, G. Liao et al., "Mesenchymal stem cells ameliorate hyperglycemia-induced endothelial injury through modulation of mitophagy," *Cell Death & Disease*, vol. 9, no. 8, p. 837, 2018.

[45] A. Pallag, G. A. Filip, D. Olteanu et al., "Equisetum arvense L. extract induces antibacterial activity and modulates oxidative stress, inflammation, and apoptosis in endothelial vascular cells exposed to hyperosmotic stress," *Oxidative Medicine and Cellular Longevity*, vol. 2018, 14 pages, 2018.

[46] R. D. Martinus and J. Goldsbury, "Endothelial TNF-α induction by Hsp60 secreted from THP-1 monocytes exposed to hyperglycaemic conditions," *Cell Stress & Chaperones*, vol. 23, no. 4, pp. 519–525, 2018.

[47] I. Castellano, P. di Tomo, N. di Pietro et al., "Anti-inflammatory activity of marine ovothiol A in an *in vitro* model of endothelial dysfunction induced by hyperglycemia," *Oxidative Medicine and Cellular Longevity*, vol. 2018, 12 pages, 2018.

[48] D. Tousoulis, N. Papageorgiou, E. Androulakis et al., "Diabetes mellitus-associated vascular impairment: novel circulating biomarkers and therapeutic approaches," *Journal of the American College of Cardiology*, vol. 62, no. 8, pp. 667–676, 2013.

[49] M. Kumar, T. Padmini, and K. Ponnuvel, "Synthesis, characterization and antioxidant activities of Schiff bases are of cholesterol," *Journal of Saudi Chemical Society*, vol. 21, pp. S322–S328, 2017.

[50] C. Aswathanarayanappa, E. Bheemappa, Y. D. Bodke, P. S. Krishnegowda, S. P. Venkata, and R. Ningegowda, "Synthesis and evaluation of antioxidant properties of novel 1,2,4-

triazole-based schiff base heterocycles," *Arch Pharm (Weinheim)*, vol. 346, no. 12, pp. 922–930, 2013.

[51] N. Revathi, M. Sankarganesh, J. Rajesh, and J. D. Raja, "Biologically active Cu(II), Co(II), Ni(II) and Zn(II) complexes of pyrimidine derivative Schiff base: DNA binding, antioxidant, antibacterial and in vitro anticancer studies," *Journal of Fluorescence*, vol. 27, no. 5, pp. 1801–1814, 2017.

[52] M. Hajrezaie, S. Golbabapour, P. Hassandarvish et al., "Acute toxicity and gastroprotection studies of a new schiff base derived copper (II) complex against ethanol-induced acute gastric lesions in rats," *PLoS One*, vol. 7, no. 12, p. e51537, 2012.

[53] V. A. Daier, E. Rivière, S. Mallet-Ladeira, D. M. Moreno, C. Hureau, and S. R. Signorella, "Synthesis, characterization and activity of imidazolate-bridged and Schiff-base dinuclear complexes as models of Cu,Zn-SOD. A comparative study," *Journal of Inorganic Biochemistry*, vol. 163, pp. 162–175, 2016.

[54] Q. Wei, J. Dong, P. Zhao et al., "DNA binding, BSA interaction and SOD activity of two new nickel(II) complexes with glutamine Schiff base ligands," *Journal of Photochemistry and Photobiology. B*, vol. 161, pp. 355–367, 2016.

[55] C. Palopoli, G. Gómez, A. Foi et al., "Dimerization, redox properties and antioxidant activity of two manganese(III) complexes of difluoro- and dichloro-substituted Schiff-base ligands," *Journal of Inorganic Biochemistry*, vol. 167, pp. 49–59, 2017.

[56] P. Zhao, S. Zhai, J. Dong et al., "Synthesis, structure, DNA interaction, and SOD activity of three nickel(II) complexes containing L-phenylalanine Schiff base and 1,10-phenanthroline," *Bioinorganic Chemistry and Applications*, vol. 2018, 16 pages, 2018.

[57] S. Maghraoui, S. Clichici, A. Ayadi et al., "Oxidative stress in blood and testicle of rat following intraperitoneal administration of aluminum and indium," *Acta Physiologica Hungarica*, vol. 101, no. 1, pp. 47–58, 2014.

[58] J. K. Holden, M. C. Lewis, M. A. Cinelli et al., "Targeting bacterial nitric oxide synthase with aminoquinoline-based inhibitors," *Biochemistry*, vol. 55, no. 39, pp. 5587–5594, 2016.

[59] J. N. Sharma, A. Al-Omran, and S. S. Parvathy, "Role of nitric oxide in inflammatory diseases," *Inflammopharmacology*, vol. 15, no. 6, pp. 252–259, 2007.

[60] M. Botta, E. Distrutti, A. Mencarelli et al., "Anti-inflammatory activity of a new class of nitric oxide synthase inhibitors that release nitric oxide," *ChemMedChem*, vol. 3, no. 10, pp. 1580–1588, 2008.

[61] S. Hamed, B. Brenner, Z. Abassi, A. Aharon, D. Daoud, and A. Roguin, "Hyperglycemia and oxidized-LDL exert a deleterious effect on endothelial progenitor cell migration in type 2 diabetes mellitus," *Thrombosis Research*, vol. 126, no. 3, pp. 166–174, 2010.

Hindawi

Research Article

Bovine Herpesvirus 1 Productive Infection Led to Inactivation of Nrf2 Signaling through Diverse Approaches

Xiaotian Fu,[1] Dongmei Chen,[2] Yan Ma,[3] Weifeng Yuan,[4] and Liqian Zhu [1]

[1]College of Veterinary Medicine, Yangzhou University and Jiangsu Co-Innovation Center for Prevention and Control of Important Animal Infectious Diseases and Zoonoses, Yangzhou 225009, China
[2]Laboratory Animal Center, Chinese Center for Disease Control and Prevention, Beijing 102206, China
[3]Keck School of Medicine, University of Southern California, Los Angeles, CA 90033, USA
[4]Institute of Animal Sciences, Chinese Academy of Agricultural Sciences, Beijing 100193, China

Correspondence should be addressed to Liqian Zhu; lzhu3596@163.com

Bovine herpesvirus type 1 (BoHV-1) is a significant cofactor for bovine respiratory disease complex (BRDC), the most important inflammatory disease in cattle. BoHV-1 infection in cell cultures induces overproduction of pathogenic reactive oxygen species (ROS) and the depletion of nuclear factor erythroid 2 p45-related factor 2 (Nrf2), a master transcriptional factor regulating a panel of antioxidant and cellular defense genes in response to oxidative stress. In this study, we reported that the virus productive infection in MDBK cells at the later stage significantly decreased the expression levels of heme oxygenase-1 (HO-1) and NAD(P)H quinone oxidoreductase-1 (NQO1) proteins, the canonical downstream targets regulated by Nrf2, inhibited Nrf2 acetylation, reduced the accumulation of Nrf2 proteins in the nucleus, and relocalized nuclear Nrf2 proteins to form dot-like staining patterns in confocal microscope assay. The differential expression of Kelch-like ECH associated protein 1 (KEAP1) and DJ-1 proteins as well as the decreased association between KEAP1 and DJ-1 promoted Nrf2 degradation through the ubiquitin proteasome pathway. These data indicated that the BoHV-1 infection may significantly suppress the Nrf2 signaling pathway. Moreover, we found that there was an association between Nrf2 and LaminA/C, H3K9ac, and H3K18ac, and the binding ratios were altered following the virus infection. Taken together, for the first time, we provided evidence showing that BoHV-1 infection inhibited the Nrf2 signaling pathway by complicated mechanisms including promoting Nrf2 degradation, relocalization of nuclear Nrf2, and inhibition of Nrf2 acetylation.

1. Introduction

Bovine herpesvirus type 1 (BoHV-1) belongs to the family *Herpesviridae* and the subfamily *Alphaherpesvirinae*. As an important pathogen for cattle of all ages and breeds, the virus infection causes diverse clinical symptoms, such as inflammation in the upper respiratory tract and reproductive system [1]. The erosion of mucosal surfaces and disruption of immune protection attributed to the virus infection may lead to a secondary infection, which consequently leads to a disease known as bovine respiratory disease complex (BRDC), the most important disease in cattle [2, 3]. Therefore, BoHV-1 is regarded as a critical cofactor for

BRDC development. The virus infection as well as the virus-induced BRDC causes great economic loss to the cattle industry worldwide [3].

Under physiological conditions, the production of reactive oxidative species (ROS) [4], such as hydrogen peroxide (H_2O_2), peroxynitrite ($OONO^-$), and hydroxyl radicals ($OH^.$), is tightly controlled by both intracellular enzymatic and nonenzymatic antioxidants responsible for ROS neutralization and removal. Therefore, ROS are generated and maintained at relatively low levels and act as second messengers to regulate diverse biological processes, such as gene expression, cell proliferation, and differentiation [5–8]. However, the overproduction of ROS induced by various factors,

including virus infection, can result in pathogenic oxidative stress [9, 10]. Accumulating studies have indicated that excessive ROS play important roles in the pathogenesis of inflammatory diseases. For example, ROS contribute to virus replication and the activation of inflammatory cytokines during the infection of both influenza virus and HSV-1 [6, 7, 11, 12]; thereby, the inhibition of ROS production is regarded as a potential therapeutic approach against virus infection [13]. The overproduction of ROS in BoHV-1-infected cells has been demonstrated to enhance viral replication, mitochondrial dysfunction, and DNA damage [4, 14, 15]. It is well established that the redox-sensitive transcription factor, NF-E2-related factor 2 (Nrf2), and Nrf2 anti-oxidant response pathways provide the primary cellular defenses against the oxidative stress [16, 17]. We have recently reported that BoHV-1 infection in MDBK cells inhibited Nrf2 expression [18].

Under normal conditions, Nrf2 is constitutively expressed and remains inactive in the cytosol by binding to its inhibitor protein Kelch-like ECH-associated protein 1 (KEAP1) to form a complex, which promotes the degradation of Nrf2 via the ubiquitin proteasome pathway [19]. In response to oxidative or electrophilic stress, Nrf2 is released from the KEAP1 complex and translocates to the nucleus, where it forms a heterodimer with small Maf (musculoaponeurotic fibrosarcoma) (sMaf) protein and binds to the DNA at the site of the antioxidant response element (ARE) [20, 21]. ARE sequences are conserved regions in the promotors of antioxidant and detoxifying genes, such as heme oxygenase-1 (HO-1), NAD(P)H quinone oxidoreductase-1 (NQO1), glutamate cysteine ligase catalytic and regulatory subunits (GCLC and GCLM), glutathione S-transferase (GST), uridine diphosphate glucuronosyltransferase (UDPGT), superoxide dismutase (SOD), catalase (CAT), glucose 6 phosphate dehydrogenase (G6PD), and glutathione peroxidase-1 (GPx) [22–24]. Recently, multiple studies have shown that the Nrf2 signaling pathway can either be stimulated or be inactivated by diverse viruses, contributing to viral pathogenesis and disease progression [23, 25]. For example, Nrf2 signaling is stimulated by the infection of influenza virus, but is suppressed during RSV infection, and the Nrf2-deficient mice exhibit much stronger inflammatory responses following either virus infection [26–29]. It is evident that intact Nrf2 signaling is essential for protecting a host against virus infection, and the dysfunction of Nrf2 signaling is potentially involved in viral pathogenesis.

Though we have recently demonstrated that BoHV-1 infection destabilized Nrf2 protein expression [18], the status of Nrf2-regulated antioxidant signaling and the mechanisms underlying Nrf2 depletion in the virus-infected cells have yet to be determined. Here, for the first time, we demonstrated that the virus infection suppressed the Nrf2 signaling pathway through multiple approaches, including inhibiting of the Nrf2 accumulation in the nucleus, inducing the relocalization of nucleus Nrf2 to form dot-like structures and the deacetylation of nucleus Nrf2, and manipulating the DJ-1/KEAP1 complex to promote the degradation of Nrf2 via the ubiquitin proteasome pathway.

2. Materials and Methods

2.1. Cells and Virus.
MDBK cells were cultured in DMEM (Gibco BRL) containing 10% horse serum (HyClone Laboratories, Logan, UT, USA). BoHV-1 (Colorado1 stain) was propagated in MDBK cells. Aliquots of the virus stocks were tittered in MDBK cells and stored at −80°C.

2.2. Antibodies and Chemicals.
The following chemicals were used in this study: tert-Butyl hydroperoxide solution (tBHP) (Sigma, cat# 458139), MG132 (Sigma, cat# 474791-1), and Trolox (MedChemExpress, cat# HY-101445). The following antibodies were used in this study: Nrf2 rabbit polyclonal antibody (Abcam, cat# ab137550), LaminA/C mouse monoclonal antibody (Santa Cruz Biotechnology, cat# sc-376248), phospho-(Ser/Thr) Phe rabbit polyclonal antibody (Cell Signaling Technology, cat# 9631), HO-1 mouse monoclonal antibody (Enzo Life Sciences, cat# ADI-OSA-110-D), NQO1 rabbit polyclonal antibody (ABclonal, cat# A0047), DJ-1 (ABclonal, cat# A0201), KEAP1 (D6B12) rabbit monoclonal antibody (Cell Signaling Technology, cat# 8047), acetyl-Histone H3 (Lys9) rabbit monoclonal antibody (Cell Signaling Technology, cat# 9649), acetyl-Histone H3 (Lys18) rabbit monoclonal antibody (Cell Signaling Technology, cat# 13998), ubiquitin mouse monoclonal antibody (Cell Signaling Technology, cat# 3936), pan acetyl Lysine rabbit polyclonal antibody (ABclonal, cat# A2391), β-actin rabbit monoclonal antibody (Cell Signaling Technology, cat# 4970), Mouse Control IgG (ABclonal, cat# AC011), rabbit control IgG (ABclonal, cat# AC005), BoHV-1 VP16 rabbit polyclonal antibody (kindly provided by Prof. Vikram Misra at the University of Saskatchewan [30]), HRP- (horseradish peroxidase-) conjugated goat anti-mouse IgG (Cell Signaling Technology, cat# 7076), and goat anti-rabbit IgG (Cell Signaling Technology, cat# 7074).

2.3. Western Blot Analysis.
MDBK cells were seeded into 60 mm dishes and cultured overnight and subsequently were infected with BoHV-1 (MOI = 0.1) for 4, 8, 16, 24, 36, and 48 hours. Cell lysates were prepared using lysis buffer (1% Triton X-100, 50 mM sodium chloride, 1 mM EDTA, 1 mM EGTA, 20 mM sodium fluoride, 20 mM sodium pyrophosphate, 1 mM phenylmethylsulfonyl fluoride, 0.5 g/mL leupeptin, 1 mM benzamidine, and 1 mM sodium orthovanadate in 20 mM Tris-HCl, pH 8.0). After centrifugation at 13,000 rpm for 10 min at 4°C, the clarified supernatants were collected and boiled together with Laemmli sample buffer for 10 min, and the samples were then separated on 8% or 10% SDS-PAGE and proteins were transferred onto PVDF membranes (Bio-Rad, cat# 1620177). After blocking with 5% nonfat milk in PBS (pH, 6.8) for 1 hour (h) at room temperature, the membranes were incubated with primary antibodies diluted in 5% bovine serum albumin in PBS (pH, 6.8), overnight at 4°C. All the primary antibodies were diluted 1 : 1000 for Western blots unless indicated specifically. After extensive washing with PBST (0.1% Tween 20 in PBS, pH 6.8), the membranes were incubated with secondary antibodies (1 : 1000) of either anti-rabbit or anti-mouse for 1 hour at room temperature. After extensive

washing with PBST, the protein bands were developed using Clarity Western ECL Substrate (Bio-Rad, cat# 1705061). The band intensity was analyzed using software ImageJ.

To analyze the effects of chemicals on the expression of indicated proteins, MDBK cells in 60 mm dishes were pretreated with either solvent DMSO or the individual chemicals at indicated concentrations for 1 h; then the cells were infected with the virus (MOI = 0.1) for 24 h in the presence of the chemicals or DMSO solvent. The cell lysates prepared using the lysis buffer as described above were subjected to Western blot analysis.

2.4. Immunoprecipitation (IP) Assay. MDBK cells grown in 60 mm dishes were mock infected or infected with BoHV-1 (MOI = 0.1). At 24 h after infection, cells were lysed with 600 μL of RIPA buffer (1x PBS, 1% NP-40, 0.5% sodium deoxycholate, 0.1% SDS) supplemented with aforementioned protease inhibitors. The cell lysates were then clarified by centrifugation at 13,000 rpm for 10 minutes and incubated with Dynabeads protein A (Life Technologies, cat# 10001D), which have been precoated with primary antibodies by incubation for 1 h at room temperature with rotation. After overnight incubation at 4°C with rotation, the beads were collected with the help of a magnet (DynaMag™) (Life Technologies, cat# 12321D). After three washings with PBS (pH 6.8), the beads were boiled in SDS-loading buffer and Western blots were performed using the indicated antibodies.

2.5. Immunofluorescence Assay (IFA). MDBK cells seeded into 2-well chamber slides (Nunc Inc., IL, USA) were mock infected or infected with BoHV-1 (MOI = 0.1) for 24 h. Cells were fixed with 4% paraformaldehyde prepared in PBS (pH 7.4) for 10 min at room temperature, permeabilized with 0.25% Triton X-100 in PBS (pH 7.4) for 10 min at room temperature, and blocked with 1% BSA in PBST (PBS+ 0.1% Tween 20) for 1 h followed by the incubation with the antibody against Nrf2 (1 : 500 dilution) and/or LaminA/C (1 : 500) in 1% BSA in PBST for 12 h at 4°C. After three washings, the cells were incubated with Alexa Fluor 488®-conjugated goat anti-rabbit IgG (H+L) (Invitrogen, cat# A-11008, 1 : 500 dilution) and/or Alexa Fluor 633®-conjugated goat anti-mouse IgG (H+L) (Invitrogen, cat# A-21052, 1 : 500 dilution) for 1 h in the dark. After three washings, DAPI (4′,6-diamidino-2-phenylindole) staining was performed to visualize nuclei. Slides were covered with coverslips by using of antifade mounting medium (Electron Microscopy Sciences, cat# 50-247-04). Images were captured by using a confocal microscope (Leica).

2.6. Relative Quantification of mRNA by qRT-PCR. Total RNA was extracted from infected cells or uninfected control cells using a TRIzol LS reagent (Ambion, cat# 10296010) following the manufacturer's instructions. Freshly prepared total RNA (1 μg) was used as a template for the synthesis of first-strand cDNA with commercial random hexamer primers using Thermoscript™ RT-PCR system Kit (Invitrogen, cat# 11146-024) following the manufacturer's instructions. The cDNA products were then used as templates for

real-time quantitative PCR to measure mRNA levels of indicated genes with gene-specific primers. For these studies, we analyzed HO-1 (forward primer: 5′-CAGAAGATGTAGCC AGAGCA-3′ and reverse primer: 5′-CATAGGGCAAG CGGTCA-3′) [31], NQO1 (forward primer: 5′-TGTATG CCATGAACTTCAATCC-3′ and reverse primer: 5′-AGTC TCGGCAGGATACTGAAAG-3′) [31], Nrf2 (forward primer: 5′-TCCAGGCGGATTCTTTACCA-3′ and reverse primer: 5′-TGACGCACCTCCCATTTCTC-3′) [32], and GAPDH (forward primer: 5′-CCATGGAGAAGGCTGG GG-3′ and reverse primer: 5′-AAGTTGTCATGGATGA CC-3′) [25].

Analysis of glyceraldehyde-3-phosphate dehydrogenase (GAPDH) mRNA was used as an internal control. Real-time PCR was carried out using the ABI 7500 fast real-time system (Applied Biosystems, CA). The expression levels of the tested genes were normalized to that of the GAPDH gene. The relative mRNA level of each gene was calculated using the method ($2^{-\Delta\Delta CT}$) by a comparison to the control.

3. Results

3.1. BoHV-1 Infection Suppressed Nrf2 Signaling. We have recently reported that the steady-state protein levels of Nrf2 are significantly reduced during BoHV-1 productive infection at the later stage [18]; however, whether the Nrf2 signaling pathway is consequently inhibited remains unknown. In order to evaluate the activity of Nrf2 signaling, we first detected the protein levels of HO-1 and NQO1, the canonical downstream targets regulated by Nrf2 signaling. Our data indicated that the virus infection altered the protein expression of Nrf2, HO-1, and NQO1 with diverse kinetics prior to 16 h after infection (Figures 1(a), 1(c), 1(d), and 1(f)). But from 24 to 48 hours post infection (hpi), the protein levels of all three molecules were consistently reduced (Figures 1(a) and 1(c)–1(f)). Particularly at 36 and 48 hpi, HO-1 protein expression was reduced to a level barely detectable. Quantitative analysis indicated that at 24 hpi the expression levels of Nrf2, HO-1, and NQO1 proteins were reduced to 23.2%, 19.3%, and 39.2% relative to the control, respectively (Figure 1(f)). To validate the correlation between virus infection and these varied protein expressions, we performed cell proliferation assay following virus infection and detected the protein expression of viral protein VP16. As shown in Figure 1(b), the cell proliferation was significantly inhibited from 16 hpi and gradually decreased until 48 hpi, which correlated with the positive detection of viral protein VP16 from 16 to 48 hpi (Figures 1(a) and 1(e)). Therefore, the virus-productive infection kinetics supported the finding that the virus infection modulated the protein expression of Nrf2, HO-1, and NQO1. In addition, we found that at 24 hpi, but not at 16 hpi, the mRNA levels of Nrf2 and NQO1 were consistent with those at the protein level (Figures 1(f) and 1(g)). Since HO-1 and NQO1 proteins are widely used indicators of Nrf2 activity, these data suggest that BoHV-1 infection at a later stage suppresses the Nrf2 signaling pathway.

Mechanistically, the Nrf2 signaling can be affected by either a ROS-dependent or ROS-independent pathway

(a)

(b)

(c)

(d)

(e)

(f)

(g)
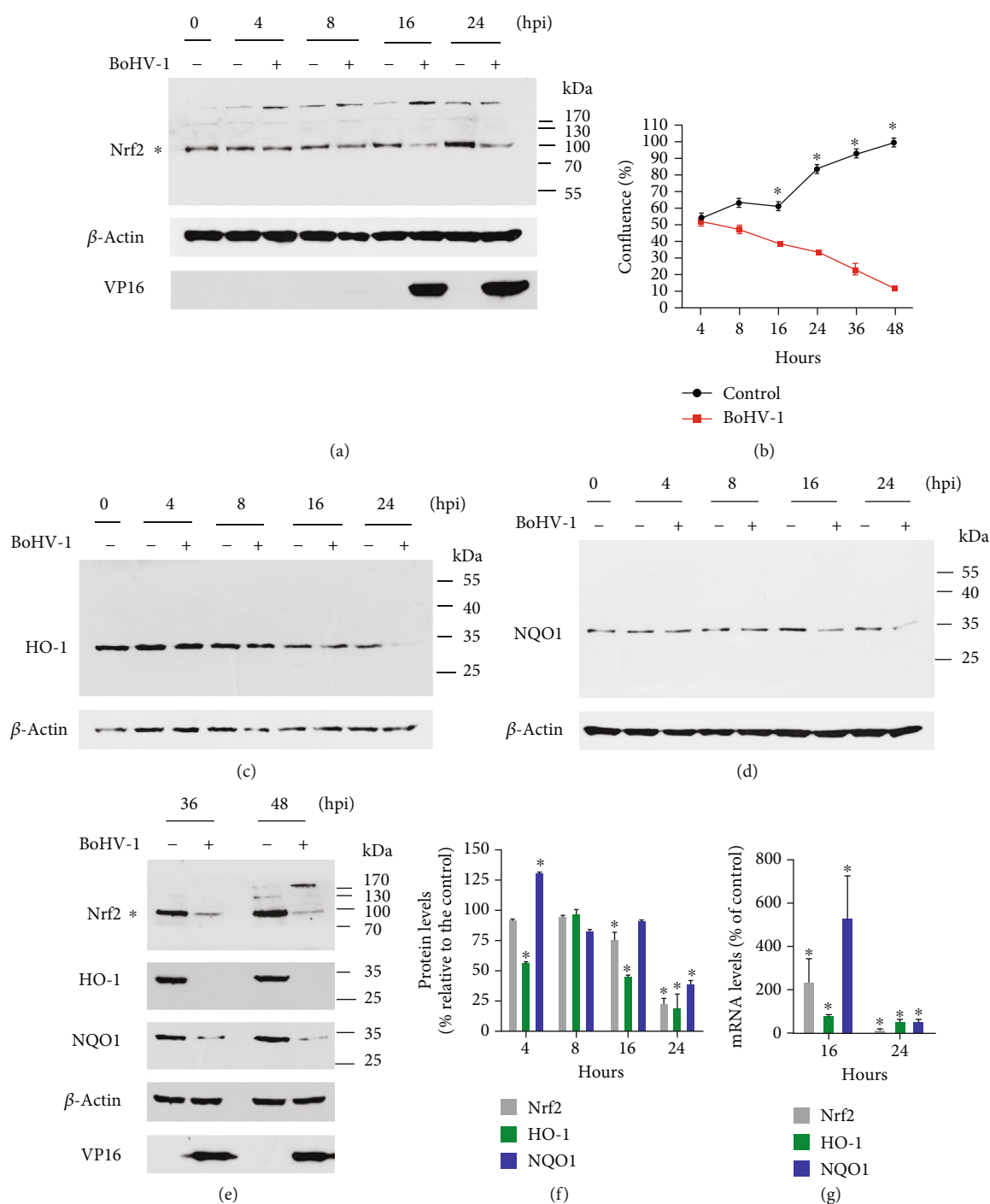
FIGURE 1: The effects of BoHV-1 infection on the expression of Nrf2-regulated downstream targets. (a, c, d, and e) MDBK cells in 60 mm dishes were mock infected or infected with BoHV-1 at an MOI of 0.1 for 4, 8, 16, 24, 36, and 48 h. The cell lysates were then prepared for Western blots to detect the expression of Nrf2, HO-1, NQO1, and VP16 using the Nrf2 antibody (Abcam, cat# ab137550, 1 : 500), HO-1 monoclonal antibody (mouse) (Enzo Life Sciences, cat# ADI-OSA-110-D, 1 : 1000), NQO1 polyclonal antibody (ABclonal, cat# A0047, 1 : 1000), and VP16 antibody (a gift from Prof. Vikram Misra at the University of Saskatchewan, 1 : 2000). (b) MDBK cells were seeded into 24-well plates. After overnight incubation, the cells were infected with BoHV-1 at an MOI of 0.1. After infection for 4, 8, 16, 24, 36, and 48 h, the cells were collected and cell numbers were counted using a Trypan-blue exclusion test. Data shown are representative of three independent experiments. (f) The band intensity was analyzed with software ImageJ. Each analysis was compared with that of uninfected control at each time point, which was arbitrarily set as 100%. These images are representative of those from three independent experiments. (g) Total RNA was prepared at 16 and 24 hpi in MDBK cells, and the mRNA levels of Nrf2, HO-1, and NQO1 were measured by qRT-PCR. Each analysis was compared with that of uninfected control, which was arbitrarily set as 100%. Data represent three independent experiments. The significance was assessed with Student's t-test ($^*P < 0.05$).

[33, 34]. Trolox, a chemical having strong capacity to neutralize intracellular ROS with minor off-target effects, has been widely used to study the interaction between ROS and Nrf2 signaling; e.g., it has been reported that Trolox contributes to Nrf2-mediated protection from injury by cigarette smoke in human and murine primary alveolar cells [35]. As expected, Trolox at a concentration of 1 and 2 mM showed no cytotoxicity to MDBK cells, but significantly reduced the virus production in a dose-dependent manner (Figures 2(i) and 2(j)). The treatment of virus-infected cells with 1 mM Trolox could partially restore Nrf2 depletion induced by virus infection albeit not to the initial level (Figures 2(a) and 2(d)). However, the Trolox treatment could not partially restore the depletion of either HO-1 or NQO1 protein at 24 hpi (Figures 2(b)–2(d)). We concluded that ROS may play a minor role in regulating Nrf2 signaling transduction during virus infection.

To confirm that the Trolox used in this study functioned properly, the effect of hydrogen peroxide (tBHP) on the activation of Nrf2 in the presence/absence of Trolox was examined. We found that either tBHP or Trolox along could stimulate the expression of both Nrf2 and HO-1 proteins, and the stimulatory effects of tBHP were further boosted by Trolox. However, neither of them had effects on the NQO1 protein expression in MDBK cells (Figures 2(e)–2(h)). These data confirmed that Trolox used in this study functioned as predicted, which validated its effects on the Nrf2 expression during virus infection.

3.2. BoHV-1 Infection Stimulated Nrf2 Degradation through the Ubiquitin Proteasome Pathway.

It has been reported that the degradation of Nrf2 protein through the ubiquitin proteasome pathway is regulated by either KEAP1-dependent or KEAP1-independent mechanisms [36]. To confirm that the ubiquitin proteasome pathway was involved in Nrf2 degradation in the virus-infected MDBK cells, the cells were exposed to proteasome inhibitor MG132 throughout viral infection as described previously [37]. We have reported that MG132 at a concentration of 1 μM had no cytotoxicity to MDBK cells [37]. The treatment of MG132 (1 μM) partially restored the Nrf2 depletion induced by the virus infection, and its protein level was increased to ~3.5-fold relative to the mock-treated infected control (Figures 3(a) and 3(b)), indicating that the ubiquitin proteasome pathway was potentially involved in the Nrf2 depletion in virus-infected cells. To provide direct evidence that Nrf2 was ubiquitinated, the lysates of either virus-infected or mock-infected cells were subjected to immunoprecipitation (IP) assay using the antibody against Nrf2; subsequently, the extents of ubiquitination of the Nrf2 protein were detected by immunoblots using the antibody against ubiquitin. To accurately determine the identity of the Nrf2 bands, both IP samples and whole cell extract (WCE) were loaded in the same gel spaced by a lane loaded by a protein ladder marker. The membrane was cut into two pieces along with the protein marker, and both ubiquitin and Nrf2 were incubated with an individual primary antibody, respectively. They were finally combined together and developed at the same time in parallel. So the

bands with molecular weights showing the same size as that in Nrf2 were regarded as the ubiquitinated Nrf2. As expected, the high levels of ubiquitin were detected in virus infected cell cultures (Figure 3(c)), which further confirmed that virus infection enhanced the ubiquitination levels of Nrf2. Collectively, these results suggested that the ubiquitin proteasome pathway was involved in the degradation of Nrf2 following virus infection.

KEAP1 is known to mediate the degradation of Nrf2 protein through the ubiquitin proteasome pathway. We then examined the effects of virus infection had on the expression of KEAP1 in MDBK cells. As shown in Figures 3(d) and 3(f), the protein levels of KEAP1 were consistently increased from 8 to 24 hpi. Particularly, it was increased approximately 4-fold at 24 hpi compared to the control. So the increased expression of KEAP1 protein may potentially contribute to Nrf2 degradation through the ubiquitin proteasome pathway.

DJ-1 can stabilize Nrf2 expression through preventing protein association between Nrf2 and KEAP1 [38, 39]. Our study demonstrated that the expression of DJ-1 protein was significantly reduced at 24 hpi (Figures 3(e) and 3(f)). Moreover, we found that virus infection destabilized the protein association between DJ-1 and KEAP1 (Figures 3(i) and 3(j)), which further supported the findings that virus infection promoted the ubiquitination of Nrf2 (Figure 3(c)). In addition, specific binding to DJ-1 by the antibody used in IP was confirmed (Figure 3(k)). It is reasonable to speculate that the reduced expression levels of DJ-1 protein result in the release of more KEAP1 from the KEAP1-DJ-1 complex, which consequently sequesters more cytosol Nrf2 and ultimately promotes Nrf2 degradation through the ubiquitin proteasome pathway. Taken together, these data implied that BoHV-1 infection promoted Nrf2 degradation partially through the regulation of the KEAP1 and DJ-1 complex.

In addition, the accumulation of DJ-1 protein in the nucleus was also inhibited at 24 hpi (Figure 3(g)). Quantitative analysis indicated that the protein levels of DJ-1 in the nucleus were decreased to ~12.15% in the virus-infected cells (at 24 hpi) relative to the mock-infected control (Figure 3(h)). It has been previously reported that nuclear translocation of DJ-1 protects neurons from cell death after oxidative stress [40]. Therefore, we speculated that the reduced accumulation of DJ-1 protein in the nucleus following virus infection is a potential pathogenic effect of the virus infection.

3.3. Virus Infection Relocalized Nuclear Nrf2 and Inhibited the Accumulation of Nrf2 Protein in the Nucleus.

To understand whether BoHV-1 infection influences the subcellular localization of Nrf2, an immunofluorescence assay (IFA) was performed at 24 hpi. Interestingly, in mock-infected MDBK cells, Nrf2 was predominantly detected in the nucleus but not in the cytosol (Figure 4(a)). Similarly, in the virus-infected cells, Nrf2 was mainly present in the nucleus rather than in the cytosol, either (Figure 4(b)). These findings were not in line with the canonical model that Nrf2 is mainly inactivated and sequestered by KEAP1 in the cytosol, in unstressed conditions, and once stimulated, it is translocated
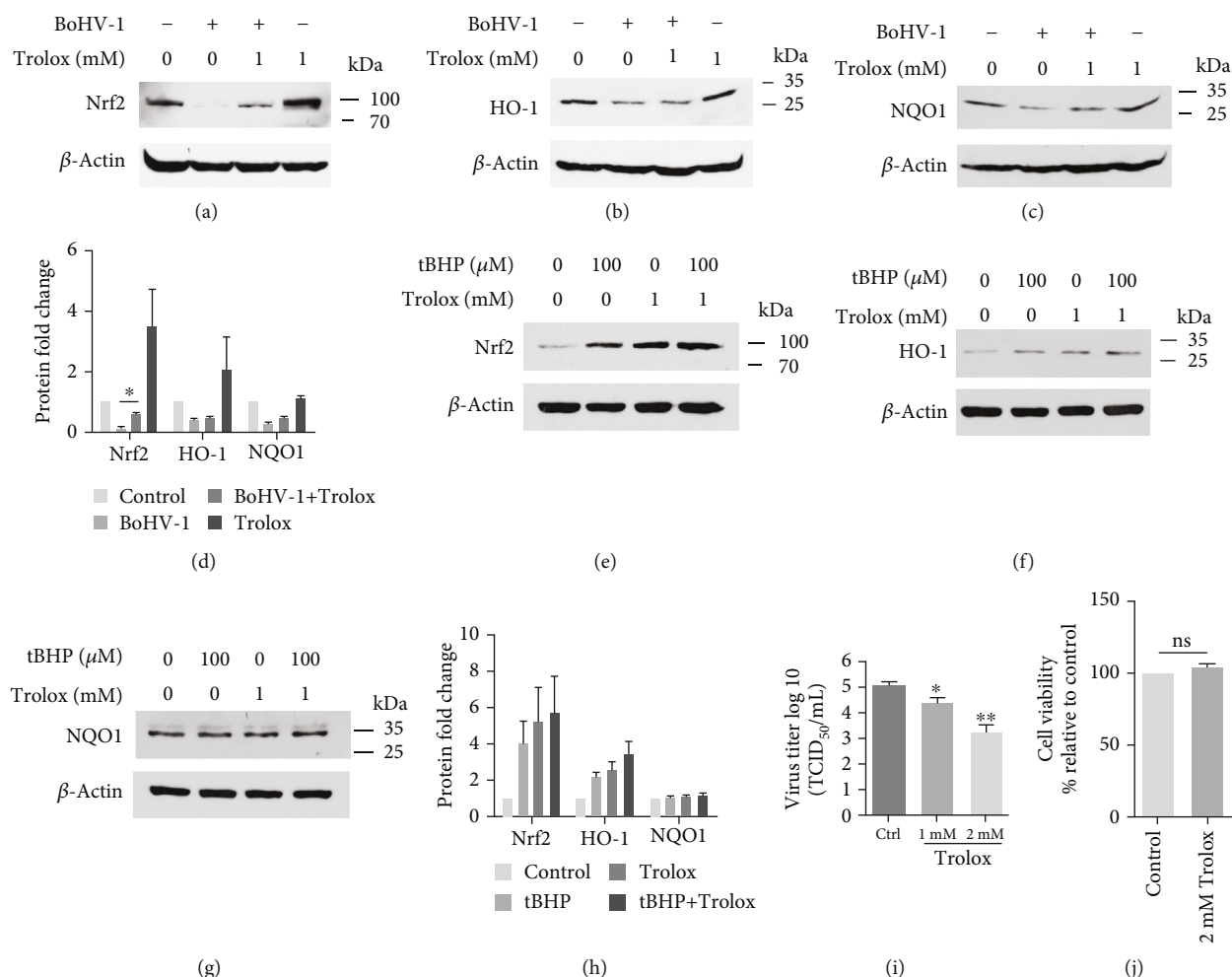
Figure 2: The effects of Trolox on the expression of Nrf2 and its downstream targets. (a, b, and c) MDBK cells in 60 mm dishes pretreated with Trolox (1 mM) or DMSO control for 1 h were infected with BoHV-1 (MOI = 0.1); in the presence of Trolox or DMSO control for 24 h, the cell lysates were prepared for Western blots to detect the expression of Nrf2 (a), HO-1 (b), and NQO1 (c). (e, f, and g) MDBK cells in 60 mm dishes pretreated with Trolox (1 mM) or DMSO control for 1 h were exposed to tBHP in the presence of Trolox or DMSO control for 2 h; the cell lysates were prepared for Western blots to detect the expression of Nrf2 (e), HO-1 (f), and NQO1 (g). (d and h) The relative band intensity was analyzed with software ImageJ, and each analysis was compared with that of uninfected control at each time point, which was arbitrarily set as 100%. Data shown are representative of three independent experiments. (i) MDBK cells in 24-well plates pretreated with Trolox at indicated concentrations or MDSO control were infected with BoHV-1 (MOI = 0.1) for 24 hours in the presence of an inhibitor or DMSO. The cell cultures were subjected to frozen-thawing twice, and viral yield was determined with the results being expressed as $TCID_{50}/mL$. (j) The cytotoxicity of Trolox in MDBK cells for 24 h was analyzed by Trypan-blue exclusion. The significance was assessed with Student's t-test ($^*P < 0.05$).

into the nucleus [36]. Of note, the virus infection destabilized Nrf2 protein steady-state expression (Figure 1(a)), so in the confocal microscopy, longer exposure time was required to detect the presence of Nrf2 protein in the virus-infected cells relative to that in the uninfected control; thus, one cannot compare Nrf2 levels between these IFA images. Our results suggested that in MDBK cells Nrf2 was mainly located in the nucleus. To examine whether Nrf2 protein in MDBK cells is active prior to viral infection, the cells were treated with Trolox; both cytoplasmic and nuclear proteins were extracted for the detection of Nrf2 proteins. As shown in Figure 5(c), the expressions of Nrf2 protein from both cytosol and nuclear fractions were significantly increased in comparison to those in the mock-treated controls (Figure 5(c)), suggest-

ing that Nrf2 was readily activated by Trolox in cell culture. Thus, these data indicated that MDBK cells used in this study were not in an activated status, which validated our novel findings that Nrf2 was mainly distributed in the nucleus rather than in the cytosol in either mock or infection contexts.

Interestingly, immunofluorescence revealed a dot-like staining pattern for nuclear Nrf2 in the virus-infected cells (Figures 4(b) and 4(c)). Following viral infection, approximately 74.5% of the cells exhibited a dot-like staining pattern in the nucleus while in mock infection control only ~4.1% of the cells show faint dot-like staining (Figure 4(d)), suggesting that virus infection led to the relocalization of Nrf2 in the nucleus.

(a)

(b)

(c)

(d)

(e)

(f)

(g)

(h)

(i)

(j)

(k)
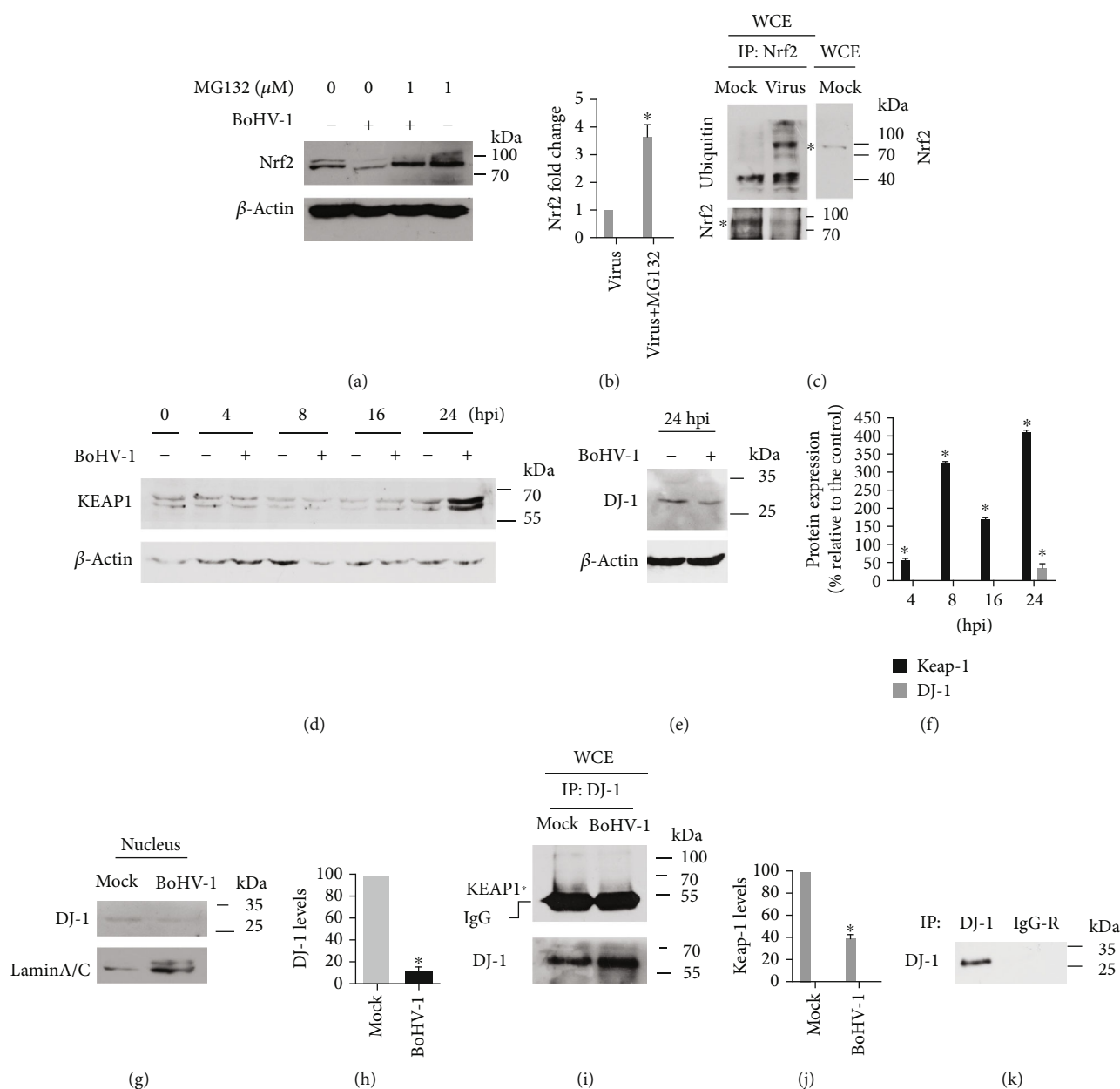
FIGURE 3: BoHV-1 infection promoted Nrf2 depletion through a proteasome pathway. (a, c, and i) MDBK cells in 60 mm dishes were infected with BoHV-1 at an MOI of 0.1 in the presence of MG132 (1 μM) or DMSO control. After infection for 24 h, the cell lysates were prepared for Western blotting to detect the expression of Nrf2 (a) or were prepared for IP using antibodies against Nrf2 (c), DJ-1 (d), and unrelated IgG (k). The IP samples were subjected to immunoblots using antibodies against ubiquitin (Cell Signaling Technology, cat# 3936, 1 : 1000) and Nrf2 (Abcam, cat# ab137550, 1 : 500), respectively. (d and e) MDBK cells in 60 mm dishes were mock infected or infected with BoHV-1 (MOI = 0.1) for an indicated time length. The cell lysates were then prepared for Western blots to detect the expression of KEAP1 and DJ-1 using antibodies against KEAP1 mAb (Cell Signaling Technology, cat# 8047, 1 : 1000) and DJ-1 (ABclonal, cat# A0201, 1 : 1000), respectively. Data shown are representative of three independent experiments. (f, h, and j) The band intensity was analyzed with software ImageJ. Each analysis was compared with that of control, which was arbitrarily set as 100%. These images are representative of those from three independent experiments. The significance was assessed with Student's t-test ($^{*}P < 0.05$). (g) MDBK cells in 60 mm dishes were mock infected or infected with BoHV-1 (MOI = 0.1) for 24 hpi. Then, the nuclear proteins were prepared using a commercial kit, and the levels of protein DJ-1 were detected by immunoblots. Data shown are representative of three independent experiments. WCE: whole cell extract.

Nuclear translocation of Nrf2 protein is essential for subsequent transactivation of its downstream target genes. Therefore, the accumulation of Nrf2 in the nucleus is a canonical indicator of Nrf2 activation. To test whether BoHV-1 productive infection altered Nrf2 nuclear accumula-

tion, MDBK cells were mock infected or infected for 24 h; nuclear proteins were purified by using a commercial kit. As a result, there was a significant decrease of the nuclear Nrf2 protein level in the virus-infected cells, relative to that in mock-infected control (Figure 5(a)). A further study

(a)

(b)

(c)

(d)
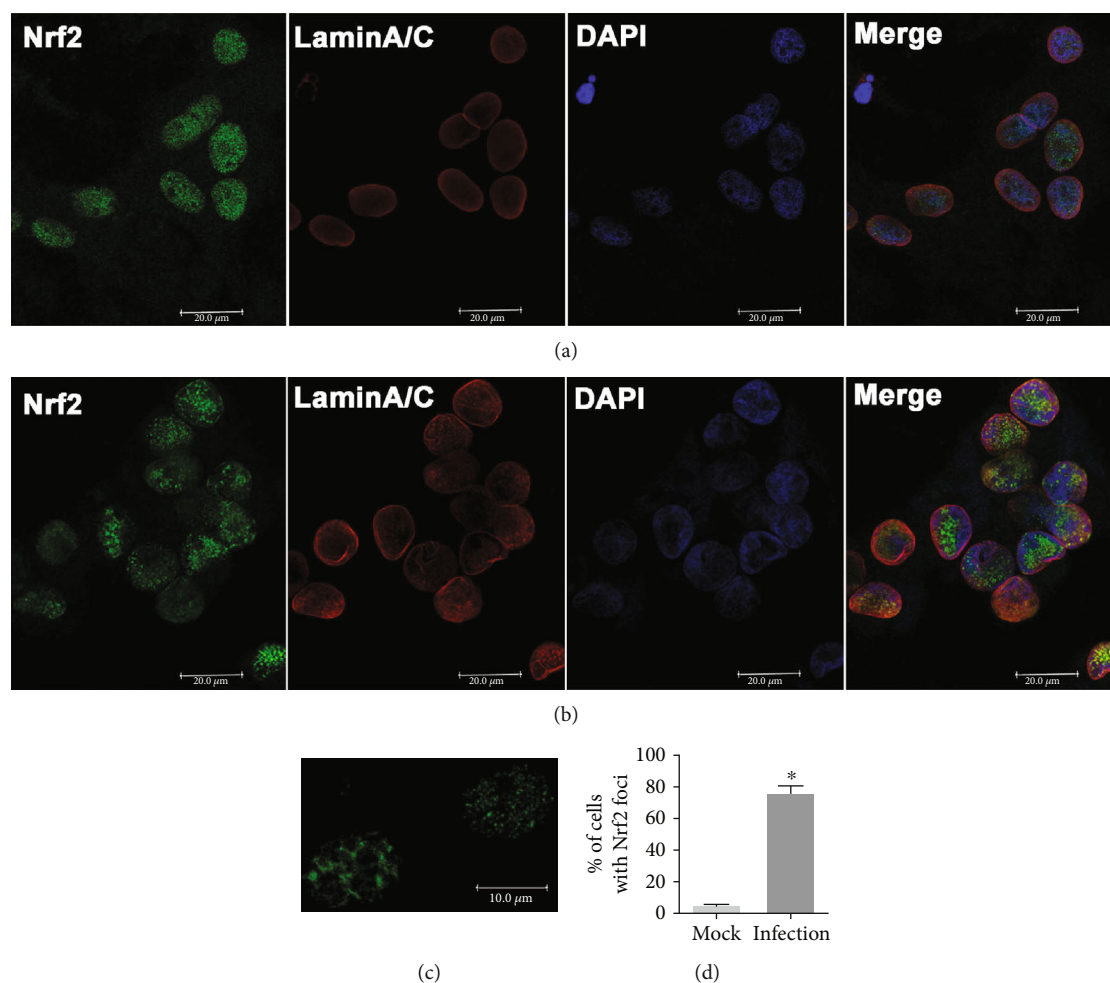
FIGURE 4: BoHV-1 infection altered the localization of nuclear Nrf2 protein. MDBK cells in 2-well chamber slides were mock infected (a) or infected with BoHV-1 (MOI = 0.1) (b) for 24 hours. After three washings with PBS, cells were fixed with 4% formaldehyde, and Nrf2 was detected by IFA using the Nrf2 antibody (1 : 500) and LaminA/C antibody (1 : 500). DAPI staining was used to stain nuclear DNA. Images were obtained by performing confocal microscopy (Leica). These images are representative of three independent experiments. (c) Zoom-in cells showing typical dot-like staining. (d) The percentage of dot-like staining-positive cells among ~400 cells was estimated from photos derived from three independent experiments. Scale bar: 200 μM.

confirmed that the nucleus protein extraction was not contaminated by cytosol protein (Figure 5(b)), which validated the finding that the virus infection inhibited the accumulation of Nrf2 protein in the nucleus.

3.4. BoHV-1 Infection Inhibited the Acetylation of Nuclear Nrf2 Protein.

Posttranslational modification, such as by acetylation and phosphorylation, is known to regulate Nrf2 transcriptional activity [41, 42]. It has been documented that the phosphorylation and acetylation of Nrf2 are critical for the nuclear translocation and transcriptional activation [43, 44]. Therefore, the effects of virus infection on the phosphorylation and acetylation of Nrf2 were further investigated. For this purpose, Nrf2 was precipitated from either nuclear protein extract or whole cell extract, and the levels of either phosphorylated or acetylated Nrf2 protein were detected by Western blot using antibodies against phospho-(Ser/Thr) Phe and acetyl Lysine, respectively. As shown in Figures 6(a) and 6(b), the expression levels of phosphorylated Nrf2 from either whole cell or nuclear extract were increased upon virus infection. Compared to the mock-infected control, the level of phosphorylated Nrf2 protein from whole cell and nuclear extract was increased to 136.1% and 223.7% at 24 hpi, respectively (Figures 6(a) and 6(b)). Therefore, the virus infection enhanced the phosphorylation of Nrf2 proteins, particularly of those located in the nucleus.

Virus infection at 24 hpi significantly decreased the acetylation levels of the nucleus Nrf2 protein, which was reduced to ~60.7% relative to that in the mock-infected control (Figure 6(c)), which is in consistent with our findings that virus infection inhibited the accumulation of Nrf2 in the nucleus (Figure 5), and depressed the expression of HO-1 and NQO1 (Figures 1(c), 1(d), and 1(f)). Interestingly, the acetylated Nrf2 from the whole cell extract was not readily detected in either mock-infected or virus-infected cell cultures (Figure 6(d)). We speculated that the acetylated Nrf2 protein mainly accumulates in the nucleus because the
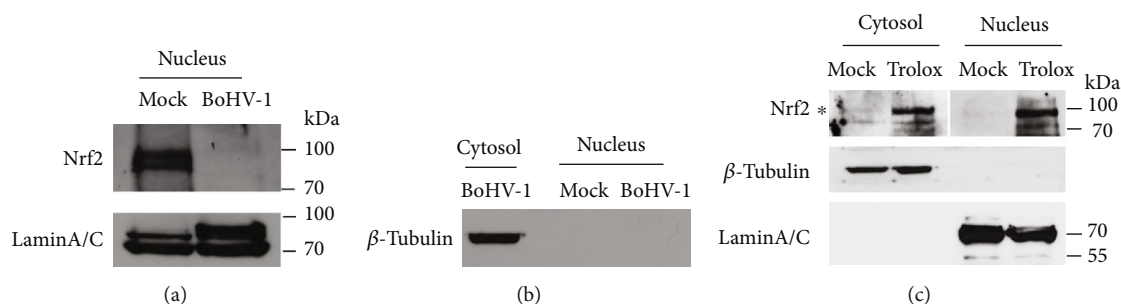
Figure 5: BoHV-1 infection altered the accumulation of Nrf2 in the nucleus. (a) MDBK cells in 60 mm dishes were mock infected or infected with BoHV-1 (MOI = 0.1) for 24 h, the cell cultures were collected for extracting nuclear proteins using commercial nuclear protein purification kit (Beyotime Biotechnology, cat# P0027). Nrf2 was detected by Western blot using the antibody against Nrf2 (Abcam, cat# ab137550). LaminA/C was detected and used as protein loading control. (b) Protein fractions of both the cytosol and nucleus were subjected to Western blots using the antibody against β-tubulin. (c) MDBK cells in 60 mm dishes were mock treated or treated with Trolox (1 mM) for 2 h; the cell lysates were collected for the purification of nuclear proteins and cytosol proteins using commercial nuclear protein purification kit (Beyotime Biotechnology, cat# P0027). Nrf2 was detected by Western blot using the antibody against Nrf2 (Abcam, cat# ab137550). LaminA/C and β-tubulin were detected to characterize whether each fraction was contaminated. These images are representative of three independent experiments.
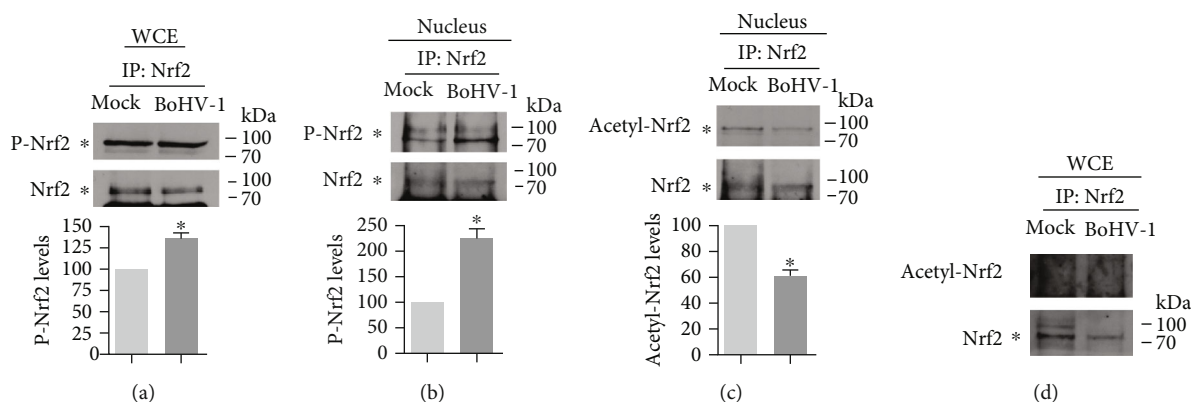
Figure 6: The posttranslational modification of Nrf2 stimulated by virus infection. MDBK cells in 60 mm dishes were mock infected or infected with BoHV-1 (MOI = 0.1) for 24 h; the cell cultures were collected to produce whole cell lysates (a and d) or to extract nuclear proteins using commercial nuclear protein purification kit (Beyotime Biotechnology, cat# P0027) (b and c). IP was performed using the antibody against Nrf2 (Abcam, cat# ab137550). Then, levels of phospho-Nrf2 in whole cell extracts (WCE) (a) and the nucleus (b) and acetylation levels of Nrf2 in the nucleus (c) and WCE (d) were detected by immunoblots using the antibody against the Nrf2 antibody (Abcam, cat# ab1375501:500), acetyl Lysine antibody (ABclonal, cat# A2391, 1 : 1000), and phospho-(Ser/Thr) Phe antibody (Cell Signaling Technology, cat# 9631, 1 : 1000). Data shown are representative of three independent experiments. The significance was assessed with Student's t-test ($^*P < 0.05$).

acetylation of Nrf2 increases its transcriptional activity and nucleus localization, whereas the deacetylation leads to Nrf2 nuclear export [42]. Taken together, BoHV-1 infection inhibited Nrf2 acetylation, further supporting our hypothesis that BoHV-1 infection inactivates the Nrf2 signaling pathway.

3.5. BoHV-1 Infection Altered the Association Ratio between Nrf2 and LaminA/C. To better understand how the virus infection relocalizes Nrf2, the antibody against LaminA/C was used for specific staining of the nuclear membrane. We found that nuclear Nrf2 proteins partially colocalized with LaminA/C in the virus-infected cells (Figure 4(b)). We speculated that Nrf2 was associated with LaminA/C. To address this issue, nuclear proteins were extracted from either mock-infected or virus-infected MDBK cells, which were then subjected to IP assay using antibodies against

either Nrf2 or LaminA/C. As a result, when the antibody against Nrf2 was used in the IP, much more LaminA/C was precipitated in the virus-infected cells (Figure 7(a)). While when IP was performed using the antibody against LaminA/C, less Nrf2 was precipitated in the virus-infected cells (Figure 7(b)). Based on these results, we assumed that if the ratio between Nrf2 and LaminA/C was arbitrarily set as 1 (Nrf2 : LaminA/C = 1) in the control, the ratio would be less than 1 (Nrf2 : LaminA/C < 1) in the virus-infected cells, suggesting that the virus infection reduced the association ratio between Nrf2 and LaminA/C. Unrelated IgG was included to do IP, which confirmed that both antibodies can be used for IP and validated that the target proteins can be specifically precipitated (Figures 7(c) and 7(d)). This was an interesting finding which needs extensive study to reveal the biological functions for this association in the future.
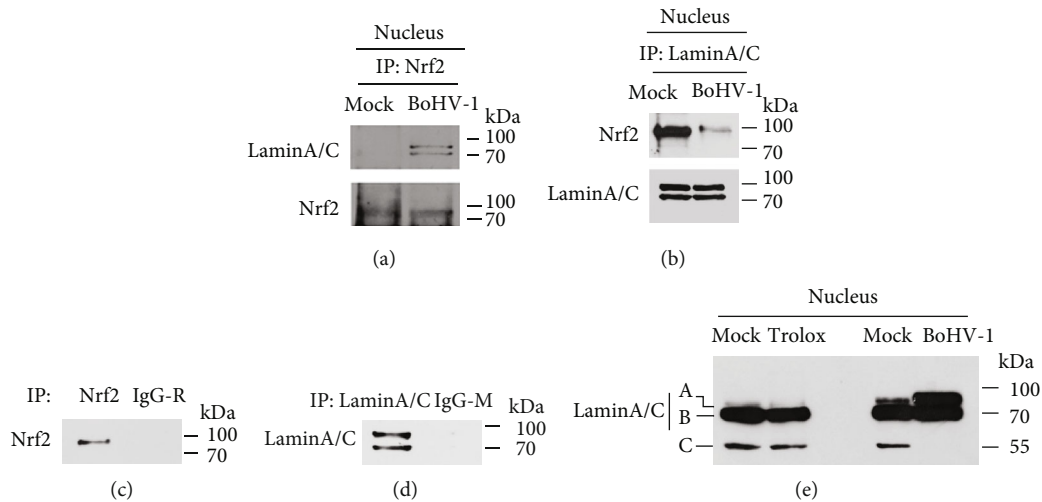
FIGURE 7: BoHV-1 affected the association between Nrf2 and LaminA/C. MDBK cells in 60 mm dishes were mock infected or infected with BoHV-1 for 24 h. Nucleus proteins were purified using commercial nuclear protein purification kit (Beyotime Biotechnology, cat# P0027). IP was performed using antibodies against Nrf2 (a), LaminA/C (b), Nrf2 and unrelated IgG (c), and LaminA/C and IgG (d) (R: rabbit; M: mouse). Then, Western blots were performed using corresponding antibodies. (e) MDBK cells in 60 mm dishes were mock treated or treated with Trolox (1 mM) for 2 h. Nucleus proteins were purified using commercial nuclear protein purification kit (Beyotime Biotechnology, cat# P0027), and LaminA/C was detected by Western blots.

The LaminA/C antibody recognizes two bands with molecular weights ranging from 65 to 70 kDa. In this study, we found that this monoclonal antibody recognized three bands which were denoted by A, B, and C in Figure 7(e), when the samples from either mock treated or treated with Trolox were applied for Western blots. However, when the samples from the virus-infected cells were applied for Western blots, band C disappeared, but the intensity of band A increased, which was largely different from that in the control. This finding indicated that BoHV-1 infection altered the LaminA/C expression pattern. Since LaminA/C is associated with Nrf2, it was reasonable to speculate that the altered expression manners of LaminA/C would affect Nrf2 relocalization in the nucleus.

3.6. BoHV-1 Infection Altered the Association Ratio between Nrf2 and H3K9ac/H3K18ac. In eukaryotes, DNA is packaged into a protein-DNA complex called chromatin. Histone H3, an important component of chromatin, can regulate the activity of chromatin through diverse epigenetic modifications, such as acetylation and phosphorylation. The acetylation of certain lysine (K) residues such as K9 and K18 in histone H3 is an indicator of transcriptionally active chromatin [45]. Whether histones, such as H3K9ac and H3K18ac, are associated with Nrf2 is currently known. To further understand how the virus infection relocalizes nuclear Nrf2, the association between Nrf2 and the acetylated H3 including H3K9ac and H3K18ac was detected. For this purpose, IP was performed using antibodies against Nrf2, H3K9ac, or H3K18ac, respectively (Figures 8(a)–8(c)). Also, unrelated IgG was included to confirm that these antibodies worked well for IP and validate that the target proteins were precipitated specifically (Figures 8(d) and 8(e)). We demonstrated that Nrf2 stably

associated with both H3K9ac and H3K18ac in both mock-infected and virus-infected MDBK cells (Figures 8(a)–8(c)). When the antibody against Nrf2 was used to do IP, much more H3K9ac and H3K18ac were precipitated in the virus-infected cells (Figure 8(a)). When IP was performed using antibodies against either H3K9ac or H3K18ac, less Nrf2 was precipitated in the virus-infected cells (Figure 8(b)). Based on these results, we assumed that if the ratio between Nrf2 and H3K9ac/H3K18ac was arbitrarily set as 1 (Nrf2 : H3K9ac/H3K18ac = 1) in the control, the ratio would be less than 1 (Nrf2 : H3K9ac/H3K18ac < 1) in the virus-infected cells, suggesting that the virus infection reduced the association ratio between Nrf2 and H3K9ac/H3K18ac. Since we have previously reported that the virus infection significantly reduced the protein levels of both H3K9ac and H3K18ac [37], the association between Nrf2 and H3K9ac/H3-K18ac supported our findings that virus infection relocalized nuclear Nrf2. It is highly possible that more Nrf2 protein was relocalized to the transcriptionally active chromatin in the virus-infected cells, which is a possible mechanism to overcome adverse effects of Nrf2 depletion during virus infection.

4. Discussion

The transcriptional activator Nrf2 plays a vital role in maintaining cellular homeostasis through regulating the expression of multiple antioxidant proteins, detoxification enzymes, and xenobiotic transporters [46, 47]. Nrf2 also regulates multiple cellular processes including cell differentiation, proliferation, and inflammation [36], which may be closely related to virus pathogenesis. BoHV-1 infection significantly reduces Nrf2 expression which is inconsistent with the report that virus infection enhances ROS production in
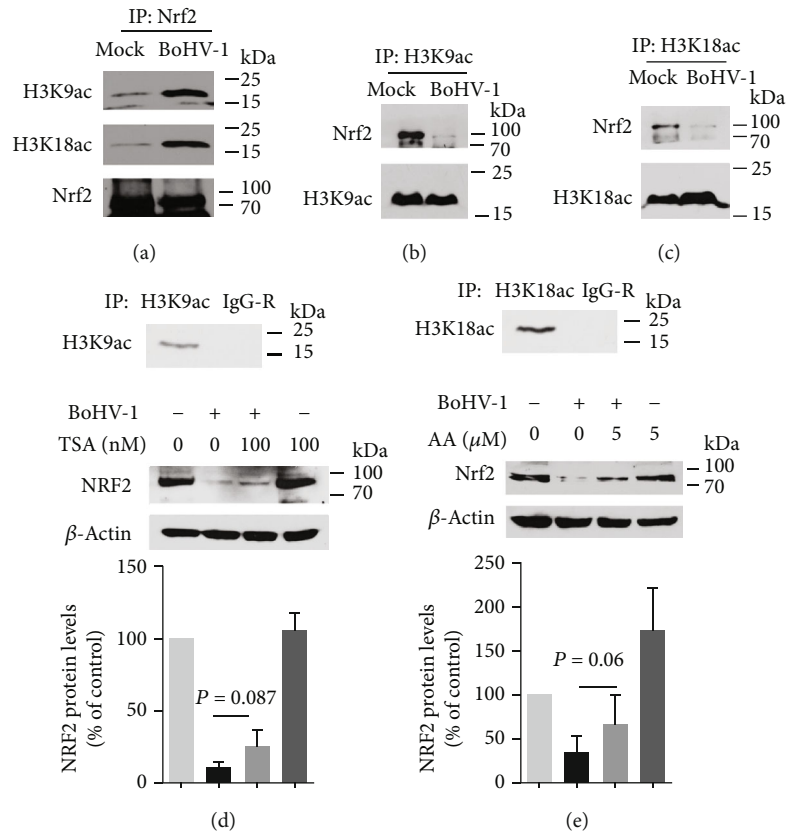
FIGURE 8: BoHV-1 affected the association between Nrf2 and H3K9ac/H3K18ac. MDBK cells in 60 mm dishes were mock infected or infected for 24 h. The cell lysates were prepared to perform IP using antibodies against Nrf2 (a), H3K9ac (b), H3K18ac (c), H3K9ac and rabbit IgG (d), and H3K18ac and rabbit IgG (e). The precipitated proteins were subjected to Western blots using the following antibodies: Nrf2 (Abcam, cat# ab137550, 1 : 1000), acetyl-Histone H3 (Lys9) rabbit mAb (Cell Signaling Technology, cat# 9649, 1 : 1000), and acetyl-Histone H3 (Lys18) rabbit mAb (Cell Signaling Technology, cat# 13998, 1 : 1000). Data shown are representative of three independent experiments. The significance was assessed with Student's t-test ($^*P < 0.05$).

cell cultures [4, 15, 18]. Here, we raised questions of whether and how the virus infection inhibits the Nrf2 signaling pathway.

In this study, we provided evidence that (i) BoHV-1 infection (after 24 hpi) significantly reduced the expression of HO-1 and NQO-1 (Figure 1), the known downstream proteins regulated by Nrf2 signaling, (ii) virus infection significantly reduced accumulation of Nrf2 in the nucleus (Figure 5), (iii) virus infection induced the deacetylation of nucleus Nrf2 (Figure 6), and (iv) virus infection led to relocalization of nuclear Nrf2 and forming a dot-like structure (Figure 4). These data unanimously suggested that BoHV-1 infection at a later stage led to the suppression of the Nrf2 signaling pathway.

HO-1 and NQO-1 are known downstream proteins regulated by Nrf2 signaling. In this study, we found that the treatment with Trolox could partially restore Nrf2 depletion induced by virus infection albeit not to the initial level, but it had no effects on the protein levels of either HO-1 or NQO-1 (Figure 2). These data implied that the virus infection hijacked the Nrf2 signaling pathway and preferentially controlled these Nrf2 downstream targets using Nrf2-independent manners.

In a canonical theory, Nrf2 is sequestered in the cytosol by forming a complex with KEAP1 which targets Nrf2 for proteasome degradation. Once activated, the complex is destructed, and therefore, Nrf2 is released and enters the nucleus where it stimulates the expression of downstream target genes. However, our data indicated that in MDBK cells either with or without infection, Nrf2 protein was readily detected in the nucleus rather than in the cytosol (Figures 4(a) and 4(b)). This is a novel finding which is in contrast to the canonical model that Nrf2 translocates to the nucleus under stimulation. We speculated that the cellular localization of Nrf2 protein is cell-type specific.

Of note, nuclear Nrf2 was relocalized following virus infection, forming dot-like structures identified by IFA (Figure 4(b)). Interestingly, partial part of Nrf2 colocalized with LaminA/C, and the association between LaminA/C and Nrf2 was confirmed by IP assay using the antibody against either Nrf2 or LaminA/C (Figure 7). Considering that the virus infection altered the expression patterns of LaminA/C and reduced the association ratio between Nrf2 and LaminA/C (Figure 7), it is reasonable to speculate that these changes may affect relocalization of nuclear Nrf2.

By using ChIP assay, it has been revealed that both phosphorylated histone H3 at serine 10 (H3S10) and Nrf2 are recruited to the promoter region of HO-1, and consequently, they coordinately stimulate HO-1 transcription in response to arsenite stimulation [48], suggesting a relationship between H3S10 and Nrf2. Here, we provided evidence showing that Nrf2 associated with activated histone H3 such as H3K9ac and H3K18ac (Figure 8). Since H3K9ac and H3K18ac are markers of transcriptional active chromatin, it is highly possible that Nrf2 preferentially binds to transcriptional active chromatin to overcome the adverse effects of Nrf2 depletion following virus infection. In addition, the virus infection reduced the association ratio between Nrf2 and H3K9ac/H3K18ac (Figure 8) and decreased the protein levels of both H3K9ac and H3K18ac [37], which potentially induce nuclear Nrf2 relocalization. This is an interesting finding which needs further study to reveal the biological effects of these associations.

Phosphorylation of Nrf2 by multiple kinases, such as PKC [44], AMPK [49], and CK2 [43], is critical for nuclear translocation and transcription activation. In this study, we found that the total phosphorylation levels of nuclear Nrf2 protein were significantly increased following virus infection (Figure 6). Of note, in this study, the phospho-(Ser/Thr) Phe antibody recognizing pan-phosphorylation sites was applied; therefore, the data represented the total phosphorylation status of Nrf2 proteins. The phosphorylation status in certain residues of Nrf2 such as Ser558 or serine 40 is critical for Nrf2 nuclear accumulation [49–51]. While the relationship between the total phosphorylation status of Nrf2 and Nrf2 activity has not been reported, our results provided a possibility that the increasing levels of phosphorylated Nrf2 proteins are negatively related to Nrf2 nuclear accumulation.

Diverse cellular factors, such as KEAP1 and DJ-1, may potentially influence Nrf2 stabilization and activation. Nrf2 expression can be regulated with KEAP1-dependent and KEAP1-independent mechanisms [36]. In this study, our findings indicated that BoHV-1 infection promoted the proteasome degradation of Nrf2 (Figure 2(a)) in line with the increased expression of KEAP1 protein following the virus infection (Figure 2(d)), suggesting that KEAP1 is potentially involved in the virus infection-induced degradation of Nrf2. DJ-1 may potentially stabilize Nrf2 expression through competitively binding to KEAP1 protein [38, 52, 53]. It has been reported that the activation of the DJ-1/Nrf2 pathway is involved in the pathogenesis of diabetic nephropathy in rats [54]. In this study, our findings indicated that BoHV-1 infection decreased DJ-1 expression, which may result in a decreased capability of binding to Nrf2 through competing with KEAP1. Immunoprecipitation using the antibody against DJ-1 further confirmed that virus infection led to a reduced capacity of binding to KEAP1. Therefore, virus infection rendered DJ-1 loss capacity to protect Nrf2 degradation which facilitated the degradation of Nrf2 through the ubiquitin proteasome pathway mediated by KEAP1.

Taken together, in this study, we provided evidences indicating that BoHV-1 infection led to an inactivation of the Nrf2 signaling pathway through complicated mechanisms such as by relocalization of nuclear Nrf2, deacetylation of nuclear Nrf2, and inhibition of Nrf2 nucleus translocation, as well as by promoting Nrf2 degradation through lost capacity of DJ-1. This study would extend our understanding of the mechanism of the virus infection-induced oxidative stress.

Data Availability

The data used to support the findings of this study are available from the corresponding author upon request.

Disclosure

Xiaotian Fu and Dongmei Chen are co-first authors.

Conflicts of Interest

The authors declare that they have no conflict of interest.

Acknowledgments

References

[1] P. D. Hodgson, P. Aich, A. Manuja et al., "Effect of stress on viral–bacterial synergy in bovine respiratory disease: novel mechanisms to regulate inflammation," *Comparative and Functional Genomics*, vol. 6, no. 4, pp. 244–250, 2005.

[2] J. A. Rice, L. Carrasco-Medina, D. C. Hodgins, and P. E. Shewen, "Mannheimia haemolytica and bovine respiratory disease," *Animal Health Research Reviews*, vol. 8, no. 2, pp. 117–128, 2007.

[3] C. Jones and S. Chowdhury, "A review of the biology of bovine herpesvirus type 1 (BHV-1), its role as a cofactor in the bovine respiratory disease complex and development of improved vaccines," *Animal Health Research Reviews*, vol. 8, no. 2, pp. 187–205, 2007.

[4] T. C. Cardoso, A. C. G. Rosa, H. L. Ferreira et al., "Bovine herpesviruses induce different cell death forms in neuronal and glial-derived tumor cell cultures," *Journal of Neurovirology*, vol. 22, no. 6, pp. 725–735, 2016.

[5] L. A. Sena and N. S. Chandel, "Physiological roles of mitochondrial reactive oxygen species," *Molecular Cell*, vol. 48, no. 2, pp. 158–167, 2012.

[6] S. Hu, W. S. Sheng, S. J. Schachtele, and J. R. Lokensgard, "Reactive oxygen species drive herpes simplex virus (HSV)-1-induced proinflammatory cytokine production by murine microglia," *Journal of Neuroinflammation*, vol. 8, no. 1, p. 123, 2011.

[7] D. Amatore, R. Sgarbanti, K. Aquilano et al., "Influenza virus replication in lung epithelial cells depends on redox-sensitive

pathways activated by NOX4-derived ROS," *Cellular Microbiology*, vol. 17, no. 1, pp. 131–145, 2015.

[8] A. Bindoli, J. M. Fukuto, and H. J. Forman, "Thiol chemistry in peroxidase catalysis and redox signaling," *Antioxidants & Redox Signaling*, vol. 10, no. 9, pp. 1549–1564, 2008.

[9] C. Tapeinos and A. Pandit, "Physical, chemical, and biological structures based on ROS-sensitive moieties that are able to respond to oxidative microenvironments," *Advanced Materials*, vol. 28, no. 27, pp. 5553–5585, 2016.

[10] R. L. Auten and J. M. Davis, "Oxygen toxicity and reactive oxygen species: the devil is in the details," *Pediatric Research*, vol. 66, no. 2, pp. 121–127, 2009.

[11] S. Ye, S. Lowther, and J. Stambas, "Inhibition of reactive oxygen species production ameliorates inflammation induced by influenza A viruses via upregulation of SOCS1 and SOCS3," *Journal of Virology*, vol. 89, no. 5, pp. 2672–2683, 2015.

[12] R. Gonzalez-Dosal, K. A. Horan, S. H. Rahbek et al., "HSV infection induces production of ROS, which potentiate signaling from pattern recognition receptors: role for S-glutathionylation of TRAF3 and 6," *PLoS Pathogens*, vol. 7, no. 9, article e1002250, 2011.

[13] L. Nencioni, R. Sgarbanti, D. Amatore et al., "Intracellular redox signaling as therapeutic target for novel antiviral strategy," *Current Pharmaceutical Design*, vol. 17, no. 35, pp. 3898–3904, 2011.

[14] L. Zhu, X. Fu, C. Yuan, X. Jiang, and G. Zhang, "Induction of oxidative DNA damage in bovine herpesvirus 1 infected bovine kidney cells (MDBK cells) and human tumor cells (A549 cells and U2OS cells)," *Viruses*, vol. 10, no. 8, p. 393, 2018.

[15] L. Zhu, C. Yuan, D. Zhang, Y. Ma, X. Ding, and G. Zhu, "BHV-1 induced oxidative stress contributes to mitochondrial dysfunction in MDBK cells," *Veterinary Research*, vol. 47, no. 1, article 47, 2016.

[16] P. Shelton and A. K. Jaiswal, "The transcription factor NF-E2-related factor 2 (Nrf2): a protooncogene?," *FASEB Journal*, vol. 27, no. 2, pp. 414–423, 2013.

[17] T. W. Kensler, N. Wakabayashi, and S. Biswal, "Cell survival responses to environmental stresses via the Keap1-Nrf2-ARE pathway," *Annual Review of Pharmacology and Toxicology*, vol. 47, no. 1, pp. 89–116, 2007.

[18] X. Fu, X. Jiang, X. Chen, L. Zhu, and G. Zhang, "The differential expression of mitochondrial function-associated proteins and antioxidant enzymes during bovine herpesvirus 1 infection: a potential mechanism for virus infection-induced oxidative mitochondrial dysfunction," *Mediators of Inflammation*, vol. 2019, Article ID 7072917, 10 pages, 2019.

[19] M. Kobayashi, L. Li, N. Iwamoto et al., "The antioxidant defense system Keap1-Nrf2 comprises a multiple sensing mechanism for responding to a wide range of chemical compounds," *Molecular and Cellular Biology*, vol. 29, no. 2, pp. 493–502, 2009.

[20] A. Raghunath, K. Sundarraj, R. Nagarajan et al., "Antioxidant response elements: discovery, classes, regulation and potential applications," *Redox Biology*, vol. 17, pp. 297–314, 2018.

[21] W. W. Wasserman and W. E. Fahl, "Functional antioxidant responsive elements," *Proceedings of the National Academy of Sciences of the United States of America*, vol. 94, no. 10, pp. 5361–5366, 1997.

[22] B. Harder, T. Jiang, T. Wu et al., "Molecular mechanisms of Nrf2 regulation and how these influence chemical modulation for disease intervention," *Biochemical Society Transactions*, vol. 43, no. 4, pp. 680–686, 2015.

[23] C. Lee, "Therapeutic modulation of virus-induced oxidative stress via the Nrf2-dependent antioxidative pathway," *Oxidative Medicine and Cellular Longevity*, vol. 2018, Article ID 6208067, 26 pages, 2018.

[24] R. Medvedev, D. Ploen, C. Spengler et al., "HCV-induced oxidative stress by inhibition of Nrf2 triggers autophagy and favors release of viral particles," *Free Radical Biology & Medicine*, vol. 110, pp. 300–315, 2017.

[25] A. Ramezani, M. P. Nahad, and E. Faghihloo, "The role of Nrf2 transcription factor in viral infection," *Journal of Cellular Biochemistry*, vol. 119, no. 8, pp. 6366–6382, 2018.

[26] B. Kosmider, E. M. Messier, W. J. Janssen et al., "Nrf2 protects human alveolar epithelial cells against injury induced by influenza A virus," *Respiratory Research*, vol. 13, no. 1, p. 43, 2012.

[27] Y. Yageta, Y. Ishii, Y. Morishima et al., "Role of Nrf2 in host defense against influenza virus in cigarette smoke-exposed mice," *Journal of Virology*, vol. 85, no. 10, pp. 4679–4690, 2011.

[28] S. M. Castro, A. Guerrero-Plata, G. Suarez-Real et al., "Antioxidant treatment ameliorates respiratory syncytial virus-induced disease and lung inflammation," *American Journal of Respiratory and Critical Care Medicine*, vol. 174, no. 12, pp. 1361–1369, 2006.

[29] H. Y. Cho, F. Imani, L. Miller-DeGraff et al., "Antiviral activity of Nrf2 in a murine model of respiratory syncytial virus disease," *American Journal of Respiratory and Critical Care Medicine*, vol. 179, no. 2, pp. 138–150, 2009.

[30] V. Misra, A. C. Bratanich, D. Carpenter, and P. O'Hare, "Protein and DNA elements involved in transactivation of the promoter of the bovine herpesvirus (BHV) 1 IE-1 transcription unit by the BHV alpha gene trans-inducing factor," *Journal of Virology*, vol. 68, no. 8, pp. 4898–4909, 1994.

[31] C. Zhang, F. Pu, A. Zhang et al., "Heme oxygenase-1 suppresses bovine viral diarrhoea virus replication *in vitro*," *Scientific Reports*, vol. 5, no. 1, article 15575, 2015.

[32] J. Opiela, D. Lipinski, R. Slomski, and L. Katska-Ksiazkiewicz, "Transcript expression of mitochondria related genes is correlated with bovine oocyte selection by BCB test," *Animal Reproduction Science*, vol. 118, no. 2-4, pp. 188–193, 2010.

[33] I. Bellezza, P. Scarpelli, S. V. Pizzo, S. Grottelli, E. Costanzi, and A. Minelli, "ROS-independent Nrf2 activation in prostate cancer," *Oncotarget*, vol. 8, no. 40, pp. 67506–67518, 2017.

[34] J. Shao, J. Huang, Y. Guo et al., "Up-regulation of nuclear factor E2-related factor 2 (Nrf2) represses the replication of SVCV," *Fish & Shellfish Immunology*, vol. 58, pp. 474–482, 2016.

[35] E. M. Messier, K. Bahmed, R. M. Tuder, H. W. Chu, R. P. Bowler, and B. Kosmider, "Trolox contributes to Nrf2-mediated protection of human and murine primary alveolar type II cells from injury by cigarette smoke," *Cell Death & Disease*, vol. 4, no. 4, article e573, 2013.

[36] H. K. Bryan, A. Olayanju, C. E. Goldring, and B. K. Park, "The Nrf2 cell defence pathway: Keap1-dependent and -independent mechanisms of regulation," *Biochemical Pharmacology*, vol. 85, no. 6, pp. 705–717, 2013.

[37] L. Zhu, X. Jiang, X. Fu, Y. Qi, and G. Zhu, "The involvement of histone H3 acetylation in bovine herpesvirus 1 replication in MDBK cells," *Viruses*, vol. 10, no. 10, p. 525, 2018.

[38] C. M. Clements, R. S. McNally, B. J. Conti, T. W. Mak, and J. P. Ting, "DJ-1, a cancer- and Parkinson's disease-associated

protein, stabilizes the antioxidant transcriptional master regulator Nrf2," *Proceedings of the National Academy of Sciences of the United States of America*, vol. 103, no. 41, pp. 15091–15096, 2006.

[39] W. Zhou, K. Bercury, J. Cummiskey, N. Luong, J. Lebin, and C. R. Freed, "Phenylbutyrate up-regulates the DJ-1 protein and protects neurons in cell culture and in animal models of Parkinson disease," *The Journal of Biological Chemistry*, vol. 286, no. 17, pp. 14941–14951, 2011.

[40] S. J. Kim, Y. J. Park, I. Y. Hwang, M. B. Youdim, K. S. Park, and Y. J. Oh, "Nuclear translocation of DJ-1 during oxidative stress-induced neuronal cell death," *Free Radical Biology and Medicine*, vol. 53, no. 4, pp. 936–950, 2012.

[41] D. Stewart, E. Killeen, R. Naquin, S. Alam, and J. Alam, "Degradation of transcription factor Nrf2 via the ubiquitin-proteasome pathway and stabilization by cadmium," *The Journal of Biological Chemistry*, vol. 278, no. 4, pp. 2396–2402, 2003.

[42] Y. Kawai, L. Garduno, M. Theodore, J. Yang, and I. J. Arinze, "Acetylation-deacetylation of the transcription factor Nrf2 (nuclear factor erythroid 2-related factor 2) regulates its transcriptional activity and nucleocytoplasmic localization," *The Journal of Biological Chemistry*, vol. 286, no. 9, pp. 7629–7640, 2011.

[43] P. L. Apopa, X. He, and Q. Ma, "Phosphorylation of Nrf2 in the transcription activation domain by casein kinase 2 (CK2) is critical for the nuclear translocation and transcription activation function of Nrf2 in IMR-32 neuroblastoma cells," *Journal of Biochemical and Molecular Toxicology*, vol. 22, no. 1, pp. 63–76, 2008.

[44] H. C. Huang, T. Nguyen, and C. B. Pickett, "Phosphorylation of Nrf2 at Ser-40 by protein kinase C regulates antioxidant response element-mediated transcription," *The Journal of Biological Chemistry*, vol. 277, no. 45, pp. 42769–42774, 2002.

[45] T. Agalioti, G. Chen, and D. Thanos, "Deciphering the transcriptional histone acetylation code for a human gene," *Cell*, vol. 111, no. 3, pp. 381–392, 2002.

[46] Q. Zhong, M. Mishra, and R. A. Kowluru, "Transcription factor Nrf2-mediated antioxidant defense system in the development of diabetic retinopathy," *Investigative Ophthalmology & Visual Science*, vol. 54, no. 6, pp. 3941–3948, 2013.

[47] M. Mishra, Q. Zhong, and R. A. Kowluru, "Epigenetic modifications of Nrf2-mediated glutamate-cysteine ligase: implications for the development of diabetic retinopathy and the metabolic memory phenomenon associated with its continued progression," *Free Radical Biology & Medicine*, vol. 75, pp. 129–139, 2014.

[48] P. D. Ray, B. W. Huang, and Y. Tsuji, "Coordinated regulation of Nrf2 and histone H3 serine 10 phosphorylation in arsenite-activated transcription of the human heme oxygenase-1 gene," *Biochimica et Biophysica Acta*, vol. 1849, no. 10, pp. 1277–1288, 2015.

[49] M. S. Joo, W. D. Kim, K. Y. Lee, J. H. Kim, J. H. Koo, and S. G. Kim, "AMPK facilitates nuclear accumulation of Nrf2 by phosphorylating at serine 550," *Molecular and Cellular Biology*, vol. 36, no. 14, pp. 1931–1942, 2016.

[50] K. Baba, H. Morimoto, and S. Imaoka, "Seven in absentia homolog 2 (Siah2) protein is a regulator of NF-E2-related factor 2 (Nrf2)," *The Journal of Biological Chemistry*, vol. 288, no. 25, pp. 18393–18405, 2013.

[51] L. Fão, S. I. Mota, and A. C. Rego, "c-Src regulates Nrf2 activity through PKCδ after oxidant stimulus," *Biochimica et Biophysica Acta (BBA) - Molecular Cell Research*, vol. 1866, no. 4, pp. 686–698, 1866.

[52] L. Gan, D. A. Johnson, and J. A. Johnson, "Keap1-Nrf2 activation in the presence and absence of DJ-1," *The European Journal of Neuroscience*, vol. 31, no. 6, pp. 967–977, 2010.

[53] P. Deshmukh, S. Unni, G. Krishnappa, and B. Padmanabhan, "The Keap1-Nrf2 pathway: promising therapeutic target to counteract ROS-mediated damage in cancers and neurodegenerative diseases," *Biophysical Reviews*, vol. 9, no. 1, pp. 41–56, 2017.

[54] Q. Sun, Z. Y. Shen, Q. T. Meng, H. Z. Liu, W. N. Duan, and Z. Y. Xia, "The role of DJ-1/Nrf2 pathway in the pathogenesis of diabetic nephropathy in rats," *Renal Failure*, vol. 38, no. 2, pp. 294–304, 2016.

Research Article

Structure-Guided Approach to Identify Potential Inhibitors of Large Envelope Protein to Prevent Hepatitis B Virus Infection

Mahboubeh Mehmankhah,[1] **Ruchika Bhat,**[2,3] **Mohammad Sabery Anvar,**[4] **Shahnawaz Ali,**[1] **Aftab Alam,**[1] **Anam Farooqui,**[1] **Fatima Amir,**[1] **Ayesha Anwer,**[1] **Saniya Khan,**[1] **Iqbal Azmi,**[5] **Rafat Ali,**[1] **Romana Ishrat,**[1] **Md. Imtaiyaz Hassan,**[1] **Zarrin Minuchehr,**[4] **and Syed Naqui Kazim** ⓘD[1]

[1]*Center for Interdisciplinary Research in Basic Sciences, Jamia Millia Islamia, New Delhi 110025, India*
[2]*Department of Chemistry, Indian Institute of Technology Delhi, New Delhi 110016, India*
[3]*Supercomputing Facility for Bioinformatics & Computational Biology (SCFBio), Indian Institute of Technology Delhi, New Delhi 110016, India*
[4]*Systems Biotechnology Department, National Institute of Genetic Engineering and Biotechnology, Tehran, Iran*
[5]*Multidisciplinary Center for Advanced Research and Studies, Jamia Millia Islamia, New Delhi 110025, India*

Correspondence should be addressed to Syed Naqui Kazim; skazim@jmi.ac.in

Hepatitis B virus (HBV) infection is one of the major causes of liver diseases, which can lead to hepatocellular carcinoma. The role of HBV envelope proteins is crucial in viral morphogenesis, infection, and propagation. Thus, blocking the pleiotropic functions of these proteins especially the PreS1 and PreS2 domains of the large surface protein (LHBs) is a promising strategy for designing efficient antivirals against HBV infection. Unfortunately, the structure of the LHBs protein has not been elucidated yet, and it seems that any structure-based drug discovery is critically dependent on this. To find effective inhibitors of LHBs, we have modeled and validated its three-dimensional structure and subsequently performed a virtual high-throughput screening against the ZINC database using RASPD and ParDOCK tools. We have identified four compounds, ZINC11882026, ZINC19741044, ZINC00653293, and ZINC15000762, showing appreciable binding affinity with the LHBs protein. The drug likeness was further validated using ADME screening and toxicity analysis. Interestingly, three of the four compounds showed the formation of hydrogen bonds with amino acid residues lying in the capsid binding region of the PreS1 domain of LHBs, suggesting the possibility of inhibiting the viral assembly and maturation process. The identification of potential lead molecules will help to discover more potent inhibitors with significant antiviral activities.

1. Introduction

Historically, one of the major human challenges has been to fight against infectious diseases; viruses are one of the causative agents of these diseases. Hepatitis B virus (HBV) infects 480-520 million people globally; this means that 1 out of every 12 people is affected, chronically [1]. Hepatitis B virus, in fact, causes about 650,000 deaths annually around the world. Sometimes, hepatitis leads to chronic liver disease and its recurrence may lead to liver fibrosis. Thus, it is the most usual cause of liver-related incidences and fatalities worldwide [2]. HBV is a small enveloped hepatotropic virus (~42 nm), having a partially double-stranded DNA genome (~3.2 kb) where the negative strand includes 3020-3320 nucleotides and the positive strand has 1700-2800 nucleotides [3, 4].

The HBV genome consists of four open reading frames (ORFs) encoding viral surface proteins (LHBs, MHBs, and SHBs also referred to as L, M, and S, respectively), polymerase (P), and core (C) and HBx (X) proteins. The LHBs has 389 amino acids (39 kDa) encoded by the PreS1, PreS2,

and S domains. The MHBs antigen includes a polypeptide encoded by PreS2 and S, whereas the SHBs contains the polypeptide encoded by the S domain only [5, 6]. Depending on genotype, the PreS1 domain has 108, 118, or 119 amino acids, the PreS2 domain has 55 amino acids, and the S domain contains 226 amino acids, also known as hepatitis B virus surface antigen (HBsAg) [7]. Thus, LHBs is divided into three main domains: PreS1 (1-108), PreS2 (109-163), and S (164-389) [7]. LHBs also contains four putative transmembrane (I-IV) regions. According to previous reports, domains PreS1 and PreS2 have a very critical role in the viral entry process [8]. It has been proven that the PreS1 domain is required for HBV morphogenesis. Deletion of some amino acids between aa 114 and 163 of the PreS2 domain did not impair the production process of the virus [9]. Amino acids 2-78 of the PreS1 domain of the LHBs protein is involved in the recognition of a hepatocyte receptor [10]. The first 77 residues of the PreS1 domain are essential for HBV infectivity [11]. This protein also has the highly conserved "a" determinant region between aa 122 and 147 which remains involved in the binding of antibodies against HBsAg. A variety of mutations have been reported within this region [12]. Therefore, this region does not seem appropriate for drug designing.

Currently available targets for the anti-HBV therapeutic approach is largely based on nucleos(t)ide analogues (NAs) targeting polymerase. However, extensive usage of NAs is gradually becoming less effective due to many reasons, the most important is the emergence of resistant mutants and their consequences [13–18]. Finding HBV entry inhibitors and appropriate neutralizing antibodies are becoming the prime focus of therapeutic intervention [19]. Hence, the importance of identifying the structure of HBV proteins is being felt more than ever. Moreover, investigating the underlying immune mechanisms and associated signaling pathways, for instance Toll-like receptors, is also an important and growing concern these days. It is needless to say that targeting any of the envelope proteins could lead to a potential threat of a disproportionate accumulation of L, M, or S proteins. The accumulation of the L protein (LHBs) coordinates with tampering of the viral assembly process [20]. Its eventuality coincides with the generation of oxidative stress within the ER, consequently altering the downstream signaling processes. Under oxidative stress, the misfolding of proteins is a predominant phenomenon which is readily sensed by mammalian cells through a signaling network referred to as unfolded protein response (UPR). UPR is induced by factors known to contribute to calcium homeostasis and protein glycosylation and those related to physiological stresses like hypoxia and glucose deprivation [21]. Altogether, they disrupt the folding of proteins in ER, consequently triggering the signaling network which involves transmembrane protein kinases, transmembrane transcription factors, and transmembrane proteases. The cumulative response culminates into UPR activation [22]. The endoplasmic reticulum (ER) serves multiple functions needed for the execution of normal cellular function and cell survival. To name a few are Ca^{2+} storage, posttranslational modification, and the folding and assembly of newly synthesized secretory proteins. In the hepatitis B virus life cycle, the ER is the venue of envelopment as well as the maturation of viral particles [23, 24]. This cellular response triggers precursor mechanisms responsible for both survival and apoptosis [25]. Hence, both the advantages and disadvantages associated with potent inhibitors of the viral envelope protein, specially the LHBs, are naturally suspected.

Unfortunately, the 3D structure of the LHBs has not yet been discovered, and the critical functions of this protein are not fully determined. Thus, determining the structure of the LHBs protein can be very significant for researchers to clarify its function. In this study, we have tried to predict the structure of the LHBs of HBV by using bioinformatics instrument (computational methods) and accessible databases. The definition of the 3D structure of the large surface protein can be effective in controlling and preventing the development of hepatitis disease and hepatocellular carcinoma (HCC) and in exploring the better and comprehensive biological mechanisms and related signaling pathways involved in the HBV life cycle in liver cells. Sufficient knowledge of this protein structure may provide beneficial targets for designing some specific drugs for a better treatment of HBV infection. At the end of the present study, we introduce four optimized small molecules with less energy bonding and low toxicity. This study may thus lead to the identification of reliable candidate drugs for inhibiting HBV infection.

2. Materials and Methods

We have utilized modern computational methods to identify potential inhibitors of LHBs. The scheme of work is illustrated in the form of a flow chart (Supplementary, Figure S1).

2.1. Target Structure Prediction. The amino acid sequence of the LHBs of HBV (genotype D, subtype ayw) was retrieved from UniProt (P03138). The retrieved sequence was used to predict the secondary structure of LHBs by the PSIPRED tool [26] which predicts the ratio of α-helices and β-sheets within a protein from its sequence. This information is useful to generate a better structure in a 3D model. The ProtParam [27, 28] was used to identify the physicochemical characteristics such as the aliphatic index and GRAVY value to determine the hydrophobic or hydrophilic nature of the protein, which helps in estimating the chemical nature of the binding pockets of the protein. Furthermore, the tertiary structure of the protein was modeled by hybrid methods involving homology, threading, and *ab initio* approaches via structure prediction tools such as the RM2TS+ server [29] and I-TASSER [30]. RM2TS+ is one among the state-of-the-art prediction tools and derives its skeletal framework from the higher order Ramachandran map. I-TASSER utilizes the knowledge of structural templates from the PDB and generates models using iterative template-based fragment assembly simulations. These servers cover the exhaustive modeling algorithm in order to yield a promising tertiary model for the LHBs protein.

The structures obtained from RM2TS+ and I-TASSER were further analyzed for their quality check using the protein structure analysis and validation (ProtSAV) [31] and RAMPAGE tools [32]. The ProtSAV server can assess the quality of a predicted protein and can determine the correctness of the predicted model by giving the score. RAMPAGE

generates the Ramachandran plot which defines whether the phi-psi value of each residue is in the allowed or disallowed location [33]. Both tools helped in analyzing if the tertiary predicted model of the LHBs protein is within the acceptable limits of the structure. The best models obtained based on the ProtSAV score and percentage allowed residues using ProtSAV and RAMPAGE, respectively, were further optimized using Galaxy refine tool. After several refinements, the 3D structure was minimized using AMBER 14 [34]. The protein was provided with a water environment of 12 Å TIP3P water model. After minimization, slow heating for 20 ps was run and the system was left in the NPT ensemble for a 20 ns run length to study its most favorable structural conformations to yield a final model of the LHBs protein.

2.2. Binding Site Prediction. The identification of active sites and experimental information about LHBs is essentially important. In order to predict the active site of the refined model, the AADS server [35] was used. AADS is a tool to predict all the possible binding pockets within a protein based on its tertiary structure with a 100% accuracy of acquiring the real binding site within the top 10 identified pockets. The final best-modeled protein obtained was submitted to the AADS server (http://www.scfbio-iitd.res.in/) which then identified the best ten potential active sites.

2.3. Hit Identification. After the binding sites of the target protein are predicted, the RASPD software [36] was used to identify the best hits from a library of a million small molecules obtained from ZINC database [37]. The protein was screened against all of the best ten binding sites using RASPD. The hit molecules were further optimized based on the Lipinski parameters such as the number of the hydrogen bond of acceptors and donors, Wiener index, volume for the protein and functional groups, and the molar refractivity and through proper ADMET profiles. The most interesting feature of RASPD is that it generates a set of hit molecules based on the complementarities of the properties. The screening was done against the million-molecule database which resulted in more than 1000 hits per binding site, out of which the top 50 hits for each site was taken for further analysis.

2.4. Molecular Docking. The screening is followed by all atom energy-based Monte Carlo protein-hit molecule docking using ParDOCK [38] for identifying the best candidates which could be selected for empirical synthesis and testing. The ParDOCK module of Sanjeevini is an automated server for protein ligand docking (http://www.scfbio-iitd.res.in). It considers the optimal position of ligands with the best configuration in binding sites of the target protein and classifies them according to their interaction energies. Thus, the best molecule is chosen based on the score of the binding energy of candidates and it is considered as the best binder to the target. The threshold kept here was -11 kcal/Mol binding energy values for the L protein-small molecule complexes.

2.5. Molecular Dynamic Simulations. From static, the energetic perspectives in terms of dynamics were taken into consideration by running 100 ns long molecular dynamic simulations mimicking the *in vitro* environment to increase the reliability of these hits as potential inhibitors and to understand their mode of interaction mechanisms. The complexes were solvated in TIP3P [39] water box molecules of 12 Å. The input for simulations was the best-docked protein inhibitor generated via ParDOCK for each inhibitor. Ligand and protein files were prepared using the AMBER 14 package for performing MD. Parameter and topology files were generated using the "ff99SB" and "GAFF" force field, respectively [40, 41]. The compounds were first subjected to 5000 steps of minimization (2500SD+2500CG) to set the water box. A further 5000 steps of hydrogen minimization (2500SD +2500CG) were performed on the complex to relieve any steric clashes. Slow heating of the solvent to 300 K over a period of 20 ps was done. Equilibration for 300 ps was also performed before letting the manufacture phase run for 100 ns with a time step of 2 femtoseconds under NPT conditions with boundary situations. Simulations were investigated through energy and density plots. The amount of pressure and temperature was kept fixed, and hydrogen atoms were finite by the SHAKE algorithm [42, 43]. The poses were written after every 100 ps. Finally, analysis of the molecular dynamic curves was carried out and PME summation [44] was used for electrostatic calculations. All the results presented here were analyzed on the last 100 ns trajectory of each system.

2.6. Toxicity Prediction. Pharmacokinetic properties and percent human oral absorption values such as absorption, distribution, metabolism, excretion, and the potential toxicity (ADMET) of the selected molecules were estimated with the admetSAR database [45], SwissADME [46], and Komputer-Assisted Technology (TOPKAT) software [47] developed by Health Designs Inc. (Discovery Studio 2.5, USA). These values provide an estimate for the drug likeness of the candidate molecules and predict their bioavailability.

3. Results

3.1. Physicochemical Characteristics. To identify the physicochemical characteristics of LHBs, the ProtParam tool was used (Supplementary, Table S1). The isoelectric point value (pI = 8.40) shows that the target protein is basic in nature. The half-life of LHBs is approximately 30 hours, and its stability lies in the middle (46.08). The aliphatic index determines the relative volume occupied by a protein and its aliphatic side chains, and the results show that LHBs has a high aliphatic index (82.24). The GRAVY value is the sum of the hydropathy values of all the residues of the protein divided by the number of amino acids of that protein, and based on this, the LHBs is considered a hydrophobic protein (0.146).

3.2. Protein Structure Prediction and Validation. For predicting the secondary structure of LHBs, the amino acid sequences were submitted to the PSIPRED server. The large envelope protein is 389 residues long, of which 26% is α-helix, 9% is β-sheet, and approximately 60% is coil (Supplementary, Figure S2). The amino acid sequences were exported to RM2TS+ and I-TASSER software which uses

both homology and *ab initio* approaches for generating three-dimensional structures (Supplementary, Figure S3). The predicted structure of LHBs was refined using "Galaxy refine," and energy was minimized using AMBER 14; MD simulations were run for 100 ns. A single polypeptide of LHBs with its boundaries determining the domains PreS1, PreS2, and S and with its residues lying within extracellular, transmembrane, and cytosolic regions has schematically been represented in Figure 1(a). The modeled structure of LHBs is shown in Figure 1(b). The refined structure has a close resemblance to the predicted secondary structure. Figure 1(b) shows three distinct domains of LHBs, also referring to the corresponding surface proteins of HBV.

After simulations, the structure was further analyzed by the structure validation tool "ProtSAV." According to the ProtSAV protocol, green is the best and the yellow color is acceptable; our modeled protein appeared in the yellow region (Figure 2(a)). Furthermore, we calculated the Ramachandran plot (RAMPAGE tool) for structural quality; we found that 94.39% of the residues are in the favored region (Figure 2(b)).

To predict the best structure of a target protein and to design especially small molecules based on drug discovery, we required accurate information about the binding pocket on the target which can inhibit the protein function. The prominent binding sites of the LHBs protein were evaluated through AADS which identified 19 potential binding sites on the LHBs structure and out of which we considered the top 10 cavities.

3.3. Hit Identification and Molecular Docking.

For finding the probable hits, the top 10 cavities of the structure which were identified by AADS were subjected to the RASPD software. The RASPD provides more than 1000 molecules against the predicted cavities of our target protein by selecting the ZINC database (-7.0 kcal/Mol to -13.5 kcal/Mol). The top 50 compounds of each cavity were taken for further scoring analysis and docking. Furthermore, all cavities were docked with compounds proposed by RASPD through the ParDOCK software. It imports the ligands with the best configuration in the target binding site and scores them based on their estimated free interaction energies using the BAPPL scoring function [48]. Finally, six compounds were selected based on the least binding energy between -11 kcal/Mol and -12.69 kcal/Mol. These were further subjected to MD simulation to check for the protein-hit interactions of over 100 ns.

3.4. MD Simulation.

All molecular dynamic simulations were carried out using AMBER 14. The overall binding free energy of the protein-hit molecule complexes throughout the 100 ns trajectories was calculated using BAPPL. To calculate the overall binding free energy between the targeted LBHs protein and the hit molecules over 100 ns long explicit simulations, the binding energies of the frames that were obtained at an interval of each nanosecond were calculated and then averaged out. A threshold of -8.0 kcal/Mol overall binding free energy for 100 ns simulations was set for proposing the molecules as potential therapeutics against the LHBs protein.

Finally, we found four out of the six screened hit molecules as potential inhibitors based on the binding free energy score during molecular dynamic simulations (Table 1). For each system simulated, the root mean squared deviation, energy (kinetic, potential, and total), density, and temperature were monitored to ensure that the standard deviation of each of these values was within acceptable limits of experimental error. The RMSD graphs of the hit molecules with promising inhibitory potential along with the above values are shown in Figure 3, which shows an overall stability within the complex. Finally, we found four out of the six compounds as potential inhibitors based on the affinity score and explicit simulation (Table 1, Table S2).

We visualized the interactions of our LHBs vs. potential ligands (complexes) using PyMOL and LigPlot (2D) (Figure 4). Our results indicate that all four selective ligands are bonded to the amino acids which are among the important regions, primarily at nucleocapsid binding residues and at a residue relevant to the entering of the virus and consequent infectivity. ZINC11882026 has been bonded by three H-bonds through Ala51 (3.33 Å); Thr104 (3.32 Å) of LHBs, which is in PreS1 (1-108); and Trp111 (3.08 Å) of LHBs; which is in PreS2 (109-163). Both of these regions are more important for NTCP receptor-mediated entry and nucleocapsid binding, respectively [8, 47, 48]. The compound ZINC00653293 is involved with Pro106 (2.9 Å) and Ala108 (3.2 Å) of LHBs; both of them are in PreS1 that signifies the nucleocapsid binding and consequent envelopment of a virus in the ER. The compound ZINC19741044 has only one H-bond with Ser90 (3.2 Å) of LHBs, which is also in the PreS1 region. The compound ZINC15000762 binds with one H-bond to Ser280 of LHBs (2.89 Å) linked to the protein which lies on the external side of the viral envelope (Table S3). Interestingly, none of them connects to the amino acids in the "a" determinant region (aa 122-147 of SHBs, corresponding to aa 286-311 of LHBs, respectively). Therefore, in case of any mutation in this region, selective ligands will still be suitable for LHBs inhibition. Therefore, our results indicate that all four selective ligands are bonded to the amino acids which are among the important regions referring to the process of entry and viral maturation. For more details, the molecular properties of each compound were also extracted from the ZINC database (http://ZINC.docking.org/), and the results indicate that our selective compounds have pharmaceutical capabilities (Table 2).

3.5. Drug Likeness Prediction.

Drug ability and toxicity of selected candidates have been computed by using admetSAR, SwissADME, and TOPKAT software. Parameters such as absorption, distribution, metabolism, excretion, and the toxicity [49–51] of selected candidates were evaluated by admetSAR (Table S4). All candidates showed positive results for the blood-brain barrier, Caco-2 permeability, and human intestinal absorption, warranting that they have no side effects about absorption. Also in terms of metabolism, various substrates and inhibitors of cytochrome P450 [52, 53] were investigated and the results are indicated in Table S4. In case of toxicity, all four compounds have
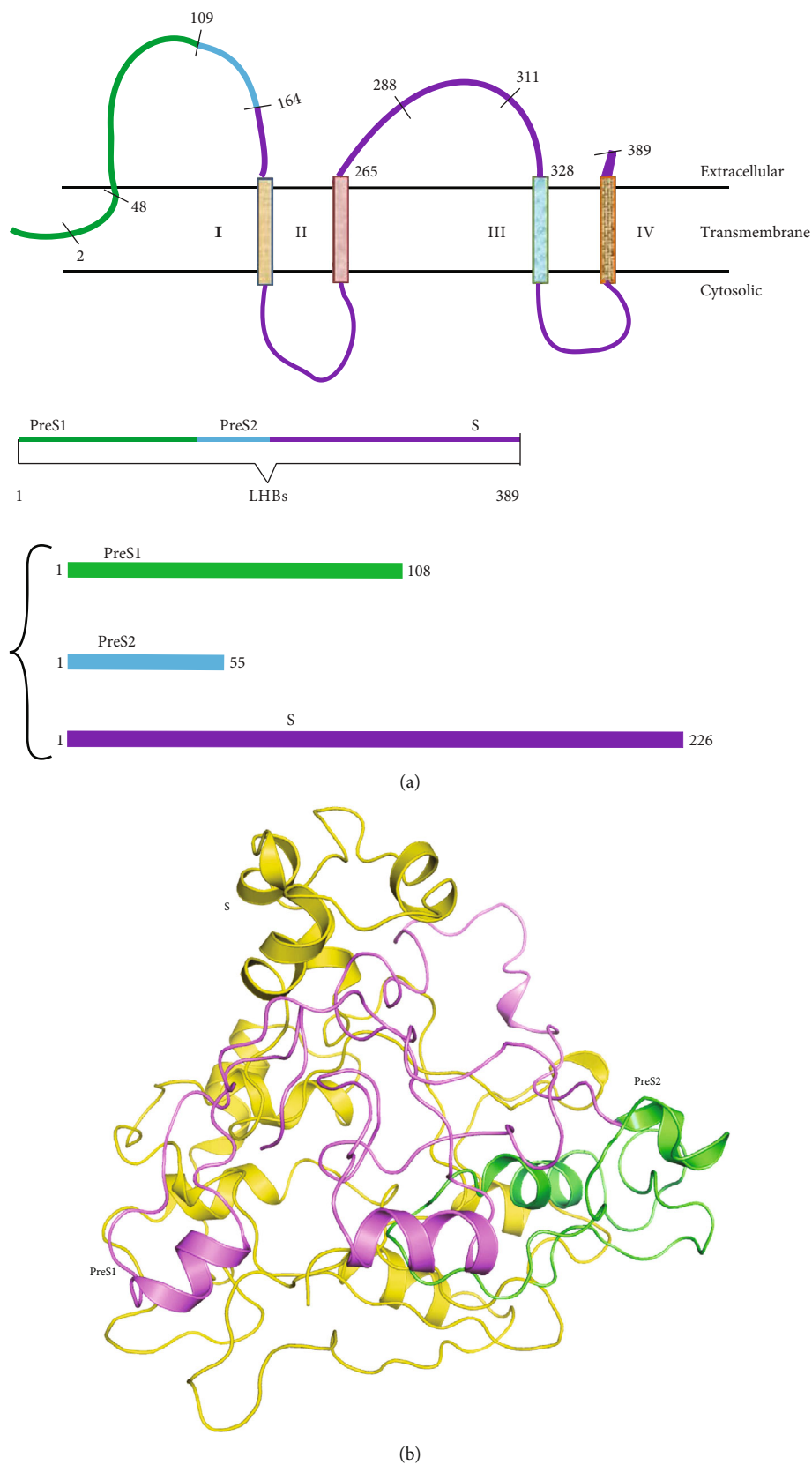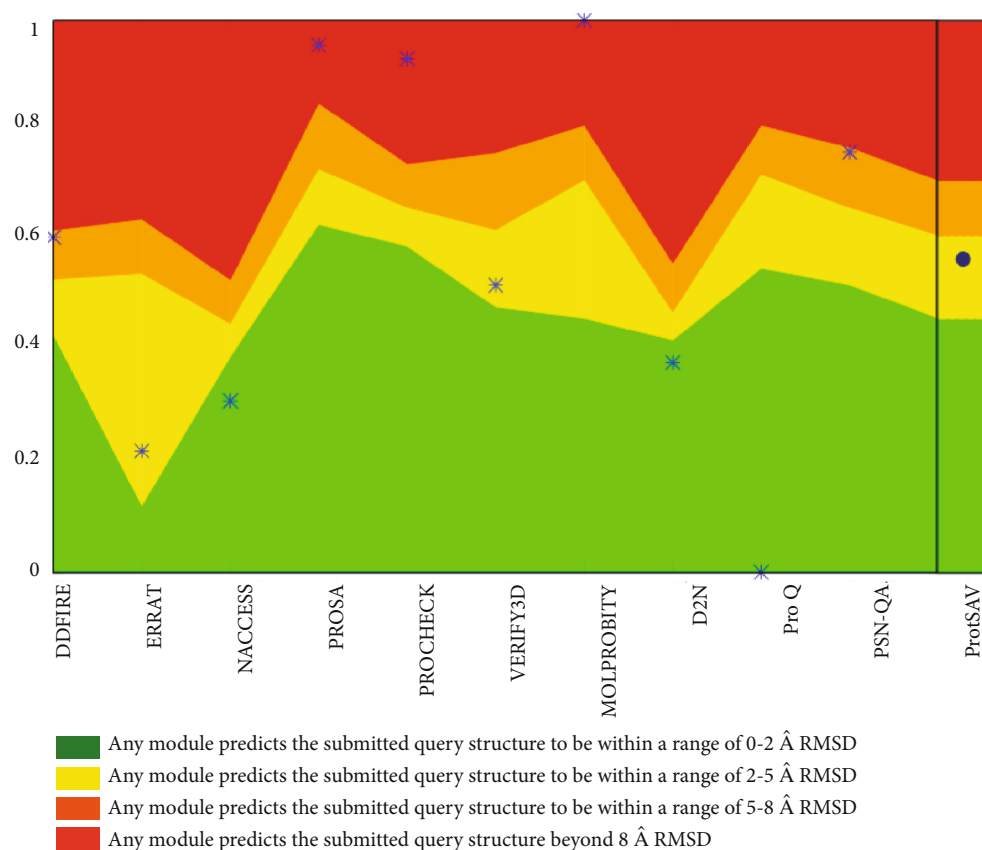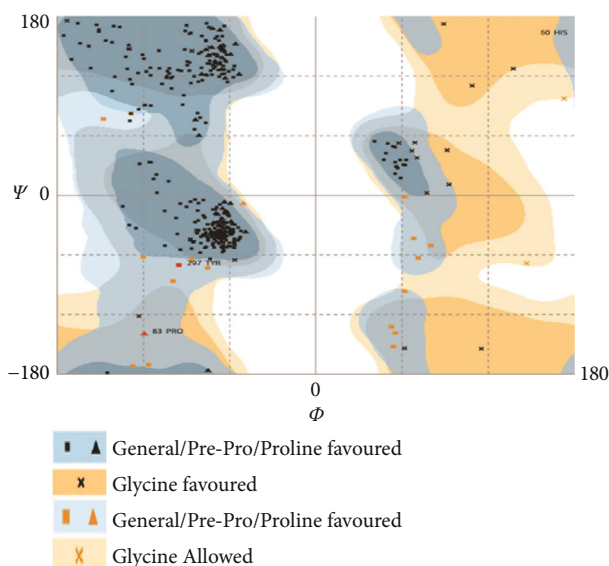
FIGURE 1: Schematic representation of the modelled protein structure of the large surface protein of HBV (LHBs). (a) Numbering and positions of amino acid residues as determinants of PreS1, PreS2, and S domains; extracellular, transmembrane, and cytosolic regions as determinants of the structure of LHBs. (b) The modeled structure of LHBs showing the PreS1, PreS2, and S domains in magenta, green, and yellow colors, respectively.

Any module predicts the submitted query structure to be within a range of 0-2 Â RMSD
Any module predicts the submitted query structure to be within a range of 2-5 Â RMSD
Any module predicts the submitted query structure to be within a range of 5-8 Â RMSD
Any module predicts the submitted query structure beyond 8 Â RMSD

(a)

General/Pre-Pro/Proline favoured
Glycine favoured
General/Pre-Pro/Proline favoured
Glycine Allowed

*Number of residues in favoured region: 365 (94.369)

(b)

FIGURE 2: (a) ProtSAV analysis: the modelled LHBs protein lies in the yellow region. (b) RAMPAGE analysis: 94.39% of the residues of LHBs lie within the favored region.

non-AMES toxicity, are noncarcinogenic, and have no carcinogenicity (three-class) required. To distinguish any unfavorable toxic properties of novel hits, TOPKAT software was also used [54]. Several descriptors such as the Ames mutagenicity test, weight of evidence carcinogenicity (v5.1) (WOE), rat oral LD50, skin irritation, skin sensitization, and aerobic biodegradability [55, 56] were investigated (Table S5).

TABLE 1: The binding affinity of top hits with LHBs are shown.

ZINC ID	ParDOCK ID	RASPD score (kcal/Mol)	ParDOCK score (kcal/Mol)	Average affinity*	Proposed
ZINC11882026	33625775	-11.4	-11.49	-8.87	Yes
ZINC00653293	21425236	-13.1	-11.75	-8.60	Yes
ZINC19741044	72860345	-13.4	-12.69	-8.33	Yes
ZINC15000762	78876711	-10.1	-12.46	-8.71	Yes
ZINC11784805	34135187	-10.5	-12.36	-4.63	No
ZINC12243260	32993271	-11.5	-12.39	-2.88	No

*Found for 100 ns scale explicit simulations.
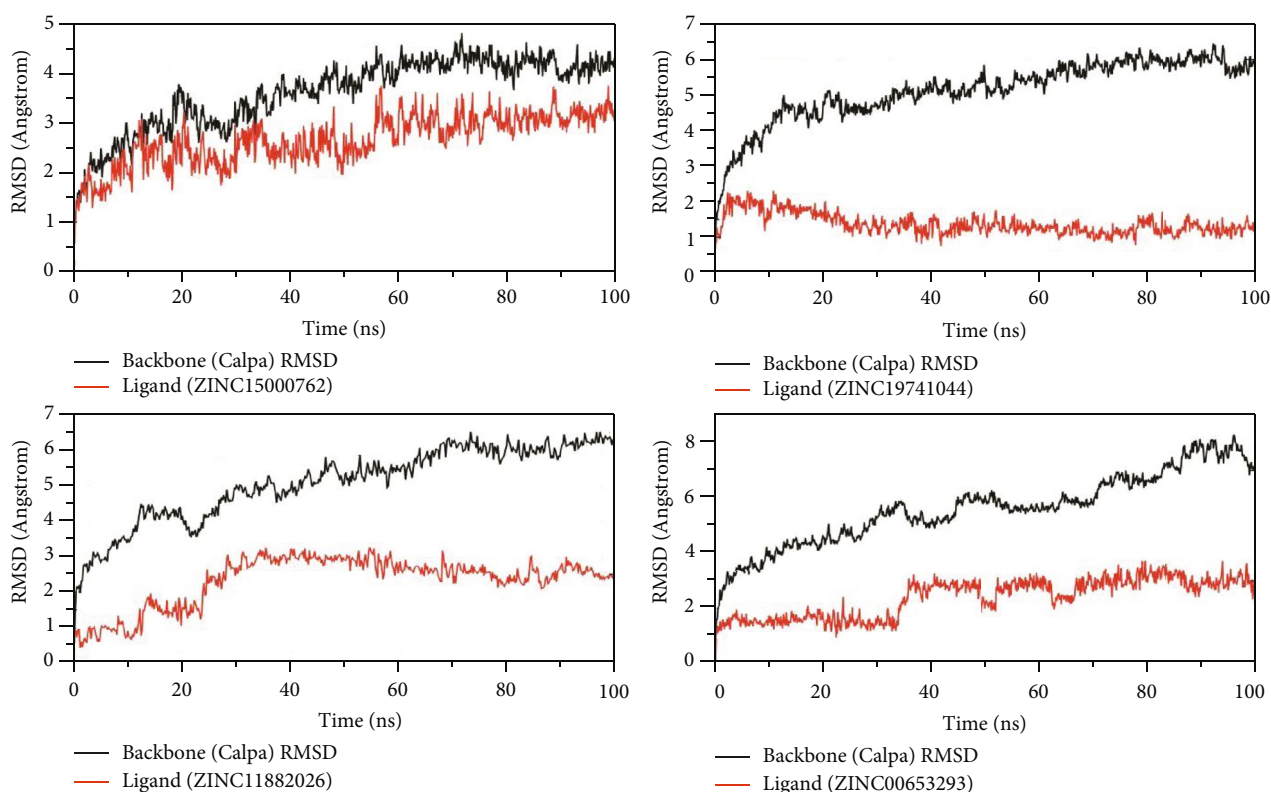
FIGURE 3: RMSD plots of the LHBs protein with corresponding ligands.

The TOPKAT results indicated that none of the compounds were mutagenic, and all of them showed a negative response to the Ames mutagenicity test. The weight of evidence carcinogenicity (WOE) was also evaluated as another toxicity predictor to determine the carcinogenicity of virtual hits, and all compounds were found to be noncarcinogenic, except compound (ZINC19741044). About skin irritation and skin sensitization, all four candidates have no skin irritancy and no skin sensitivity effect, and of these compounds, only compound ZINC00653293 and ZINC15000762 were predicted to be aerobic biodegradable. The comparative ADMET data and TOPKAT results of virtual hits with a standard drug proposed that selected hits may be used as inhibitor molecules for HBV.

4. Discussion

4.1. Structurally Validated Modeled LHBs Occupy Significant Numbers of Residues in the Favored Region. The surface open reading frame (S-ORF) of the hepatitis B virus genome encodes proteins of three distinct types; namely, large (L), middle (M), and small (S) surface proteins, also referred to as LHBs, MHBs, and SHBs, respectively. All of them share common C terminals [5]. The S protein is also referred to as HBsAg and is the most abundant among these three proteins. Its expression is not directly dependent on the L and M envelope protein expression. However, in order to accomplish the normal viral life cycle, the presence of the proper proportion of all the three envelope proteins is essential. If

(a)   (b)   (c)   (d)

(e)   (f)   (g)   (h)
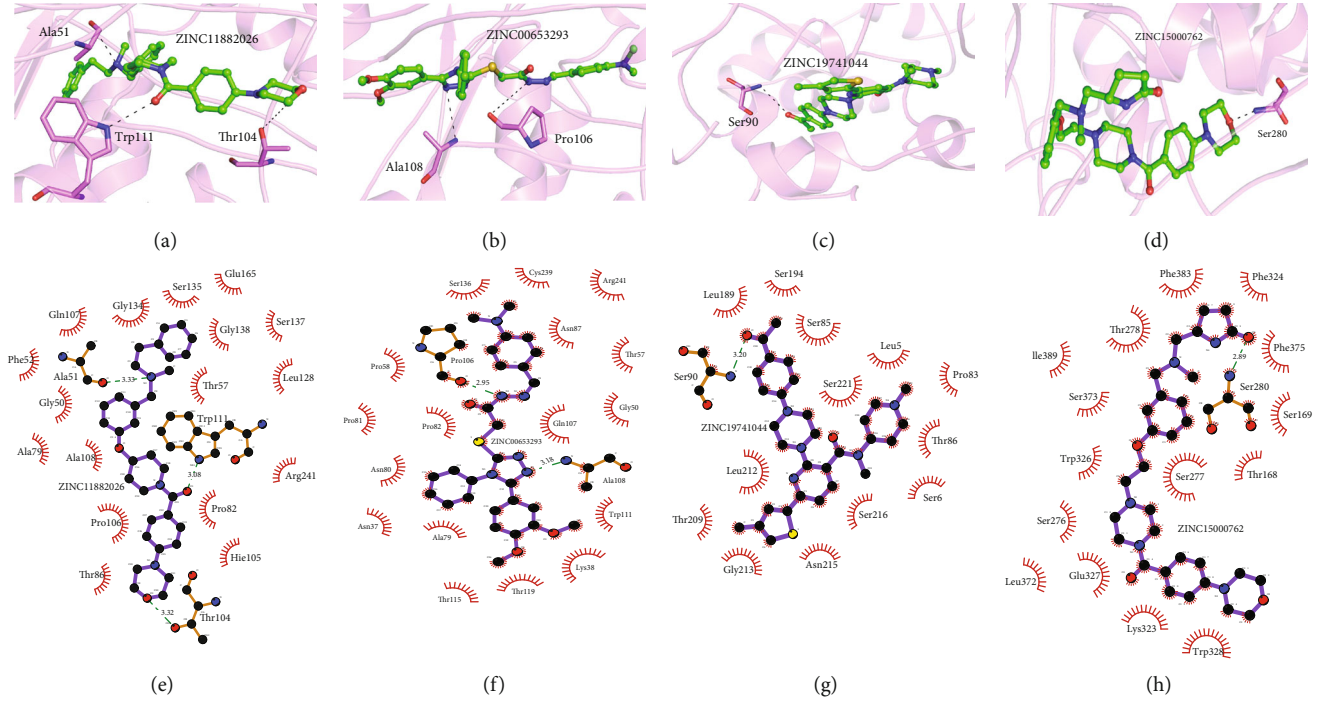
FIGURE 4: The binding patterns (a–d) and 2D representations (e–h) of LHBs in-complexed with ligands are shown: (a, e) 11882026, (b, f) 00653293, (c, g) 19741044, and (d, h) 15000762.

TABLE 2: Molecular properties of selected ligands.

Compound ID	ALogP ($\leq$5)	Molecular weight	H-bond acceptors ($\leq$10)	H-bond donors ($\leq$5)	Apolar desolvation (kcal/Mol)	Polar desolvation (kcal/Mol)	Rotatable bonds ($\leq$10)
ZINC11882026	3.78	514.69	6	1	-1.52	-49.29	9
ZINC00653293	1.91	515.614	9	0	-5.09	-14.77	6
ZINC19741044	4.02	532.734	7	1	13.34	-52.43	6
ZINC15000762	1.70	536.697	9	2	7.87	-57.67	10

LHBs is overexpressed, an indirect hindrance appears in HBsAg secretion [57]. In spite of many studies performed on the pathogenicity of the large HBV surface protein (LHBs) over the past two decades, there is still not much information about the 3D structure of this protein. Several evidences indicate that LHBs is expressed in liver cells and plays a prominent role in chronic hepatitis B even in the development of HCC. On the other hand, with regard to the realization of this fact that the fundamental role of this protein in vaccine development is undeniable, our motivation to predict the 3D structure and perform a geometry optimization was conceived more than ever.

In this study, the LHBs of HBV genotype D has carefully been modeled with the aid of RM2TS+ and I-TASSER and subsequently has the best possible refinements. The purpose of the selection of genotype D is that it is the most prevalent genotype among the Indian population. The amino acid sequences of LHBs were elaborately analyzed, and efforts were made to predict the best optimized structure. The potential LHBs structure was subjected to ProtSAV and

RAMPAGE. Thus, the obtained structure of LHBs lies in the acceptable yellow region (Figure 2(a)) with 94.39% of the residues occupying the favored region (Figure 2(b)). Our findings provided basic insights into the 3D structure of LHBs and introduced four novel compounds having the best interconnection with the most important structural and functional regions of this protein. It is important to mention that LHBs performs many different functions, right from the viral entry to the hepatocytes until the maturation of infectious virions within the endoplasmic reticulum (ER). The protein facilitates the adherence of infectious virions to the heparansulphate proteoglycan on the surface of hepatocytes. The myristoylated N-terminal of the PreS1 domain of the L protein subsequently binds to the sodium taurocholate cotransporting polypeptide (NTCP), the potent receptor identified during the last few years [58]. The PreS1 sequence (2-48) specifically interacts with NTCP [8, 59]. Furthermore, aa 49-75 is also needed for infection. The definitive function of this sequence is not fully established, but it has widely been assumed that aa 49-75 is involved in targeting the NTCP

[59]. There is a spacer region towards the C-terminal to the NTCP binding site which consists of a nucleocapsid binding sequence, essentially needed for the envelopment process of HBV [8].

4.2. Identification of Potential Compounds That Possess the Best Features of Binding Affinity with LHBs. The present study has elaborately been undertaken to create a reliable model to display the construction of LHBs using exhaustive computational approaches, and subsequently, identification of potential compounds showing high affinity with the LHBs protein was carried out. The interactions of LHBs vs. potential ligands (complexes) were visualized in PyMOL (3D) and LigPlot (2D). Four selective ligands, ZINC11882026, ZINC19741044, ZINC00653293, and ZINC15000762 were identified establishing covalent linkages with the amino acids significantly essential for the viral entry process and viral nucleocapsid envelopment. To the best of our knowledge, these compounds as well respective amino acids have for the first time been explored in this study, which apparently could be of relevance in antiviral drug design and related studies. The obtained insight into the modeled protein and the identification of potential inhibitory compounds could be an important milestone in search for the alternative therapies against HBV infection.

The structural organization of L, M, and S proteins and their consequent functions, on one hand are guided in an orchestrated manner, and on the other hand, these critical sequences and structural organization provide enormous space to explore the newer therapeutic approaches for the improvement in HBV-related disease management over a period of time. Interestingly, all the four ligands show a desired affinity with the NTCP binding region (aa 2-48), the most important newly discovered entry receptor. The one which has the closest proximity and forms a hydrogen bond at Ala51 (3 aa downstream) is ZINC11882026. It is perceived that blocking Ala51 with the help of this compound may have some influence on inhibiting the viral entry process. The rest of the residues (111, 104, 106, 108, and 90) are being targeted by ZINC11882026, 00653293, and 19741044 (Figure 4 and Table S3). It is quite interesting to point out that these residues are lying within the so-called spacer region of LHBs, which is supposed to be involved in NC binding that is the envelopment and maturation process of the encapsidated viral genome undergoing in the ER. In the present study, we were able to identify the ligands targeting the spacer region of LHBs for the first time. In other words, the envelopment and morphogenesis of the virus could potentially be inhibited with the help of these ligands.

Only the receptor inhibitor Myrcludex B at a median contraction of 80 pmol/L has been known till date. It is a synthetic N-acylated PreS1 lipopeptide and has been shown to block the NTCP and virus entry process, both *in vitro* and *in vivo* [60, 61]. There was lack of information regarding capsid binding inhibitors. The present study exhaustively searched, analyzed, and identified three inhibitors at the capsid binding locus of LHBs and one at the suspected extension of the receptor. The combination of these compounds in varying permutation combinations could be a novel approach for the simultaneous inhibition of entry/infection and capsid binding/envelopment, thus, targeting the early as well as later phases of viral infection at the same time. However, these warrant an urgent need of testing these newly identified compounds singly or in combination in a cell culture system.

4.3. The Binding Affinity of Identified Compounds and Regulation of Cellular Redox Homeostasis-Associated Therapeutic Advantages Might Outnumber the Disadvantages. Careful modeling of LHBs followed by the identification of entry as well as capsid binding inhibitors having maximum suitability to be used as potential drugs might be of important significance in search of newer therapeutic approaches in order to overcome the difficulties associated with extensive use of nucleoside analogues. However, the suspected accumulation of disproportionate levels of the large surface proteins, in the absence of capsid binding and assembly of the virus, and thus, the possible downstream consequences like the generation of oxidative stress and activation of resultant pathways, at this stage cannot be ruled out. Three of the four inhibitors, namely, ZINC11882026, ZINC00653293, and ZINC19741044, make hydrogen bonds with amino acid residues lying in the capsid binding region of the PreS1 domain of LHBs (Figure 4 and Table S3). The expected result of the usage of these inhibitors may coincide with the viral assembly process. The logical consequences could lead to the accumulation of LHBs within the ER and the possible eventuality could also be related to the disproportionate existence of the L, M, and S envelope proteins intracellularly. The cumulative effect might be reflected in the generation of oxidative stress. It is of quite relevance to critically apprehend the advantages as well as disadvantages of the potential inhibitors. Nevertheless, experimental validation would essentially be needed.

As reported earlier, viral infection may trigger the UPR as a consequence of the overloading of the ER. Viral infection-mediated ER stress, on one hand may promote cell suicide as a strategy to avoid viral replication and spreading, while on the other hand may contribute to innumerable deleterious consequences [62, 63], primarily related to the production of overwhelming levels of reactive oxygen species (ROS). The predominant forms are anionic superoxide (O_2^-) and hydrogen peroxide (H_2O_2) [64, 65]. We apprehend a couple of possible consequences in response to the binding affinity shown by potential compounds with the LHBs identified in this study. Firstly, the possibility of a decreased or impaired encapsidation process might enhance the accumulation of LHBs and/or MHBs in the ER. As a result, the generated stress could be a major contributory cause to the production of more H_2O_2. This could lead to an increased number of disulfide bridge formation during the folding of a protein, involving enzymes such as endoplasmic reticulum oxidoreductin-1 alpha (Ero1α). The relevant signaling pathway might get triggered consequently. Secondly, in response to stress signals, Ca^{2+} might be released from the ER and taken up by mitochondria via the mitochondrial uniporter (MCU). The point of contact between the ER and mitochondria has a major role to play while triggering Ero1α/Ca^{2+} in

this signaling pathway. The activated pathways might involve mitochondrial accumulation of Ca^{2+} in order to trigger signaling and downstream processes [22]. The point of contact between the ER and mitochondria is established by the inositol triphosphate receptor (IP3R) and the voltage-dependent anion channel protein (VDAC). There is a direct impact on the functioning of the electron transport chain (ETC) by the Ca^{2+} level inside the mitochondria with consequences of an increase in ROS production [22].

We had previously demonstrated in one of our studies the intracellular reactive oxygen species production culminating into mitochondrial depolarization. However, the study was an elaborated comparative account of hepatitis B virus X protein mutants K130M, V131I, and KV130/131MI to investigate their roles in fibrosis, cirrhosis, and hepatocellular carcinoma. It was found that the expression of KV130/131MI induced cell proliferation and altered the expression of cell cycle regulatory genes in favor of cell proliferation, intracellular reactive oxygen species (ROS) production, and mitochondrial depolarization [66]. Hence, it is quite understandable that the present study highlighting the binding affinity of newly identified compounds with LHBs might enhance ROS production through Ca^{2+}-mediated alterations in mitochondrial functioning and unfolded protein response.

However, the activation of the Nrf2/ARE pathway is a parallel cascade of signaling in order to provide the rescue operation sensed through the deleterious effects of ROS. The hepatitis B virus induces this pathway of antioxidant defense [20, 67]. Both the transfected cell lines with the HBV genome as well biopsy samples from CHB patients have demonstrated the salvage pathway. Several independent studies have shown the increased levels of Nrf2-dependent phase II enzymes such as glutathione synthetase (GSS) and glutathione reductase [24, 68]. The activation of Nrf2/ARE is known to be triggered by HBx and LHBs also in in vitro cell cultures [67]. PERK, one of the transmembrane kinases, is very important in PERK-dependent activation of Nrf2 and is critical for survival signaling. PERK-dependent phosphorylation leads to the nuclear accumulation of Nrf2 and increased transcription of Nrf2 target genes [69]. PERK function is needed for cellular response to ER stress [23]. Nrf2 confers a protective advantage to stressed cells with the help of an interesting rescue operation that its activation contributes to the maintenance of glutathione levels. Glutathione functions as a buffer/neutralization component at the time of accumulation of reactive oxygen species during the unfolded protein response. Logically, the deleterious effects of Nrf2 or PERK deficiencies could be attenuated by the restoration of cellular glutathione levels or Nrf2 activity.

Based on the findings indicating the appreciable affinity of the inhibitor compounds identified in this study and their high degree of suitability as a drug seen with the help of reliable computational methods (Tables S4 and S5), these compounds could be of great importance in the future. However, it is difficult to predict if these compounds would act as an antiviral either by suppressing the viral load directly or by reducing the opportunity for newer infection of the uninfected hepatocytes in *in vitro* conditions (transformed cell lines). Again, whether the magnitude of ER stress and generation of ROS would be substantial or there will be no or only a minimal level of such stress due to the apprehended accumulation of LHBs cannot be predicted at present.

It must be emphasized here that all the previous studies and their findings discussed here are based on several types of point as well as deletion mutants within the S-ORF, more specifically in the functionally critical residues of the PreS1 and PreS2 domains of LHBs. Several mutations in S-ORFs lead to ER stress in hepatocytes through the accumulation of HBV virions and in the general consequent development of hepatocellular carcinoma and liver damage. Most studies have employed specific types of deletion mutants in LHBs [70, 71]. It is important to mention here that mutations disturbing amino acids 88-108 of PreS1 and the first five amino acids of PreS2, where most of the newly identified compounds in our present study are supposed to interact, have been believed to varyingly influence the capsid binding with the eventuality of interference with HBV assembly. However, the M protein-deficient HBV consisting of arbitrary PreS2 sequences within the L protein has been shown to be infectious [72]. However, because of the presumed lack of viral assembly due to a deficient M protein, the sustainability of the infection still remains unanswered.

Based on the available literature, we still believe that the identified compounds in the present study would be potential inhibitors, primarily for the residues lying within the nucleocapsid binding region at the carboxy terminal region of PreS1 of LHBs (aa90, 104, 106, 108, and 111). The most effective compounds, referred to as ZINC11882026, might have the best inhibitory effects both by virtue of establishing a covalent bond at aa 51 (a suspected residue at the locus within PreS1 facilitating the entry process) and by interacting with aa 104 and 111, which are responsible for NC binding and viral maturation. Both of the significant processes of the viral life cycle, one at the early events of infections and another at the late events related to viral maturation and morphogenesis, may simultaneously be blocked hand in hand with this compound. It is theoretically conceived that ZINC11882026 may regulate both the early and late phases of viral life cycles, thereby controlling the overaccumulation of LHBs and other viral proteins within the ER and cytosol. This could also be attributed to the regulation of the deleterious effects of ROS production and oxidative stress generation; consequently, signaling pathways responsible for tumor genesis might not cross the limits that generally accelerate the process of liver damage. Furthermore, the combination of compound ZINC11882026 with any of the other three compounds could also be of significant relevance in inhibiting the viral life cycle without deregulating the underlying molecular mechanisms pertaining to the signaling cascades of oncogenesis and/or apoptosis by maintaining the desired proportion of L, M, and S proteins. The fourth compound with ZINC15000762 has been shown to interact with serine aa 280 of LHBs which is in fact the aa 117 of the major surface protein (SHBs or HBsAg). This residue lies within the well-known major hydrophilic region (MHR) of HBsAg (aa 100-160). Dual possible impacts may be attributed by this inhibitor: the first

is viral infectivity and the other could be its influence on the antigenicity of HBsAg. The region is also known as the antigenic loop (AGL), and researchers have demonstrated that the residues of AGL, transmembrane-II (Trn-II), and transmembrane-III (Trns-III) are required for infectivity, particularly Gly-119, Pro-120, Cys-121, Arg-122, and Cys-124 [62]. However, the identified residue Ser-117 (Ser-280 with reference to LHBs) in thus study, being present in AGL, might have a role in infectivity also. However, it may not have as much significance with respect to antigenicity like the other residues of MHR. It is quite logical to appreciate that, in addition to many other important features, a good antiviral must have the primary quality of being a good inhibitor of the viral life cycle without significantly modulating antigenicity, particularly for these viral proteins which are involved in eliciting the host immune response. In light of the concept, the inhibitor ZINC15000762 establishes covalent linkage with Ser-117 (with reference to SHBs or HBsAg), and although it would not be able to influence the antigenicity of HBsAg substantially, it may inhibit the infectivity process, in accordance with previous studies. The resulting situation would possibly be a favorable situation in order to present the infectious virions or subviral particles to the immune response of the host and consequently eliminate the existing infection with simultaneous inhibitions of newer infectivity. Nevertheless, the biochemical significance of the amino acid (ser-117) and its presence in AGL could be of relevance to prevent infectivity if inhibited by ZINC15000762.

To conclude, the LHBs modeled with utmost precision and care and the identification of biologically potent inhibitors with the best possible therapeutic features are novel findings, which possibly could be of positive impact in the search of newer therapeutic approaches against hepatitis B virus infection. The expected ROS generation and ER stress development could be managed by using the combination of compounds in order to maintain the proportionate expression and accumulation of large, major, and middle surface proteins, for the purpose of accomplishing normal encapsidation and envelopment processes as generally seen in wild-type HBV.

Data Availability

The amino acid sequence of LHBs of HBV (genotype D, subtype ayw) was retrieved from the UniProt (P03138). The data for the ligands were obtained from the ZINC database. These data and other data used to carry out the study and to support the findings of this study are included within the article and in the supplementary information files.

Conflicts of Interest

The authors declare that they have no conflicts of interest.

Authors' Contributions

All authors have given approval to the final version of the manuscript.

Supplementary Materials

Figure S1: diagrammatic representation of a structure-guided approach to design potential inhibitors of the LHBs protein. Figure S2: distribution of α-helix (pink), β-sheet (yellow), and coil (black) in the LHBs protein. Figure S3: the structures which were obtained from RM2TS+ and I-TASSER were further analyzed using various tools such as ProtSAV and Protein Structure Analysis and Validation, but in order to get a better structure, the MD was run for 20 ns. Table S1: physiological properties of the LHBs protein. Table S2: 2D structure of the identified ligands from the ZINC database. Table S3: comparative analysis of hydrogen bonds in LHBs and four ligands. Table S4: computationally predicted ADME properties of the identified compounds 1-5 by admetSAR and SwissADME. NS: nonsubstrate; S: substrate; NI: noninhibitor; NT: nontoxicity; NC: noncarcinogen; NR: not required. Table S5: TOPKAT values of the identified compounds. NM: nonmutagen; NC: noncarcinogen; C: carcinogen; NI: nonirritant; NS: nonsensitive; S: sensitive. (Supplementary Materials)

References

[1] A. E. Mitchell and H. M. Colvin, *Hepatitis and Liver Cancer: A National Strategy for Prevention and Control of Hepatitis B and C*, National Academies Press, 2010.

[2] E. B. Keeffe, D. T. Dieterich, S. H. B. Han et al., "A treatment algorithm for the management of chronic hepatitis B virus infection in the United States: 2008 update," *Clinical Gastroenterology and Hepatology*, vol. 6, no. 12, pp. 1315–1341, 2008.

[3] T. Inoue and Y. Tanaka, "Hepatitis B virus and its sexually transmitted infection – an update," *Microbial Cell*, vol. 3, no. 9, pp. 419–436, 2016.

[4] T. J. Liang, "Hepatitis B: the virus and disease," *Hepatology*, vol. 49, no. S5, pp. S13–S21, 2009.

[5] E. Karataş, S. Erensoy, U. S. Akarca, and R. Sertöz, "Analysis of hepatitis B virus (HBV) preS1, preS2 and S gene regions from patient groups infected with HBV genotype D," *Mikrobiyoloji Bulteni*, vol. 52, no. 1, pp. 23-24, 2018.

[6] T. T.-C. Yen, A. Yang, W.-T. Chiu et al., "Hepatitis B virus PreS2-mutant large surface antigen activates store-operated calcium entry and promotes chromosome instability," *Oncotarget*, vol. 7, no. 17, pp. 23346–23360, 2016.

[7] R. Prange and R. E. Streeck, "Novel transmembrane topology of the hepatitis B virus envelope proteins," *The EMBO Journal*, vol. 14, no. 2, pp. 247–256, 1995.
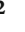
[8] S. Urban, R. Bartenschlager, R. Kubitz, and F. Zoulim, "Strategies to inhibit entry of HBV and HDV into hepatocytes," *Gastroenterology*, vol. 147, no. 1, pp. 48–64, 2014.

[9] J. Le Seyec, P. Chouteau, I. Cannie, C. Guguen-Guillouzo, and P. Gripon, "Role of the pre-S2 domain of the large envelope protein in hepatitis B virus assembly and infectivity," *Journal of Virology*, vol. 72, no. 7, pp. 5573–5578, 1998.

[10] J. Le Seyec, P. Chouteau, I. Cannie, C. Guguen-Guillouzo, and P. Gripon, "Infection process of the hepatitis B virus depends on the presence of a defined sequence in the pre-S1 domain," *Journal of Virology*, vol. 73, no. 3, pp. 2052–2057, 1999.

[11] C. Lepere-Douard, M. Trotard, J. le Seyec, and P. Gripon, "The first transmembrane domain of the hepatitis B virus large envelope protein is crucial for infectivity," *Journal of Virology*, vol. 83, no. 22, pp. 11819–11829, 2009.

[12] R. Rezaee, M. Poorebrahim, S. Najafi et al., "Impacts of the G145R mutation on the structure and immunogenic activity of the hepatitis B surface antigen: a computational analysis," *Hepatitis Monthly*, vol. 16, no. 7, article e39097, 2016.

[13] F. A. Di Lello, E. Ridruejo, A. P. Martínez, P. S. Pérez, R. H. Campos, and D. M. Flichman, "Molecular epidemiology of hepatitis B virus mutants associated with vaccine escape, drug resistance and diagnosis failure," *Journal of Viral Hepatitis*, vol. 26, no. 5, pp. 552–560, 2019.

[14] H.-y. Zhang, L. G. Liu, C. Y. Ye et al., "Evolution of drug-resistant mutations in HBV genomes in patients with treatment failure during the past seven years (2010–2016)," *Virus Genes*, vol. 54, no. 1, pp. 41–47, 2018.

[15] F. Zoulim and S. Locarnini, "Hepatitis B virus resistance to nucleos(t)ide analogues," *Gastroenterology*, vol. 137, no. 5, pp. 1593–1608.e2, 2009.

[16] A. S. Lok, F. Zoulim, S. Locarnini et al., "Antiviral drug-resistant HBV: standardization of nomenclature and assays and recommendations for management," *Hepatology*, vol. 46, no. 1, pp. 254–265, 2007.

[17] S. Locarnini, "Molecular virology and the development of resistant mutants: implications for therapy," *Seminars in Liver Disease*, vol. 25, pp. 9–19, 2005.

[18] S. A. Locarnini and L. Yuen, "Molecular genesis of drug-resistant and vaccine-escape HBV mutants," *Antiviral Therapy*, vol. 15, no. 3, Part B, pp. 451–461, 2010.

[19] J. Petersen, M. Dandri, W. Mier et al., "Prevention of hepatitis B virus infection in vivo by entry inhibitors derived from the large envelope protein," *Nature Biotechnology*, vol. 26, no. 3, pp. 335–341, 2008.

[20] K.-H. Peiffer, S. Akhras, K. Himmelsbach et al., "Intracellular accumulation of subviral HBsAg particles and diminished Nrf2 activation in HBV genotype G expressing cells lead to an increased ROI level," *Journal of Hepatology*, vol. 62, no. 4, pp. 791–798, 2015.

[21] S. B. Cullinan and J. A. Diehl, "PERK-dependent activation of Nrf2 contributes to redox homeostasis and cell survival following endoplasmic reticulum stress," *Journal of Biological Chemistry*, vol. 279, no. 19, pp. 20108–20117, 2004.

[22] A. V. Ivanov, V. T. Valuev-Elliston, D. A. Tyurina et al., "Oxidative stress, a trigger of hepatitis C and B virus-induced liver carcinogenesis," *Oncotarget*, vol. 8, no. 3, 2017.

[23] H. P. Harding, Y. Zhang, A. Bertolotti, H. Zeng, and D. Ron, "*Perk* is essential for translational regulation and cell survival during the unfolded protein response," *Molecular Cell*, vol. 5, no. 5, pp. 897–904, 2000.

[24] H. Li, W. Zhu, L. Zhang et al., "The metabolic responses to hepatitis B virus infection shed new light on pathogenesis and targets for treatment," *Scientific Reports*, vol. 5, no. 1, p. 8421, 2015.

[25] J.-S. Pan, M.-Z. Hong, and J.-L. Ren, "Reactive oxygen species: a double-edged sword in oncogenesis," *World Journal of Gastroenterology*, vol. 15, no. 14, pp. 1702–1707, 2009.

[26] L. J. McGuffin, K. Bryson, and D. T. Jones, "The PSIPRED protein structure prediction server," *Bioinformatics*, vol. 16, no. 4, pp. 404-405, 2000.

[27] J. D. Bendtsen, L. J. Jensen, N. Blom, G. von Heijne, and S. Brunak, "Feature-based prediction of non-classical and leaderless protein secretion," *Protein Engineering Design and Selection*, vol. 17, no. 4, pp. 349–356, 2004.

[28] E. Gasteiger, C. Hoogland, A. Gattiker et al., "Protein identification and analysis tools on the ExPASy server," in *The Proteomics Protocols Handbook*, pp. 571–607, Humana Press, 2005.

[29] D. DasGupta, R. Kaushik, and B. Jayaram, "From Ramachandran maps to tertiary structures of proteins," *The Journal of Physical Chemistry B*, vol. 119, no. 34, pp. 11136–11145, 2015.

[30] J. Yang, R. Yan, A. Roy, D. Xu, J. Poisson, and Y. Zhang, "The I-TASSER suite: protein structure and function prediction," *Nature Methods*, vol. 12, no. 1, pp. 7-8, 2015.

[31] A. Singh, R. Kaushik, A. Mishra, A. Shanker, and B. Jayaram, "ProTSAV: a protein tertiary structure analysis and validation server," *Biochimica et Biophysica Acta (BBA) - Proteins and Proteomics*, vol. 1864, no. 1, pp. 11–19, 2016.

[32] W. Wang, M. Xia, J. Chen et al., "Data set for phylogenetic tree and RAMPAGE Ramachandran plot analysis of SODs in *Gossypium raimondii* and *G. arboreum*," *Data in Brief*, vol. 9, pp. 345–348, 2016.

[33] G. Mukherjee and B. Jayaram, "A rapid identification of hit molecules for target proteins via physicochemical descriptors," *Physical Chemistry Chemical Physics*, vol. 15, no. 23, pp. 9107–9116, 2013.

[34] Y. Hu, B. Sherborne, T. S. Lee, D. A. Case, D. M. York, and Z. Guo, "The importance of protonation and tautomerization in relative binding affinity prediction: a comparison of AMBER TI and Schrödinger FEP," *Journal of Computer-Aided Molecular Design*, vol. 30, no. 7, pp. 533–539, 2016.

[35] T. Singh, D. Biswas, and B. Jayaram, "*AADS* - an automated active site identification, docking, and scoring protocol for protein targets based on physicochemical descriptors," *Journal of Chemical Information and Modeling*, vol. 51, no. 10, pp. 2515–2527, 2011.

[36] A. Soni, K. Pandey, P. Ray, and B. Jayaram, "Genomes to hits in silico - a country path today, a highway tomorrow: a case study of Chikungunya," *Current Pharmaceutical Design*, vol. 19, no. 26, pp. 4687–4700, 2013.

[37] J. J. Irwin and B. K. Shoichet, "ZINC - a free database of commercially available compounds for virtual screening," *Journal of Chemical Information and Modeling*, vol. 45, no. 1, pp. 177–182, 2005.

[38] A. Gupta, A. Gandhimathi, P. Sharma, and B. Jayaram, "ParDOCK: an all atom energy based Monte Carlo docking protocol for protein-ligand complexes," *Protein & Peptide Letters*, vol. 14, no. 7, pp. 632–646, 2007.

[39] P. Mark and L. Nilsson, "Structure and dynamics of the TIP3P, SPC, and SPC/E water models at 298 K," *The Journal of Physical Chemistry A*, vol. 105, no. 43, pp. 9954–9960, 2001.

[40] C. I. Bayly, P. Cieplak, W. Cornell, and P. A. Kollman, "A well-behaved electrostatic potential based method using charge restraints for deriving atomic charges: the RESP model," *The Journal of Physical Chemistry*, vol. 97, no. 40, pp. 10269–10280, 1993.

[41] W. D. Cornell, P. Cieplak, C. I. Bayly, and P. A. Kollman, "Application of RESP charges to calculate conformational energies, hydrogen bond energies, and free energies of solvation," *Journal of the American Chemical Society*, vol. 115, no. 21, pp. 9620–9631, 2002.

[42] H. C. Andersen, "Rattle: a "velocity" version of the shake algorithm for molecular dynamics calculations," *Journal of Computational Physics*, vol. 52, no. 1, pp. 24–34, 1983.

[43] V. Kräutler, W. F. van Gunsteren, and P. H. Hünenberger, "A fast SHAKE algorithm to solve distance constraint equations for small molecules in molecular dynamics simulations," *Journal of Computational Chemistry*, vol. 22, no. 5, pp. 501–508, 2001.

[44] M. Valiev, E. J. Bylaska, N. Govind et al., "NWChem: a comprehensive and scalable open-source solution for large scale molecular simulations," *Computer Physics Communications*, vol. 181, no. 9, pp. 1477–1489, 2010.

[45] F. Cheng, W. Li, Y. Zhou et al., "admetSAR: A Comprehensive Source and Free Tool for Assessment of Chemical ADMET Properties," *Journal of Chemical Information and Modeling*, vol. 52, no. 11, pp. 3099–3105, 2012.

[46] A. Daina, O. Michielin, and V. Zoete, "SwissADME: a free web tool to evaluate pharmacokinetics, drug-likeness and medicinal chemistry friendliness of small molecules," *Scientific Reports*, vol. 7, no. 1, article 42717, 2017.

[47] K. Enslein, V. K. Gombar, and B. W. Blake, "Use of SAR in computer-assitted prediction of carcinogenicity and mutagenicity of chemicals by the *TOPKAT* program," *Mutation Research/Fundamental and Molecular Mechanisms of Mutagenesis*, vol. 305, no. 1, pp. 47–61, 1994.

[48] T. Jain and B. Jayaram, "An all atom energy based computational protocol for predicting binding affinities of protein–ligand complexes," *FEBS Letters*, vol. 579, no. 29, pp. 6659–6666, 2005.

[49] W. J. Egan and G. Lauri, "Prediction of intestinal permeability," *Advanced Drug Delivery Reviews*, vol. 54, no. 3, pp. 273–289, 2002.

[50] W. J. Egan, K. M. Merz, and J. J. Baldwin, "Prediction of drug absorption using multivariate statistics," *Journal of Medicinal Chemistry*, vol. 43, no. 21, pp. 3867–3877, 2000.

[51] A. Cheng and K. M. Merz, "Prediction of aqueous solubility of a diverse set of compounds using quantitative structure–property relationships," *Journal of Medicinal Chemistry*, vol. 46, no. 17, pp. 3572–3580, 2003.

[52] H. van de Waterbeemd and E. Gifford, "ADMET in silico modelling: towards prediction paradise?," *Nature Reviews Drug Discovery*, vol. 2, no. 3, pp. 192–204, 2003.

[53] C. de Graaf, N. P. E. Vermeulen, and K. A. Feenstra, "Cytochrome P450 in silico: an integrative modeling approach," *Journal of Medicinal Chemistry*, vol. 48, no. 8, pp. 2725–2755, 2005.

[54] A. Alam, N. Tamkeen, N. Imam et al., "Pharmacokinetic and molecular docking studies of plant-derived natural compounds to exploring potential anti-Alzheimer activity," in *In Silico Approach for Sustainable Agriculture*, pp. 217–238, Springer, 2018.

[55] A. Cheng and S. L. Dixon, "In silico models for the prediction of dose-dependent human hepatotoxicity," *Journal of Computer-Aided Molecular Design*, vol. 17, no. 12, pp. 811–823, 2003.

[56] X. Xia, E. G. Maliski, P. Gallant, and D. Rogers, "Classification of kinase inhibitors using a Bayesian model," *Journal of Medicinal Chemistry*, vol. 47, no. 18, pp. 4463–4470, 2004.

[57] K. Molnar-Kimber, V. Jarocki-Witek, S. K. Dheer et al., "Distinctive properties of the hepatitis B virus envelope proteins," *Journal of Virology*, vol. 62, no. 2, pp. 407–416, 1988.

[58] H. Yan, G. Zhong, G. Xu et al., "Sodium taurocholate cotransporting polypeptide is a functional receptor for human hepatitis B and D virus," *eLife*, vol. 1, article e00049, 2012.

[59] K. Watashi, S. Urban, W. Li, and T. Wakita, "NTCP and beyond: opening the door to unveil hepatitis B virus entry," *International Journal of Molecular Sciences*, vol. 15, no. 2, pp. 2892–2905, 2014.

[60] D. Glebe, S. Urban, E. V. Knoop et al., "Mapping of the hepatitis B virus attachment site by use of infection-inhibiting preS1 lipopeptides and tupaia hepatocytes," *Gastroenterology*, vol. 129, no. 1, pp. 234–245, 2005.

[61] P. Gripon, I. Cannie, and S. Urban, "Efficient inhibition of hepatitis B virus infection by acylated peptides derived from the large viral surface protein," *Journal of Virology*, vol. 79, no. 3, pp. 1613–1622, 2005.

[62] H. C. Wang, W. Huang, M. D. Lai, and I. J. Su, "Hepatitis B virus pre-S mutants, endoplasmic reticulum stress and hepatocarcinogenesis," *Cancer Science*, vol. 97, no. 8, pp. 683–688, 2006.

[63] J. H. Lin, P. Walter, and T. S. B. Yen, "Endoplasmic reticulum stress in disease pathogenesis," *Annual Review of Pathology: Mechanisms of Disease*, vol. 3, no. 1, pp. 399–425, 2008.

[64] M. Gutowski and S. Kowalczyk, "A study of free radical chemistry: their role and pathophysiological significance," *Acta Biochimica Polonica*, vol. 60, no. 1, 2013.

[65] O. Augusto and S. Miyamoto, "Oxygen radicals and related species," in *Principles of Free Radical Biomedicine*, vol. 1, pp. 19–42, Nova Science Publishers, Inc., 2011.

[66] Z. I. Siddiqui, S. R. Farooqui, S. A. Azam et al., "A comparative study of hepatitis B virus X protein mutants K130M, V131I and KV130/131MI to investigate their roles in fibrosis, cirrhosis and hepatocellular carcinoma," *Journal of Viral Hepatitis*, vol. 24, no. 12, pp. 1121–1131, 2017.

[67] S. Schaedler, J. Krause, K. Himmelsbach et al., "Hepatitis B virus induces expression of antioxidant response element-regulated genes by activation of Nrf2," *Journal of Biological Chemistry*, vol. 285, no. 52, pp. 41074–41086, 2010.

[68] T. Severi, C. Ying, J. R. Vermeesch et al., "Hepatitis B virus replication causes oxidative stress in HepAD38 liver cells," *Molecular and Cellular Biochemistry*, vol. 290, no. 1-2, pp. 79–85, 2006.

[69] S. B. Cullinan, D. Zhang, M. Hannink, E. Arvisais, R. J. Kaufman, and J. A. Diehl, "Nrf2 is a direct PERK substrate and effector of PERK-dependent cell survival," *Molecular and Cellular Biology*, vol. 23, no. 20, pp. 7198–7209, 2003.

[70] Y.-H. Hsieh, I. J. Su, H. C. Wang et al., "Pre-S mutant surface antigens in chronic hepatitis B virus infection induce oxidative stress and DNA damage," *Carcinogenesis*, vol. 25, no. 10, pp. 2023–2032, 2004.

[71] P. K. Chua, R. Y. L. Wang, M. H. Lin, T. Masuda, F. M. Suk, and C. Shih, "Reduced secretion of virions and hepatitis B virus (HBV) surface antigen of a naturally occurring HBV variant correlates with the accumulation of the small S envelope protein in the endoplasmic reticulum and Golgi apparatus," *Journal of Virology*, vol. 79, no. 21, pp. 13483–13496, 2005.

[72] Y. Ni, J. Sonnabend, S. Seitz, and S. Urban, "The pre-s2 domain of the hepatitis B virus is dispensable for infectivity but serves a spacer function for L-protein-connected virus assembly," *Journal of Virology*, vol. 84, no. 8, pp. 3879–3888, 2010.

Research Article

Hepatitis C Virus RNA-Dependent RNA Polymerase Is Regulated by Cysteine S-Glutathionylation

Marina K. Kukhanova [ID],[1] Vera L. Tunitskaya [ID],[1] Olga A. Smirnova [ID],[1] Olga A. Khomich,[1,2] Natalia F. Zakirova [ID],[1] Olga N. Ivanova [ID],[1] Rustam Ziganshin [ID],[3] Birke Bartosch [ID],[2] Sergey N. Kochetkov [ID],[1] and Alexander V. Ivanov [ID][1]

[1]Engelhardt Institute of Molecular Biology, Russian Academy of Sciences, Moscow, Russia
[2]Université Claude Bernard Lyon 1, INSERM 1052, CNRS 5286, Centre Léon Bérard, Centre de Recherche en Cancérologie de Lyon, Lyon 69434, France
[3]Shemyakin-Ovchinnikov Institute of Bioorganic Chemistry, Russian Academy of Sciences, Moscow, Russia

Correspondence should be addressed to Alexander V. Ivanov; aivanov@yandex.ru

Hepatitis C virus (HCV) triggers massive production of reactive oxygen species (ROS) and affects expression of genes encoding ROS-scavenging enzymes. Multiple lines of evidence show that levels of ROS production contribute to the development of various virus-associated pathologies. However, investigation of HCV redox biology so far remained in the paradigm of oxidative stress, whereas no attention was given to the identification of redox switches among viral proteins. Here, we report that one of such redox switches is the NS5B protein that exhibits RNA-dependent RNA polymerase (RdRp) activity. Treatment of the recombinant protein with reducing agents significantly increases its enzymatic activity. Moreover, we show that the NS5B protein is subjected to S-glutathionylation that affects cysteine residues 89, 140, 170, 223, 274, 521, and either 279 or 295. Substitution of these cysteines except C89 and C223 with serine residues led to the reduction of the RdRp activity of the recombinant protein in a primer-dependent assay. The recombinant protein with a C279S mutation was almost inactive in vitro and could not be activated with reducing agents. In contrast, cysteine substitutions in the NS5B region in the context of a subgenomic replicon displayed opposite effects: most of the mutations enhanced HCV replication. This difference may be explained by the deleterious effect of oxidation of NS5B cysteine residues in liver cells and by the protective role of S-glutathionylation. Based on these data, redox-sensitive posttranslational modifications of HCV NS5B and other proteins merit a more detailed investigation and analysis of their role(s) in the virus life cycle and associated pathogenesis.

1. Introduction

Hepatitis C virus (HCV) is a widespread human pathogen that in 80% cases establishes persistent replication in the liver [1]. The WHO estimates 0.5-2% of the world population to be chronic hepatitis C (CHC) carriers. CHC is often accompanied by persistent inflammation, fibrosis, and various metabolic disorders in the liver [2]. All these pathologies contribute to a possible development of liver cirrhosis and hepatocellular carcinoma. Together with hepatitis B virus (HBV), HCV accounts for approximately 80% of HCC cases

in the world [3]. Since 2011, multiple compounds that target enzymatic activity and/or functions of the HCV protease (NS3 protein), RNA-dependent RNA polymerase (RdRp, NS5B protein), and the regulatory NS5A protein were approved for the treatment of CHC [4]. Using treatment combinations, sustained virological response rates have reached 95-99% (for example, [5–7]). At the same time, clearance of the infection does not reduce risks of the development of liver cirrhosis and cancer to the initial level, observed in the uninfected population [8]. Scarce studies provided evidence that even acute hepatitis C that clears

spontaneously leads to an elevated rate of liver pathologies. So, the investigation of the interplay between the virus and host cell processes requires additional endeavors.

One of the factors that contributes to liver pathologies is the disturbance of the redox status of the host cell (reviewed in [8]). It results from enhanced production of reactive oxygen species (ROS) and altered expression of ROS-scavenging enzymes. ROS represent a spectrum of short-lived oxygen intermediates including hydroxyl radicals (HO·), superoxide anions ($O_2^{·-}$), hydrogen peroxide (H_2O_2), and others [9]. As several types of ROS have a very high oxidizing potential towards various biological molecules, enhanced ROS production above the levels that can be scavenged by the host antioxidant systems was considered hazardous for cells. At the same time, there are mounting pieces of evidence that ROS play signaling and regulatory functions and thus are indispensable for cells [10]. So, in recent years, the redox community shifted away from measuring and identifying ROS towards the identification and investigation of redox switches, *such as oxidation* of cysteine -SH groups into sulfenic (-SOH) or sulfinic (-SO_2H) acid residues, and S-glutathionylation (*i.e.*, coupling to glutathione via disulfide bond), and to assess the consequent impact on protein structure, stability, and function. Oxidation changes for example the enzymatic activity of protein phosphatases (PTPs) [11] and thus affects signaling pathways, hyperoxidation-driven gain of chaperone activity by peroxiredoxins [12], and redox-driven glutathionylation of Na^+/K^+-ATPase that abolishes their activity and thus changes the levels of monovalent ions in cells [13].

However, much less is known about redox biology of viral infections. With few exceptions, studies so far focused on the investigation of mechanisms by which various viruses augment ROS production and solicit expression of antioxidant enzymes such as catalase (CAT), superoxide dismutases (SOD), or glutathione peroxidases (GPx) (as reviewed in [8, 14, 15] and other reviews). In addition, some efforts were given to establishing correlations between levels of ROS production and virus-associated pathologies [8, 14–17]. In contrast, almost no attention was given to a possibility of redox posttranslational modification of viral proteins and their role in virus life cycle and pathogenesis. The only exceptions are the reported S-glutathionylation of retroviral proteases [18–20], nsP2 of chikungunya virus [21] and of NS5 protein of Zika, and dengue [22].

There are many pieces of evidence that show that HCV triggers massive ROS production that is even higher than that observed in HBV infections. HCV induces mitochondrial dysfunction and induces ROS-producing enzymes such as NADPH oxidases (Nox) 1 and 4 [23–26], cytochrome P450 2E1 [23, 24], and ER oxidoreductin 1α (Ero1α) [23]. HCV also affects the expression of antioxidant enzymes including those regulated by the Nrf2 transcription factor, although the results from different groups remain controversial [27–29]. Several studies also suggest that replication [30] and production of infectious virions [31] are suppressed by lipid peroxides whose production is augmented by the infection. However, a possibility of a direct modulation of HCV protein functions by ROS or other reactive species, as well

as redox-sensitive cysteine modifications, remains unexplored. In the presence of the virus or its proteins, production of hydrogen peroxide is augmented, which can lead to oxidation of cysteine residues. In addition, HCV causes elevation of the levels of oxidized glutathione that may drive S-glutathionylation of cellular and viral proteins. So, our goal was to investigate if the NS5B protein is subjected to S-glutathionylation and if such a modification may play a role in regulation of NS5B RNA polymerase activity.

2. Experimental Section

2.1. Reagents. The plasmid pJFH1-SGR and Huh7.5 cells were courteously provided by Prof. C.M. Rice (The Rockefeller University, New York, USA) and Apath, L.L.C. (St. Louis, MI, USA). Restriction endonucleases were from Fermentas (Vilnius, Lithuania), and oligonucleotides were synthesized by Evrogen JSC (Moscow, Russia). DNA purification kits and DNA polymerases were also provided by Evrogen. Ni-NTA-agarose and Rosetta(DE3) *Escherichia coli* were purchased from Novagen (Madison, WI, USA). Most of other reagents were from Sigma-Aldrich (St. Louis, MO, USA) if not stated otherwise.

2.2. Construction of the Plasmids. The plasmid pET21-2c-NS5BΔ21 encoding the C-terminally truncated protein of the JFH1 isolate was constructed using the two-cistron vector described previously [32]. The protein-encoding DNA fragment was amplified from the plasmid pJFH1-SGR using the oligonucleotides 5′-AATGAATTCCATGT CATACTCCTGGAC-3′ and 5′-AATCTCGAGGCGGGGT CGGGCGCGC-3′. The resulting DNA fragment was digested with endonucleases *Eco*RI and *Xho*I and cloned into the respective sites of the vector pET-21-2c.

Construction of the plasmids for the expression of NS5B mutants with cysteine-to-serine substitutions was performed according to an approach of Ho et al. [33]. Briefly, the fragments containing the mutation were amplified from the plasmid pET21-2c-NS5BΔ21 using two parts each using the oligonucleotides listed in Table S1. A typical reaction contained 5-10 ng of template DNA, 5 pmol of each flanking primer and mutagenic primer, 200 μM of each dNTP, and 2 units of Tersus polymerase mix (Evrogen) in the recommended buffer. Amplification was obtained after 20 cycles of 15 sec at 95°C, 15 sec at 60°C, and 60 sec at 72°C. Then, 15-30 ng the resulting products representing the "Head" and the "Tail" of the target fragment bearing the mutation were mixed together and subjected to additional 12 rounds of PCR, using 5 pmol of each flanking primer. The products were isolated by agarose gel electrophoresis with subsequent extraction using a Cleanup Standard kit (Evrogen), digested with endonucleases listed in Table S1, and cloned into the plasmid pET21-2c-NS5BΔ21 instead of the nonmutated fragment.

Construction of the plasmids encoding HCV subgenomic replicons with substitutions in the NS5B-coding region was performed similarly, using the plasmid pSGR-JFH1 and the oligonucleotides listed in Table S2. The mutants with substitutions of C89S, C179S, C146S, and C223S were done

by amplification of pairs of fragments constituting the region between BsrGI and SnaBI sites, whereas the mutants C274S, C279S, C295S, and D318N, and C521S were constructed by amplification of the SnaBI-EcoRV fragment. In the latter case, the analysis of insert orientation was performed. In case of the C521S mutant, the single SnaBI-EcoRV fragment was amplified, digested with these endonucleases, and cloned as discussed above.

The sequence of all constructs was confirmed by sequencing in Center "Genome" (EIMB, Moscow, Russia).

2.3. Expression and Purification of the NS5B Δ21 Protein. Wild-type and mutant forms of the NS5B protein were expressed in *E.coli* Rosetta(DE3) strain and purified on the Ni-NTA column as described previously [32] with the exception of absence 2-mercaptoethanol during purification.

2.4. RNA Polymerase Activity Assay. The RNA-dependent RNA polymerase activity of the NS5B protein was measured in primer-dependent and primer-independent assays as described previously [32, 34]. When required, the protein was preincubated with 10 mM dithiothreitol, 1 mM GSH, or 1 mM GSSG in the reaction buffer (20 mM Tris-HCl, pH 7.5, 20 mM KCl, 4 mM $MgCl_2$) for 10 min in ice prior to the addition of the template or template/primer complex and nucleoside triphosphates to initiate the enzymatic reaction. The reaction was carried out in accordance with the published procedure [32], with the exception of usage of 1 μM UTP.

2.5. Western Blotting. The NS5B protein (0.1-2 μg) mixed with a Laemmli loading lacking DTT or 2-mercaptoethanol was incubated at 40°C for 10 min, applied onto 10% SDS-PAGE, and transferred onto a nitrocellulose membrane (GE Healthcare, Little Chalfont, UK) in 25 mM Tris, 192 mM glycine, and 20% methanol, which was blocked with 5% nonfat milk in phosphate-buffered saline (PBS) for 1 h at room temperature (RT). The membrane was probed with a primary antibody to S-glutathionylated proteins (Millipore, MAB5310, 1 : 1000) in PBS supplemented with 0.1% Tween-20 (PBS-T) or with a serum of the rabbit immunized with the recombinant NS5B protein [35] in 5% nonfat milk in PBS-T at 4°C overnight and washed 3 times for 10 min with PBS-T followed by incubation with a secondary antibody: anti-mouse antibody (Santa-Cruz Biotechnology, sc-2005, 1 : 5,000) or anti-rabbit antibody (Santa-Cruz Biotechnology, sc-2005, 1 : 5,000) in PBS-T for 1 h at RT. After three additional washing steps with PBS-T, immunoblots were visualized using an ECL pico detection system (Thermo Fisher Scientific, Rockford, IL, USA).

2.6. Mass Spectrometry. The identification of cysteine residues of the NS5B protein that undergo S-glutathionylation was performed by MALDI-TOF MS. The protein was incubated alone or in the presence of 170 μM GSSG for 30 min at room temperature, then with a Laemmli buffer lacking reducing agent for 5 min at 98°C, and loaded onto a 10% SDS-polyacrylamide gel. The band corresponding to NS5B was excised and subjected to in-gel digestion by trypsin [36]. For in-gel digestion, trypsin was dissolved in 50 mM

ammonium bicarbonate buffer solution in a concentration of 13 ng/μl correspondingly just before use. The MALDI-TOF MS analysis of the resulting peptide fragments was performed using an Ultraflex II TOF/TOF mass spectrometer (Bruker Daltonics, Germany) with a reflector positive ion mode. Tryptic fragments in solution (1 μl) were transferred onto the MTP 384 target plate polished steel TF mass spectrometric target and mixed with a 1 μl of a matrix solution consisting of 2,4-dihydroxybenzoic acid (201346, Bruker Daltonics) in concentrations of 20 mg/ml, 50% acetonitrile in water, and 0.1% TFA. Results of 4000 laser impulses (200 impulses from 20 different points of one spot) were summed up for every spectrum. The MS data were processed using Bruker Daltonics Flex Analysis 2.4 software, and the accuracy of mass determination of peptides was fixed to 100 ppm. The correlation of the MS data with the protein sequence was done using Bruker Daltonics BioTools 3.0 software.

2.7. HCV Replicons. HCV subgenomic replicons were obtained by *in vitro* transcription of the RNAs from pSGR-JFH1 plasmids encoding the wild-type or mutated NS5B protein and its delivery into Huh7.5 cells by electroporation according to the standard protocol [37] and selection of the G418-resistant colonies. The cells were harvested at passages 3, 5, and 8.

2.8. Reverse Transcription and Real-Time PCR. HCV RNA levels were quantified by reverse transcription and real-time PCR and normalized to levels of mRNA encoding glucuronidase B (GUS). Briefly, total RNA was purified with a TRIzol reagent and cDNA was synthesized with random hexamer primer and RevertAid reverse transcriptase (Thermo Fisher Scientific, Rockford, IL, USA) according to the manufacturer's specifications. PCR was performed using primers for HCV (5′-GTCTAGCCATGGCGTT AGTA-3′ and 5′-CTCCCGGGGCACTCGCAAGC-3′) and GUS (5′-CGTGGTTGGAGAGCTCATTTGGAA-3′ and 5′-ATTCCCCAGCACTCTCGTCGGT-3′). A standard reaction mixture (13 μl) contained the respective primers, cDNA equivalent to 50 ng total RNA, and qPCRmix-HS SYBR (Evrogen). The real-time PCR thermal conditions were 55°C for 5 min, 95°C for 10 min, followed by 40 cycles each at 95°C for 10 s, and 57°C for 1 min (signal collection temperature). The results were analyzed by the $\Delta\Delta Ct$ approach.

2.9. Alignment of NS5B Sequences. For alignment, the following NS5B protein sequences (591 amino acid sequences of C-terminal part of the HCV polyprotein) of the corresponding HCV isolates (genotypes) were selected: 1a (H77, AAB66324), 1a (TN, ABR25251), 1a (DH6), 1a (HCV1, AAA45676), 1b (Con1, CAB46677), 1b (J4, AAC15725), 1b (DH1, KY427256), 2a (JFH1, BAB32872), 2a (JFH2, BAM28690), 2a (J6, BAA00792), 2b (J8, AFJ14788), 3a (S52, ADF97232), 4a (ED43, ADF97234), 5a (SA13, AAC61696), 6a (EUHK2, CAA72801), and 7a (QC69 accession ABN05226). Alignment was performed using
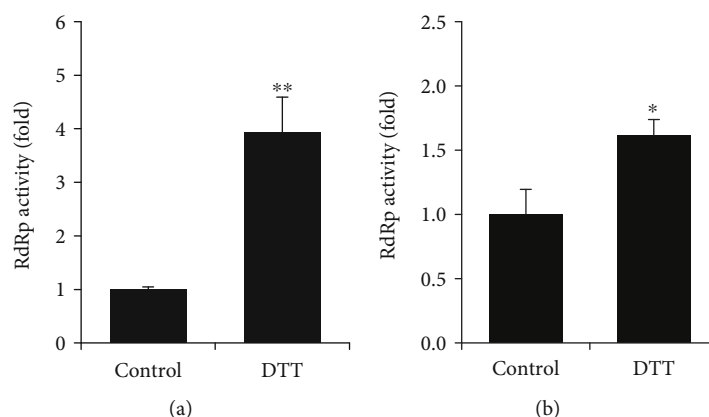
FIGURE 1: Primer-dependent (a) and *de novo* (b) RdRp activity of the recombinant NS5BΔ21 protein is stimulated in the presence of dithiothreitol. The results are presented as the mean ± SD. The control represents the untreated recombinant protein. $^*p < 0.05$ and $^{**}p < 0.001$ (Mann-Whitney test).

Clustal Omega online service [38] at https://www.ebi.ac.uk/Tools/msa/clustalo/ site.

2.10. Statistical Analysis. Statistical analysis was performed using GraphPad software (GraphPad Software, San Diego, CA, USA). The results are presented as the means ± SD. Significant differences between two groups were determined using the Mann-Whitney test, whereas multiple comparisons were accessed by the Kruskal-Wallis method with the Benjamini and Hochberg procedure. Statistical differences between the activities of the mutated NS5B proteins in the absence and presence of DTT were analyzed by multiple paired Student's *t*-test.

3. Results

3.1. RNA-Dependent RNA Polymerase Activity of NS5B Protein Is Redox-Dependent. Purification of various DNA and RNA polymerases and measurement of their enzymatic activity are often performed in the presence of reducing agents such as 2-mercaptoethanol or dithiothreitol. However, to our knowledge, the reasons for the addition of these reagents are unknown. We asked therefore whether the protein's function is dependent on the presence of reducing agents. So, first, we investigated whether the RdRp activity of NS5B protein changes upon the addition of reducing agents. As the most widely used cell model for HCV replication is based on the virus genome of the JFH1 isolate of 2a genotype (gt), we expressed NS5B of 2a gt in *E.coli* and purified the recombinant protein using the vector previously developed for the expression of the polymerase of Con1 isolate [32]. It should be noted that NS5B was expressed as a truncated form lacking the C-terminal membrane-spanning motif comprising 21 amino acid residues (NS5BΔ21). In order to preserve the state of cysteine residues, purification was performed in the absence of reducing agents (i.e., DTT or 2-mercaptoethanol) that are routinely used in the field. The measurement of RdRp activity was performed in two assays: an efficient primer-dependent assay based on a polyA-oligoU primer-template complex and a primer-

independent (*i.e.*, *de novo*) assay in which the template was presented by $3'$UTR of an antigenomic RNA strand [39]. In both cases, the activity was measured by incorporation of $[\alpha-^{32}P]$UTP into RNA. The results are presented in Figure 1. It can be seen that in assays, the addition of DTT caused a significant increase in the RdRp activity of the NS5BΔ21 protein. In addition, the treatment of the protein with hydrogen peroxide led to a decrease in its enzymatic activity (Figure S1). This indicates that the NS5B protein acts as a redox switch.

3.2. NS5B Is Subject to S-Glutathionylation That Reduces RdRp Activity of the Recombinant Protein. S-Glutathionylation is one of the cysteine modifications that can be removed by reducing agents. To investigate whether the NS5B protein is subjected to S-glutathionylation, the recombinant NS5BΔ21 protein was treated with the oxidized glutathione (GSSG) (Figure 2(a)) with subsequent analysis by Western blotting using antibodies to glutathionylated cysteine residues (anti-PSSG). As additional controls, NS5BΔ21 was treated with DTT or GSH. Strikingly, the western blotting revealed that the untreated recombinant NS5BΔ21 protein contained glutathionylated cysteines, and treatment with GSSG further increased the degree of this posttranslational modification (Figure 2(b)). Treatment with a reduced glutathione or DTT, in contrast, removed glutathione residues (Figure 2(b)), presumably by dithiol-disulfide exchange (Figure 2(a)).

Treatment of the NS5BΔ21 protein with GSSG reduced the levels of its activity in primer-dependent and primer-independent assays, whereas GSH stimulated it (Figures (2(c)) and 2(d)). Noteworthy, however, the effect of GSH was less pronounced than in the case of DTT treatment, as shown above (Figure 1). But the lower activity of reduced glutathione is in line with its lower reducing potential ($E' = -264$ mV at pH 7.4), compared to that of DTT ($E' = -360$ mV) [40]. Thus, the HCV NS5B protein is subject to S-glutathionylation, which modulates protein RdRp activity.
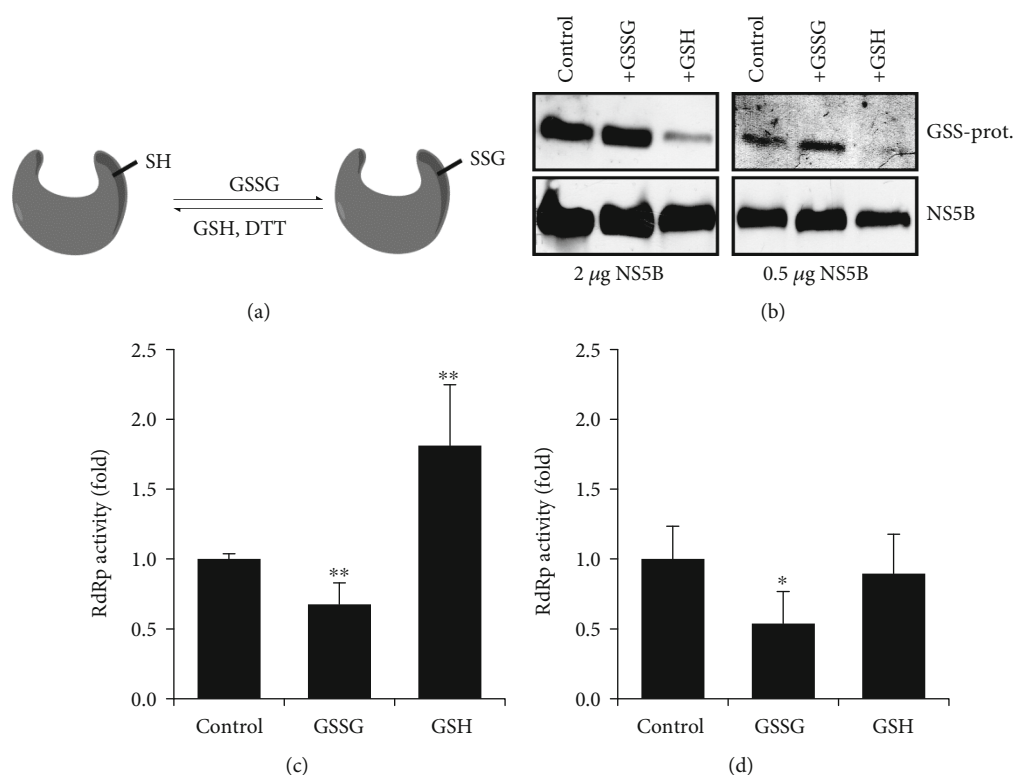
FIGURE 2: The recombinant NS5BΔ21 protein is subjected to S-glutathionylation which leads to reduction of RdRp activity. (a) A scheme showing impact of oxidized (GSSG) and reduced (GSH) glutathione on protein S-glutathionylation. (b) A western blot showing S-glutathionylation of the NS5BΔ21 protein. (c, d) RdRp activity of the NS5BΔ21 protein treated with glutathione isoforms or DTT, measured in primer-dependent (c) and primer-independent (d) assays. The results are presented as the mean ± SD. The control represents the untreated recombinant protein. $^*p < 0.05$ and $^{**}p < 0.01$ (Mann-Whitney test).

3.3. Identification of Cysteine Residues That Are Subjected to S-Glutathionylation.

The next step was the identification of the glutathionylated amino acid residues. For that purpose, a widely used in-gel digestion procedure with trypsin was performed with subsequent analysis of the resulting peptides by MALDI mass spectrometry analysis. Two types of samples were analyzed: the recombinant freshly purified NS5BΔ21 protein and the same protein treated with oxidized glutathione. In both cases, the detected peptides covered 75-85% of the total protein and most of the cysteine residues. Among the cysteine residues that escaped detection in a few experiments were C14 and C39 (one experiment) and C366 (one experiment). But it should be noted that in other repeat experiments the corresponding peptides were detected thus allowing to draw conclusions about their possible modification.

The results of analysis are summarized in Table 1. As one can see, within the untreated protein, up to four cysteine residues were subjected to S-glutathionylation. Two of them were identified unambiguously: C89 and C146. S-Glutathionylation of cysteines at other positions varied between the samples. In one sample, glutathionylation was seen for the residues 170 and 274. In the other, no S-glutathionylation of C170 was detected. In contrast, two glutathione residues were found in a peptide spanning from aa 271-298 that displayed three cysteine residues at positions 274, 279, and 295. The difference in the glutathionylation status of Cys170 and cysteines of a 271-298 amino acid region

might be explained by a lower level of S-glutathionylation of the respective residues in one of these samples, probably lower than the detection limit.

In the protein preincubated with GSSG, seven glutathione residues were found in the peptide digest (Table 1). As in the previous case, three of them were at cysteines 89, 146, and 274. In one out of two samples, glutathionylation was also detected for C521. Again, in both samples, the peptide aa 271-298 with two glutathione residues was seen. Taken into account that one of them should be at C274, the second one should be either at C279 or at C295. Finally, in one of the samples, the peptide aa 223-259 (bearing C223 and C243) with one glutathione residue was detected accompanied by the nonglutathionylated peptide aa 235-250. The latter indicates that another site of S-glutathionylation is presented by C223. Indeed, the second sample contained the glutathionylated peptide aa 212-231 which supported the localization of this site. It is also worth noting that in all samples, oxidation of thiols of C89, C521, and C223 and one of the pair C279/C295 into sulfenic and sulfinic acids was detected. Thus, these results indicated that the NS5B protein is glutathionylated at cysteine residues 89, 146, 170, 223, 274, 279, 295, and 521.

To find out which of these cysteine residues are conserved among HCV isolates, multiple alignment of NS5B protein variants derived from genotypes 1-7 was performed. For genotypes 1a, 1b, and 2a, three strains each were included.

TABLE 1: Cysteine residues of the recombinant NS5BΔ21 protein that are subjected to S-glutathionylation.

Protein		14	39	89	146	170	223	243	274	279	295	303	316	366	521
							Cysteine residue								
The recombinant NS5BΔ21	Exp1	−	−	+	+	+	−	−	+	−	−	−	−	−	−
The recombinant NS5BΔ21	Exp2	−	−	+	+	−	−	−		Two[1]	−	−	−	−	−
NS5BΔ21, treated with GSSG	Exp1	−	−	+	+	−	+[2]	−		Two[3]		−	−	−	+
NS5BΔ21, treated with GSSG	Exp2	−	−	+	+	−	+[2]	−		Two[3]		−	−	−	+

[1,2,3]The peptide comprising aa 271-298 with three cysteines (C274, C279, and C295) contained two glutathione residues. In the same analysis, no glutathionylation was revealed in a peptide of aa 271-280. A peptide aa 223-259 with two cysteines (C223 and C243) contained one glutathione residue. In a similar sample, the peptide of aa 235-250 was not glutathionylated. The peptide comprising aa 271-298 contained two glutathione residues. In the same analysis, a glutathionylated peptide of aa 251-278 is implying that one of the residues is at C274, and the second is either at C279 or C295.

TABLE 2: Variability of amino acid residues of the NS5B protein from HCV genotypes 1-7 at positions, in which the protein of JFH-1 isolate contains cysteine residues.

Gt	Isolate	14	39	**89**	**146**	**170**	**223**	243	**274**	**279**	**295**	303	316	366	**521**
	H77	C	S	**C**	**C**	**C**	**C**	C	**C**	**C**	**C**	C	C	C	**C**
1a	TN	C	S	**C**	**C**	**C**	**C**	C	**C**	**C**	**C**	C	C	C	**C**
	HCV1	C	S	**C**	**C**	**C**	**C**	C	**C**	**C**	**C**	C	C	C	**C**
	Con1	C	A	**C**	**C**	**C**	**C**	C	**C**	**C**	**C**	C	C	C	**C**
1b	J4	C	A	**C**	**C**	**C**	**C**	C	**C**	**C**	**C**	C	N	C	**C**
	DH1	C	A	**C**	**C**	**C**	**C**	C	**C**	**C**	**C**	C	C	C	**C**
	JFH1	C	C	**C**	**C**	**C**	**C**	C	**C**	**C**	**C**	C	C	C	**C**
2a	JFH2	C	C	**C**	**C**	**C**	**C**	C	**C**	**C**	**C**	C	C	C	**C**
	J6	C	C	**C**	**C**	**C**	**C**	C	**C**	**C**	**C**	C	C	C	**C**
2b	J8	C	S	**C**	**C**	**C**	**C**	C	**C**	**C**	**C**	C	C	C	**C**
3a	S52	C	S	**C**	**C**	**C**	**C**	C	**C**	**C**	**C**	A	C	C	**C**
4a	ED43	C	A	**C**	A	**C**	**C**	C	**C**	**C**	**C**	I	C	C	**C**
5a	SA13	C	S	**C**	A	**C**	**C**	C	**C**	**C**	**C**	C	C	C	**C**
6a	EUHK2	C	S	**C**	**C**	**C**	**C**	C	**C**	**C**	**C**	C	C	C	**C**
7a	QC69	S	S	A	**C**	**C**	**C**	C	V	**C**	**C**	A	C	C	**C**

The alignment is shown in Supplementary figure S1, whereas Table 2 represents a summary for cysteine residues. First, the NS5B proteins from the different genotypes contained different quantities of cysteine residues: 14 for genotype 2 and 7 isolates to 21-23 for genotype 1 isolate. The residues 170, 223, 243, 279, 295, 366, and 521 were conserved among all genotypes, and cysteines 14, 89, 274, and 316 were also highly conserved: they are present in the NS5B protein of all genotypes except for one of the analyzed isolates. On the other side, cysteines 39, 146, and 303 were absent in at least two genotypes. It should also be worth noting that several genotypes were bearing cysteines in other positions that were absent in case of JFH1 and other genotype 2 polymerases (Figure S2). So, among eight cysteine residues of the NS5B protein that are subjected to S-glutathionylation NS5B, five were conservative, and two others were highly conserved among all genotypes.

3.4. Substitution of Most Glutathionylated Cysteine Residues in NS5BΔ21 Protein Leads to Reduced Enzymatic Activity of the Recombinant Protein. To analyze the role of glutathiony-lation of the identified cysteines in maintaining the enzymatic activity of the viral polymerase, a panel of NS5BΔ21 with single C→S substitution was constructed. The rationale for such mutations was to exchange the sulfhydryl group (-SH) with a hydroxyl group (-OH) that cannot be coupled with GSH or be oxidized. The expression and purification of the protein forms were carried out according to the same protocol used for the wild-type enzyme. The degree of their S-glutathionylation was analyzed using the same anti-PSSG antibodies as described above. As can be seen from Figure 3(a), not a single substitution prevented the NS5B protein from coupling with glutathione. Moreover, several mutant forms exhibited a somewhat enhanced degree of glutathionylation.

RdRp activity was then measured in a primer-dependent assay in which the same amount of the protein was present in the reaction mixture. Using the wild-type protein, no differences were observed in the *de novo* system, but the overall higher levels of nucleotide incorporation were obtained, thus ensuring better reproducibility and lower level of error. The substitution of residues 89 and 223 did not affect RdRp

(a)

(b)
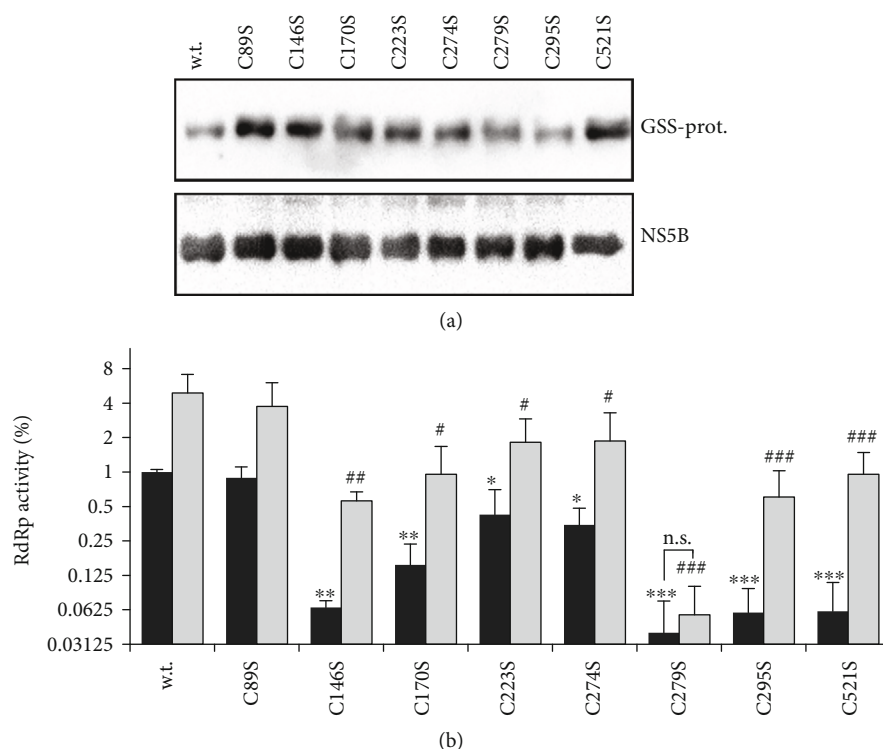
Figure 3: Most cysteine-to-serine substitutions in NS5BΔ21 decrease its enzymatic activity but do not affect its ability to be activated by a reducing agent. (a) Western blot for anti-PSSG. (b) Primer-dependent RNA polymerase activity of NS5BΔ21 mutant forms in the absence and presence of a reducing agent. The results are presented as the mean ± SD. Statistically significant differences between the activities of the mutated NS5B proteins and the wild-type enzyme were analyzed using the Kruskal-Wallis method with the Benjamini and Hochberg procedure. Influence of DTT on activity of each NS5B form was analyzed using multiple t-tests.

activity, and the change of C174 for serine only moderately reduced activity (Figure 3(b)). In contrast, other substitutions decreased the activity by >10-fold. The greatest reduction was observed for the C279S mutant, for which the incorporation of a radioactive nucleotide into RNA was close to the background. Moreover, this substitution also blocked the increase of RdRp activity upon treatment with the reducing agent. These results show that glutathionylation of several NS5B cysteines inhibits the polymerase activity of the protein.

3.5. Substitution of Most Glutathionylated Cysteine Residues in NS5B Protein in the Context of the Viral Subgenomic Replicon Enhanced HCV Replication. In order to verify the role of NS5B cysteine residues that are glutathionylated, on polymerase activity in the context of a viral proteome, similar mutations were introduced into a subgenomic JFH1 replicon. All the corresponding RNAs produced by in vitro transcription were electroporated into Huh7.5 cells and grown in the presence of the selection agent G418. As a negative control, the replication-incompetent variant displaying a substitution of the catalytic Asp318 with asparagine was electroporated. The results are presented in Figure 4. First, in neither out of four independent experiments, cells with an NS5B C89S substitution could be selected. This may indicate that this residue in indispensable for maintaining replication in liver cells. Substitution of C146 did not affect HCV replication efficacy.
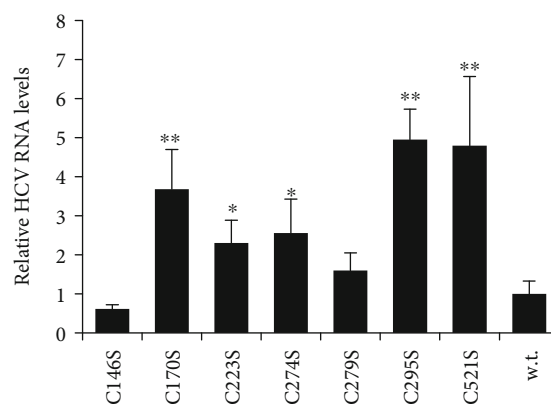
Figure 4: Most cysteine-to-serine substitutions in NS5B upregulate the replication of the subgenomic HCV subgenomic replicon. The results are presented as the mean ± SD. Statistical differences in replication rates between mutation-bearing and wild-type replicons were accessed by the Kruskal-Wallis method with the Benjamini and Hochberg procedure. $^*p < 0.05$; $^{**}p < 0.001$.

Substitutions of C179, 295, or 512 with serine residues significantly enhanced the replication of the viral genome. A less pronounced stimulation was observed for C223 and C274 substitutions. Finally, substitutions of C146 or C279 had no notable effect on HCV replication.

4. Discussion

Numerous reports show that hepatitis C virus alters the redox state of infected cells (summarized in [23] and other reviews) with focus on the identification of HCV-induced ROS sources and levels, identification of ROS-scavenging enzymes, and search for redox-sensitive pathways that may be implicated in virus pathogenesis. In contrast, no attempts have been made so far to analyze the impact of ROS on viral proteins in terms of redox-sensitive or redox-dependent posttranslational modifications and how these ROS-induced posttranslational modifications may change structural or enzymatic properties of viral proteins and affect virus replication as well as the development of the associated liver diseases. It is widely accepted that effects by which ROS and reactive nitrogen species deregulate any particular process are based on their ability to induce redox-sensitive posttranslational modifications. Many of those are presented by covalent modifications or cysteine thiol groups: oxidation to sulfenic (-SOH), sulfinic (-SO$_2$H), or even sulfonic (-SO$_3$H) acids [41]; S-glutathionylation (a formation of a mixed disulfide with glutathione) [42]; nitrosation (commonly referred to as nitrosylation—a conversion of the -SH group into the -SNO group) [43]; and many others. Numerous papers show that these posttranslational modifications play crucial roles in the regulation of many cellular enzymes and other proteins [17, 41, 43]. Among these, S-glutathionylation has a prominent role in the regulation of many pathophysiological events [42]. During last year, it became clear that this cysteine modification is implicated in the development of lung fibrosis [44], asthma [45], neural disorders such as Friedrich's ataxia [46], and other pathologies, whereas targeted regulation of S-glutathionylation in cells and tissues presents a novel strategy to treat at least some of these diseases [44]. In contrast, there are almost no data on existence of these modifications in case of proteins of HCV or other infections.

We show here that the hepatitis C virus NS5B protein that represents an RNA-dependent RNA polymerase undergoes S-glutathionylation. This finding expands the small list of viral proteins that are subject to this redox-sensitive posttranslational modification. Besides NS5B, S-glutathionylation was described for the proteases of human immunodeficiency and human T-lymphotropic viruses [18–20], the nsP2 protein of chikungunya virus [21], and NS5 protein of Zika and dengue [22]. Zika and dengue viruses belong to the *Flaviviridae*-family, though to a different genus. Chikungunya virus is a member of the *Togaviridae* family that is comprised of small enveloped viruses whose genome is presented by a single-stranded nonfragmented (+) strand RNA. The NS5 protein of Zika and dengue viruses that is subject to S-glutathionylation exhibits two types of enzymatic activities: guanylyltransferase, RNA guanine-N^7-methyltransferase, nucleoside 2′-O-methyltransferase, and RdRp [22]. S-Glutathionylation moderately decreases at least two of them: guanylyltransferase and RdRp. The nsP2 protein of Chikungunya virus is a protease, and its S-glutathionylation suppresses this activity [21]. Similarly, S-glutathionylation of HIV protease inhibits its enzymatic activity by preventing

its dimerization [18, 19]. In our case, this posttranslational modification also decreased the enzymatic activity of the NS5B protein of HCV; however, the underlying mechanisms remain unknown.

S-Glutathionylation of NS5B was shown for the recombinant protein only. Unfortunately, we could not verify S-glutathionylation of the HCV NS5B protein expressed in liver cells due to technical restrictions. We tried to immuno-precipitate the protein with either NS5B or PSSG antibodies or treatment of the HCV-infected Huh7.5 cells with a bio-tinylated glutathione (Bio-GEE). All these approaches did not show the presence of the NS5B in the precipitates, most probably due to very weak affinity of the antibodies to this protein. Two commercially available antibodies and one in-house produced polyclonal antibody that were used for the detection of NS5B had a detection limit of 30 ng per lane of a gel. So, future endeavors should require introduction of any high affinity tag to the NS5B protein which cannot be done in the context of HCV infectious or noninfectious replication systems.

Based on existing crystal structures, it could be speculated that glutathionylation of several cysteine residues may block RdRp activity by introducing a bulky tripeptide moiety close to sites that are critical for catalysis. The first example is C223 that is located in a palm subdomain in a proximity to aspartate residue D220, which coordinates one of the magnesium ions, D225 which forms a hydrogen bond with a 2′-hydroxyl of an incoming triphosphate, or R222 that also interacts with NTP [47]. The second example is C89 that is close to the residues that form a tunnel for the RNA primer [48]. Surprisingly, the mutants with cysteines 89 or 223 substituted to serine residues exhibited enzymatic activity similar to that of the wild-type protein. In contrast, the RdRp activity of the C170S and C274S mutants was only moderately reduced. The latter is in contrast to a study of Murakami's group that demonstrated a significant reduction in the enzymatic activity of C274A mutant polymerase [49, 50]. However, such discrepancy could be explained by a different isolate of virus (JK-1 isolate of a 1b genotype compared to JFH1 isolate of 2a gt used in the present study) or by the difference in amino acid residue to which the cysteine was substituted. Next, C146S, C279S, C195S, and C521S mutant exhibited significantly reduced RdRp activity compared to the wild-type enzyme. However, the activities of all of them except C179S were upregulated by pretreatment with DTT. Again, the result for C279 is in contradiction to the papers of Murakami's group [49, 50], where C279A substitution did not affect the RdRp activity of the NS5B protein. But again, differences in viral isolate or substitution may account for this discrepancy. Nevertheless, these results indicate that several cysteine residues are important for maintaining enzymatic activity of the polymerase.

To verify that the substitutions of the cysteine residues in NS5B proteins lead to the abovementioned changes in its enzymatic activity, respective substitutions were introduced into a subgenomic HCV replicon. Stable cells lines were selected and obtained and used to measure HCV RNA levels. Strikingly, this system led to absolutely different results: a C89S mutation that had no effect on RdRp activity in vitro

did not support HCV replication, whereas a series of mutations that did diminish the activity of the recombinant enzyme up-regulated HCV replication in cells. The most pronounced difference was seen in the case of the C279S mutant. This suggests the existence of at least two factors that influence RdRp activity. First, S-glutathionylation or other cysteine modifications inhibit the polymerase in cells. Second, the recombinant NS5B protein has a preference for cysteine compared to serine in the respective positions. However, it cannot be excluded that these cysteine residues can undergo other redox-sensitive modifications such as sulfenation or even sulfination that also decrease RdRp activity. It is accepted that oxidation of thiol groups into sulfenic groups may precede S-glutathionylation either through reaction with GSH or through an enzyme-catalyzed process [51]. There are several examples that both oxidation and S-glutathionylation occur for cysteine residues with reduced pKa. Mass spectrometric analysis in this study revealed both oxidized forms for several cysteines that were subjected to S-glutathionylation. Though we cannot rule out a possibility of spontaneous oxidation of these residues by air oxygen, it is tempting to speculate that at least deep oxidation (i.e., into sulfinic acids) seen for C89, C521, C223, and a pair C179/C295 could reflect a high potential of these residues to redox-sensitive posttranslational modifications. So, future studies of a wide range of cysteine modifications of the NS5B protein are required.

Both S-glutathionylation and sulfenation of cysteines rely upon hydrogen peroxide [41]. HCV infection is known to trigger enhanced production of ROS and to increase cytoplasmic H_2O_2 levels in particular [23, 25]. Long-lasting HCV infection also causes a significant increase in oxidized glutathione levels [31]. These facts assume that HCV infection should favor protein S-glutathionylation. As glutathionylation of the NS5B protein inhibits its enzymatic activity, one might expect a negative effect of hydrogen peroxide on virus replication. Indeed, Choi et al. reported inhibition of HCV replication by nontoxic doses of H_2O_2.

5. Conclusions

To sum up, we have shown that the NS5B protein of hepatitis C virus is subjected to S-glutathionylation and that this modification alters enzymatic activity. At the same time, results from the cell system suggest the existence of other modifications of NS5B cysteine residues that also can affect RdRp activity of the protein. So, these data point out to the necessity of future investigations of redox-sensitive posttranslational modifications of the HCV NS5B proteins as well as of other virus proteins and their role in HCV replication.

Data Availability

No data were used to support this study.

Conflicts of Interest

The authors declare that they have no conflicts of interest.

Authors' Contributions

Marina K. Kukhanova and Vera L. Tunitskaya contributed equally to this work.

Supplementary Materials

Figure S1: primer-dependent RdRp activity of the recombinant NS5BΔ21 protein is inhibited by treatment with hydrogen peroxide. Control represents the untreated recombinant protein. Figure S2: alignment of the NS5B protein derived from the virus of genotypes 1-7 and conservativeness of cysteine residues. Table S1: structure of oligonucleotides used for site-directed mutagenesis in the plasmid pET-2c-NS5BΔ21. Table S2: structure of oligonucleotides used for site-directed mutagenesis in the plasmid pSGR-JFH1. (Supplementary Materials)

References

[1] http://www.who.int/mediacentre/factsheets/fs164/en/.

[2] J. K. Mitchell, S. M. Lemon, and D. R. McGivern, "How do persistent infections with hepatitis C virus cause liver cancer?," *Current Opinion in Virology*, vol. 14, pp. 101–108, 2015.

[3] C. de Martel, D. Maucort-Boulch, M. Plummer, and S. Franceschi, "World-wide relative contribution of hepatitis B and C viruses in hepatocellular carcinoma," *Hepatology*, vol. 62, no. 4, pp. 1190–1200, 2015.

[4] R. D'Ambrosio, E. Degasperi, M. Colombo, and A. Aghemo, "Direct-acting antivirals: the endgame for hepatitis C?," *Current Opinion in Virology*, vol. 24, pp. 31–37, 2017.

[5] M. Bourlière, S. C. Gordon, S. L. Flamm et al., "Sofosbuvir, velpatasvir, and voxilaprevir for previously treated HCV infection," *New England Journal of Medicine*, vol. 376, no. 22, pp. 2134–2146, 2017.

[6] G. R. Foster, N. Afdhal, S. K. Roberts et al., "Sofosbuvir and velpatasvir for HCV genotype 2 and 3 infection," *New England Journal of Medicine*, vol. 373, no. 27, pp. 2608–2617, 2015.

[7] J. J. Feld, I. M. Jacobson, C. Hézode et al., "Sofosbuvir and velpatasvir for HCV genotype 1, 2, 4, 5, and 6 infection," *New England Journal of Medicine*, vol. 373, no. 27, pp. 2599–2607, 2015.

[8] A. V. Ivanov, V. T. Valuev-Elliston, D. A. Tyurina et al., "Oxidative stress, a trigger of hepatitis C and B virus-induced liver carcinogenesis," *Oncotarget*, vol. 8, no. 3, 2017.

[9] M. Gutowski and S. Kowalczyk, "A study of free radical chemistry: their role and pathophysiological significance," *Acta Biochimica Polonica*, vol. 60, no. 1, p. 1, 2013.

[10] C. R. Reczek and N. S. Chandel, "ROS-dependent signal transduction," *Current Opinion in Cell Biology*, vol. 33, pp. 8–13, 2015.

[11] C. C. Winterbourn, "Reconciling the chemistry and biology of reactive oxygen species," *Nature Chemical Biology*, vol. 4, no. 5, pp. 278–286, 2008.

[12] E. A. Veal, Z. E. Underwood, L. E. Tomalin, B. A. Morgan, and C. S. Pillay, "Hyperoxidation of peroxiredoxins: gain or loss of function?," *Antioxidants & Redox Signaling*, vol. 28, no. 7, pp. 574–590, 2018.

[13] I. Y. Petrushanko, S. Yakushev, V. A. Mitkevich et al., "S-Glutathionylation of the Na,K-ATPase Catalytic α Subunit Is a Determinant of the Enzyme Redox Sensitivity," *The Journal of Biological Chemistry*, vol. 287, no. 38, pp. 32195–32205, 2012.

[14] A. V. Ivanov, V. T. Valuev-Elliston, O. N. Ivanova et al., "Oxidative stress during HIV infection: mechanisms and consequences," *Oxidative Medicine and Cellular Longevity*, vol. 2016, Article ID 8910396, 18 pages, 2016.

[15] O. Khomich, S. Kochetkov, B. Bartosch, and A. Ivanov, "Redox Biology of Respiratory Viral Infections," *Viruses*, vol. 10, no. 8, p. 392, 2018.

[16] J. Choi, "Oxidative stress, endogenous antioxidants, alcohol, and hepatitis C: pathogenic interactions and therapeutic considerations," *Free Radical Biology & Medicine*, vol. 52, no. 7, pp. 1135–1150, 2012.

[17] J. Choi, N. L. B. Corder, B. Koduru, and Y. Wang, "Oxidative stress and hepatic Nox proteins in chronic hepatitis C and hepatocellular carcinoma," *Free Radical Biology & Medicine*, vol. 72, pp. 267–284, 2014.

[18] D. A. Davis, C. A. Brown, F. M. Newcomb et al., "Reversible oxidative modification as a mechanism for regulating retroviral protease dimerization and activation," *Journal of Virology*, vol. 77, no. 5, pp. 3319–3325, 2003.

[19] D. A. Davis, K. Dorsey, P. T. Wingfield et al., "Regulation of HIV-1 protease activity through cysteine modification," *Biochemistry*, vol. 35, no. 7, pp. 2482–2488, 1996.

[20] D. A. Davis, F. M. Newcomb, D. W. Starke, D. E. Ott, J. J. Mieyal, and R. Yarchoan, "Thioltransferase (Glutaredoxin) Is Detected Within HIV-1 and Can Regulate the Activity of Glutathionylated HIV-1 Protease in Vitro," *The Journal of Biological Chemistry*, vol. 272, no. 41, pp. 25935–25940, 1997.

[21] C. Saisawang, A. Kuadkitkan, D. R. Smith, S. Ubol, and A. J. Ketterman, "Glutathionylation of chikungunya nsP2 protein affects protease activity," *Biochimica et Biophysica Acta - General Subjects*, vol. 1861, no. 2, pp. 106–111, 2017.

[22] C. Saisawang, A. Kuadkitkan, P. Auewarakul, D. R. Smith, and A. J. Ketterman, "Glutathionylation of dengue and Zika NS5 proteins affects guanylyltransferase and RNA dependent RNA polymerase activities," *PLoS One*, vol. 13, no. 2, p. e0193133, 2018.

[23] A. Ivanov, O. Smirnova, I. Petrushanko et al., "HCV core protein uses multiple mechanisms to induce oxidative stress in human hepatoma Huh7 cells," *Viruses*, vol. 7, no. 6, pp. 2745–2770, 2015.

[24] O. A. Smirnova, O. N. Ivanova, B. Bartosch et al., "Hepatitis C virus NS5A protein triggers oxidative stress by inducing NADPH oxidases 1 and 4 and cytochrome P450 2E1," *Oxidative Medicine and Cellular Longevity*, vol. 2016, Article ID 8341937, 10 pages, 2016.

[25] N. S. R. De Mochel, S. Seronello, S. H. Wang et al., "Hepatocyte NAD(P)H oxidases as an endogenous source of reactive oxygen species during hepatitis C virus infection," *Hepatology*, vol. 52, no. 1, pp. 47–59, 2010.

[26] H. E. Boudreau, S. U. Emerson, A. Korzeniowska, M. A. Jendrysik, and T. L. Leto, "Hepatitis C virus (HCV) proteins induce NADPH oxidase 4 expression in a transforming growth factor beta-dependent manner: a new contributor to HCV-induced oxidative stress," *Journal of Virology*, vol. 83, no. 24, pp. 12934–12946, 2009.

[27] D. Burdette, M. Olivarez, and G. Waris, "Activation of transcription factor Nrf2 by hepatitis C virus induces the cell-survival pathway," *The Journal of General Virology*, vol. 91, no. 3, pp. 681–690, 2010.

[28] M. Carvajal-Yepes, K. Himmelsbach, S. Schaedler et al., "Hepatitis C virus impairs the induction of cytoprotective Nrf2 target genes by delocalization of small Maf proteins," *The Journal of Biological Chemistry*, vol. 286, no. 11, pp. 8941–8951, 2011.

[29] Y. Jiang, H. Bao, Y. Ge et al., "Therapeutic targeting of GSK3β enhances the Nrf2 antioxidant response and confers hepatic cytoprotection in hepatitis C," *Gut*, vol. 64, no. 1, pp. 168–179, 2015.

[30] D. Yamane, D. R. McGivern, E. Wauthier et al., "Regulation of the hepatitis C virus RNA replicase by endogenous lipid peroxidation," *Nature Medicine*, vol. 20, no. 8, pp. 927–935, 2014.

[31] C. Brault, P. Lévy, S. Duponchel et al., "Glutathione peroxidase 4 is reversibly induced by HCV to control lipid peroxidation and to increase virion infectivity," *Gut*, vol. 65, no. 1, pp. 144–154, 2016.

[32] A. V. Ivanov, A. N. Korovina, V. L. Tunitskaya et al., "Development of the system ensuring a high-level expression of hepatitis C virus nonstructural NS5B and NS5A proteins," *Protein Expression and Purification*, vol. 48, no. 1, pp. 14–23, 2006.

[33] S. N. Ho, H. D. Hunt, R. M. Horton, J. K. Pullen, and L. R. Pease, "Site-directed mutagenesis by overlap extension using the polymerase chain reaction," *Gene*, vol. 77, no. 1, pp. 51–59, 1989.

[34] A. V. Ivanov, V. L. Tunitskaya, O. N. Ivanova et al., "Hepatitis C virus NS5A protein modulates template selection by the RNA polymerase in in vitro system," *FEBS Letters*, vol. 583, no. 2, pp. 277–280, 2009.

[35] A. V. Ivanov, O. A. Smirnova, O. N. Ivanova, O. V. Masalova, S. N. Kochetkov, and M. G. Isaguliants, "Hepatitis C virus proteins activate NRF2/ARE pathway by distinct ROS-dependent and independent mechanisms in HUH7 cells," *PLoS One*, vol. 6, no. 9, p. e24957, 2011.

[36] A. Shevchenko, H. Tomas, J. Havli, J. V. Olsen, and M. Mann, "In-gel digestion for mass spectrometric characterization of proteins and proteomes," *Nature Protocols*, vol. 1, no. 6, pp. 2856–2860, 2006.

[37] T. Kato, T. Date, M. Miyamoto et al., "Efficient replication of the genotype 2a hepatitis C virus subgenomic replicon," *Gastroenterology*, vol. 125, no. 6, pp. 1808–1817, 2003.

[38] W. Li, A. Cowley, M. Uludag et al., "The EMBL-EBI bioinformatics web and programmatic tools framework," *Nucleic Acids Research*, vol. 43, no. W1, pp. W580–W584, 2015.

[39] S. Reigadas, M. Ventura, L. Sarih-Cottin, M. Castroviejo, S. Litvak, and T. Astier-Gin, "HCV RNA-dependent RNA polymerase replicates in vitro the 3′ terminal region of the minus-strand viral RNA more efficiently than the 3′ terminal region of the plus RNA," *European Journal of Biochemistry*, vol. 268, no. 22, pp. 5857–5867, 2001.

[40] K. X. Chan, P. D. Mabbitt, S. Y. Phua et al., "Sensing and signaling of oxidative stress in chloroplasts by inactivation of

the SAL1 phosphoadenosine phosphatase," *Proceedings of the National Academy of Sciences of the United States of America*, vol. 113, no. 31, pp. E4567–E4576, 2016.

[41] M. Lo Conte and K. S. Carroll, "The redox biochemistry of protein sulfenylation and sulfinylation," *The Journal of Biological Chemistry*, vol. 288, no. 37, pp. 26480–26488, 2013.

[42] J. Zhang, Z. W. Ye, S. Singh, D. M. Townsend, and K. D. Tew, "An evolving understanding of the S-glutathionylation cycle in pathways of redox regulation," *Free Radical Biology & Medicine*, vol. 120, pp. 204–216, 2018.

[43] N. Gould, P. T. Doulias, M. Tenopoulou, K. Raju, and H. Ischiropoulos, "Regulation of protein function and signaling by reversible cysteine S-nitrosylation," *The Journal of Biological Chemistry*, vol. 288, no. 37, pp. 26473–26479, 2013.

[44] V. Anathy, K. G. Lahue, D. G. Chapman et al., "Reducing protein oxidation reverses lung fibrosis," *Nature Medicine*, vol. 24, no. 8, pp. 1128–1135, 2018.

[45] S. M. Hoffman, X. Qian, J. D. Nolin et al., "Ablation of glutaredoxin-1 modulates house dust mite-induced allergic airways disease in mice," *American Journal of Respiratory Cell and Molecular Biology*, vol. 55, no. 3, pp. 377–386, 2016.

[46] M. Sparaco, L. M. Gaeta, F. M. Santorelli et al., "Friedreich's ataxia: oxidative stress and cytoskeletal abnormalities," *Journal of the Neurological Sciences*, vol. 287, no. 1-2, pp. 111–118, 2009.

[47] S. Bressanelli, L. Tomei, A. Roussel et al., "Crystal structure of the RNA-dependent RNA polymerase of hepatitis C virus," *Proceedings of the National Academy of Sciences of the United States of America*, vol. 96, no. 23, pp. 13034–13039, 1999.

[48] D. O'Farrell, R. Trowbridge, D. Rowlands, and J. Jager, "Substrate complexes of hepatitis C virus RNA polymerase (HC-J4): structural evidence for nucleotide import and de-novo initiation," *Journal of Molecular Biology*, vol. 326, no. 4, pp. 1025–1035, 2003.

[49] Y. Ma, T. Shimakami, H. Luo, N. Hayashi, and S. Murakami, "Mutational analysis of hepatitis C virus NS5B in the subgenomic replicon cell culture," *The Journal of Biological Chemistry*, vol. 279, no. 24, pp. 25474–25482, 2004.

[50] W. Qin, T. Yamashita, Y. Shirota, Y. Lin, W. Wei, and S. Murakami, "Mutational analysis of the structure and functions of hepatitis C virus RNA-dependent RNA polymerase," *Hepatology*, vol. 33, no. 3, pp. 728–737, 2001.

[51] D. M. Townsend, Y. Manevich, L. He, S. Hutchens, C. J. Pazoles, and K. D. Tew, "Novel role for glutathione S-transferase pi. Regulator of protein S-glutathionylation following oxidative and nitrosative stress," *The Journal of Biological Chemistry*, vol. 284, no. 1, pp. 436–445, 2009.

Review Article

Flaviviridae Viruses and Oxidative Stress: Implications for Viral Pathogenesis

Zhenzhen Zhang,[1,2] **Liang Rong,**[1,2] **and Yi-Ping Li** [1,2,3]

[1]*Institute of Human Virology and Zhongshan School of Medicine, Sun Yat-sen University, Guangzhou 510080, China*
[2]*Key Laboratory of Tropical Disease Control (Sun Yat-sen University), Ministry of Education, Guangzhou 510080, China*
[3]*Program of Pathobiology, The Fifth Affiliated Hospital and Zhongshan School of Medicine, Sun Yat-sen University, Guangdong, China*

Correspondence should be addressed to Yi-Ping Li; lyiping@mail.sysu.edu.cn

Oxidative stress is induced once the balance of generation and neutralization of reactive oxygen species (ROS) is broken in the cell, and it plays crucial roles in a variety of natural and diseased processes. Infections of *Flaviviridae* viruses trigger oxidative stress, which affects both the cellular metabolism and the life cycle of the viruses. Oxidative stress associated with specific viral proteins, experimental culture systems, and patient infections, as well as its correlations with the viral pathogenesis attracts much research attention. In this review, we primarily focus on hepatitis C virus (HCV), dengue virus (DENV), Zika virus (ZIKV), Japanese encephalitis virus (JEV), West Nile virus (WNV), and tick-borne encephalitis virus (TBEV) as representatives of *Flaviviridae* viruses and we summarize the mechanisms involved in the relevance of oxidative stress for virus-associated pathogenesis. We discuss the current understanding of the pathogenic mechanisms of oxidative stress induced by *Flaviviridae* viruses and highlight the relevance of autophagy and DNA damage in the life cycle of viruses. Understanding the crosstalk between viral infection and oxidative stress-induced molecular events may offer new avenues for antiviral therapeutics.

1. Introduction

The *Flaviviridae* is a family of viruses that comprise more than 100 species. These viruses include those that have been grouped into one of four genera (*Flavivirus*, *Pestivirus*, *Pegivirus*, and *Hepacivirus*) [1], as well as a number of unclassified species. Natural hosts of *Flaviviridae* viruses are primarily humans and other mammals, and the viruses spread mainly through arthropod vectors (e.g., mosquitoes and ticks; *Flavivirus*) and blood-associated transmission (*Hepacivirus*). Medically important *Flaviviridae* viruses include dengue virus (DENV), Zika virus (ZIKV), yellow fever virus (YFV), Japanese encephalitis virus (JEV), West Nile virus (WNV), tick-borne encephalitis virus (TBEV), and hepatitis C virus (HCV) [1]. Major clinical manifestations associated with the infections of these viruses include hemorrhagic syndromes [2], neurological complications (e.g., encephalitis, Guillain-Barré-syndrome (GBS), and microcephaly) [3, 4], and hepatitis [5]. After entry into the cell through receptor-mediated endocytosis, the life cycle of *Flaviviridae* viruses is completed entirely in the cytoplasm. Many host cellular factors have been identified as being involved in the viral infection, and the various steps of the life cycle or viral products interfere with the homeostasis of cellular metabolism, thus triggering a stress pressure to the host cell. In general, cellular metabolism steadily produces reactive oxygen species (ROS), as a byproduct of the normal aerobic metabolism, by a variety of enzymes in mitochondria, endoplasmic reticulum (ER), and peroxisome compartments, and simultaneously the oxide is removed to keep the balance [6, 7]. ROS are reactive chemical species containing oxygen, for example, hydrogen peroxide (H_2O_2), superoxide anion ($O_2^{\bullet-}$), hydroxyl radical ($^{\bullet}OH$), and singlet oxygen ($^1O_2$). In a biological context, ROS are oxidants and mediators of cell injury, disease, homeostasis, and signaling activation [6, 7]. Once the balance between the accumulation

of ROS and the removal of the oxide is broken, an oxidative stress is established. The ultimate consequences of oxidative stress are tissue damage, inflammation response, and cell death [8, 9]. To maintain a favorable environment for cell survival and to restore the balance of oxidation and antioxidant systems, the cell generally restricts the use of nutrients and energy through, for example, reducing protein synthesis [10, 11]. It is noted that oxidative stress as a mere imbalance between ROS production and neutralization is being substituted by a concept of redox pathophysiology, which focuses on searching for exact reactions between ROS or oxidation products with exact groups of proteins and the consequences of these reactions.

Thus, an updated definition of "an imbalance between oxidants and antioxidants in favor of the oxidants, leading to a disruption of redox signaling and control and/or molecular damage" is being introduced for oxidative stress [12]. A variety of viral infections have been found to trigger oxidative stress and thus interfere with the normal function of the host cell. Therefore, the maintenance and restoration of a favorable intracellular environment are vitally important for the host to combat against virus infection. Several *Flaviviridae* viruses have been demonstrated to trigger oxidative stress in the infected cell, which include the viruses of the *Flavivirus* genus, DENV [13–15], ZIKV [16, 17], JEV [18–20], WNV [21, 22], and TBEV [23], as well as *Hepacivirus* HCV [24–28].

Among *Flaviviridae* viruses, HCV infection and the induction of oxidative stress have been more extensively studied. HCV is a major cause of liver disease, and majority of infected patients develop chronic infection, which increases the risk of developing liver cirrhosis, liver failure, and eventually hepatocellular carcinoma (HCC). Globally, chronic HCV infection affects 71 million people, and HCV-associated diseases lead to 400,000 deaths per year [29]. Direct-acting antiviral agents (DAAs) have been approved recently for the treatment of HCV infection and have dramatically increased the cure rate up to 90% [30]. However, a vaccine for HCV is still unavailable. Besides, new challenges arising from the limited access and high cost of DAA, emergence of drug resistance, impaired neutralizing immunity, and unawareness of infection, as well as the unceasing progression of HCC and risk of reinfection after virus clearance have compromised the global eradication and elimination of HCV infection [31]. Many reports have described the production of ROS in HCV-infected cells and in the liver tissue and lymphocytes from HCV-infected patients [24, 27, 28, 32, 33]. Almost all HCV proteins have been demonstrated to be involved in the induction of oxidative stress, of which core and NS5A proteins are evidenced as the main inducers.

DENV, ZIKV, JEV, WNV, and YFV are mosquito-transmitted viruses, mainly prevalent in tropical and subtropical regions, and cause major health and economic problems. Although most of the infections are asymptomatic or present as mild illness, a portion of the infected patients develops severe symptoms and may result in death. DENV infection could lead to severe symptoms, including dengue hemorrhagic fever (DHF) and dengue shock syndrome (DSS) [34–36]. ZIKV infection may cause serious neurologi-

cal complications, including GBS in adults and the microcephaly birth defect in infants [37–39]. The birth defect along with its sexual and transplacental transmission makes ZIKV unique and distinct from other flaviviruses [40]. JEV infection causes acute encephalitis and, frequently, neurological sequelae, which lead to the loss of more disability-adjusted life years (DALY) than any other arthropod-borne virus [41, 42]. A small portion of WNV and TBEV (tick transmitted) can also result in severe neurological symptoms (e.g. encephalitis, meningitis, or meningoencephalitis) and may lead to mortality [42, 43]. To date, there is no specific antiviral treatment available for the infections of these flaviviruses. Vaccines for human use are only available for JEV and DENV. However, JEV vaccines are not effective against all clinical JEV isolates, while DENV vaccines can only be used in dengue endemic regions and in the individuals of a specific age range [44].

Accumulating evidences have linked the oxidative stress to the pathogenesis of these vector-borne flaviviruses [45]. In this review, we focus on the infection of six viruses, including HCV, DENV, ZIKV, JEV, WNV, and TBEV. We aim to summarize the reported data regarding the role of oxidative stress in viral pathogenesis and the crosstalk between virus, elevated ROS levels, and oxidative stress-induced molecular events. In addition, autophagy and DNA damage are representatively summarized for HCV, DENV, and ZIKV.

2. Virion Structure and Life Cycle of *Flaviviridae* Viruses

Although *Flaviviridae* viruses share a high similarity in the replication cycle, some specific features differ from each other in terms of virion, genome, replication, etc. The virion of *Flaviviridae* viruses has enveloped, icosahedral, and spherical geometries with a diameter of about 40-60 nm [1, 46]. The viral genome is a positive single-stranded RNA of 9.6-12.3 kb, consisting of one large open reading frame (ORF) flanked by untranslated regions (UTRs) at each end. In the $5'$UTR, the *Flavivirus* genus carries a methylated nucleotide cap (type I cap), while viruses from other genera possess an internal ribosome entry site (IRES), important for the initiation of RNA translation [1, 47]. All members of the family lack a $3'$-terminal poly(A) tract. After entry into the cell, the genomic RNA is uncoated and is directly recognized as a mRNA template by the translation machinery of the host cell to synthesize a large polyprotein precursor. The polyprotein is co- or posttranslationally processed by viral and cellular proteases to produce individual viral proteins, including structural and nonstructural (NS) proteins. Structural proteins form the virion, which is usually comprised of a single core protein (capsid in flaviviruses; C) and two or three envelope proteins. NS proteins are mainly involved in building up the replication complex and regulating RNA replication, viral assembly, and host responses. NS1 is unique to flaviviruses and is the only NS protein residing in the lumen of the ER. The NS1 and NS2A of flaviviruses are required for RNA replication and production of an infectious particle. The NS2B of flaviviruses or the NS4A of HCV acts as a cofactor for

the NS3 protease and recruits NS3 to the ER membrane. NS3 is a multifunctional protein with serine protease, RNA helicase, and nucleoside triphosphatase (NTPase) activities that are essential for RNA replication. The NS4A of flaviviruses is an integral membrane protein involved in membrane rearrangement to form the viral replication complex, while the NS4B of HCV functions in this aspect. The NS5 of flaviviruses and the NS5B of HCV both possess RNA-dependent RNA polymerase activity responsible for viral RNA synthesis. In addition, HCV NS5A is a phosphoprotein involved in the interactions with host factors and in RNA binding. HCV p7 is a small protein with ion channel activity. p7 and NS2 of HCV support the assembly and release of virions, which may diverge mechanically from the flaviviruses [1]. Despite a high degree of similarity in the genome organization and the mechanism of RNA replication, important differences exist between flaviviruses and hepacivirus, including the way in which these viruses utilize cellular resources to favor their propagation and possible clinical outcome, likely reflecting the use of distinct host cellular pathways.

3. Source and Cellular Response of ROS

ROS are byproducts of aerobic metabolism in various cell compartments, including the mitochondria and ER, and function as fine-tuning modulators of numerous normal physiological processes [7]. It is well known that ROS could be both beneficial and deleterious to the cell, depending on the source and cellular response of ROS [48]. Oxidative stress induced by unbalanced ROS production and scavenging contributes to physiological disorders, such as metabolic dysfunction and neurodegeneration [49], inflammatory activation [50], and infectious diseases [8, 51]. As a natural defense system, the cell regularly produces antioxidants or adopt other mechanisms to eliminate the ROS to keep the balance of antioxidation and oxidation. Thus, the development of antioxidants and strategies are emerging as potential therapeutic approaches for diseases related to the oxidative stress.

3.1. Mitochondria: Source and Target of ROS.
Mitochondria are the powerhouse of eukaryotic cells responsible for the majority of oxygen consumption inside the cell, supplying 90% of cellular energy; they are also the major producers of intracellular ROS. Mitochondrial respiration depends on electron transfer and a proton gradient to drive ATP synthesis, and in this process, ROS are produced as natural byproducts. The superoxide is primarily produced by an electron leak from electron transport chains (ETC) in mitochondria and through the oxidation of nicotinamide-adenine dinucleotide phosphate (NADPH) by NAPH oxidases (NOXs), as well as by enzymes including pyruvate and 2-oxoglutarate dehydrogenases [52–56]. The superoxide produced is rapidly converted into hydrogen peroxide by superoxide dismutases (SODs) and into hydroxyl radicals through reactions with metal cations within the cell [56]. The ROS produced mostly target the mitochondrial DNA (mtDNA) and are believed to induce mtDNA degradation, owing to the close proximity of

the mitochondrial genome to the ETC. In addition to mtDNA damage, excessive ROS accumulation in the mitochondria could trigger mitochondrial outer membrane permeabilization (MOMP), which facilitates the release of cytochrome C (apoptosis activator) into the cytosol and the activation of caspase-3 (key apoptosis effector) [57–59]. Upon induction of MOMP, the capacity of mitochondrial Ca^{2+} buffering is decreased. As a consequence, mitochondrial Ca^{2+} is overloaded, and thus ROS is generated. Although it is incompletely certain whether increased ROS are a consequence of mitochondrial dysfunction or damage, it is clear that the increased ROS levels and oxidative stress that resulted from mitochondrial dysfunction have now been convincingly correlated to a variety of human pathological states, including infection of pathogens [60, 61].

3.2. Endoplasmic Reticulum (ER) and ROS.
ER is an organelle containing complex and dynamic tubules, which serve as the site of the storage of Ca^{2+}, folding and secretory pathways of proteins, and lipid synthesis. Growing evidences have shown that the oxidation of proteins in ER is responsible for the generation of ROS that cause oxidative stress [58, 62, 63]. Considering the intimate cross-talks between ER and mitochondria [64], which form very dynamic platforms termed mitochondria-associated membranes (MAM), the ER-associated oxidative stress could induce mitochondrial Ca^{2+} overload, unfolding protein response (UPR), and autophagy, as well as involvements in virus infection [65, 66]. Such stress responses may switch a process from being physiologically beneficial to one that signals cell damage [58].

3.3. Antioxidant Defense Systems.
To counteract oxidative stress, eukaryotic cells have evolved antioxidant defense systems, which are composed of antioxidant molecules that inhibit oxidants from reacting with other molecules by ETC, thereby minimizing damage and maintaining cellular redox homeostasis [67, 68]. The molecules of antioxidant defense systems can be endogenous and exogenous. The endogenous (or adaptive) antioxidants consist of both enzymatic (e.g., peroxiredoxins, SOD, catalase, and glutathione peroxidase) and nonenzymatic components (e.g. vitamin C, vitamin E, uric acid, metal binding proteins, polyamines, bilirubin, carotenoids, and glutathione). However, only vitamin E is found to act as a ROS scavenger with visible efficacy, whereas other molecules, albeit they can scavenge ROS *in vitro*, do not act so *in vivo*, but are considered to affect redox-sensitive pathways [69]. Yet, it has also been reported that the antioxidant effects of vitamin E are only displayed *in vitro* and not *in vivo*; thus, it remains a matter of controversy as to whether or not vitamin E is useful for protecting the body from ROS-induced oxidative stress [70]. Many of these antioxidants are encoded by the Nrf2- (nuclear factor erythroid 2-related factor 2-) Keap1 (kelch-like ECH-associated protein 1) pathway [67, 71–74]. Nrf2 is a transcription factor that regulates the expression of numerous ROS detoxifying and antioxidant genes [72, 75]. Under basal physiology, Nrf2 is sequestered in the cytosol by interacting with Keap1, which facilitates the ubiquitination of Nrf2 and proteasomal degradation, thus limiting the expression of

Nrf2-regulated genes. Upon cellular oxidative stress, the conformation of Keap1 is changed and thus Nrf2 is released and no longer degraded. Newly synthesized Nrf2 is accumulated and translocated to the nucleus, where it forms a heterodimer with small Maf (sMaf) proteins and binds to the antioxidant response element (ARE). The binding of Nrf2 to ARE initiates ARE-dependent transcriptions of antioxidant defense enzymes, thus building up antioxidant defenses to attenuate cellular oxidative stress and to return the cell to a basal state. Exogenous antioxidants are derived from the diet and supplements, such as tiron (4,5-dihydroxy-1,3-benzenedisulfonic acid; a ROS scavenger), carotenoids, and flavonoids. Most of the endogenous and exogenous antioxidants are localized within the cytosol, and a small portion are localized within the mitochondria [76]. Antioxidant systems are manipulated by *Flaviviridae* viruses and are associated with HCV chronic infection [26] and the immune and apoptotic responses against DENV infection via Nrf2-dependent regulation of ROS production [13]. Although it is a hope and an attempt to modulate the antioxidants for therapeutic purpose, a large challenge exists, mainly in delivering antioxidants to diseased tissue or dysfunctional cells without affecting normal tissue.

4. Oxidative Stress and Viral Infections

Oxidative stress induced by virus infection was first described in the study of Sendai virus infection of phagocytes in 1979 [77]. In this study, the binding of the Sendai virus to the cell was demonstrated to quickly activate a membrane-bound NADPH-linked dehydrogenase. This enzyme forms a superoxide anion and hydrogen peroxide, which together with ROS, reacts with polyunsaturated fatty acids, carbohydrates, or artificial easily oxidized substrates such as luminol (5-amino-2,3-dihydro-1,4-phthalazinedione), and finally leads to the induction of chemiluminescence. Since then, many viruses have been demonstrated to cause cell damage by generating ROS and changing redox homeostasis [33, 78–80]. The induction of oxidative stress may also activate the antiviral inflammatory signaling pathways [81–84], thus contributing to viral pathogenesis. For example, DENV infection induces NOX-dependent oxidative stress, which activates interferon regulatory factor 3 (IRF-3), IRF-7, and signal transducer and activator of transcription 1 (STAT-1), as well as nuclear factor kappa-light-chain-enhancer of activated B cell- (NF-κB-) mediated antiviral responses, and associates with the severe damage of virally infected cells [13]. DENV can also induce oxidative stress in liver cells, leading to the production of CCL5 and the activation of the transcriptional regulator CCAAT/enhancer-binding protein β (C/EBPβ) [85]. High levels of circulating proinflammatory cytokines such as IL-1β or tumor necrosis factor α (TNF-α) also correlates with severe dengue fever in DENV-infected patients [86]. Oxidative stress caused by other viruses, such as Rift Valley fever virus (RVFV; a mosquito-borne virus), could also activate inflammatory regulators NF-κB and p53 responses, which in turn modulates cytokine expression, apoptosis, and cell death [82]. The respiratory syncytial virus (RSV) also activates NOX-dependent IRF-3 [87], and NOX2-derived ROS are required for the host cell to trigger an efficient retinoic acid-inducible gene 1- (RIG-I-) mediated activation of IRF-3 and downstream antiviral genes through the regulation of mitochondrial antiviral signaling protein (MAVS) [83]. In turn, ROS may facilitate viral replication, depending on the cell type and the virus involved [51]. Flaviviruses and alphaviruses may use oxidative stress produced during infection to help temporally control genome RNA capping and genome replication [21]. DENV infection is able to activate ER stress-regulated autophagy to limit apoptosis of the cell and thus increase the potential of DENV replication [88]. To counteract the oxidation from the high chemical reactivity of ROS, cells have evolved antioxidant mechanisms to maintain redox homeostasis. Although varying in the ability to induce ROS, viruses share a common pathogenic pathway to defend against oxidative stress. Modulation of Nrf2/ARE signaling is a universal strategy for viruses to trigger antioxidant responses [89].

4.1. Oxidative Stress in HCV Infection. Mitochondria are the major sources of ROS inside hepatocytes and liver-resident blood cells. Excessive production of ROS is a leading factor that contributes to liver inflammation, fibrogenesis, and hepatic carcinogenesis [50], which are common sequelae of chronic HCV infection. It is well known that HCV triggers oxidative stress and modifies antioxidant systems, leading to chronic hepatitis C and extrahepatic manifestations such as type 2 diabetes mellitus [90–94], cardiovascular diseases [95–98], autoimmune or lymphoproliferative disorders [99–101], glomerulopathies [102], and neurological diseases [103–107]. Biomarkers of oxidative stress could be detected both in chronic HCV patients and in various *in vitro* systems including replicon systems and infectious cell culture systems [26, 33, 108, 109]. The induction of oxidative stress by HCV has been summarized recently in excellent reviews [26–28, 110]. Most of the HCV proteins are involved in the induction of oxidative stress, including the core, E1, E2, NS3, NS4B, and NS5A [111–121]. It is worth noting that the HCV core protein serves as a key regulator causing calcium perturbations and ROS production, and multiple mechanisms are exploited by the HCV core to induce oxidative stress. The core is localized to mitochondria and MAM with ER and induces the efflux of Ca^{2+} from ER to mitochondria, which causes glutathione (GSH) oxidation and consequent complex I glutathionylation, and thus sustaining and amplifying the oxidized mitochondrial environment [114]. The N terminal of the core (36 residues) induces the production of ROS through transforming growth factor β1- (TGF-β1-) dependent expression of NOX1 and NOX4, while the rest of the core upregulates ROS transcription via cytochrome P450 2E1 and induces oxidoreductin-1α, thus triggering Ca^{2+} efflux from ER to mitochondria via the mitochondrial Ca^{2+} uniporter, leading to the generation of superoxide anions [119]. Both the HCV core and NS5A proteins have been shown to induce ER stress, leading to cytoplasmic Ca^{2+} release via the inhibition of the sarcoplasmic/endoplasmic reticulum calcium ATPase (SERCA) and the induction of a passive leak of Ca^{2+}, respectively [33, 122]. NS5A-induced Ca^{2+} release triggers ROS production in mitochondria, leading to the

activation of NF-κB and STAT-3 [118]. Envelope proteins E1 and/or E2 induce stress indicator CCAAT/enhancer-binding protein-homologous protein (CHOP) [123] and accumulation of ROS and activation of Nrf2 [124]. E2 upregulates collagen-α-related production of ROS in the hepatic stellate cells and contributes to fibrosis [116]. HCV NS3 can trigger oxidative stress in human monocytes via the activation of NADPH oxidases [112]. NS4B induces oxidative stress and associates with the activation of the phosphatidylinositol 3 kinase- (PI3K-) Akt pathway [125]. In addition, HCV infection triggers MOMP accompanied by ROS production, leading to DNA damage and STAT-3 activation, and this activation is achieved by the core, E1, and NS3 proteins [126]. As STAT-3 has been identified as an oncogene, its activation may lead to downstream proliferative responses. Furthermore, the HCV replicon also causes oxidative stress to activate STAT-3 signaling which involves p38 MAPK, JNK, JAK2, and Src kinases, which eventually contributes to the stimulation of HCV RNA replication [109].

In spite of these observations, studies also report the inhibitory effect of elevated ROS levels on viral genome replication. ROS, within the range of a biologically relevant concentration, could suppress HCV RNA replication in human hepatoma cells [127]. HCV replication is susceptible to the cellular redox state [128], and some adaptive mutations that permitted in vitro infection of HCV genomes adaptive mutations permitted by *in vitro* virus production are found to confer resistance to peroxidation [128, 129]; this study also indicates that NS4A and NS5B are involved in the viral susceptibility to lipid peroxidation [128]. Another study reports that besides the induction of oxidative stress, HCV also induces ROS scavenger glutathione peroxidase 4 (GPx4) to control lipid peroxidation and to increase virion infectivity [130]. A recent study describes that a marked increase in oxidative stress in liver cell cultures favors viral replication in the acute phase of HCV *in vitro* infection, while HCV replication and apoptosis are observed at low levels during the chronic phase; concomitantly, the restoration of reducing redox condition is recorded [131]. The conflicting results about the relevance of ROS for the HCV life cycle may be due to the concentration of ROS or the stage of HCV infection.

The modulation of oxidative stress for a therapeutic purpose is being exploited for HCV infection. Promising results have been obtained by modifying the antioxidant defense mechanisms, which include antioxidant agents (mainly the glutathione system and thioredoxin), antioxidant enzyme systems (superoxide dismutase, catalase, GSH peroxidase, and heme oxygenase-1 (HO-1)), and natural and synthetic antioxidants (vitamins C and E, N-acetylcysteine, silymarin, etc.) (reviewed in [132, 133]). The inhibition of glycogen synthase kinase 3β (GSK3β) enhances the Nrf2 antioxidant response, thus conferring protection in HCV-infected cells and hepatitis C patients [134]. Nevertheless, along with its therapeutic potential, there are concerns on antioxidant therapy. Taking vitamins as an example, several studies report that the serum levels of vitamins (β-carotene (provitamin A) and vitamins B, C, and D) are significantly reduced in chronic hepatitis C patients [135–137], but the underlying mechanisms are unclear. These vitamins may have been seriously depleted in the patients; therefore, high doses of primary antioxidants (vitamins) should be administered to restore and, thereafter, to maintain serum and tissue concentrations at normal levels. Thus, the use of antioxidants necessitates early restoration of optimal concentrations in the liver and plasma. However, the results of clinical studies about the efficiency of vitamins for chronic hepatitis C are still controversial [138]. It has been reported that vitamin D2 inhibited HCV RNA replication [139], while vitamin E enhanced HCV RNA replication [140]. No significant effect of antioxidant supplements on the sustained virologic response has also been reported for chronic hepatitis C patients [138]. In addition, antioxidant treatment often involves a wide variety of drugs or mixtures and may have toxic or uncertain effects [133, 141]. Moreover, the pathology of viral diseases are ultimately the result of complex cellular reactions and host-virus interactions, and it remains to be clarified how antioxidant therapy modulates the cell redox state and treats HCV infection [141, 142]. Together, although many natural compounds have the ability to scavenge ROS or to activate endogenous defense systems, thus offering an indirect protection to the cell [143], with the current knowledge and uncertainties on the effect of antioxidants, targeting the redox-sensitive pathways as a complementary strategy to HCV therapy requires further investigations.

4.2. Oxidative Stress in DENV Infection. Similar to HCV, changes of redox status in the host cell are a common result of DENV infection. Currently, oxidative damage has been reported in severe DENV patients [144–146], indicating a correlation between oxidative stress and viral pathogenesis. DENV is shown to stimulate oxidative stress leading to chemokine RANTES secretion through the activating nuclear factor for IL-6 expression (NF-IL-6) signaling [85]. A recent study reports that changes in redox homeostasis and induction of oxidative stress are associated with the enhanced viral replication in monocytes from glucose-6-phosphate dehydrogenase- (G6PD-) deficient patients [14]. G6PD provides the reduced form of NADPH for various cellular reactions including GSH recycling and superoxide anion production via NADPH oxidase and nitric oxide (NO) synthesis; thus, G6PD deficiency weakens antioxidant defenses and increases oxidative stress in the cell. The G6PD deficiency alters the cellular redox into an abnormal state, and such oxidative state may benefit DENV replication. Thus, G6PD-deficient patients were found to have a higher virus load, and this may also be a link to the presence of severe dengue. This study laterally supports the link between cellular oxidative state and susceptibility to DENV infection. In primary human monocyte-derived dendritic cells (Mo-DC), DENV infection induces NOX-dependent oxidative stress that regulates the magnitude of the activation of innate antiviral immune responses and stimulates apoptosis [13]. More recently, the extent of oxidative stress has been associated with the disease severity in DENV-infected patients [146, 147]. The level of oxidative stress is found to be maximal in DSS followed by DHF, and its level is minimal in dengue fever [147], suggesting a correlation between the level of oxidative stress and DENV-induced pathogenesis.

In addition, DENV can manipulate antioxidant systems to favor its replication. In line with this notion, DENV serotype 2 (DENV2) infection alters the host intracellular GSH levels, and inhibition of GSH synthesis promotes DENV2 replication in liver cells and *in vivo* [148, 149], implicating antioxidant molecules as a potential therapeutic agent for the treatment of viral infections via the inhibition of oxidative stress. Induction of antioxidant enzyme HO-1 effectively inhibits DENV replication in Huh7 cells [150]. The inhibition of antioxidant pathways regulated by Nrf2 increases DENV-associated immune and apoptotic responses in Mo-DC [13]. Furthermore, the addition of garlic diallyl disulfide (DADS), diallyl sulfide (DAS), and alliin has been found to reduce DENV-mediated oxidative stress [151]. DAS is a selective inhibitor of cytochrome P450 2E1, which is shown to be upregulated by the HCV core and NS5A, respectively [119, 120]. These studies show that modulation of the antioxidant systems has a potential for the development of DENV therapy; however, more studies are required.

4.3. Oxidative Stress in the Infections of ZIKV. To date, there are very few reports about the effects of ROS on the ZIKV life cycle and ZIKV-induced pathogenesis; this is perhaps due to the fact that ZIKV began to attract research interest after its outbreak in recent years. A recent study shows that Nrf2-mediated signaling affects embryo survival, redox biology, and ZIKV susceptibility in the mosquito *Aedes aegypti* [152], thus linking oxidative stress and ZIKV infection. ZIKV infection can trigger ER stress (or UPR) in the cerebral cortex of infected postmortem human fetuses as well as in cultured human neural stem cells. Oxidative stress and ER stress are related states that occur frequently in diseases involving inflammation and viral infection [153]. One consequence of oxidative stress is the disruption of the correct oxidative environment within the ER, leading to the misfolding of proteins and ER stress [154, 155]. Meanwhile, protein misfolding in the ER may also result in excessive ROS production and therefore oxidative stress. The role of oxidative stress and the underlying molecular details during ZIKV infection needs to be further investigated.

4.4. Oxidative Stress in the Infections of JEV, WNV, and TBEV. Many continuous cell lines can support the production of JEV, and early studies show that JEV infection produces the toxic oxygen species in neutrophils [156], ROS intermediates in murine neuroblastoma cells [19], and superoxide anion and nitric oxide in rat cortical glial cells [157]. UV-inactivated JEV causes oxidative stress in mouse neuronal N18 cells [18]. Subsequently, in human astrocytoma and astroglioma cell lines, JEV infection is found to lead to ROS production and to regulate RANTES [158]. JEV induces massive inflammatory responses, which upregulates ROS [159]. The production of ROS is involved in the oxidative stress-induced apoptosis [160]. JEV infection of human promonocyte cells downregulates thioredoxin and induces ROS and ASK1-ERK/p38 MAPK signaling, and all are associated with JEV-induced apoptosis [20]. In the rat model, JEV is able to cause an imbalance of oxidants and antioxidant systems in different brain regions [161]. These studies suggest

that oxidative stress contributes as a key factor in the pathogenesis of JEV infection. Besides, the therapeutic efficacy of antioxidants, including minocycline, arctigenin, fenofibrate, and curcumin, has been studied for their potential for the treatment of JEV infection [162].

Less studies are reported for the impact of WNV and TBEV on oxidative stress. The WNV infection of rabbit PBMCs induces the transcription of HO-1 and inducible NO synthase (iNOS), suggesting that oxidative stress may be involved [163]. However, natural WNV strain infections do not induce stress granules (SGs) and some WNV strains could inhibit the SG formation induced by arsenite treatment [22]. SGs are cytoplasmic messenger ribonucleoprotein structures (mRNPs) that are assembled in response to environmental stresses such as oxidative stress, and they contain an array of RNA-binding proteins, translation initiation factors, large and small ribosomal subunit protein components, and mRNAs. The mRNAs are primarily released from polysomes and sequestered into SGs as an adaptive response in eukaryotic cells [164]. The interaction of viral RNA and proteins with TIA-1/TIAR is found to interfere with the formation of SGs [165]. Thus, WNV induced both ROS and the antioxidant responses; however, the infected cells do not display characteristics of oxidative stress, since the antioxidant responses counteract the negative effects of ROS [22]. Thus, the cellular redox status is thought to be beneficial for the life cycle of WNV so far. The overexpression of TBEV NS1 triggers ROS production and activates the Nrf2/ARE pathway, yet its correlations with TBEV-induced damage of the central nervous system remains unclear [23].

5. Autophagy and Virus Infections

Viruses have evolved diverse strategies to exploit cellular processes and to escape from host defenses. One such central pathway is autophagy, an evolutionarily conserved mechanism that recycles damaged or unwanted cellular materials to maintain cell homeostasis. In resting cells, autophagy is suppressed by the mammalian target of rapamycin (mTOR) serine/threonine kinase. Autophagy is induced by cell stresses, such as starvation, ER stress, and pathogen infections, each of which leads to the dephosphorylation and inactivation of TOR [166]. Autophagy begins with the sequestration of intracellular components into a crescent-shaped isolation membrane [166, 167]. Isolation membranes contain autophagy proteins ATG5, ATG8 (known as LC3 in mammals), and ATG12. During the maturation process, the cytosolic microtubule-associated protein light chain 3 (LC3I) is conjugated to phosphatidylethanolamine, producing the membrane-bound, lipidated form of LC3II mediated by the ATG5-ATG12 conjugate [168]. This lipidated form of LC3 mediates membrane tethering and fusion to extend the isolation membrane by recruiting membranes from multiple sources, leading to the formation of large double-membrane vesicles known as autolysosomes [169], which subsequently fuse with endosomes/lysosomes where sequestered substrates are degraded [170, 171].

Since viral infections cause cell stress, autophagy is frequently induced as a byproduct of infections. However,

virus-induced autophagy is not merely a passive process [170]. It has been shown that positive-stranded RNA viruses could manipulate autophagic machinery to evade host immune responses and facilitate viral replication [170, 172–175]. In accord with these phenomena, the increased formation of autophagosomes has been observed in HCV, DENV, and ZIKV-infected cells [176–178]. Additionally, autophagy can play dual roles of both proviral and antiviral functions depending on the virus type and the steps of the viral life cycle. Despite much efforts, the molecular mechanisms for how autophagy is induced during virus infection remain elusive. Many positive-stranded RNA viruses replicate in ER-mitochondria contact membranes, causing new membrane synthesis and rearrangement through the induction of UPR, many of the processes involving oxidative stress [179].

Although the role of autophagy in HCV and ZIKV infection is established (for recent reviews for HCV, see [180], and for ZIKV, see [181, 182]), the specific molecular mechanisms involved in the modulation of autophagy by *Flaviviridae* viruses have yet to be fully clarified. This review here focuses on the interplay between oxidative stress, autophagy, and virus-induced pathogenesis.

5.1. Oxidative Stress, Autophagy, and HCV Infection. Accumulating evidences have demonstrated that HCV infection induces autophagy in cell culture and in the hepatocytes of chronically infected patients [183]. Autophagy has been reported to function at the early stages of HCV infection such as the translation of incoming viral RNA. The induction of autophagy is required to sustain the survival of virally infected cells, which is an important characteristic of HCV chronic infection [184–187]. HCV RNA transfection blocks lysosomal fusion with autophagosomes, the membranes of which provide replication sites for HCV [188]. Several studies suggest that HCV induces the UPR *in vitro* [189–191] and in liver biopsies of HCV-infected patients [192]. The HCV-induced UPR in turn activates the autophagic pathway to promote viral RNA replication in human hepatoma cells [189]. The UPR-autophagy pathway could suppress the innate immune responses by repressing the production of interferon- (IFN-) β or of interferon-stimulated genes (ISGs) through the HCV-derived pathogen-associated molecular pattern (PAMP) [184, 189]. However, the molecular mechanism(s) for HCV-induced UPR remains unclear. Besides autophagy, HCV induces mitophagy to promote its persistent infection [193], and inhibition of mitophagy by knockdown of parkin attenuates HCV replication [81]. These results suggest that autophagy has mostly been attributed to a proviral function in HCV. However, a recent study demonstrates that an ER transmembrane protein SCOTIN recruited the NS5A protein to the autophagosomal compartment, where autophagic degradation of NS5A has taken place, thereby inhibiting HCV replication [194].

Oxidative stress is known to induce the autophagic machinery [195, 196]. As already mentioned, HCV infection is associated with elevated ROS levels and oxidative stress, which in turn activates autophagy to favor HCV particle release [197]. Oxidative stress induced by HCV infection triggers the phosphorylation of the autophagic adaptor pro-

tein p62 on Ser349 that is involved in the induction of autophagy. Consequently, phosphorylated p62 increases its binding to Keap1, thereby releasing Nrf2 from the Keap1-Nrf2 complex. In HCV-positive cells, sMafs are bound to NS3 at the replicon complexes on the cytoplasmic face of the ER, thus preventing its translocation to the nucleus. Free Nrf2 is trapped via delocalized sMaf proteins and is therefore prevented from its entry into the nucleus to induce antioxidant defenses, which in turn favors the release of viral particles. In addition, HCV-induced sequestration of Nrf2 at the replicon complex is core dependent, but how the core participates in this process remains to be investigated. Taken together, it is possible that the interplay between HCV-induced oxidative stress and the Nrf2 signaling elevates the ROS, leading to the induction of autophagy, thereby favoring HCV infection (Figure 1). Given that a functional association between a dysfunctional autophagy and Nrf2 pathway activation has been identified in HCC [198], oxidative stress by the inhibition of Nrf2 triggers autophagy and thus may be involved in chronic HCV infection-related HCC. It is worth noting that several papers also suggest that HCV can activate the Nrf2 pathway. On one hand, HCV-mediated Nrf2 activation contributes to the survival of HCV-infected Huh7 cells, which provides important clues to the understanding of the mechanisms of chronic liver disease induced by oxidative stress associated with HCV infection [199]. Conversely, at an early stage, the expression of HCV proteins in Huh7 cells induces a strong upregulation of the antioxidant defense system. These events may underlie the harmful effects of HCV-induced oxidative stress during the acute stage of hepatitis C [124]. Thus, the difference in Nrf2 status during HCV infection may depend on cell types and infection stages.

5.2. Oxidative Stress, Autophagy, and Flavivirus Infection. Since the initial characterization of autophagy in hepatocyte cells during DENV2 infection was reported in 2008 [200], several reports have demonstrated the proviral role of autophagy in DENV2 infection. NS1 is reported to partially colocalize with autophagosomes in hepatocytes, and inhibiting lysosomal fusion with autophagosomes increases viral replication, implying a role for immature autophagosomes in the DENV2 life cycle [201]. DENV3 also induces autophagy; however, the role of autophagy in its life cycle may differ from that for DENV2 as a lysosomal fusion inhibitor decreases DENV3 replication [202]. Moreover, a recent report shows that NS4A can induce autophagosome formation during DENV infection and protect the infected cells from apoptosis in renal epithelial cells and thus contribute to prolonged viral replication [203]. Additionally, DENV has been shown to induce the proliferation of LC3-containing membranes [204], and inhibition of cellular autophagy deranges DENV virion maturation [205]. Similar to HCV, the UPR-autophagy pathways have been shown to modulate the DENV-associated PAMP-induced innate immune response, implying that DENV exploits the UPR-autophagy pathways to escape from the innate immune response [189]. However, autophagy also has the potential to limit DENV replication. A recent study demonstrates that autophagy activity is increased and supports DENV
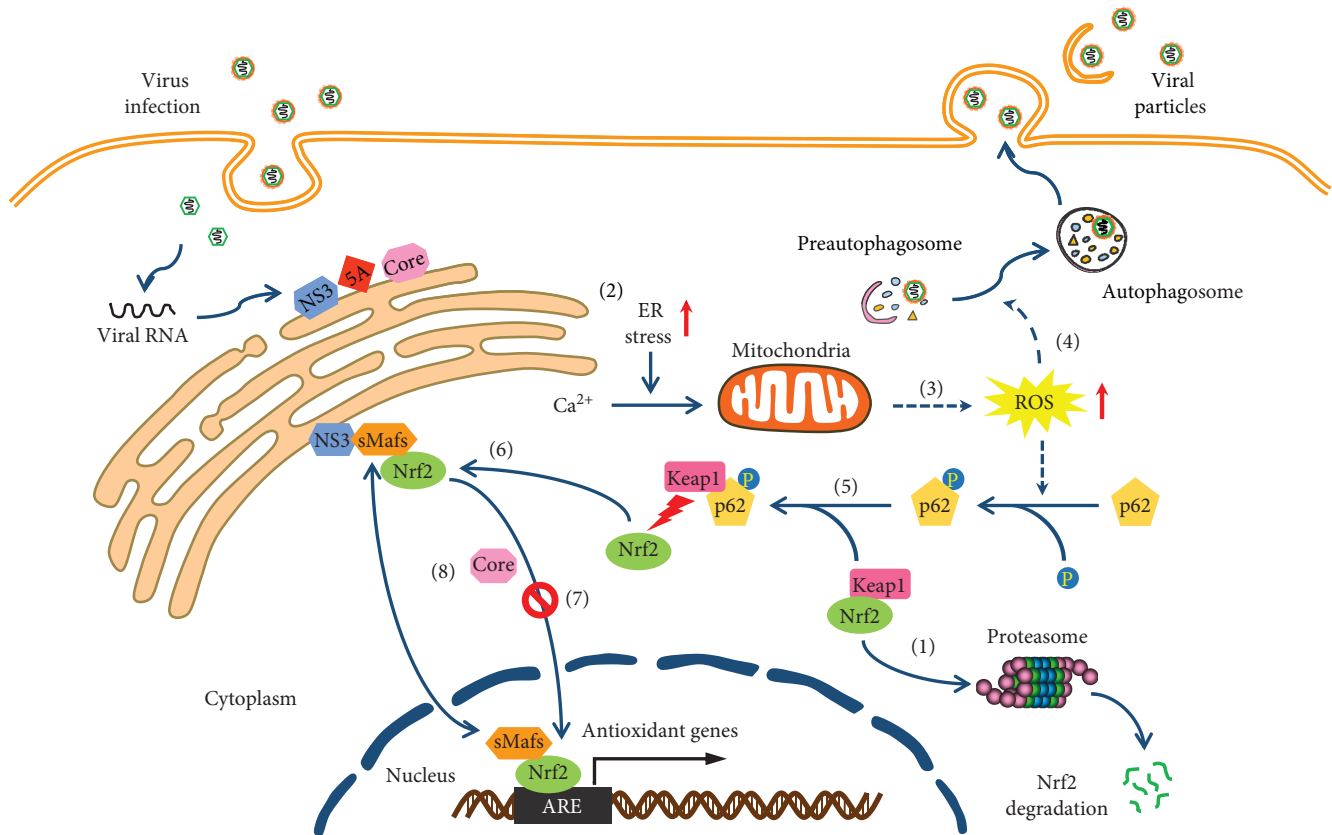
FIGURE 1: Proposed model for the interplay between HCV infection and ROS production, Nrf2 signaling, and autophagy. (1) Under homeostatic conditions, Keap1 sequesters Nrf2 in the cytosol, where it mediates proteasomal degradation of Nrf2. (2) HCV infection induces ER stress and alters ER calcium homeostasis. (3) The uptake of calcium in the mitochondria triggers ROS formation. (4) Oxidant stress induced by HCV infection induces the phosphorylation of p62 and autophagy. (5) Consequently, phosphorylated p62 increases its binding to Keap1, thereby releasing Nrf2 from the Keap1-Nrf2 complex. (6) Free Nrf2 is trapped via delocalized sMaf proteins that are associated with NS3 at the replication complex on the cytoplasmic face of the ER, (7) and thus preventing its translocation to the nucleus to induce antioxidant defenses, which in turn favors the release of viral particles. (8) In addition, HCV-induced sequestration of Nrf2 at the replication complex is core dependent, but how the core participates in this process remains unclear.

replication during early infection, and at the later stage of infection specific autophagy suppression provides a viral replication advantage, suggesting the shifts of autophagy from a virus-supporting to a virus-suppressing process [176]. In addition to general autophagy, DENV-induced selective autophagy is termed as lipophagy, resulting in the release of free fatty acids (FFA), which undergoes oxidation in the mitochondria to generate ATP, and thus producing a metabolically favorable environment for viral replication [206]. Furthermore, DENV and ZIKV subvert reticulophagy through viral protease NS2B3-dependent cleavage of ER-localized reticulophagy receptor FAM134B [207].

To date, relatively few studies have been done on the role of autophagy under the infection of ZIKV. The precise molecular mechanisms involved in ZIKV-induced autophagy have not been fully elucidated. It has been demonstrated that autophagic vesicles are accumulated following ZIKV infection in both *in vitro* and *in vivo* models, suggesting the induction of autophagy in ZIKV infection. Similar to DENV, ZIKV can also induce the formation of LC3-containing membranes [175, 178, 208]. However, in contrast to DENV,

where NS4A-induced autophagy confers protection from cell death, NS4A and NS4B of ZIKV dysregulate autophagy through AKT1-mTOR inhibition, leading to increased cell death and impeded neurogenesis in fetal neural stem cells [178]. Moreover, one study demonstrates that noncanonical secretory autophagy may contribute to the spread of ZIKV [209]. Recently, a study showed that ZIKV infection activates autophagic activity in human trophoblast cells and in the mouse placenta, and inhibition of the autophagy signaling reduces ZIKV vertical transmission and limits placental damage and fetal death, therefore providing a foundation for developing therapeutics targeting autophagy to reduce maternal-fetal transmission of ZIKV [210]. Furthermore, ZIKV triggers ER stress and UPR in the cerebral cortex of infected postmortem human fetuses as well as in cultured human neural stem cells, suggesting a potential role of oxidative stress in ZIKV-induced autophagy [211]. Given that oxidative stress plays a critical role in the induction of autophagy, in the future, more work is required to determine the interplay between oxidative stress and autophagy during DENV and ZIKV infections.

6. Oxidative Stress, DNA Damage, and Viral Infection

DNA is usually restricted within the nucleus and mitochondria of eukaryotic cells. RNA viruses are known to cause DNA damage, leading to the escape of self-DNA into the cytoplasm [212]. The presence of cytosolic DNA of mammalian cells serves as a danger signal that activates innate immune responses [213]. DNA damage can induce cell apoptosis, inflammatory immune responses, and deleterious mutations that increase the risk of tumorigenesis and contribute to the pathogenesis of RNA viruses [212, 214]. Therefore, the molecular basis for RNA virus-mediated DNA damage response remains an important area of study that will likely provide key insights into the modulation of host cell functions by these pathogens.

Growing evidences demonstrate that HCV increases the production of the hydroxyl radical and peroxynitrite close to the cell nucleus, therefore inflicting DNA damage. Further study shows that HCV increases the generation of the superoxide and H_2O_2 in proximity to the hepatocyte nucleus and that the source of ROS is primarily NOX1 and NOX4 [215]. During HCV infection, the core and NS3 proteins induce oxidative stress through the activation of iNOS, which in turn causes DNA damage and thereby results in the increased mutagenesis of cellular genes, including protooncogenes and tumor suppressor genes [216]. The core, E1, and NS3 proteins can also cause DNA damage and the activation of oncogene STAT-3 via ROS [126]. NS3/4A impairs DNA repair efficiency and enhances cellular sensitivity to DNA damage [217]. All of these contribute to the HCV-related hepatocarcinogenesis. Although the DNA repair mechanisms of the host cell have specifically evolved to counteract DNA damage, studies have suggested that the suppression of DNA repair might be a crucial consequence of chronic oxidative stress in HCV-infected cells [218]. The accumulation of DNA damage response in HCV-infected cells suggests that HCV-associated oxidative stress may overwhelm cellular antioxidant and DNA repair mechanisms, leading ultimately to neoplastic transformation. In line with this result, DNA damage is observed in PBMCs from HCV-infected patients and B cells *in vitro* [219]. The HCV core protein inhibits the formation of the complex of DNA damage sensor proteins and oxidatively damages DNA repair, resulting in DNA damage and hypersensitivity to DNA-damaging reagents. In addition, the HCV-triggered induction of ROS and the perturbation of DNA repair enzyme *NEIL1* expression may be involved in the progression of liver disease suggesting that antioxidant and antiviral therapies can reverse these deleterious effects of HCV in part by restoring the function of the DNA repair enzymes [220].

To date, only a few studies are reported on the role of DNA damage and the infection of DENV and ZIKV. A recent study demonstrates that DENV NS2B targets the DNA sensor cyclic GMP-AMP synthase (cGAS) for lysosomal degradation to avoid the detection of mtDNA during infection [221]. Similar to DENV, ZIKV infection induces a release of mtDNA which is identified as a ligand for cGAS, thereby eliciting inflammation to evade antiviral response [222]. As mtDNA is a major target of oxidative stress, the interplay between oxidative stress, mtDNA-associated inflammatory responses, and DENV or ZIKV-induced pathogenesis is a field of increasing interest.

7. Conclusions and Future Perspective

Flaviviridae virus infection induces oxidative stress, which affects both the cellular metabolism and the life cycle of the viruses. In the past decades, much progress has been made in understanding the interplay between oxidative stress and *Flaviviridae* viruses, especially for HCV and DENV. It is already known that oxidative stress plays dual roles in regulating viral replication; nevertheless, the underlying mechanisms are still unclear. More studies have shown that the Nrf2/ARE pathway is a common antioxidant system for HCV, DENV, and ZIKV; however, only few reports are done for JEV, TBEV, and WNV regarding oxidative stress and antioxidants. Arctigenin is found to have antioxidant and antiviral activities against the infection of JEV [223], and morpholino lowers the oxidative stress induced by JEV [224]. The TBEV NS1 protein both triggers ROS production and activates the Nrf2/ARE pathway [23]. Echinochrome A is reported to have antioxidant properties suppressing TBEV [225]. WNV could upregulate Nrf2 [22]. Fine-tuning the balance between ROS generation and detoxifying upon the infections of viruses requires more effort not only for JEV, TBEV, and WNV, which is hampered largely because of the lack of knowledge, but also for HCV, DENV, and ZIKV in the future. Knowledge gained from HCV, DENV, or other viruses may facilitate the study of the modulation of the oxidative stress in JEV, WNV, and TBEV infections. Once the mechanisms are elucidated, they may provide new insights into viral pathogenesis and the development of new therapeutics.

Understanding the role of oxidative stress and ROS-mediated DNA damage or autophagy might lead to new discoveries in pathology and novel strategies for interventions and clinical management. Moreover, the challenges involved in researching cellular ROS in viral infection are as follows: (1) Many positive-stranded RNA viruses replicate in ER-derived membranes, causing new membrane synthesis and rearrangement which are reorganized into viral replication organelles. While the architecture of these replication organelles is relatively defined, little is known about the viral and host factors orchestrating their biogenesis upon induction of oxidative stress. (2) HCV-induced ROS is required for the establishment of acute and chronic liver diseases. However, little is known about the role of oxidative stress in HCV-induced extrahepatic manifestations such as insulin resistance and neuronal disorders. (3) Although much of the available evidence supports the involvement of ROS in HCV and DENV-associated diseases, the interplay among viral proteins, cellular factors and enzymes for ROS production remains to be clarified. Thus, a better understanding of the underlying molecular mechanisms might help develop the study of the pathogenesis and antiviral therapies against the infections of *Flaviviridae* viruses. (4) In contrast to the chronic infection by HCV, apoptosis is usually the ultimate

outcome of cells infected with DENV and ZIKV. It is of interest to determine why oxidative stress and associated molecular events such as autophagy and mtDNA damage can lead to different responses in the host cell. (5) Recent studies have shown that ZIKV has oncolytic activity against glioblastoma stem cells (GSCs), suggesting that the engineering of ZIKV may provide a therapeutic modality against glioblastoma [226–229]. As ZIKV selectively infects and kills GSCs relative to normal neuronal cells, it is of great interest to determine the role of oxidative stress in this process. (6) The role of oxidative stress in other flavivirus infections requires more effort.

Disclosure

Conflicts of Interest

The authors declare that there is no conflict of interests regarding the publication of this paper.

Acknowledgments

References

[1] C. J. Neufeldt, M. Cortese, E. G. Acosta, and R. Bartenschlager, "Rewiring cellular networks by members of the *Flaviviridae* family," *Nature Reviews Microbiology*, vol. 16, no. 3, pp. 125–142, 2018.

[2] S. B. Halstead and S. N. Cohen, "Dengue hemorrhagic fever at 60 years: early evolution of concepts of causation and treatment," *Microbiology and Molecular Biology Reviews*, vol. 79, no. 3, pp. 281–291, 2015.

[3] T. dos Santos, A. Rodriguez, M. Almiron et al., "Zika Virus and the Guillain–Barré Syndrome — Case Series from Seven Countries," *The New England Journal of Medicine*, vol. 375, no. 16, pp. 1598–1601, 2016.

[4] B. Hoen, B. Schaub, A. L. Funk et al., "Pregnancy outcomes after ZIKV infection in French territories in the Americas," *The New England Journal of Medicine*, vol. 378, no. 11, pp. 985–994, 2018.

[5] H. H. Thein, Q. Yi, G. J. Dore, and M. D. Krahn, "Estimation of stage-specific fibrosis progression rates in chronic hepatitis C virus infection: a meta-analysis and meta-regression," *Hepatology*, vol. 48, no. 2, pp. 418–431, 2008.

[6] Y. M. Go and D. P. Jones, "Redox compartmentalization in eukaryotic cells," *Biochimica et Biophysica Acta (BBA) - General Subjects*, vol. 1780, no. 11, pp. 1273–1290, 2008.

[7] J. Roy, J.-M. Galano, T. Durand, J.-Y. le Guennec, and J. C.-Y. Lee, "Physiological role of reactive oxygen species as promoters of natural defenses," *The FASEB Journal*, vol. 31, no. 9, pp. 3729–3745, 2017.

[8] G. Pizzino, N. Irrera, M. Cucinotta et al., "Oxidative stress: harms and benefits for human health," *Oxidative Medicine and Cellular Longevity*, vol. 2017, Article ID 8416763, 13 pages, 2017.

[9] A. Dandekar, R. Mendez, and K. Zhang, "Cross talk between ER stress, oxidative stress, and inflammation in health and disease," *Methods in Molecular Biology*, vol. 1292, pp. 205–214, 2015.

[10] A. Ruggieri, E. Dazert, P. Metz et al., "Dynamic oscillation of translation and stress granule formation mark the cellular response to virus infection," *Cell Host & Microbe*, vol. 12, no. 1, pp. 71–85, 2012.

[11] K. Onomoto, M. Yoneyama, G. Fung, H. Kato, and T. Fujita, "Antiviral innate immunity and stress granule responses," *Trends in Immunology*, vol. 35, no. 9, pp. 420–428, 2014.

[12] H. Sies, "Oxidative stress: a concept in redox biology and medicine," *Redox Biology*, vol. 4, pp. 180–183, 2015.

[13] D. Olagnier, S. Peri, C. Steel et al., "Cellular oxidative stress response controls the antiviral and apoptotic programs in dengue virus-infected dendritic cells," *PLoS Pathogens*, vol. 10, no. 12, article e1004566, 2014.

[14] A. A. al-alimi, S. A. Ali, F. M. al-Hassan, F. M. Idris, S.-Y. Teow, and N. Mohd Yusoff, "Dengue virus type 2 (DENV2) induced oxidative responses in monocytes from glucose-6-phosphate dehydrogenase (G6PD)-deficient and G6PD normal subjects," *PLoS Neglected Tropical Diseases*, vol. 8, no. 3, article e2711, 2014.

[15] T. H. Chen, P. Tang, C. F. Yang et al., "Antioxidant defense is one of the mechanisms by which mosquito cells survive dengue 2 viral infection," *Virology*, vol. 410, no. 2, pp. 410–417, 2011.

[16] G. Li, M. Poulsen, C. Fenyvuesvolgyi et al., "Characterization of cytopathic factors through genome-wide analysis of the Zika viral proteins in fission yeast," *Proceedings of the National Academy of Sciences of the United States of America*, vol. 114, no. 3, pp. E376–E385, 2017.

[17] R. Amorim, A. Temzi, B. D. Griffin, and A. J. Mouland, "Zika virus inhibits eIF2α-dependent stress granule assembly," *PLoS Neglected Tropical Diseases*, vol. 11, no. 7, article e0005775, 2017.

[18] R. J. Lin, C. L. Liao, and Y. L. Lin, "Replication-incompetent virions of Japanese encephalitis virus trigger neuronal cell death by oxidative stress in a culture system," *The Journal of General Virology*, vol. 85, no. 2, pp. 521–533, 2004.

[19] S. L. Raung, M. D. Kuo, Y. M. Wang, and C. J. Chen, "Role of reactive oxygen intermediates in Japanese encephalitis virus infection in murine neuroblastoma cells," *Neuroscience Letters*, vol. 315, no. 1-2, pp. 9–12, 2001.

[20] T. C. Yang, C. C. Lai, S. L. Shiu et al., "Japanese encephalitis virus down-regulates thioredoxin and induces ROS-mediated ASK1-ERK/p38 MAPK activation in human

promonocyte cells," *Microbes and Infection*, vol. 12, no. 8-9, pp. 643–651, 2010.

[21] R. C. Gullberg, J. Jordan Steel, S. L. Moon, E. Soltani, and B. J. Geiss, "Oxidative stress influences positive strand RNA virus genome synthesis and capping," *Virology*, vol. 475, pp. 219–229, 2015.

[22] M. Basu, S. C. Courtney, and M. A. Brinton, "Arsenite-induced stress granule formation is inhibited by elevated levels of reduced glutathione in West Nile virus-infected cells," *PLoS Pathogens*, vol. 13, no. 2, article e1006240, 2017.

[23] Y. V. Kuzmenko, O. A. Smirnova, A. V. Ivanov, E. S. Starodubova, and V. L. Karpov, "Nonstructural protein 1 of tick-borne encephalitis virus induces oxidative stress and activates antioxidant defense by the Nrf2/ARE pathway," *Intervirology*, vol. 59, no. 2, pp. 111–117, 2016.

[24] N. de Maria, A. Colantonl, S. Fagiuoli et al., "Association between reactive oxygen species and disease activity in chronic hepatitis C," *Free Radical Biology & Medicine*, vol. 21, no. 3, pp. 291–295, 1996.

[25] F. Farinati, R. Cardin, N. de Maria et al., "Iron storage, lipid peroxidation and glutathione turnover in chronic anti-HCV positive hepatitis," *Journal of Hepatology*, vol. 22, no. 4, pp. 449–456, 1995.

[26] A. Ivanov, B. Bartosch, O. Smirnova, M. Isaguliants, and S. Kochetkov, "HCV and oxidative stress in the liver," *Viruses*, vol. 5, no. 2, pp. 439–469, 2013.

[27] R. Medvedev, D. Ploen, and E. Hildt, "HCV and oxidative stress: implications for HCV life cycle and HCV-associated pathogenesis," *Oxidative Medicine and Cellular Longevity*, vol. 2016, Article ID 9012580, 13 pages, 2016.

[28] K. Rebbani and K. Tsukiyama-Kohara, "HCV-induced oxidative stress: battlefield-winning strategy," *Oxidative Medicine and Cellular Longevity*, vol. 2016, Article ID 7425628, 7 pages, 2016.

[29] WHO, *Global hepatitis report 2017. Geneva: global hepatitis Programme*, Department of HIV/AIDS, World Health Organization, 2017, https://afro.who.int/sites/default/files/2017-2006/9789241565455-eng.pdf.

[30] M. P. Manns, M. Buti, E. Gane et al., "Hepatitis C virus infection," *Nature Reviews. Disease Primers*, vol. 3, no. 1, 2017.

[31] R. Bartenschlager, T. F. Baumert, J. Bukh et al., "Critical challenges and emerging opportunities in hepatitis C virus research in an era of potent antiviral therapy: considerations for scientists and funding agencies," *Virus Research*, vol. 248, pp. 53–62, 2018.

[32] F. Farinati, R. Cardin, P. Degan et al., "Oxidative DNA damage in circulating leukocytes occurs as an early event in chronic HCV infection," *Free Radical Biology & Medicine*, vol. 27, no. 11-12, pp. 1284–1291, 1999.

[33] M. Isaguliants, O. Smirnova, A. V. Ivanov et al., "Oxidative stress induced by HIV1 reverse transcriptase modulates the enzyme's performance in gene immunization," *Human Vaccines & Immunotherapeutics*, vol. 9, no. 10, pp. 2111–2119, 2014.

[34] N. E. Murray, M. B. Quam, and A. Wilder-Smith, "Epidemiology of dengue: past, present and future prospects," *Clinical Epidemiology*, vol. 5, pp. 299–309, 2013.

[35] S. B. Halstead, "Pathogenesis of dengue: dawn of a new era," *F1000Res*, vol. 4, no. 4, 2015.

[36] A. Wilder-Smith, E. E. Ooi, O. Horstick, and B. Wills, "Dengue," *Lancet*, vol. 393, no. 10169, pp. 350–363, 2019.

[37] J. P. Messina, M. U. Kraemer, O. J. Brady et al., "Mapping global environmental suitability for Zika virus," *eLife*, vol. 5, 2016.

[38] N. Wikan and D. R. Smith, "Zika virus: history of a newly emerging arbovirus," *The Lancet Infectious Diseases*, vol. 16, no. 7, pp. e119–e126, 2016.

[39] T. C. Pierson and M. S. Diamond, "The emergence of Zika virus and its new clinical syndromes," *Nature*, vol. 560, no. 7720, pp. 573–581, 2018.

[40] M. J. Counotte, C. R. Kim, J. Wang et al., "Sexual transmission of Zika virus and other flaviviruses: a living systematic review," *PLoS Medicine*, vol. 15, no. 7, article e1002611, 2018.

[41] L. Turtle and T. Solomon, "Japanese encephalitis—the prospects for new treatments," *Nature Reviews. Neurology*, vol. 14, no. 5, pp. 298–313, 2018.

[42] O. A. Maximova and A. G. Pletnev, "Flaviviruses and the central nervous system: revisiting neuropathological concepts," *Annual Review of Virology*, vol. 5, no. 1, pp. 255–272, 2018.

[43] F. X. Heinz and K. Stiasny, "Flaviviruses and flavivirus vaccines," *Vaccine*, vol. 30, no. 29, pp. 4301–4306, 2012.

[44] T. Ishikawa, A. Yamanaka, and E. Konishi, "A review of successful flavivirus vaccines and the problems with those flaviviruses for which vaccines are not yet available," *Vaccine*, vol. 32, no. 12, pp. 1326–1337, 2014.

[45] A. L. C. Valadão, R. S. Aguiar, and L. B. de Arruda, "Interplay between inflammation and cellular stress triggered by *Flaviviridae* viruses," *Frontiers in Microbiology*, vol. 7, p. 1233, 2016.

[46] C. L. Murray, C. T. Jones, and C. M. Rice, "Architects of assembly: roles of *Flaviviridae* non-structural proteins in virion morphogenesis," *Nature Reviews. Microbiology*, vol. 6, no. 9, pp. 699–708, 2008.

[47] P. Simmonds, P. Becher, J. Bukh et al., "ICTV virus taxonomy profile: *Flaviviridae*," *The Journal of General Virology*, vol. 98, no. 1, pp. 2-3, 2017.

[48] E. Panieri, V. Gogvadze, E. Norberg, R. Venkatesh, S. Orrenius, and B. Zhivotovsky, "Reactive oxygen species generated in different compartments induce cell death, survival, or senescence," *Free Radical Biology & Medicine*, vol. 57, pp. 176–187, 2013.

[49] Z. Zhang, L. Liu, X. Jiang, S. Zhai, and D. Xing, "The essential role of Drp1 and its regulation by S-nitrosylation of Parkin in dopaminergic neurodegeneration: implications for Parkinson's disease," *Antioxidants & Redox Signaling*, vol. 25, no. 11, pp. 609–622, 2016.

[50] K. de Andrade, F. Moura, J. dos Santos, O. de Araújo, J. de Farias Santos, and M. Goulart, "Oxidative stress and inflammation in hepatic diseases: therapeutic possibilities of N-acetylcysteine," *International Journal of Molecular Sciences*, vol. 16, no. 12, pp. 30269–30308, 2015.

[51] F. C. Camini, C. C. da Silva Caetano, L. T. Almeida, and C. L. de Brito Magalhaes, "Implications of oxidative stress on viral pathogenesis," *Archives of Virology*, vol. 162, no. 4, pp. 907–917, 2017.

[52] A. A. Starkov, G. Fiskum, C. Chinopoulos et al., "Mitochondrial α-ketoglutarate dehydrogenase complex generates reactive oxygen species," *The Journal of Neuroscience*, vol. 24, no. 36, pp. 7779–7788, 2004.

[53] D. B. Zorov, M. Juhaszova, and S. J. Sollott, "Mitochondrial reactive oxygen species (ROS) and ROS-induced ROS

release," *Physiological Reviews*, vol. 94, no. 3, pp. 909–950, 2014.

[54] A. Ambrus, N. S. Nemeria, B. Torocsik et al., "Formation of reactive oxygen species by human and bacterial pyruvate and 2-oxoglutarate dehydrogenase multienzyme complexes reconstituted from recombinant components," *Free Radical Biology & Medicine*, vol. 89, pp. 642–650, 2015.

[55] L. Tretter and V. Adam-Vizi, "Generation of reactive oxygen species in the reaction catalyzed by α-ketoglutarate dehydrogenase," *The Journal of Neuroscience*, vol. 24, no. 36, pp. 7771–7778, 2004.

[56] M. Schieber and N. S. Chandel, "ROS function in redox signaling and oxidative stress," *Current Biology*, vol. 24, no. 10, pp. R453–R462, 2014.

[57] D. R. Green and G. Kroemer, "The pathophysiology of mitochondrial cell death," *Science*, vol. 305, no. 5684, pp. 626–629, 2004.

[58] S. Marchi, S. Patergnani, S. Missiroli et al., "Mitochondrial and endoplasmic reticulum calcium homeostasis and cell death," *Cell Calcium*, vol. 69, pp. 62–72, 2018.

[59] I. R. Indran, M. P. Hande, and S. Pervaiz, "Tumor cell redox state and mitochondria at the center of the non-canonical activity of telomerase reverse transcriptase," *Molecular Aspects of Medicine*, vol. 31, no. 1, pp. 21–28, 2010.

[60] J. Dan Dunn, L. A. Alvarez, X. Zhang, and T. Soldati, "Reactive oxygen species and mitochondria: a nexus of cellular homeostasis," *Redox Biology*, vol. 6, pp. 472–485, 2015.

[61] M. P. Simula and V. De Re, "Hepatitis C virus-induced oxidative stress and mitochondrial dysfunction: a focus on recent advances in proteomics," *Proteomics. Clinical Applications*, vol. 4, no. 10-11, pp. 782–793, 2010.

[62] M. J. Berridge, M. D. Bootman, and H. L. Roderick, "Calcium signalling: dynamics, homeostasis and remodelling," *Nature Reviews. Molecular Cell Biology*, vol. 4, no. 7, pp. 517–529, 2003.

[63] A. Görlach, P. Klappa, and D. T. Kietzmann, "The endoplasmic reticulum: folding, calcium homeostasis, signaling, and redox control," *Antioxidants & Redox Signaling*, vol. 8, no. 9-10, pp. 1391–1418, 2006.

[64] R. Rizzuto, P. Pinton, W. Carrington et al., "Close contacts with the endoplasmic reticulum as determinants of mitochondrial Ca^{2+} responses," *Science*, vol. 280, no. 5370, pp. 1763–1766, 1998.

[65] I. K. Lee, S. A. Lee, H. Kim, Y. S. Won, and B. J. Kim, "Induction of endoplasmic reticulum-derived oxidative stress by an occult infection related S surface antigen variant," *World Journal of Gastroenterology*, vol. 21, no. 22, pp. 6872–6883, 2015.

[66] O. Smirnova, B. Bartosch, N. Zakirova, S. Kochetkov, and A. Ivanov, "Polyamine metabolism and oxidative protein folding in the ER as ROS-producing systems neglected in virology," *International Journal of Molecular Sciences*, vol. 19, no. 4, p. 1219, 2018.

[67] J. Soeur, J. Eilstein, G. Lereaux, C. Jones, and L. Marrot, "Skin resistance to oxidative stress induced by resveratrol: from Nrf2 activation to GSH biosynthesis," *Free Radical Biology & Medicine*, vol. 78, pp. 213–223, 2015.

[68] Y. Wu, M. S. Matsui, J. Z. S. Chen et al., "Antioxidants add protection to a broad-spectrum sunscreen," *Clinical and Experimental Dermatology*, vol. 36, no. 2, pp. 178–187, 2011.

[69] H. J. Forman, K. J. A. Davies, and F. Ursini, "How do nutritional antioxidants really work: nucleophilic tone and Parahormesis versus free radical scavenging in vivo," *Free Radical Biology & Medicine*, vol. 66, pp. 24–35, 2014.

[70] T. Miyazawa, G. C. Burdeos, M. Itaya, K. Nakagawa, and T. Miyazawa, "Vitamin E: regulatory redox interactions," *IUBMB Life*, vol. 71, no. 4, pp. 430–441, 2019.

[71] S. Magesh, Y. Chen, and L. Hu, "Small molecule modulators of Keap1-Nrf2-ARE pathway as potential preventive and therapeutic agents," *Medicinal Research Reviews*, vol. 32, no. 4, pp. 687–726, 2012.

[72] Z. Ungvari, Z. Bagi, A. Feher et al., "Resveratrol confers endothelial protection via activation of the antioxidant transcription factor Nrf2," *American Journal of Physiology. Heart and Circulatory Physiology*, vol. 299, no. 1, pp. H18–H24, 2010.

[73] S. G. Rhee, S. W. Kang, T. S. Chang, W. Jeong, and K. Kim, "Peroxiredoxin, a novel family of peroxidases," *IUBMB Life*, vol. 52, no. 1, pp. 35–41, 2001.

[74] R. K. Gupta, A. K. Patel, N. Shah et al., "Oxidative stress and antioxidants in disease and cancer: a review," *Asian Pacific Journal of Cancer Prevention*, vol. 15, no. 11, pp. 4405–4409, 2014.

[75] M. Kobayashi, L. Li, N. Iwamoto et al., "The antioxidant defense system Keap1-Nrf2 comprises a multiple sensing mechanism for responding to a wide range of chemical compounds," *Molecular and Cellular Biology*, vol. 29, no. 2, pp. 493–502, 2009.

[76] M. L. Jauslin, T. Meier, R. A. Smith, and M. P. Murphy, "Mitochondria-targeted antioxidants protect Friedreich ataxia fibroblasts from endogenous oxidative stress more effectively than untargeted antioxidants," *The FASEB Journal*, vol. 17, no. 13, pp. 1972–1974, 2003.

[77] E. Peterhans, "Sendai virus stimulates chemiluminescence in mouse spleen cells," *Biochemical and Biophysical Research Communications*, vol. 91, no. 1, pp. 383–392, 1979.

[78] Y. H. Lee, C. L. Lai, S. H. Hsieh, C. C. Shieh, L. M. Huang, and B. A. Wu-Hsieh, "Influenza a virus induction of oxidative stress and MMP-9 is associated with severe lung pathology in a mouse model," *Virus Research*, vol. 178, no. 2, pp. 411–422, 2013.

[79] M. L. Reshi, Y. C. Su, and J. R. Hong, "RNA viruses: ROS-mediated cell death," *International Journal of Cell Biology*, vol. 2014, Article ID 467452, 16 pages, 2014.

[80] O. Khomich, S. Kochetkov, B. Bartosch, and A. Ivanov, "Redox biology of respiratory viral infections," *Viruses*, vol. 10, no. 8, p. 392, 2018.

[81] S. J. Kim, G. H. Syed, and A. Siddiqui, "Hepatitis C virus induces the mitochondrial translocation of Parkin and subsequent mitophagy," *PLoS Pathogens*, vol. 9, no. 3, article e1003285, 2013.

[82] A. Narayanan, M. Amaya, K. Voss et al., "Reactive oxygen species activate NFκB (p65) and p53 and induce apoptosis in RVFV infected liver cells," *Virology*, vol. 449, pp. 270–286, 2014.

[83] A. Soucy-Faulkner, E. Mukawera, K. Fink et al., "Requirement of NOX2 and reactive oxygen species for efficient RIG-I-mediated antiviral response through regulation of MAVS expression," *PLoS Pathogens*, vol. 6, no. 6, article e1000930, 2010.

[84] M. Strengert, R. Jennings, S. Davanture, P. Hayes, G. Gabriel, and U. G. Knaus, "Mucosal reactive oxygen species are

required for antiviral response: role of Duox in influenza a virus infection," *Antioxidants & Redox Signaling*, vol. 20, no. 17, pp. 2695–2709, 2014.

[85] Y. L. Lin, C. C. Liu, J. I. Chuang et al., "Involvement of oxidative stress, NF-IL-6, and RANTES expression in dengue-2-virus-infected human liver cells," *Virology*, vol. 276, no. 1, pp. 114–126, 2000.

[86] Y. Jaiyen, P. Masrinoul, S. Kalayanarooj, R. Pulmanausahakul, and S. Ubol, "Characteristics of dengue virus-infected peripheral blood mononuclear cell death that correlates with the severity of illness," *Microbiology and Immunology*, vol. 53, no. 8, pp. 442–450, 2009.

[87] H. Indukuri, S. M. Castro, S. M. Liao et al., "Ikkepsilon regulates viral-induced interferon regulatory factor-3 activation via a redox-sensitive pathway," *Virology*, vol. 353, no. 1, pp. 155–165, 2006.

[88] E. Datan, S. G. Roy, G. Germain et al., "Dengue-induced autophagy, virus replication and protection from cell death require ER stress (PERK) pathway activation," *Cell Death & Disease*, vol. 7, no. 3, article e2127, 2016.

[89] A. Ramezani, M. P. Nahad, and E. Faghihloo, "The role of Nrf2 transcription factor in viral infection," *Journal of Cellular Biochemistry*, vol. 119, no. 8, pp. 6366–6382, 2018.

[90] M. Eslam, M. A. Khattab, and S. A. Harrison, "Insulin resistance and hepatitis C: an evolving story," *Gut*, vol. 60, no. 8, pp. 1139–1151, 2011.

[91] M. Taskoparan, E. Serin, H. S. Gokturk et al., "Early effect of peginterferon alpha2b plus ribavirin treatment on blood pressure and insulin resistance in patients with chronic hepatitis C," *Hepatogastroenterology*, vol. 58, no. 107-108, pp. 875–879, 2011.

[92] L. Serfaty and J. Capeau, "Hepatitis C, insulin resistance and diabetes: clinical and pathogenic data," *Liver International*, vol. 29, Supplement 2, pp. 13–25, 2009.

[93] E. G. Meissner, Y. J. Lee, A. Osinusi et al., "Effect of sofosbuvir and ribavirin treatment on peripheral and hepatic lipid metabolism in chronic hepatitis C virus, genotype 1-infected patients," *Hepatology*, vol. 61, no. 3, pp. 790–801, 2015.

[94] E. Vanni, E. Bugianesi, and G. Saracco, "Treatment of type 2 diabetes mellitus by viral eradication in chronic hepatitis C: myth or reality?," *Digestive and Liver Disease*, vol. 48, no. 2, pp. 105–111, 2016.

[95] Y. C. Hsu, J. T. Lin, H. J. Ho et al., "Antiviral treatment for hepatitis C virus infection is associated with improved renal and cardiovascular outcomes in diabetic patients," *Hepatology*, vol. 59, no. 4, pp. 1293–1302, 2014.

[96] R. J. Wong, F. Kanwal, Z. M. Younossi, and A. Ahmed, "Hepatitis C virus infection and coronary artery disease risk: a systematic review of the literature," *Digestive Diseases and Sciences*, vol. 59, no. 7, pp. 1586–1593, 2014.

[97] B. Terrier, A. Karras, P. Cluzel et al., "Presentation and prognosis of cardiac involvement in hepatitis C virus-related vasculitis," *The American Journal of Cardiology*, vol. 111, no. 2, pp. 265–272, 2013.

[98] S. Petta, M. Maida, F. S. Macaluso et al., "Hepatitis C virus infection is associated with increased cardiovascular mortality: a meta-analysis of observational studies," *Gastroenterology*, vol. 150, no. 1, pp. 145–155.e4, 2016.

[99] A. L. Zignego, C. Giannini, and L. Gragnani, "HCV and lymphoproliferation," *Clinical & Developmental Immunology*, vol. 2012, article 980942, 8 pages, 2012.

[100] A. L. Zignego, L. Gragnani, A. Piluso et al., "Virus-driven autoimmunity and lymphoproliferation: the example of HCV infection," *Expert Review of Clinical Immunology*, vol. 11, no. 1, pp. 15–31, 2015.

[101] F. Gulli, U. Basile, L. Gragnani et al., "Autoimmunity and lymphoproliferation markers in naive HCV-RNA positive patients without clinical evidences of autoimmune/lymphoproliferative disorders," *Digestive and Liver Disease*, vol. 48, no. 8, pp. 927–933, 2016.

[102] A. Ozkok and A. Yildiz, "Hepatitis C virus associated glomerulopathies," *World Journal of Gastroenterology*, vol. 20, no. 24, pp. 7544–7554, 2014.

[103] L. Goldstein, H. Fogel-Grinvald, and I. Steiner, "Hepatitis B and C virus infection as a risk factor for Parkinson's disease in Israel—a nationwide cohort study," *Journal of the Neurological Sciences*, vol. 398, pp. 138–141, 2019.

[104] K. J. Wangensteen, E. L. Krawitt, R. W. Hamill, and J. T. Boyd, "Hepatitis C virus infection: a risk factor for Parkinson's disease," *Journal of Viral Hepatitis*, vol. 23, no. 7, p. 535, 2016.

[105] H. H. Tsai, H. H. Liou, C. H. Muo, C. Z. Lee, R. F. Yen, and C. H. Kao, "Hepatitis C virus infection as a risk factor for Parkinson disease: a nationwide cohort study," *Neurology*, vol. 86, no. 9, pp. 840–846, 2016.

[106] J. T. Boyd, C.-H. Kao, K. J. Wangensteen, E. L. Krawitt, R. W. Hamill, and H.-H. Tsai, "Hepatitis C virus infection as a risk factor for Parkinson disease: a nationwide cohort study," *Neurology*, vol. 87, no. 3, p. 342, 2016.

[107] W. Y.-Y. Wu, K. H. Kang, S. L. S. Chen et al., "Hepatitis C virus infection: a risk factor for Parkinson's disease," *Journal of Viral Hepatitis*, vol. 22, no. 10, pp. 784–791, 2015.

[108] S. Mahmood, M. Kawanaka, A. Kamei et al., "Immunohistochemical evaluation of oxidative stress markers in chronic hepatitis C," *Antioxidants & Redox Signaling*, vol. 6, no. 1, pp. 19–24, 2004.

[109] G. Waris, J. Turkson, T. Hassanein, and A. Siddiqui, "Hepatitis C virus (HCV) constitutively activates STAT-3 via oxidative stress: role of STAT-3 in HCV replication," *Journal of Virology*, vol. 79, no. 3, pp. 1569–1580, 2005.

[110] C. Vasallo and P. Gastaminza, "Cellular stress responses in hepatitis C virus infection: mastering a two-edged sword," *Virus Research*, vol. 209, pp. 100–117, 2015.

[111] M. Okuda, K. Li, M. R. Beard et al., "Mitochondrial injury, oxidative stress, and antioxidant gene expression are induced by hepatitis C virus core protein," *Gastroenterology*, vol. 122, no. 2, pp. 366–375, 2002.

[112] C. Bureau, J. Bernad, N. Chaouche et al., "Nonstructural 3 protein of hepatitis C virus triggers an oxidative burst in human monocytes via activation of NADPH oxidase," *The Journal of Biological Chemistry*, vol. 276, no. 25, pp. 23077–23083, 2001.

[113] M. V. García-Mediavilla, S. Sánchez-Campos, P. González-Pérez et al., "Differential contribution of hepatitis C virus NS5A and core proteins to the induction of oxidative and nitrosative stress in human hepatocyte-derived cells," *Journal of Hepatology*, vol. 43, no. 4, pp. 606–613, 2005.

[114] M. Korenaga, T. Wang, Y. Li et al., "Hepatitis C virus core protein inhibits mitochondrial electron transport and increases reactive oxygen species (ROS) production," *The Journal of Biological Chemistry*, vol. 280, no. 45, pp. 37481–37488, 2005.

[115] C. Piccoli, R. Scrima, G. Quarato et al., "Hepatitis C virus protein expression causes calcium-mediated mitochondrial bioenergetic dysfunction and nitro-oxidative stress," *Hepatology*, vol. 46, no. 1, pp. 58–65, 2007.

[116] H. Ming-Ju, H. Yih-Shou, C. Tzy-Yen, and C. Hui-Ling, "Hepatitis C virus E2 protein induce reactive oxygen species (ROS)-related fibrogenesis in the HSC-T6 hepatic stellate cell line," *Journal of Cellular Biochemistry*, vol. 112, no. 1, pp. 233–243, 2011.

[117] S. Li, L. Ye, X. Yu et al., "Hepatitis C virus NS4B induces unfolded protein response and endoplasmic reticulum overload response-dependent NF-κB activation," *Virology*, vol. 391, no. 2, pp. 257–264, 2009.

[118] G. Gong, G. Waris, R. Tanveer, and A. Siddiqui, "Human hepatitis C virus NS5A protein alters intracellular calcium levels, induces oxidative stress, and activates STAT3 and NF-κB," *Proceedings of the National Academy of Sciences of the United States of America*, vol. 98, no. 17, pp. 9599–9604, 2001.

[119] A. Ivanov, O. Smirnova, I. Petrushanko et al., "HCV core protein uses multiple mechanisms to induce oxidative stress in human hepatoma Huh7 cells," *Viruses*, vol. 7, no. 6, pp. 2745–2770, 2015.

[120] O. A. Smirnova, O. N. Ivanova, B. Bartosch et al., "Hepatitis C virus NS5A protein triggers oxidative stress by inducing NADPH oxidases 1 and 4 and cytochrome P450 2E1," *Oxidative Medicine and Cellular Longevity*, vol. 2016, Article ID 8341937, 10 pages, 2016.

[121] J. Jansons, I. Sominskaya, N. Petrakova et al., "The immunogenicity in mice of HCV core delivered as DNA is modulated by its capacity to induce oxidative stress and oxidative stress response," *Cell*, vol. 8, no. 3, p. 208, 2019.

[122] N. Dionisio, M. V. Garcia-Mediavilla, S. Sanchez-Campos et al., "Hepatitis C virus NS5A and core proteins induce oxidative stress-mediated calcium signalling alterations in hepatocytes," *Journal of Hepatology*, vol. 50, no. 5, pp. 872–882, 2009.

[123] S. W. Chan and P. A. Egan, "Hepatitis C virus envelope proteins regulate CHOP via induction of the unfolded protein response," *The FASEB Journal*, vol. 19, no. 11, pp. 1510–1512, 2005.

[124] A. V. Ivanov, O. A. Smirnova, O. N. Ivanova, O. V. Masalova, S. N. Kochetkov, and M. G. Isaguliants, "Hepatitis C virus proteins activate NRF2/ARE pathway by distinct ROS-dependent and independent mechanisms in HUH7 cells," *PLoS One*, vol. 6, no. 9, article e24957, 2011.

[125] G. Waris, D. J. Felmlee, F. Negro, and A. Siddiqui, "Hepatitis C virus induces proteolytic cleavage of sterol regulatory element binding proteins and stimulates their phosphorylation via oxidative stress," *Journal of Virology*, vol. 81, no. 15, pp. 8122–8130, 2007.

[126] K. Machida, K. T. H. Cheng, C. K. Lai, K. S. Jeng, V. M. H. Sung, and M. M. C. Lai, "Hepatitis C virus triggers mitochondrial permeability transition with production of reactive oxygen species, leading to DNA damage and STAT3 activation," *Journal of Virology*, vol. 80, no. 14, pp. 7199–7207, 2006.

[127] J. Choi, K. J. Lee, Y. Zheng, A. K. Yamaga, M. M. C. Lai, and J. H. Ou, "Reactive oxygen species suppress hepatitis C virus RNA replication in human hepatoma cells," *Hepatology*, vol. 39, no. 1, pp. 81–89, 2004.

[128] D. Yamane, D. R. McGivern, E. Wauthier et al., "Regulation of the hepatitis C virus RNA replicase by endogenous lipid peroxidation," *Nature Medicine*, vol. 20, no. 8, pp. 927–935, 2014.

[129] Y. P. Li, S. Ramirez, S. B. Jensen, R. H. Purcell, J. M. Gottwein, and J. Bukh, "Highly efficient full-length hepatitis C virus genotype 1 (strain TN) infectious culture system," *Proceedings of the National Academy of Sciences of the United States of America*, vol. 109, no. 48, pp. 19757–19762, 2012.

[130] C. Brault, P. Lévy, S. Duponchel et al., "Glutathione peroxidase 4 is reversibly induced by HCV to control lipid peroxidation and to increase virion infectivity," *Gut*, vol. 65, no. 1, pp. 144–154, 2016.

[131] S. Anticoli, D. Amatore, P. Matarrese et al., "Counteraction of HCV-induced oxidative stress concurs to establish chronic infection in liver cell cultures," *Oxidative Medicine and Cellular Longevity*, vol. 2019, Article ID 6452390, 14 pages, 2019.

[132] S. A. Lozano-Sepulveda, O. L. Bryan-Marrugo, C. Cordova-Fletes, M. C. GutierrezRuiz, and A. M. Rivas-Estilla, "Oxidative stress modulation in hepatitis C virus infected cells," *World Journal of Hepatology*, vol. 7, no. 29, pp. 2880–2889, 2015.

[133] J. Choi, "Oxidative stress, endogenous antioxidants, alcohol, and hepatitis C: pathogenic interactions and therapeutic considerations," *Free Radical Biology & Medicine*, vol. 52, no. 7, pp. 1135–1150, 2012.

[134] Y. Jiang, H. Bao, Y. Ge et al., "Therapeutic targeting of GSK3β enhances the Nrf2 antioxidant response and confers hepatic cytoprotection in hepatitis C," *Gut*, vol. 64, no. 1, pp. 168–179, 2015.

[135] S. Petta, C. Cammà, C. Scazzone et al., "Low vitamin D serum level is related to severe fibrosis and low responsiveness to interferon-based therapy in genotype 1 chronic hepatitis C," *Hepatology*, vol. 51, no. 4, pp. 1158–1167, 2010.

[136] R. M. Souza dos Santos, A. F. de Bem, E. Colpo, I. Bertoncello, C. W. Nogueira, and J. B. T. Rocha, "Plasmatic vitamin C in nontreated hepatitis C patients is negatively associated with aspartate aminotransferase," *Liver International*, vol. 28, no. 1, pp. 54–60, 2008.

[137] C. C. Lin and M. C. Yin, "Vitamins B depletion, lower iron status and decreased antioxidative defense in patients with chronic hepatitis C treated by pegylated interferon alfa and ribavirin," *Clinical Nutrition*, vol. 28, no. 1, pp. 34–38, 2009.

[138] G. Bjelakovic, L. L. Gluud, D. Nikolova, M. Bjelakovic, A. Nagorni, and C. Gluud, "Meta-analysis: antioxidant supplements for liver diseases—the Cochrane Hepato-biliary group," *Alimentary Pharmacology & Therapeutics*, vol. 32, no. 3, pp. 356–367, 2010.

[139] M. Yano, M. Ikeda, K. Abe et al., "Comprehensive analysis of the effects of ordinary nutrients on hepatitis C virus RNA replication in cell culture," *Antimicrobial Agents and Chemotherapy*, vol. 51, no. 6, pp. 2016–2027, 2007.

[140] M. Nakamura, H. Saito, M. Ikeda et al., "An antioxidant resveratrol significantly enhanced replication of hepatitis C virus," *World Journal of Gastroenterology*, vol. 16, no. 2, pp. 184–192, 2010.

[141] M. Esrefoglu, "Oxidative stress and benefits of antioxidant agents in acute and chronic hepatitis," *Hepatitis Monthly*, vol. 12, no. 3, pp. 160–167, 2012.

[142] E. Gabbay, E. Zigmond, O. Pappo et al., "Antioxidant therapy for chronic hepatitis C after failure of interferon: results of phase II randomized, double-blind placebo controlled clinical

trial," *World Journal of Gastroenterology*, vol. 13, no. 40, pp. 5317–5323, 2007.

[143] M. C. Myhrstad, H. Carlsen, O. Nordstrom, R. Blomhoff, and J. O. Moskaug, "Flavonoids increase the intracellular glutathione level by transactivation of the gamma-glutamylcysteine synthetase catalytical subunit promoter," *Free Radical Biology & Medicine*, vol. 32, no. 5, pp. 386–393, 2002.

[144] R. C. S. Seet, C.-Y. J. Lee, E. C. H. Lim et al., "Oxidative damage in dengue fever," *Free Radical Biology & Medicine*, vol. 47, no. 4, pp. 375–380, 2009.

[145] L. Gil, G. Martínez, R. Tápanes et al., "Oxidative stress in adult dengue patients," *The American Journal of Tropical Medicine and Hygiene*, vol. 71, no. 5, pp. 652–657, 2004.

[146] R. Soundravally, S. L. Hoti, S. A. Patil et al., "Association between proinflammatory cytokines and lipid peroxidation in patients with severe dengue disease around defervescence," *International Journal of Infectious Diseases*, vol. 18, pp. 68–72, 2014.

[147] R. Soundravally, P. Sankar, Z. Bobby, and S. L. Hoti Deputy Dir, "Oxidative stress in severe dengue viral infection: association of thrombocytopenia with lipid peroxidation," *Platelets*, vol. 19, no. 6, pp. 447–454, 2009.

[148] Y. Tian, W. Jiang, N. Gao et al., "Inhibitory effects of glutathione on dengue virus production," *Biochemical and Biophysical Research Communications*, vol. 397, no. 3, pp. 420–424, 2010.

[149] J. Wang, Y. Chen, N. Gao et al., "Inhibitory effect of glutathione on oxidative liver injury induced by dengue virus serotype 2 infections in mice," *PLoS One*, vol. 8, no. 1, article e55407, 2013.

[150] C. K. Tseng, C. K. Lin, Y. H. Wu et al., "Human heme oxygenase 1 is a potential host cell factor against dengue virus replication," *Scientific Reports*, vol. 6, no. 1, article 32176, 2016.

[151] A. Hall, A. Troupin, B. Londono-Renteria, and T. Colpitts, "Garlic organosulfur compounds reduce inflammation and oxidative stress during dengue virus infection," *Viruses*, vol. 9, no. 7, p. 159, 2017.

[152] V. Bottino-Rojas, O. A. C. Talyuli, L. Carrara et al., "The redox-sensing gene Nrf2 affects intestinal homeostasis, insecticide resistance, and Zika virus susceptibility in the mosquito *Aedes aegypti*," *The Journal of Biological Chemistry*, vol. 293, no. 23, pp. 9053–9063, 2018.

[153] A. C. Chen, L. Burr, and M. A. McGuckin, "Oxidative and endoplasmic reticulum stress in respiratory disease," *Clinical & Translational Immunology*, vol. 7, no. 6, article e1019, 2018.

[154] S. S. Cao and R. J. Kaufman, "Endoplasmic reticulum stress and oxidative stress in cell fate decision and human disease," *Antioxidants & Redox Signaling*, vol. 21, no. 3, pp. 396–413, 2014.

[155] S. Z. Hasnain, "Endoplasmic reticulum and oxidative stress in immunopathology: understanding the crosstalk between cellular stress and inflammation," *Clinical & Translational Immunology*, vol. 7, no. 7, article e1035, 2018.

[156] S. Srivastava, N. Khanna, S. K. Saxena, A. Singh, A. Mathur, and T. N. Dhole, "Degradation of Japanese encephalitis virus by neutrophils," *International Journal of Experimental Pathology*, vol. 80, no. 1, pp. 17–24, 1999.

[157] S. L. Liao, S. L. Raung, and C. J. Chen, "Japanese encephalitis virus stimulates superoxide dismutase activity in rat glial cul-

tures," *Neuroscience Letters*, vol. 324, no. 2, pp. 133–136, 2002.

[158] M. K. Mishra, K. L. Kumawat, and A. Basu, "Japanese encephalitis virus differentially modulates the induction of multiple pro-inflammatory mediators in human astrocytoma and astroglioma cell-lines," *Cell Biology International*, vol. 32, no. 12, pp. 1506–1513, 2008.

[159] A. Ghoshal, S. Das, S. Ghosh et al., "Proinflammatory mediators released by activated microglia induces neuronal death in Japanese encephalitis," *Glia*, vol. 55, no. 5, pp. 483–496, 2007.

[160] D. Ghosh and A. Basu, "Japanese encephalitis—a pathological and clinical perspective," *PLoS Neglected Tropical Diseases*, vol. 3, no. 9, article e437, 2009.

[161] S. Kumar, U. K. Misra, J. Kalita, V. K. Khanna, and M. Y. Khan, "Imbalance in oxidant/antioxidant system in different brain regions of rat after the infection of Japanese encephalitis virus," *Neurochemistry International*, vol. 55, no. 7, pp. 648–654, 2009.

[162] Y. Zhang, Z. Wang, H. Chen, Z. Chen, and Y. Tian, "Antioxidants: potential antiviral agents for Japanese encephalitis virus infection," *International Journal of Infectious Diseases*, vol. 24, pp. 30–36, 2014.

[163] M. J. Uddin, W. W. Suen, N. A. Prow, R. A. Hall, and H. Bielefeldt-Ohmann, "West Nile virus challenge alters the transcription profiles of innate immune genes in rabbit peripheral blood mononuclear cells," *Frontiers in Veterinary Science*, vol. 2, p. 76, 2015.

[164] N. Kedersha, G. Stoecklin, M. Ayodele et al., "Stress granules and processing bodies are dynamically linked sites of mRNP remodeling," *The Journal of Cell Biology*, vol. 169, no. 6, pp. 871–884, 2005.

[165] M. M. Emara and M. A. Brinton, "Interaction of TIA-1/TIAR with West Nile and dengue virus products in infected cells interferes with stress granule formation and processing body assembly," *Proceedings of the National Academy of Sciences of the United States of America*, vol. 104, no. 21, pp. 9041–9046, 2007.

[166] T. Wileman, "Aggresomes and autophagy generate sites for virus replication," *Science*, vol. 312, no. 5775, pp. 875–878, 2006.

[167] T. Wileman, "Aggresomes and pericentriolar sites of virus assembly: cellular defense or viral design?," *Annual Review of Microbiology*, vol. 61, no. 1, pp. 149–167, 2007.

[168] T. Hanada, N. N. Noda, Y. Satomi et al., "The Atg12-Atg5 conjugate has a novel E3-like activity for protein lipidation in autophagy," *The Journal of Biological Chemistry*, vol. 282, no. 52, pp. 37298–37302, 2007.

[169] H. Nakatogawa, Y. Ichimura, and Y. Ohsumi, "Atg8, a ubiquitin-like protein required for autophagosome formation, mediates membrane tethering and hemifusion," *Cell*, vol. 130, no. 1, pp. 165–178, 2007.

[170] Y. Choi, J. W. Bowman, and J. U. Jung, "Autophagy during viral infection—a double-edged sword," *Nature Reviews. Microbiology*, vol. 16, no. 6, pp. 341–354, 2018.

[171] E. Itakura, C. Kishi-Itakura, and N. Mizushima, "The hairpin-type tail-anchored SNARE syntaxin 17 targets to autophagosomes for fusion with endosomes/lysosomes," *Cell*, vol. 151, no. 6, pp. 1256–1269, 2012.

[172] M. Dreux and F. V. Chisari, "Viruses and the autophagy machinery," *Cell Cycle*, vol. 9, no. 7, pp. 1295–1307, 2014.

[173] J. Shi and H. Luo, "Interplay between the cellular autophagy machinery and positive-stranded RNA viruses," *Acta Biochimica et Biophysica Sinica Shanghai*, vol. 44, no. 5, pp. 375–384, 2012.

[174] M. Ait-Goughoulte, T. Kanda, K. Meyer, J. S. Ryerse, R. B. Ray, and R. Ray, "Hepatitis C virus genotype 1a growth and induction of autophagy," *Journal of Virology*, vol. 82, no. 5, pp. 2241–2249, 2008.

[175] E. Abernathy, R. Mateo, K. Majzoub et al., "Differential and convergent utilization of autophagy components by positive-strand RNA viruses," *PLoS Biology*, vol. 17, no. 1, article e2006926, 2019.

[176] P. Metz, A. Chiramel, L. Chatel-Chaix et al., "Dengue virus inhibition of autophagic flux and dependency of viral replication on proteasomal degradation of the autophagy receptor p62," *Journal of Virology*, vol. 89, no. 15, pp. 8026–8041, 2015.

[177] L. Wang, Y. Tian, and J. H. J. Ou, "HCV induces the expression of Rubicon and UVRAG to temporally regulate the maturation of autophagosomes and viral replication," *PLoS Pathogens*, vol. 11, no. 3, article e1004764, 2015.

[178] Q. Liang, Z. Luo, J. Zeng et al., "Zika virus NS4A and NS4B proteins deregulate Akt-mTOR signaling in human fetal neural stem cells to inhibit neurogenesis and induce autophagy," *Cell Stem Cell*, vol. 19, no. 5, pp. 663–671, 2016.

[179] K. D. Tardif, G. Waris, and A. Siddiqui, "Hepatitis C virus, ER stress, and oxidative stress," *Trends in Microbiology*, vol. 13, no. 4, pp. 159–163, 2005.

[180] D. Ploen and E. Hildt, "Hepatitis C virus comes for dinner: how the hepatitis C virus interferes with autophagy," *World Journal of Gastroenterology*, vol. 21, no. 28, pp. 8492–8507, 2015.

[181] A. I. Chiramel and S. M. Best, "Role of autophagy in Zika virus infection and pathogenesis," *Virus Research*, vol. 254, pp. 34–40, 2018.

[182] R. Gratton, A. Agrelli, P. Tricarico, L. Brandão, and S. Crovella, "Autophagy in Zika virus infection: a possible therapeutic target to counteract viral replication," *International Journal of Molecular Sciences*, vol. 20, no. 5, article E1048, p. 1048, 2019.

[183] M. Dreux and F. V. Chisari, "Impact of the autophagy machinery on hepatitis C virus infection," *Viruses*, vol. 3, no. 8, pp. 1342–1357, 2011.

[184] S. Shrivastava, A. Raychoudhuri, R. Steele, R. Ray, and R. B. Ray, "Knockdown of autophagy enhances the innate immune response in hepatitis C virus-infected hepatocytes," *Hepatology*, vol. 53, no. 2, pp. 406–414, 2011.

[185] S. Shrivastava, J. Bhanja Chowdhury, R. Steele, R. Ray, and R. B. Ray, "Hepatitis C virus upregulates Beclin1 for induction of autophagy and activates mTOR signaling," *Journal of Virology*, vol. 86, no. 16, pp. 8705–8712, 2012.

[186] S. Shrivastava, P. Devhare, N. Sujijantarat et al., "Knockdown of autophagy inhibits infectious hepatitis C virus release by the exosomal pathway," *Journal of Virology*, vol. 90, no. 3, pp. 1387–1396, 2016.

[187] I. Tanida, M. Fukasawa, T. Ueno, E. Kominami, T. Wakita, and K. Hanada, "Knockdown of autophagy-related gene decreases the production of infectious hepatitis C virus particles," *Autophagy*, vol. 5, no. 7, pp. 937–945, 2014.

[188] D. Sir, C. F. Kuo, Y. Tian et al., "Replication of hepatitis C virus RNA on autophagosomal membranes," *The Journal of Biological Chemistry*, vol. 287, no. 22, pp. 18036–18043, 2012.

[189] P.-Y. Ke and S. S.-L. Chen, "Activation of the unfolded protein response and autophagy after hepatitis C virus infection suppresses innate antiviral immunity in vitro," *The Journal of Clinical Investigation*, vol. 121, no. 1, pp. 37–56, 2011.

[190] D. Sir, W. L. Chen, J. Choi, T. Wakita, T. S. B. Yen, and J. H. J. Ou, "Induction of incomplete autophagic response by hepatitis C virus via the unfolded protein response," *Hepatology*, vol. 48, no. 4, pp. 1054–1061, 2008.

[191] K. D. Tardif, K. Mori, and A. Siddiqui, "Hepatitis C virus subgenomic replicons induce endoplasmic reticulum stress activating an intracellular signaling pathway," *Journal of Virology*, vol. 76, no. 15, pp. 7453–7459, 2002.

[192] T. Asselah, I. Bièche, A. Mansouri et al., "In vivo hepatic endoplasmic reticulum stress in patients with chronic hepatitis C," *The Journal of Pathology*, vol. 221, no. 3, pp. 264–274, 2010.

[193] S. J. Kim, G. H. Syed, M. Khan et al., "Hepatitis C virus triggers mitochondrial fission and attenuates apoptosis to promote viral persistence," *Proceedings of the National Academy of Sciences of the United States of America*, vol. 111, no. 17, pp. 6413–6418, 2014.

[194] N. Kim, M. J. Kim, P. S. Sung, Y. C. Bae, E. C. Shin, and J. Y. Yoo, "Interferon-inducible protein SCOTIN interferes with HCV replication through the autolysosomal degradation of NS5A," *Nature Communications*, vol. 7, no. 1, p. 10631, 2016.

[195] R. Kiffin, U. Bandyopadhyay, and A. M. Cuervo, "Oxidative stress and autophagy," *Antioxidants & Redox Signaling*, vol. 8, no. 1-2, pp. 152–162, 2006.

[196] G. Filomeni, D. De Zio, and F. Cecconi, "Oxidative stress and autophagy: the clash between damage and metabolic needs," *Cell Death and Differentiation*, vol. 22, no. 3, pp. 377–388, 2015.

[197] R. Medvedev, D. Ploen, C. Spengler et al., "HCV-induced oxidative stress by inhibition of Nrf2 triggers autophagy and favors release of viral particles," *Free Radical Biology & Medicine*, vol. 110, pp. 300–315, 2017.

[198] D. Bartolini, K. Dallaglio, P. Torquato, M. Piroddi, and F. Galli, "Nrf2-p62 autophagy pathway and its response to oxidative stress in hepatocellular carcinoma," *Translational Research*, vol. 193, pp. 54–71, 2018.

[199] D. Burdette, M. Olivarez, and G. Waris, "Activation of transcription factor Nrf2 by hepatitis C virus induces the cell-survival pathway," *The Journal of General Virology*, vol. 91, no. 3, pp. 681–690, 2010.

[200] Y. R. Lee, H. Y. Lei, M. T. Liu et al., "Autophagic machinery activated by dengue virus enhances virus replication," *Virology*, vol. 374, no. 2, pp. 240–248, 2008.

[201] M. Panyasrivanit, A. Khakpoor, N. Wikan, and D. R. Smith, "Co-localization of constituents of the dengue virus translation and replication machinery with amphisomes," *The Journal of General Virology*, vol. 90, no. 2, pp. 448–456, 2009.

[202] A. Khakpoor, M. Panyasrivanit, N. Wikan, and D. R. Smith, "A role for autophagolysosomes in dengue virus 3 production in HepG2 cells," *The Journal of General Virology*, vol. 90, no. 5, pp. 1093–1103, 2009.

[203] J. E. McLean, A. Wudzinska, E. Datan, D. Quaglino, and Z. Zakeri, "Flavivirus NS4A-induced autophagy protects cells against death and enhances virus replication," *The Journal of Biological Chemistry*, vol. 286, no. 25, pp. 22147–22159, 2011.

[204] S. Miller and J. Krijnse-Locker, "Modification of intracellular membrane structures for virus replication," *Nature Reviews. Microbiology*, vol. 6, no. 5, pp. 363–374, 2008.

[205] R. Mateo, C. M. Nagamine, J. Spagnolo et al., "Inhibition of cellular autophagy deranges dengue virion maturation," *Journal of Virology*, vol. 87, no. 3, pp. 1312–1321, 2013.

[206] N. S. Heaton and G. Randall, "Dengue virus-induced autophagy regulates lipid metabolism," *Cell Host & Microbe*, vol. 8, no. 5, pp. 422–432, 2010.

[207] N. J. Lennemann and C. B. Coyne, "Dengue and Zika viruses subvert reticulophagy by NS2B3-mediated cleavage of FAM134B," *Autophagy*, vol. 13, no. 2, pp. 322–332, 2017.

[208] R. Hamel, O. Dejarnac, S. Wichit et al., "Biology of Zika virus infection in human skin cells," *Journal of Virology*, vol. 89, no. 17, pp. 8880–8896, 2015.

[209] Z. W. Zhang, Z. L. Li, and S. Yuan, "The role of secretory autophagy in Zika virus transfer through the placental barrier," *Frontiers in Cellular and Infection Microbiology*, vol. 6, p. 206, 2017.

[210] B. Cao, L. A. Parnell, M. S. Diamond, and I. U. Mysorekar, "Inhibition of autophagy limits vertical transmission of Zika virus in pregnant mice," *The Journal of Experimental Medicine*, vol. 214, no. 8, pp. 2303–2313, 2017.

[211] I. Gladwyn-Ng, L. Cordón-Barris, C. Alfano et al., "Stress-induced unfolded protein response contributes to Zika virus-associated microcephaly," *Nature Neuroscience*, vol. 21, no. 1, pp. 63–71, 2018.

[212] E. Ryan, R. Hollingworth, and R. Grand, "Activation of the DNA damage response by RNA viruses," *Biomolecules*, vol. 6, no. 1, p. 2, 2016.

[213] X. Cai, Y. H. Chiu, and Z. J. Chen, "The cGAS-cGAMP-STING pathway of cytosolic DNA sensing and signaling," *Molecular Cell*, vol. 54, no. 2, pp. 289–296, 2014.

[214] M. A. Luftig, "Viruses and the DNA damage response: activation and antagonism," *Annual Review of Virology*, vol. 1, no. 1, pp. 605–625, 2014.

[215] N. S. R. de Mochel, S. Seronello, S. H. Wang et al., "Hepatocyte NAD(P)H oxidases as an endogenous source of reactive oxygen species during hepatitis C virus infection," *Hepatology*, vol. 52, no. 1, pp. 47–59, 2010.

[216] K. Machida, K. T. H. Cheng, V. M. H. Sung, K. J. Lee, A. M. Levine, and M. M. C. Lai, "Hepatitis C virus infection activates the immunologic (type II) isoform of nitric oxide synthase and thereby enhances DNA damage and mutations of cellular genes," *Journal of Virology*, vol. 78, no. 16, pp. 8835–8843, 2004.

[217] C.-K. Lai, K.-S. Jeng, K. Machida, Y.-S. Cheng, and M. M. C. Lai, "Hepatitis C virus NS3/4A protein interacts with ATM, impairs DNA repair and enhances sensitivity to ionizing radiation," *Virology*, vol. 370, no. 2, pp. 295–309, 2008.

[218] J. F. van Pelt, T. Severi, T. Crabbé et al., "Expression of hepatitis C virus core protein impairs DNA repair in human hepatoma cells," *Cancer Letters*, vol. 209, no. 2, pp. 197–205, 2004.

[219] K. Machida, G. McNamara, K. T. H. Cheng et al., "Hepatitis C virus inhibits DNA damage repair through reactive oxygen and nitrogen species and by interfering with the ATM-NBS1/Mre11/Rad50 DNA repair pathway in monocytes and hepatocytes," *Journal of Immunology*, vol. 185, no. 11, pp. 6985–6998, 2010.

[220] S. Pal, S. J. Polyak, N. Bano et al., "Hepatitis C virus induces oxidative stress, DNA damage and modulates the DNA repair enzyme NEIL1," *Journal of Gastroenterology and Hepatology*, vol. 25, no. 3, pp. 627–634, 2010.

[221] S. Aguirre, P. Luthra, M. T. Sanchez-Aparicio et al., "Dengue virus NS2B protein targets cGAS for degradation and prevents mitochondrial DNA sensing during infection," *Nature Microbiology*, vol. 2, no. 5, 2017.

[222] Y. Zheng, Q. Liu, Y. Wu et al., "Zika virus elicits inflammation to evade antiviral response by cleaving cGAS via NS1-caspase-1 axis," *The EMBO Journal*, vol. 37, no. 18, p. e99347, 2018.

[223] V. Swarup, J. Ghosh, M. K. Mishra, and A. Basu, "Novel strategy for treatment of Japanese encephalitis using arctigenin, a plant lignan," *The Journal of Antimicrobial Chemotherapy*, vol. 61, no. 3, pp. 679–688, 2008.

[224] A. Nazmi, K. Dutta, and A. Basu, "Antiviral and neuroprotective role of octaguanidinium dendrimer-conjugated morpholino oligomers in Japanese encephalitis," *PLoS Neglected Tropical Diseases*, vol. 4, no. 11, article e892, 2010.

[225] S. Fedoreyev, N. Krylova, N. Mishchenko et al., "Antiviral and antioxidant properties of echinochrome a," *Marine Drugs*, vol. 16, no. 12, p. 509, 2018.

[226] J. A. Lubin, R. R. Zhang, and J. S. Kuo, "Zika virus has oncolytic activity against glioblastoma stem cells," *Neurosurgery*, vol. 82, no. 5, pp. E113–E114, 2018.

[227] Z. Zhu, M. J. Gorman, L. D. McKenzie et al., "Zika virus has oncolytic activity against glioblastoma stem cells," *The Journal of Experimental Medicine*, vol. 214, no. 10, pp. 2843–2857, 2017.

[228] Q. Chen, J. Wu, Q. Ye et al., "Treatment of human glioblastoma with a live attenuated Zika virus vaccine candidate," *MBio*, vol. 9, no. 5, 2018.

[229] C. Kaid, E. Goulart, L. C. Caires-Júnior et al., "Zika virus selectively kills aggressive human embryonal CNS tumor cells in vitro and in vivo," *Cancer Research*, vol. 78, no. 12, 2018.

Review Article

ROS Generation and Antioxidant Defense Systems in Normal and Malignant Cells

Anastasiya V. Snezhkina (ID)**, Anna V. Kudryavtseva** (ID)**, Olga L. Kardymon,**
Maria V. Savvateeva (ID)**, Nataliya V. Melnikova** (ID)**, George S. Krasnov** (ID)**,**
and Alexey A. Dmitriev (ID)

Engelhardt Institute of Molecular Biology, Russian Academy of Sciences, Moscow 119991, Russia

Correspondence should be addressed to Anastasiya V. Snezhkina; leftger@rambler.ru and Alexey A. Dmitriev; alex_245@mail.ru

Reactive oxygen species (ROS) are by-products of normal cell activity. They are produced in many cellular compartments and play a major role in signaling pathways. Overproduction of ROS is associated with the development of various human diseases (including cancer, cardiovascular, neurodegenerative, and metabolic disorders), inflammation, and aging. Tumors continuously generate ROS at increased levels that have a dual role in their development. Oxidative stress can promote tumor initiation, progression, and resistance to therapy through DNA damage, leading to the accumulation of mutations and genome instability, as well as reprogramming cell metabolism and signaling. On the contrary, elevated ROS levels can induce tumor cell death. This review covers the current data on the mechanisms of ROS generation and existing antioxidant systems balancing the redox state in mammalian cells that can also be related to tumors.

1. Introduction

Reactive oxygen species (ROS) are formed as natural by-products of normal cell activity and participate in cellular signaling [1]. The increase in ROS levels has harmful effects on cell homeostasis, structures, and functions and results in oxidative stress. As such, the disturbance of cellular redox balance is a risk factor for the development of various pathologies [2].

Tumor cells are characterized by a high level of ROS. ROS overproduction can result from changes in many processes, such as oxidative phosphorylation (OXPHOS), transition metal ions, oxidase activity, protein folding, thymidine, and polyamine catabolism [3–7]. ROS can be generated both in various cellular compartments and in the tumor microenvironment.

ROS have a dual role in cancer development; on one hand, they can promote molecular genetic alterations that are necessary for tumor initiation, growth, and progression,

as well as acquisition of treatment resistance [8]. On the other hand, permanent elevated ROS levels have cytotoxic effects, inducing activation of apoptotic pathways or inhibiting resistance to anticancer treatments [9].

In this review, we discuss the main sources of ROS production in animal cells and the antioxidant defense systems that could be implicated in the redox state of cancer cells (to a significant or less significant extent).

2. Sources of ROS Generation and Antioxidant Defense Systems

2.1. Mitochondria. Mitochondria are a prime source of endogenous ROS due to its main role in oxidative ATP production, in which molecular oxygen (O_2) is reduced to water in the electron transport chain. The superoxide radical ($O_2^{\bullet-}$) is produced at a number of sites in the mitochondria, including complex I (sites IQ and IF), complex III (site IIIQo), glycerol 3-phosphate dehydrogenase, Q oxidoreductase, pyruvate

dehydrogenase, and 2-oxoglutarate dehydrogenase [10]. All the sites release superoxide radical into the mitochondrial matrix (MM), and two of them, complex III (site IIIQo) and glycerol 3-phosphate dehydrogenase, also generate ROS into the intermembrane mitochondrial space (IMS). Manganese superoxide dismutase (Mn-SOD) converts the superoxide radical to hydrogen peroxide (H_2O_2) in the MM, while Cu- and Zn-SOD convert the superoxide radical in the IMS or cytosol [11]. The H_2O_2 in the MM can further be converted by mitochondrial aconitase to a hydroxyl radical ($^\bullet OH$) via a Fenton reaction [12]. One more site of ROS production in the mitochondria is the cytochrome (CYP) catalytic cycle. CYP enzymes metabolize a wide range of organic substrates (lipids, steroid hormones, xenobiotics, and others) to give rise to superoxide radical and H_2O_2 as by-products [13]. Several CYP family members were shown to be present in the mitochondrial membrane of steroidogenic organs, as well as in the liver and kidney [14]. Furthermore, several other mammalian proteins, such as NADH-cytochrome $b5$ reductase [15], dihydroorotate dehydrogenase [16, 17], complex II (succinate dehydrogenase) [18], and monoamine oxidases (MAO) [19], were shown to generate ROS in the mitochondria.

Mitochondria are protected from ROS by multiple defense systems and antioxidants: glutathione peroxidases (GPXs), thioredoxin peroxidases (TRXPs), superoxide dismutases (SODs), peroxiredoxins (PRDXs), glutathione (GSH), thioredoxin 2 (TRX2), glutaredoxin 2 (GRX2), cytochrome c oxidase (complex IV), coenzyme Q, ascorbic acid, tocopherol, vitamin E, and carotene [20–26]. Moreover, catalase (CAT), which commonly detoxifies H_2O_2 in the peroxisome, was found in rat heart mitochondria (but not in other tissues) [27, 28].

Mitochondrion-generated ROS were widely shown to be implicated in various human pathologies, including inflammation, cancer, mitochondrial and neurodegenerative diseases, diabetes, chronic diseases, and aging [3, 29–32]. Elevated ROS levels and mitochondrial dysfunction, present in many cancers, lead to oxidative damage of cellular structures, in particular, genomic and mitochondrial DNA, somatic mutations, genome instability, activation of oncogenes and inactivation of tumor suppressor genes, and alterations in metabolic and signaling pathways with simultaneous activation of compensatory antioxidant mechanisms, that all contribute to cell transformation [33]. However, overproduction of ROS can also promote tumor cell apoptosis and such strategies have effectively been used for anticancer treatment [34].

2.2. Transition Metal Ions. One of the major mechanisms of metal carcinogenicity is the ability of transition metal ions to induce oxidative stress [35]. Fenton and Haber-Weiss reactions are frequently responsible for ROS generation in living cells [36]. During these reactions, H_2O_2 is decomposed with the participation of metal ions, such as iron (Fe), copper (Cu), zinc (Zn), and aluminum (Al), leading to the production of hydroxyl radical ($^\bullet OH$) and hydroxyl anion (OH^-) [37]. Other carcinogenic metal ions (antimony, arsenic, chromium, cobalt, nickel, and vanadium)

were also supposed to be able to generate ROS in cellular redox reactions [36]. The hydroxyl radicals produced can attack the DNA, causing oxidative DNA adduct formation. The adducts 8-hydroxy-2′-deoxyguanosine (8-OHdG) and 8-oxo-7,8-dihydro-2′-deoxyguanosine (8-oxodG) are the most predominant, resulting from the addition of hydroxyl radicals to guanine. These compounds are widely considered as markers of endogenous oxidative DNA damage as well as a risk factor for cancer development [38].

2.3. Peroxisome Activity. Peroxisomes have multiple functions in living cells, including fatty acid β-oxidation and α-oxidation as well as metabolism of purines, polyamines, amino acids, glyoxylate, reactive oxygen and nitrogen species (RNS), transition metal ions, and others [39, 40]. Peroxisomes generate a wide range of ROS and RNS: H_2O_2, superoxide radical ($O_2^{\bullet -}$), hydroxyl radical ($^\bullet OH$), nitric oxide ($NO^\bullet$), and peroxynitrite ($ONOO^-$) [41].

The peroxisome was first described as an H_2O_2-producing and H_2O_2-degrading organelle [42]. Despite the presence of CAT, peroxisomes are one of the main sources of H_2O_2 [43, 44]. H_2O_2 is released as a by-product during the normal catalytic activity of many peroxisomal enzymes, and it can also be generated by the spontaneous or enzymatic dismutation of the superoxide radical [45]. H_2O_2 can generate hydroxyl radicals ($^\bullet OH$) via a Fenton reaction [46].

Peroxisomes produce superoxide radicals ($O_2^{\bullet -}$) in both the matrix and membrane. In the matrix, two enzymes are responsible for $O_2^{\bullet -}$ generation, xanthine oxidoreductase (XOR), and urate oxidase (UO) [47, 48]. XOR catalyzes the formation of uric acid during purine metabolism that is further converted to allantoin by UO. Both enzymes generate $O_2^{\bullet -}$ and H_2O_2. However, UO expression was not detected in humans and some primates indicating that uric acid is a terminal compound of purine metabolism [49]. The other source of superoxide radicals is an electron transport chain in the peroxisomal membrane [50]. Moreover, XOR also catalyzes the reduction of nitrates and nitrites to nitric oxide ($NO^\bullet$) [51]. $NO^\bullet$ can also be produced from L-arginine, in a reaction catalyzed by nitric oxide synthase (NOS) [52]. The reaction of $O_2^{\bullet -}$ with $NO^\bullet$ results in a highly reactive compound called peroxynitrite ($ONOO^-$) [53].

Several antioxidant systems regulate ROS levels in peroxisomes and defend cells from oxidative damage. These include a number of enzymes, such as CAT, superoxide dismutases, peroxiredoxins, glutathione S-transferases (GST), and epoxide hydrolase 2 (EPHX2), as well as nonenzymatic low-molecular weight antioxidants, which are reviewed in detail elsewhere [39, 45, 50].

Changes in redox homeostasis contribute to cancer development and progression [54]. The peroxisome maintains cellular oxidative balance, and dysregulation of its activity is associated with carcinogenesis. Thus, reduced CAT activity leads to ROS generation and oxidative stress resulting in DNA damage and genome instability promoting cancer development. Decreased CAT expression has been shown in hepatocellular carcinoma and colon, lung, kidney, and prostate cancers, as well as in precancer states, such

as prostatic intraepithelial neoplasia (PIN) and cervical intraepithelial neoplasia (CIN) [55–60]. In several cases, decreased CAT activity was associated with a reduced number of peroxisomes [57, 61].

2.4. Endoplasmic Reticulum.

The endoplasmic reticulum (ER) has many general cellular functions, such as protein folding, synthesis, transport, and posttranslational modifications, as well as lipid metabolism and calcium storage [62]. Alterations in the folding pathway lead to accumulation of misfolded and unfolded proteins in the ER lumen resulting in ER stress. This disrupts cell homeostasis and initiates the unfolded protein response (UPR) [63, 64]. UPR triggers ROS production, and ROS, in turn, can promote ER stress [65, 66]. In tumor cells, the UPR signaling pathway serves as an adaptive to the stress mechanism supporting their survival and propagation [67]. However, if ER stress is prolonged, the UPR triggers tumor cell apoptosis [68].

Oxidative protein folding gives rise to a highly oxidative environment in the ER lumen [69]. Protein disulfide isomerase (PDI) catalyzes thiol-disulfide exchange reactions, which form a native disulfide bond in proteins [70]. During this process, PDI is oxidized by endoplasmic reticulum oxidoreductin-1 (ERO1), which accepts electrons from a reduced PDI and transfers them to molecular oxygen, thereby generating H_2O_2 [69, 71]. ERO1 also catalyzes the conversion of glutathione (GSH) to glutathione disulfide (GSSG), besides PDI oxidation. Accumulation of both H_2O_2 and oxidized glutathione causes ER stress. Furthermore, the ratio between GSH and GSSG is an essential marker of the redox status in the ER lumen. Moreover, GSH was proposed as a potential protection mechanism from ER-associated ROS damage [72]. PDI and ERO1 were found to be upregulated in different types of cancer and were implicated in cancer progression and metastasis. PDI and ERO1 overexpression has been found in patients with non-small cell lung cancer (NSCLC) and was significantly associated with shorter overall survival [73]. Expression of several members of the PDI family was upregulated in ovarian and colorectal cancers [74, 75] while ERO1 overexpression was correlated with the progression and metastasis of breast cancer, as well as with poor survival and high recurrence rates in gastric cancer [76–78]. ERO1 knockout led to the reduced growth of colorectal cancer cells under hypoxic conditions [79]. Elevated ERO1 expression was associated with poor prognosis in cervical cancer [80]. In the same study, ERO1 knockout inhibited tumor growth and migration of cervical cancer cells.

PDI is also involved in H_2O_2 generation through interconnections with NOX1 and NOX4, which belong to the nicotinamide adenine dinucleotide phosphate (NADPH) oxidase protein family [81, 82]. In addition, NOX4 occurs in the NOX4-p22^{phox} complex in the ER membrane and is involved in releasing H_2O_2 in the ER lumen [83]. One more site of ROS generation in the ER is the microsomal monooxygenase (MMO) system. This is a multienzyme system consisting of multiple cytochrome P450 species, NADPH-P450 reductase (NPR), and cytochrome b_5 [84]. MMO catalyzes the oxygenation of hydrophobic exogenous compounds and some endogenous substrates, resulting in a production of superoxide radicals and H_2O_2 [85, 86]. Increased MMO-derived ROS production and greater rates of microsomal lipid peroxidation were shown to be associated with the activation of cytochrome P450 2E1 (CYP2E1) [87, 88].

2.5. Thymidine Catabolism.

Thymidine phosphorylase (TP) is a rate-limiting enzyme in thymidine catabolism that catalyzes the reversible conversion of thymidine to thymine and 2-deoxy-D-ribose-1-phosphate (DR1P) [89]. TP is upregulated in many tumors and plays an important role in angiogenesis, apoptosis evasion, invasion, and metastasis, as well as in chemotherapy response [90]. Recently, Tabata and coauthors have revealed that TP activity increases NADPH levels via the pentose phosphate pathway (PPP) which activates NADPH oxidase-dependent production of ROS in cancer cells [6, 91]. Previously, it was shown that the addition of thymidine to a TP-overexpressing bladder carcinoma cell line induces cellular oxidative stress [92]. The authors proposed another potential mechanism of TP-induced ROS production. This mechanism is based on excess 2dDR1P produced during thymidine phosphorylation that could be further subjected to transition metal-catalyzed oxidation, leading to ROS generation.

2.6. Polyamine Catabolism.

The natural polyamines (PAs), putrescine, spermidine, and spermine, are involved in multiple basic cellular functions, including growth, proliferation, differentiation, apoptosis, migration, and protection from stresses. They are involved in protein posttranslational modifications, regulation of ion channels, maintenance of nucleic acid, and protein structure and stability, as well as cell-cell communications [93]. PA content and catabolism are strongly regulated at different levels by key enzymes in the biosynthesis and transport systems [94]. However, dysregulation of PA catabolism is frequently observed in cancer [95].

In mammals, putrescine is the first polyamine of the PA catabolism. It is synthesized with the participation of ornithine decarboxylase (ODC). Putrescine is further converted to higher polyamines, spermidine and spermine, a reaction catalyzed by spermidine synthase (SPDS) and spermine synthase (SPMS), respectively. S-Adenosylmethionine decarboxylase (AdoMetDC) supplies the aminopropyl groups in these reactions. The activities of ODC and AdoMetDC are considered to be a rate-limiting factors of PA biosynthesis. The other branch of PA catabolism involves the interconversion cycles where spermine is degraded to spermidine and spermidine to putrescine with the generation of toxic-reactive aldehydes and ROS. Spermine oxidase (SMO) catalyzes the conversion of spermine to spermidine, which is accompanied by 3-aminopropanal and H_2O_2 release. Spermidine and spermine can also be converted to prior polyamines, with the help of spermidine/spermine-N1-acetyltransferase (SSAT) and acetylpolyamine oxidase (APAO/PAOX). N-Acetyl-3-aminopropanaldehyde and H_2O_2 are produced as by-products of these reactions [94, 96]. Additionally, another degradative enzyme related to PA catabolism is a diamine oxidase (DAO) that oxidizes putrescine to H_2O_2, ammonia, and 4-aminobutanal.

However, as putrescine is present in relatively low amounts in most mammalian tissues, this reaction does not generate significant amounts of ROS [97].

Increased PA catabolism can lead to an elevated level of ROS and oxidative stress. Overexpression of SMOX and SAT1, which encode the SMO and SSAT enzymes, respectively, was shown to be interconnected with infection, inflammation, and high risk of cancer. Several studies have reported that bacterial cytotoxins upregulate the expression of SMOX. The Helicobacter pylori virulence factor, cytotoxin-associated gene A (CagA) protein, promotes an increase in the SMOX mRNA level and enzyme activity in both human and animal gastric epithelial cells. This results in a significant increase in extra- and intracellular H_2O_2, leading to DNA damage and apoptosis, which can further contribute to inflammation and carcinogenesis [98, 99]. Using a gerbil model, it was shown that H. pylori infection induces overexpression of SMO and oxidative DNA damage and is associated with a high risk of gastric dysplasia and adenocarcinoma [100]. Furthermore, SMO expression was increased in gastric cancer patients infected with H. pylori [101]. In the same study, it was reported that activation of EGFR and ERBB2 signaling is involved in H. pylori-induced upregulation of SMOX.

Enterotoxigenic Bacteroides fragilis (ETBF) infection results in chronic inflammation and can promote colorectal carcinogenesis [102]. B. fragilis toxin (BFT) has also been reported to increase SMOX expression leading to ROS generation and DNA damage in colonic epithelial cells [103]. A study involving patients with colorectal cancer has revealed that SMOX overexpression could be caused by the activation of the transcription factor C/EBPβ, which is involved in the regulation of inflammation and immunity, rather than the ETBF infection [104]. The association of increased SMOX expression and chronic inflammation was also observed in several precancerous conditions such as prostatic intrae-pithelial neoplasia (PIN) and chronic hepatitis [105–107]. Interestingly, drug-induced modulation of polyamine catabolism in hepatic cells results in them undergoing an epithelial-mesenchymal transition- (EMT-) like dedifferentiation, which is not, however, associated with elevated ROS levels [108]. This can indicate that ROS overproduction caused by increased polyamine catabolism together with chronic inflammation could be a precursor event of cancer development, but not tumor progression (with respect to metastasis).

On the contrary, an antioxidant role of polyamines has been proposed. Multiple protection mechanisms from oxidative damage with PA participation were reported: direct ROS scavenging [109, 110], changes in DNA structure and conformation which reduce the possibility of its interactions with reactive species [109, 111–114], formation of chelates with metals at low concentration which prevents ROS generation, particularly hydroxyl radicals [115], or a combination of these mechanisms. Additionally, PA metabolism was linked to p53-mediated ferroptosis in response to oxidative stress [116]. This mechanism is based on p53-induced SSAT activation, in the presence of high levels of ROS, leading to downstream modulation of the expression of ferroptosis components.

2.7. Oxidase Activity.
Diamine oxidase (DAO) is a copper-containing amine oxidase that catalyzes the oxidation of polyamines, such as histamine, putrescine, spermidine, and to a lesser extent spermine [97, 117]. All these reactions generate H_2O_2. DAO activity in mammals varies and was found to be tissue specific. As such, high DAO activity was found in the placenta, kidneys, lungs, small intestine, and liver [118, 119]. Moreover, elevated DAO activity was found in prostate, breast, ovarian, cervical, and endometrial cancers [120–122] and a decrease in activity was found in colorectal cancer [123]. Increased plasma/serum DAO activity was detected in patients with endometrial, lung, and thyroid cancers [124–126]. Moreover, serum/plasma DAO activity has been proposed as an indicator of mucosal injury during chemotherapy and can be used for monitoring anticancer drug toxicity [127, 128].

Acetylpolyamine oxidase (APAO/PAOX) is related to flavin adenine dinucleotide- (FAD-) containing enzymes and catalyzes the oxidation of both spermidine and spermine in peroxisomes. Depending on the substrate, N1-acetylspermine or N1-acetylspermidine, APAO produces spermidine or putrescine, respectively, generating H_2O_2 as a by-product [129]. The presence of starting substrates of APAO is controlled by SSAT activity [130]. Induction of the SSAT/APAO pathway can increase oxidative stress; however, it seems to have a more significant contribution than the one-step spermine oxidation reaction catalyzed by SMO [131].

Spermine oxidase (SMO) is a FAD-dependent oxidase that acts directly on spermine generating spermidine, H_2O_2, and 3-aminopropanal [132, 133]. Unlike APAO, SMO is not a peroxisomal enzyme and is located in cytoplasm or nucleus [134]. SMO activity can produce higher levels of oxidative cellular damage [135]. Elevated expression of SMOX was shown in prostate and colorectal cancers [104, 105]. Furthermore, SMOX overexpression followed by downstream oxidative damage, chronic inflammation, and carcinogenesis is often induced by infections (discussed above).

Xanthine oxidoreductase (XOR) is a molybdenum iron-sulfur flavin hydroxylase that exists in two forms, xanthine dehydrogenase (XDH) and xanthine oxidase (XOD). XDH can be converted to XOD either irreversibly by proteolysis or reversibly by modification of cysteine residues [136, 137]. The enzyme catalyzes the oxidation of hypoxanthine to xanthine or xanthine to uric acid during purine metabolism [138]. Both XDH and XOD generate H_2O_2 and $O_2^{\bullet-}$ through NADH oxidation [139]. Nevertheless, for XDH, NAD+ is a more preferable substrate compared to oxygen, and therefore, it cannot directly produce ROS [140]. XOR-released superoxide radicals rapidly react with nitric oxide ($NO^{\bullet}$) generating peroxynitrite ($ONOO^-$). $NO^{\bullet}$, in turn, is produced by NOS activity or even by XOR under hypoxic conditions [141]. The association of XOR with neoplastic transformation was first reported many years ago [142]. Decreased XOR activity was frequently found in many animal and human tumors [143]. XOR activity was increased in meningioma, astrocytoma, and laryngeal and colorectal cancers [144–146]. This indicates that dysregulation of purine metabolism and ROS levels can play a role in tumor pathogenesis.

Cytochrome P450 (CYP) oxidase is part of the microsomal electron transport system. It belongs to the CYP superfamily of integral membrane proteins that catalyze the oxidation of numerous organic substrates, accompanied by the reduction of molecular oxygen [147]. CYP enzymes also have peroxygenase and peroxidase activity, using H_2O_2 either for direct oxidation of substrates or as a donor of oxygen atoms [148]. The prosthetic heme group in CYP enzymes is essential for their activity [149]. H_2O_2 and superoxide radicals are produced during the CYP monooxygenase cycle; the former can be further decomposed to hydroxyl radicals ($^•OH$) in the presence of ferrous iron via a Fenton reaction [150]. CYP enzymes are predominantly located in the endoplasmic reticulum and mitochondria and are expressed in many mammalian tissues [151]. CYP-related ROS generation depends on CYP isoforms, content and type of substrates, pH, ionic strength, the action of cytochrome $b5$, oxygen concentration, oligomerization, and so on [150, 152, 153]. Studies have shown that CYP2E1 induces higher ROS production than other CYP enzymes and that its activation or overexpression leads to increased ROS levels [152, 154]. CYP enzyme activity can promote carcinogenesis through increased ROS production. As such, overexpression of CYP family genes was observed in many cancers [150].

The NADPH oxidase (NOX) family includes seven members: NOX1, NOX2, NOX3, NOX4, NOX5, dual oxidase 1 (DUOX1), and DUOX2 [155]. These are transmembrane proteins that transfer an electron from the NADPH substrate to FAD across biological membranes in order to reduce oxygen to a superoxide radical [156]. Dysregulation of NOX activity leads to elevated ROS production that can contribute to tumorigenesis, cell transformation, tumor growth, angiogenesis, and metastasis. NOX-derived ROS were shown to be implicated in many common cancer types (e.g., bladder, colorectal, breast, kidney, lung, and prostate cancers), as well as acute myeloid leukemia and non-Hodgkin's lymphoma [157–161]. Moreover, NOX family members are involved in host defense and innate immunity. NOX could be activated by various infectious agents resulting in increased ROS production which promotes the death of the infected cells as well as an inflammatory response [162]. Toll-like receptors (TLRs) located at the plasma membrane recognize conserved structures of bacteria, viruses, or fungi and trigger downstream signaling. TLRs interact with NOX, leading to increased ROS generation, as well as subsequent activation of the transcription factor NF-κB, and production of cytokines and chemokines [163–165]. Nucleotide-binding oligomerization domain- (NOD-) like receptors (NLRs) can also recognize components of the bacterial cell wall and other bacterial molecules (e.g., RNA, toxins, and ligands). NLR family members, NACHT lectin-like receptor and PYD domain-containing proteins (NLRPs), promote the assembly of inflammasomes and mediate the activation of inflammatory caspases [166]. ROS were shown to be required for the activation of NLRP3-mediated inflammasomes, and NOX, as one of the main sources of ROS production, can be involved in NLR signaling [167]. The important role of NOX-produced ROS in the NLR system was also reported

by Lipinski et al. [168]. Additionally, hepatitis C virus (HCV) infection can induce NOX1 and NOX4 expression, leading to increased ROS generation in hepatocytes [169]. It was shown that HCV modulates NOX4 through TGF-beta [169, 170]. Moreover, HCV can induce immune dysfunction via HCV nonstructural protein 3- (NS3-) induced release of ROS from phagocytes, resulting in the apoptosis of T lymphocytes, natural killer (NK) cells, and NKT cells [171, 172].

Cyclooxygenases (COX) and lipoxygenases (LOX) participate in polyunsaturated fatty acid (PUFA) metabolism, by producing bioactive eicosanoids. COX and LOX oxygenate arachidonic acid resulting in the formation of prostaglandin G2 and H2 (PGG2/PGH2) and fatty acid hydroperoxide, respectively, a reaction that is accompanied by ROS release [173]. Peroxyl radicals (ROO$^•$) and alkoxyl radicals (RO$^•$) are intermediates of the hydroperoxide metabolism. Moreover, the arachidonic acid pathway itself could be responsible for ROS generation via NADPH oxidase activation [174]. In spite of the similarity between COX/LOX-catalyzing reactions, they have a completely different sequence, structure, cellular localization, and tissue expression [175]. COX is present in three isoforms - constitutive (COX-1), inducible (COX-2), and splice variant of COX-1 (COX-3) [176]. The PTGS1 gene encodes for both COX-1 and COX-3 isoenzymes; however, COX-3 activity in humans remains unclear [177, 178]. PTGS2 encodes for COX-2. COX-1 predominantly regulates basal prostaglandin metabolism and normal tissue homeostasis [179]. COX-2 is induced by proinflammatory stimuli, cytokines, and growth factors in response to inflammation, tissue injury, and tumorigenesis [180, 181]. COX-2 overexpression and increased prostaglandin biosynthesis have been found in both the precancer stages and various tumors [173, 182–184]. COX1 was upregulated in breast, cervical, ovarian, endometrial, and colorectal cancers, as well as in cholangiocarcinoma [185–190].

LOX constitutes a large family of nonheme iron-containing dioxygenases; five LOX isoenzymes were found in humans (5-LOX, 12-LOX, 12R-LOX, two 15-LOX, and 3-LOX/E-LOX). Dysregulated LOX expression was observed in various tumors and animal models. A dual role of LOX in tumorigenesis has been proposed, as they can be involved in both neoplastic transformation and tumor suppression [173].

Monoamine oxidases A and B (MAOA and MAOB) are mitochondrial FAD-dependent enzymes encoded by separate genes [191, 192]. They catalyze the oxidative deamination of monoamines, including monoamine neurotransmitters (e.g., norepinephrine, dopamine, serotonin, and epinephrine), exogenous dietary amines, and drugs, generating H_2O_2 and aldehydes as by-products [193, 194]. Excessive MAO activity leads to enhanced ROS production and mitochondrial damage and is implicated in aging, cardiovascular diseases, neurodegenerative disorders, and cancer [195–197]. Increased MAOA expression was found in lung, prostate, and breast cancers, as well as hepatocellular carcinoma and cholangiocarcinoma [198–203]. Moreover, several studies suggested that MAOA can promote cancer progression through induction of EMT [197, 198]. Conversely, MAOA was downregulated in a number of cancer tissues

and significantly differed between them [204]. In this case, the potential mechanism of tumor progression can be related to an increase in the amounts of MAOA substrate epinephrine [205, 206].

Lysyl oxidase is a family of copper-dependent enzymes that play a primary role in the remodeling of the extracellular matrix (ECM). They catalyze the conversion of specific lysine residues into reactive aldehyde groups in collagen and elastin, forming protein crosslinks [207]. The lysyl oxidase catalytic cycle also produces H_2O_2, which can increase oxidative stress thereby promoting carcinogenesis. Overexpression of lysyl oxidase and its involvement in tumor progression and metastasis were shown in various cancers [208–214].

2.8. Signaling Pathways. The PI3K/AKT/PTEN signaling pathway is implicated in NOX-derived ROS production [215]. PTEN (phosphatase and tensin homolog) is a tumor suppressor responsible for the negative regulation of PI3K/AKT signaling. Loss of *PTEN* expression or mutations in the gene, as well as dysregulation of the PI3K/AKT signaling pathway, were frequently found in many tumors [216, 217].

NOXs are multimeric enzymes consisting of several proteins that are distributed between the membrane and cytosol when inactive. Upon activation by different stimuli, the cytosolic subunits interact with integral membrane subunits, forming the functional NOX enzymes which can generate ROS [218]. It was shown that PI3K/AKT inhibitors can reduce NOX-dependent ROS generation through the inhibition of NOX subunit translocation into the membrane. In addition, membrane depolarization with downstream PI3K/AKT and (protein kinase C) PKC activation causes NOX assembly and ROS production [215]. Moreover, oxidative stress inhibits PTEN-induced PI3K/AKT signaling, which promotes both the expression of cell survival genes and ROS production [219]. Such mechanisms may contribute to tumor cell proliferation and growth under oxidative conditions. Several other enzymes, including PKC, mitogen-activated protein kinases (MAPK), cAMP-dependent protein kinases (PKA), p21-activated kinases (PAK), and PKB/AKT, can modulate the activation of NOXs through phosphorylation of their cytosolic subunits, thereby increasing the level of ROS [220]. All the aforementioned enzymes were shown to be greatly involved in cancer development [221–223].

Transcription factor p53 is a widely known tumor suppressor, involved in regulating the expression of various genes encoding for both ROS-producing and antioxidant-related components [224]. p53 induces the expression of glutathione peroxidase 1 (GPX1) and mitochondrial superoxide dismutase 2, both components of the key antioxidant defense system [225, 226]. Moreover, p53 regulates the expression of sestrins (*SESN1* and *SESN2*) that are required for peroxiredoxins regeneration [227]. Phosphate-activated mitochondrial glutaminase (GLS2) converts glutamine to glutamate, which is a precursor for glutathione synthesis. GLS2 expression can be induced by p53 in response to DNA damage or oxidative stress to promote antioxidant defense by controlling the GSH/GSSG ratio [228]. Other p53-inducible antioxidant genes are *TIGAR* and *ALDH4*. TIGAR negatively regulates glycolysis and decreases intracel-

lular ROS levels [229], while aldehyde dehydrogenase 4 (ALDH4) is a NAD+-dependent enzyme that catalyzes the second step of the proline degradation pathway in the mitochondrial matrix [230]. Overexpression of *ALDH4* in p53-null cells inhibits ROS generation and apoptosis [231].

The function of prooxidant p53 is based on its ability to regulate the expression of genes encoding for prooxidant enzymes, such as PUMA (the p53-upregulated modulator of apoptosis), p66Shc (66 kDa Src collagen homologue (Shc) adaptor protein), and other proteins encoded by a group of p53-induced genes (PIGs). PUMA overexpression induces BCL2-associated X (BAX) protein-dependent ROS generation (predominantly superoxide radicals and H_2O_2) and apoptosis in colorectal cancer cells [232]. p66Shc generates mitochondrial H_2O_2 as signaling molecules for the induction of apoptosis [233]. PIG is a family of proteins, whose several members were shown to influence the cell redox status. P53-induced activation of PIGs results in increased ROS levels and mitochondria-derived apoptosis in colorectal cancer cells [234]. It was shown that p53 promotes the expression of *PIG3*, *BAX*, and *PUMA* leading to an increase in intracellular ROS levels and induction of apoptosis. Moreover, the authors have demonstrated that p53 induction is associated with the excessive ROS release by mitochondria, which supports its prooxidant role [235].

3. Role of Glycolysis and the Pentose Phosphate Pathway in Antioxidant Defense

Glycolysis and the pentose phosphate pathway are involved in ROS detoxification. Glycolysis occurs in living cells both in anaerobic and aerobic conditions. Aerobic glycolysis generates pyruvate that is converted to acetyl-CoA with the release of carbon dioxide in the mitochondrial tricarboxylic acid (TCA) cycle, while in the absence of oxygen, lactate is produced [236]. Most tumor cells use anaerobic glycolysis even in the presence of oxygen; this phenomenon is termed the "Warburg effect" [237]. Glycolysis reprogramming allows tumor cells to redirect this process to support *de novo* nucleotide synthesis during proliferation [238]. Dysregulation in the expression of genes encoding for key glycolytic components has been found in many tumors [239–246]. Increased glycolysis in tumor cells can reduce ROS production via a decrease in OXPHOS activity [247].

The NADPH/NADP+ ratio is important for antioxidant defense; NADPH acts as a donor of reductive potential to glutathione and thioredoxin reductases. The main source of NADPH is the oxidative branch of the pentose phosphate pathway (ox-PPP) [248]. Glucose-6-phosphate (G6P) derived from glucose phosphorylation by hexokinases (HKs) is reduced to 6-phosphogluconate and NADPH via glucose-6-phosphate dehydrogenase (G6PD) during the first step of ox-PPP. In the next step, 6-phosphogluconate dehydrogenase (6PG) catalyzes the oxidative decarboxylation of 6-phosphogluconate to ribulose-5-phosphate (Ru5P) providing the additional NADPH [249]. The NADP+/NADPH ratio regulates G6PD and 6PG activity in order to produce more NADPH for oxidative stress prevention [250]. Several glycolytic enzymes, such as phosphofructokinase-1 (PFK1),

TABLE 1: ROS and major mechanisms of their generation and detoxification.

ROS	Generation	Detoxification
Superoxide radical ($O_2^{\bullet-}$)	Mitochondrial respiratory chain Electron transport chain in the peroxisomal membrane Superoxide dismutases CYP catalytic cycle Mitochondrial enzymes (glycerol 3-phosphate dehydrogenase, 2-oxoglutarate dehydrogenase, NADH-cytochrome b5 reductase, etc.) Xanthine oxidoreductase	Superoxide dismutases Polyamines
Hydrogen peroxide (H_2O_2)	Spontaneous dismutation of superoxide radicals Polyamine catabolism Thymidine catabolism NADPH oxidases Monoamine oxidases Lysyl oxidases Dihydroorotate dehydrogenase CYP catalytic cycle Peroxisomal enzymes (acyl-CoA oxidases, d-amino acid oxidase, d-aspartate oxidase, etc.) Microsomal monooxygenase (MMO) system Normal protein folding/unfolded protein response Polyunsaturated fatty acid metabolism	Polyamines Glutathione peroxidases Thioredoxin peroxidases Catalase Peroxiredoxins Glutathione S-transferases Glutaredoxins Thioredoxins Nonenzymatic scavengers* Glycolysis Pentose phosphate pathway
Hydroxyl radical ($^{\bullet}OH$)	Fenton and Haber-Weiss reactions Thymidine catabolism (supposed) Aconitase via Fenton reaction	$^{\bullet}OH$ has a very short half-life and is very rapidly involved in other reactions Polyamines
Singlet oxygen (O_2)	Nonphotosensitized mechanisms of O_2 generation**	O_2 is rapidly implicated in many oxidation reactions Polyamines
Hydroperoxyl radical ($HOO^{\bullet}$)	Protonated form of $O_2^{\bullet-}$	Nonenzymatic scavengers
Peroxyl radical ($ROO^{\bullet}$)	Polyunsaturated fatty acid metabolism	Nonenzymatic scavengers
Alkoxyl radical ($RO^{\bullet}$)	Polyunsaturated fatty acid metabolism	Nonenzymatic scavengers

*Described in [150, 269]; **well reviewed in [270].

glyceraldehyde 3-phosphate dehydrogenase (GAPDH), and pyruvate kinase (PK), as well as the TP53-inducible glycolysis and apoptosis regulator (TIGAR), are involved in the redirection of glycolytic flux through the ox-PPP in order to reduce the ROS level [251]. Moreover, the acceleration of glycolysis and PPP in a tumor cell can protect it from oxidative damage [252].

4. Tumor Microenvironment

Solid tumors are commonly infiltrated with different types of cells, including cancer-associated fibroblasts (CAFs), immune cells, pericytes, adipocytes, and other tissue-associated cells. This forms a distinct tumor microenvironment that comprises cell-cell and cell-extracellular matrix interactions, as well as many soluble factors [253, 254]. The latter include vascular endothelial growth factors (VEGFs), fibroblast growth factors (FGFs), angiopoietins (ANGs), transforming growth factors (TNFs), ROS, chemokines, cytokines, exosomes, microRNAs, Ca^{2+}, K^+, Na^+, H^+, and other ions [255–257]. The tumor microenvironment plays an essential role in tumor initiation, progression, and metastasis [258]. It is also involved in the resistance to targeted therapy, radiation, and chemotherapy, as well as sensitivity to immunotherapy [259, 260].

Relatively stable ROS, such as H_2O_2, which is produced at a high level by tumor cells, can diffuse into the extracellular space. H_2O_2 can freely cross membranes; however, the cells seem to regulate H_2O_2 transport by changes in membrane lipid composition, thereby maintaining cellular H_2O_2 concentration [261]. Aquaporins (AQPs) have also been found to be transporters of H_2O_2 [262, 263]. Moreover, superoxide dismutase 3 (SOD3, EC-SOD) and NADPH oxidase provide extracellular ROS sources. SOD3, which is located in the extracellular space, catalyzes the dismutation of the superoxide anion into H_2O_2 [264], while several NOX isoforms generate H_2O_2 and $O_2^{\bullet-}$ outside cells [156, 265]. Extracellular ROS signaling in tumor cells with the participation of SOD and NOX enzymes has been well described by Bauer et al. [266]. Briefly, NOX located in the plasma membrane produces $O_2^{\bullet-}$ into the extracellular space. The superoxide radical, in turn, dismutates to H_2O_2 during the hypochlorous
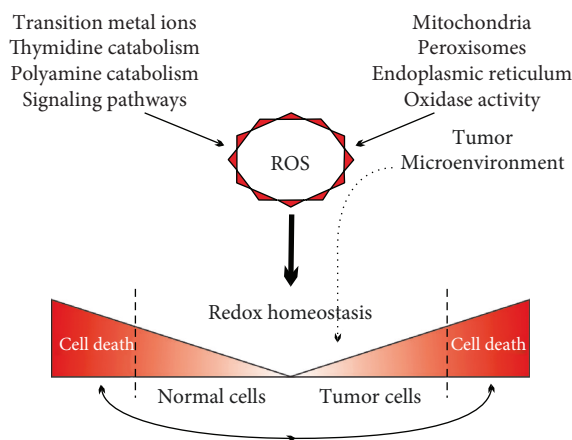
FIGURE 1: Main sources of ROS production in normal and tumor cells.

acid (HOCl) pathway. Peroxidases (POD) use the H_2O_2 as a substrate to generate HOCl, which further reacts with hydroxyl anions (OH^-) leading to the formation of hydroxyl radicals ($^\bullet OH$). NOX-generated $O_2^{\bullet-}$ is reduced to H_2O_2 either by SOD3 or spontaneously; membrane CAT decomposes the produced H_2O_2 thereby inhibiting HOCl signaling. CAT can also decompose peroxynitrite ($ONOO^-$) derived from the reaction between NO and H_2O_2 that prevents hydroxyl radical formation through the NO/peroxynitrite pathway.

Apart from tumor cells, cancer-associated fibroblasts also release extracellular H_2O_2 that induces oxidative stress in normal fibroblasts, triggering their reprogramming to CAFs and promoting field cancerization, epithelial cell transformation and growth, and cancer aggressiveness [267]. Immune cells, such as myeloid-derived suppressor cells (MDSCs), tumor-associated macrophages (TAMs), regulatory T cells (Tregs), neutrophils, eosinophils, and mononuclear phagocytes, can also generate ROS (mainly H_2O_2) into the tumor microenvironment [253, 268].

The major mechanisms of ROS generation and detoxification are presented in Table 1 and Figure 1.

5. Conclusions

ROS are generated by multiple cellular processes and can be overproduced in response to different stimuli. Normal cells can maintain oxidative homeostasis owing to the activity of various antioxidant systems which control ROS production through changes in metabolic and signaling pathways. Upon a permanent increase in ROS levels, the antioxidant defense mechanisms can promote cell death. However, oxidative stress damages many molecules, cell structures, and functions leading to the development of pathological states, such as inflammation, aging, neurodegenerative disorders, and cancer. ROS are greatly implicated in tumorigenesis, and summarizing the current data on ROS biology is important for understanding the mechanisms of tumor initiation, promotion, and progression, as well as for treatment development.

Conflicts of Interest

The authors declare that there is no conflict of interest regarding the publication of this paper.

References

[1] J. Zhang, X. Wang, V. Vikash et al., "ROS and ROS-mediated cellular signaling," *Oxidative Medicine and Cellular Longevity*, vol. 2016, Article ID 4350965, 18 pages, 2016.

[2] A. A. Alfadda and R. M. Sallam, "Reactive oxygen species in health and disease," *Journal of Biomedicine and Biotechnology*, vol. 2012, Article ID 936486, 14 pages, 2012.

[3] A. V. Kudryavtseva, G. S. Krasnov, A. A. Dmitriev et al., "Mitochondrial dysfunction and oxidative stress in aging and cancer," *Oncotarget*, vol. 7, no. 29, pp. 44879–44905, 2016.

[4] P. Storz, "Reactive oxygen species in tumor progression," *Frontiers in Bioscience*, vol. 10, no. 1-3, pp. 1881–1896, 2005.

[5] T. B. Dansen and K. W. Wirtz, "The peroxisome in oxidative stress," *IUBMB Life*, vol. 51, no. 4, pp. 223–230, 2001.

[6] S. Tabata, R. Ikeda, M. Yamamoto et al., "Thymidine phosphorylase enhances reactive oxygen species generation and interleukin-8 expression in human cancer cells," *Oncology Reports*, vol. 28, no. 3, pp. 895–902, 2012.

[7] R. Amendola, M. Cervelli, G. Tempera et al., "Spermine metabolism and radiation-derived reactive oxygen species for future therapeutic implications in cancer: an additive or adaptive response," *Amino Acids*, vol. 46, no. 3, pp. 487–498, 2014.

[8] S. Kumari, A. K. Badana, G. Murali Mohan, G. Shailender, and R. R. Malla, "Reactive oxygen species: a key constituent in cancer survival," *Biomarker Insights*, vol. 13, article 1177271918755391, 2018.

[9] S. Galadari, A. Rahman, S. Pallichankandy, and F. Thayyullathil, "Reactive oxygen species and cancer paradox: to promote or to suppress?," *Free Radical Biology & Medicine*, vol. 104, pp. 144–164, 2017.

[10] M. D. Brand, "The sites and topology of mitochondrial superoxide production," *Experimental Gerontology*, vol. 45, no. 7-8, pp. 466–472, 2010.

[11] A. Okado-Matsumoto and I. Fridovich, "Subcellular distribution of superoxide dismutases (SOD) in rat liver: Cu,Zn-SOD in mitochondria," *Journal of Biological Chemistry*, vol. 276, no. 42, pp. 38388–38393, 2001.

[12] J. Vasquez-Vivar, B. Kalyanaraman, and M. C. Kennedy, "Mitochondrial aconitase is a source of hydroxyl radical. An electron spin resonance investigation," *Journal of Biological Chemistry*, vol. 275, no. 19, pp. 14064–14069, 2000.

[13] H. Yasui, S. Hayashi, and H. Sakurai, "Possible involvement of singlet oxygen species as multiple oxidants in p450 catalytic reactions," *Drug Metabolism and Pharmacokinetics*, vol. 20, no. 1, pp. 1–13, 2005.

[14] T. Omura, "Mitochondrial P450s," *Chemico-Biological Interactions*, vol. 163, no. 1-2, pp. 86–93, 2006.

[15] S. A. Whatley, D. Curti, F. D. Gupta et al., "Superoxide, neuroleptics and the ubiquinone and cytochrome b_5 reductases in brain and lymphocytes from normals and schizophrenic patients," *Molecular Psychiatry*, vol. 3, no. 3, pp. 227–237, 1998.

[16] H. J. Forman and J. Kennedy, "Dihydroorotate-dependent superoxide production in rat brain and liver. A function of the primary dehydrogenase," *Archives of Biochemistry and Biophysics*, vol. 173, no. 1, pp. 219–224, 1976.

[17] M. Hey-Mogensen, R. L. S. Goncalves, A. L. Orr, and M. D. Brand, "Production of superoxide/H_2O_2 by dihydroorotate dehydrogenase in rat skeletal muscle mitochondria," *Free Radical Biology & Medicine*, vol. 72, pp. 149–155, 2014.

[18] L. Zhang, L. Yu, and C. A. Yu, "Generation of superoxide anion by succinate-cytochrome$c$ reductase from bovine heart mitochondria," *Journal of Biological Chemistry*, vol. 273, no. 51, pp. 33972–33976, 1998.

[19] N. Kaludercic, J. Mialet-Perez, N. Paolocci, A. Parini, and F. Di Lisa, "Monoamine oxidases as sources of oxidants in the heart," *Journal of Molecular and Cellular Cardiology*, vol. 73, pp. 34–42, 2014.

[20] T. Rabilloud, M. Heller, M. P. Rigobello, A. Bindoli, R. Aebersold, and J. Lunardi, "The mitochondrial antioxidant defence system and its response to oxidative stress," *Proteomics*, vol. 1, no. 8, pp. 1105–1110, 2001.

[21] I. Hanukoglu, "Antioxidant protective mechanisms against reactive oxygen species (ROS) generated by mitochondrial P450 systems in steroidogenic cells," *Drug Metabolism Reviews*, vol. 38, no. 1-2, pp. 171–196, 2006.

[22] M. Mari, A. Morales, A. Colell, C. Garcia-Ruiz, and J. C. Fernandez-Checa, "Mitochondrial glutathione, a key survival antioxidant," *Antioxidants & Redox Signaling*, vol. 11, no. 11, pp. 2685–2700, 2009.

[23] Y. Orii, "The cytochrome c peroxidase activity of cytochrome oxidase," *Journal of Biological Chemistry*, vol. 257, no. 16, pp. 9246–9248, 1982.

[24] R. E. Beyer, "The participation of coenzyme Q in free radical production and antioxidation," *Free Radical Biology & Medicine*, vol. 8, no. 6, pp. 545–565, 1990.

[25] M. R. Fernando, J. M. Lechner, S. Lofgren, V. N. Gladyshev, and M. F. Lou, "Mitochondrial thioltransferase (glutaredoxin 2) has GSH-dependent and thioredoxin reductase-dependent peroxidase activities *in vitro* and in lens epithelial cells," *The FASEB Journal*, vol. 20, no. 14, pp. 2645–2647, 2006.

[26] A.-J. L. Ham and D. C. Liebler, "Vitamin E oxidation in rat liver mitochondria," *Biochemistry*, vol. 34, no. 17, pp. 5754–5761, 1995.

[27] R. Radi, J. F. Turrens, L. Y. Chang, K. M. Bush, J. D. Crapo, and B. A. Freeman, "Detection of catalase in rat heart mitochondria," *Journal of Biological Chemistry*, vol. 266, no. 32, pp. 22028–22034, 1991.

[28] C. D. Phung, J. A. Ezieme, and J. F. Turrens, "Hydrogen peroxide metabolism in skeletal muscle mitochondria," *Archives of Biochemistry and Biophysics*, vol. 315, no. 2, pp. 479–482, 1994.

[29] I. G. Kirkinezos and C. T. Moraes, "Reactive oxygen species and mitochondrial diseases," *Seminars in Cell & Developmental Biology*, vol. 12, no. 6, pp. 449–457, 2001.

[30] A. Rimessi, M. Previati, F. Nigro, M. R. Wieckowski, and P. Pinton, "Mitochondrial reactive oxygen species and inflammation: molecular mechanisms, diseases and promising therapies," *The International Journal of Biochemistry & Cell Biology*, vol. 81, Part B, pp. 281–293, 2016.

[31] P. Newsholme, E. P. Haber, S. M. Hirabara et al., "Diabetes associated cell stress and dysfunction: role of mitochondrial and non-mitochondrial ROS production and activity," *The Journal of Physiology*, vol. 583, no. 1, pp. 9–24, 2007.

[32] A. van der Vliet, Y. M. W. Janssen-Heininger, and V. Anathy, "Oxidative stress in chronic lung disease: from mitochondrial dysfunction to dysregulated redox signaling," *Molecular Aspects of Medicine*, vol. 63, pp. 59–69, 2018.

[33] K. Księżakowska-Łakoma, M. Żyła, and J. R. Wilczyński, "Mitochondrial dysfunction in cancer," *Przeglad Menopauzalny = Menopause review*, vol. 2, no. 2, pp. 136–144, 2014.

[34] Z. Zou, H. Chang, H. Li, and S. Wang, "Induction of reactive oxygen species: an emerging approach for cancer therapy," *Apoptosis*, vol. 22, no. 11, pp. 1321–1335, 2017.

[35] D. Beyersmann and A. Hartwig, "Carcinogenic metal compounds: recent insight into molecular and cellular mechanisms," *Archives of Toxicology*, vol. 82, no. 8, pp. 493–512, 2008.

[36] M. Valko, K. Jomova, C. J. Rhodes, K. Kuca, and K. Musilek, "Redox- and non-redox-metal-induced formation of free radicals and their role in human disease," *Archives of Toxicology*, vol. 90, no. 1, pp. 1–37, 2016.

[37] S. I. Liochev and I. Fridovich, "The Haber-Weiss cycle—70 years later: an alternative view," *Redox Report*, vol. 7, no. 1, pp. 55–57, 2002.

[38] A. Valavanidis, T. Vlachogianni, and C. Fiotakis, "8-Hydroxy-2′-deoxyguanosine (8-OHdG): a critical biomarker of oxidative stress and carcinogenesis," *Journal of Environmental Science and Health Part C: Environmental Carcinogenesis & Ecotoxicology Reviews*, vol. 27, no. 2, pp. 120–139, 2009.

[39] L. A. Del Río and E. López-Huertas, "ROS generation in peroxisomes and its role in cell signaling," *Plant and Cell Physiology*, vol. 57, no. 7, pp. 1364–1376, 2016.

[40] I. Singh, "Biochemistry of peroxisomes in health and disease," *Molecular and Cellular Biochemistry*, vol. 167, no. 1-2, pp. 1–29, 1997.

[41] S. Di Meo, T. T. Reed, P. Venditti, and V. M. Victor, "Role of ROS and RNS sources in physiological and pathological conditions," *Oxidative Medicine and Cellular Longevity*, vol. 2016, Article ID 1245049, 44 pages, 2016.

[42] C. De Duve and P. Baudhuin, "Peroxisomes (microbodies and related particles)," *Physiological Reviews*, vol. 46, no. 2, pp. 323–357, 1966.

[43] R. Fritz, J. Bol, U. Hebling et al., "Compartment-dependent management of H_2O_2 by peroxisomes," *Free Radical Biology & Medicine*, vol. 42, no. 7, pp. 1119–1129, 2007.

[44] A. Boveris, N. Oshino, and B. Chance, "The cellular production of hydrogen peroxide," *Biochemical Journal*, vol. 128, no. 3, pp. 617–630, 1972.

[45] M. Fransen, M. Nordgren, B. Wang, and O. Apanasets, "Role of peroxisomes in ROS/RNS-metabolism: implications for

human disease," *Biochimica et Biophysica Acta (BBA) - Molecular Basis of Disease*, vol. 1822, no. 9, pp. 1363–1373, 2012.

[46] M. Valko, H. Morris, and M. T. Cronin, "Metals, toxicity and oxidative stress," *Current Medicinal Chemistry*, vol. 12, no. 10, pp. 1161–1208, 2005.

[47] J. M. C. Gutteridge and B. Halliwell, "Comments on review of free radicals in biology and medicine, second edition, by Barry Halliwell and John M. C. Gutteridge," *Free Radical Biology & Medicine*, vol. 12, no. 1, pp. 93-94, 1992.

[48] L. M. Sandalio, V. M. Fernandez, F. L. Ruperez, and L. A. Del Rio, "Superoxide free radicals are produced in glyoxysomes," *Plant Physiology*, vol. 87, no. 1, pp. 1–4, 1988.

[49] N. Usuda, M. K. Reddy, T. Hashimoto, M. S. Rao, and J. K. Reddy, "Tissue specificity and species differences in the distribution of urate oxidase in peroxisomes," *Laboratory Investigation*, vol. 58, no. 1, pp. 100–111, 1988.

[50] L. M. Sandalio, M. Rodriguez-Serrano, M. C. Romero-Puertas, and L. A. del Rio, "Role of peroxisomes as a source of reactive oxygen species (ROS) signaling molecules," *Sub-cellular Biochemistry*, vol. 69, pp. 231–255, 2013.

[51] R. Harrison, "Structure and function of xanthine oxidoreductase: where are we now?," *Free Radical Biology & Medicine*, vol. 33, no. 6, pp. 774–797, 2002.

[52] L. A. Del Rio, "Peroxisomes as a cellular source of reactive nitrogen species signal molecules," *Archives of Biochemistry and Biophysics*, vol. 506, no. 1, pp. 1–11, 2011.

[53] P. Pacher, J. S. Beckman, and L. Liaudet, "Nitric oxide and peroxynitrite in health and disease," *Physiological Reviews*, vol. 87, no. 1, pp. 315–424, 2007.

[54] E. Panieri and M. M. Santoro, "ROS homeostasis and metabolism: a dangerous liason in cancer cells," *Cell Death & Disease*, vol. 7, no. 6, article e2253, 2016.

[55] C. Lauer, A. Volkl, S. Riedl, H. D. Fahimi, and K. Beier, "Impairment of peroxisomal biogenesis in human colon carcinoma," *Carcinogenesis*, vol. 20, no. 6, pp. 985–989, 1999.

[56] J. Chung-man Ho, S. Zheng, S. A. Comhair, C. Farver, and S. C. Erzurum, "Differential expression of manganese superoxide dismutase and catalase in lung cancer," *Cancer Research*, vol. 61, no. 23, pp. 8578–8585, 2001.

[57] W. M. Frederiks, K. S. Bosch, K. A. Hoeben, J. van Marle, and S. Langbein, "Renal cell carcinoma and oxidative stress: the lack of peroxisomes," *Acta Histochemica*, vol. 112, no. 4, pp. 364–371, 2010.

[58] D. G. Bostwick, E. E. Alexander, R. Singh et al., "Antioxidant enzyme expression and reactive oxygen species damage in prostatic intraepithelial neoplasia and cancer," *Cancer*, vol. 89, no. 1, pp. 123–134, 2000.

[59] M. Y. Cho, J. Y. Cheong, W. Lim et al., "Prognostic significance of catalase expression and its regulatory effects on hepatitis B virus X protein (HBx) in HBV-related advanced hepatocellular carcinomas," *Oncotarget*, vol. 5, no. 23, pp. 12233–12246, 2014.

[60] I. Vuillaume, Y. Decroix, R. Calvayrac et al., "Catalase-associated abnormalities and H_2O_2 increase in pre-neoplastic and neoplastic lesions of the human lower female genital tract and their near adjacent epithelia," *Biomedicine & Pharmacotherapy*, vol. 45, no. 10, pp. 435–444, 1991.

[61] J. A. Litwin, K. Beier, A. Volkl, W. J. Hofmann, and H. D. Fahimi, "Immunocytochemical investigation of catalase and peroxisomal lipid β-oxidation enzymes in human hepatocellular tumors and liver cirrhosis," *Virchows Archiv*, vol. 435, no. 5, pp. 486–495, 1999.

[62] D. S. Schwarz and M. D. Blower, "The endoplasmic reticulum: structure, function and response to cellular signaling," *Cellular and Molecular Life Sciences*, vol. 73, no. 1, pp. 79–94, 2016.

[63] M. Schroder and R. J. Kaufman, "ER stress and the unfolded protein response," *Mutation Research*, vol. 569, no. 1-2, pp. 29–63, 2005.

[64] P. Scriven, N. J. Brown, A. G. Pockley, and L. Wyld, "The unfolded protein response and cancer: a brighter future unfolding?," *Journal of Molecular Medicine*, vol. 85, no. 4, pp. 331–341, 2007.

[65] C. X. C. Santos, L. Y. Tanaka, J. Wosniak Jr., and F. R. M. Laurindo, "Mechanisms and implications of reactive oxygen species generation during the unfolded protein response: roles of endoplasmic reticulum oxidoreductases, mitochondrial electron transport, and NADPH oxidase," *Antioxidants & Redox Signaling*, vol. 11, no. 10, pp. 2409–2427, 2009.

[66] W. S. Wu, "The signaling mechanism of ROS in tumor progression," *Cancer and Metastasis Reviews*, vol. 25, no. 4, pp. 695–705, 2007.

[67] A. Papaioannou and E. Chevet, "Driving cancer tumorigenesis and metastasis through UPR signaling," *Current Topics in Microbiology and Immunology*, vol. 414, pp. 159–192, 2018.

[68] H. J. Clarke, J. E. Chambers, E. Liniker, and S. J. Marciniak, "Endoplasmic reticulum stress in malignancy," *Cancer Cell*, vol. 25, no. 5, pp. 563–573, 2014.

[69] B. P. Tu and J. S. Weissman, "Oxidative protein folding in eukaryotes: mechanisms and consequences," *The Journal of Cell Biology*, vol. 164, no. 3, pp. 341–346, 2004.

[70] L. Ellgaard and L. W. Ruddock, "The human protein disulphide isomerase family: substrate interactions and functional properties," *EMBO Reports*, vol. 6, no. 1, pp. 28–32, 2005.

[71] E. Zito, "ERO1: a protein disulfide oxidase and H_2O_2 producer," *Free Radical Biology & Medicine*, vol. 83, pp. 299–304, 2015.

[72] H. M. Zeeshan, G. H. Lee, H. R. Kim, and H. J. Chae, "Endoplasmic reticulum stress and associated ROS," *International Journal of Molecular Sciences*, vol. 17, no. 3, p. 327, 2016.

[73] K. M. Kim, A. R. An, H. S. Park et al., "Combined expression of protein disulfide isomerase and endoplasmic reticulum oxidoreductin 1-α is a poor prognostic marker for non-small cell lung cancer," *Oncology Letters*, vol. 16, no. 5, pp. 5753–5760, 2018.

[74] S. Samanta, S. Tamura, L. Dubeau et al., "Expression of protein disulfide isomerase family members correlates with tumor progression and patient survival in ovarian cancer," *Oncotarget*, vol. 8, no. 61, pp. 103543–103556, 2017.

[75] Z. Yang, J. Liu, Q. Shi et al., "Expression of protein disulfide isomerase A3 precursor in colorectal cancer," *OncoTargets and Therapy*, vol. 11, pp. 4159–4166, 2018.

[76] G. Kutomi, Y. Tamura, T. Tanaka et al., "Human endoplasmic reticulum oxidoreductin 1-α is a novel predictor for poor prognosis of breast cancer," *Cancer Science*, vol. 104, no. 8, pp. 1091–1096, 2013.

[77] S. Y. Seol, C. Kim, J. Y. Lim et al., "Overexpression of endoplasmic reticulum oxidoreductin 1-α (ERO1L) is associated with poor prognosis of gastric cancer," *Cancer Research and Treatment*, vol. 48, no. 4, pp. 1196–1209, 2016.

[78] B. Zhou, G. Wang, S. Gao et al., "Expression of ERO1L in gastric cancer and its association with patient prognosis," *Experimental and Therapeutic Medicine*, vol. 14, no. 3, pp. 2298–2302, 2017.

[79] N. Takei, A. Yoneda, K. Sakai-Sawada, M. Kosaka, K. Minomi, and Y. Tamura, "Hypoxia-inducible ERO1α promotes cancer progression through modulation of integrin-β1 modification and signalling in HCT116 colorectal cancer cells," *Scientific Reports*, vol. 7, no. 1, p. 9389, 2017.

[80] Y. Zhang, T. Li, L. Zhang et al., "Targeting the functional interplay between endoplasmic reticulum oxidoreductin-1α and protein disulfide isomerase suppresses the progression of cervical cancer," *EBioMedicine*, vol. 41, pp. 408–419, 2019.

[81] A. C. Androwiki, L. Camargo Lde, S. Sartoretto et al., "Protein disulfide isomerase expression increases in resistance arteries during hypertension development. Effects on Nox1 NADPH oxidase signaling," *Frontiers in Chemistry*, vol. 3, p. 24, 2015.

[82] M. Janiszewski, L. R. Lopes, A. O. Carmo et al., "Regulation of NAD(P)H oxidase by associated protein disulfide isomerase in vascular smooth muscle cells," *Journal of Biological Chemistry*, vol. 280, no. 49, pp. 40813–40819, 2005.

[83] M. Zana, Z. Péterfi, H. A. Kovács et al., "Interaction between p22^{phox} and Nox4 in the endoplasmic reticulum suggests a unique mechanism of NADPH oxidase complex formation," *Free Radical Biology & Medicine*, vol. 116, pp. 41–49, 2018.

[84] D. R. Davydov, "Microsomal monooxygenase as a multienzyme system: the role of P450-P450 interactions," *Expert Opinion on Drug Metabolism & Toxicology*, vol. 7, no. 5, pp. 543–558, 2011.

[85] J. Rashba-Step and A. I. Cederbaum, "Generation of reactive oxygen intermediates by human liver microsomes in the presence of NADPH or NADH," *Molecular Pharmacology*, vol. 45, no. 1, pp. 150–157, 1994.

[86] S. C. Bondy and S. Naderi, "Contribution of hepatic cytochrome P450 systems to the generation of reactive oxygen species," *Biochemical Pharmacology*, vol. 48, no. 1, pp. 155–159, 1994.

[87] Q. Chen, M. Galleano, and A. I. Cederbaum, "Cytotoxicity and apoptosis produced by arachidonic acid in Hep G2 cells overexpressing human cytochrome P4502E1," *Journal of Biological Chemistry*, vol. 272, no. 23, pp. 14532–14541, 1997.

[88] M. Ingelman-Sundberg, M. J. Ronis, K. O. Lindros, E. Eliasson, and A. Zhukov, "Ethanol-inducible cytochrome P4502E1: regulation, enzymology and molecular biology," *Alcohol and Alcoholism*, vol. 2, pp. 131–139, 1994.

[89] M. Friedkin and D. Roberts, "The enzymatic synthesis of nucleosides. I. Thymidine phosphorylase in mammalian tissue," *Journal of Biological Chemistry*, vol. 207, no. 1, pp. 245–256, 1954.

[90] Y. Y. Elamin, S. Rafee, N. Osman, K. J. O'Byrne, and K. Gately, "Thymidine phosphorylase in cancer; enemy or friend?," *Cancer Microenvironment*, vol. 9, no. 1, pp. 33–43, 2016.

[91] S. Tabata, M. Yamamoto, H. Goto et al., "Thymidine catabolism promotes NADPH oxidase-derived reactive oxygen species (ROS) signalling in KB and yumoto cells," *Scientific Reports*, vol. 8, no. 1, article 6760, 2018.

[92] N. S. Brown, A. Jones, C. Fujiyama, A. L. Harris, and R. Bicknell, "Thymidine phosphorylase induces carcinoma cell oxidative stress and promotes secretion of angiogenic factors," *Cancer Research*, vol. 60, no. 22, pp. 6298–6302, 2000.

[93] A. E. Pegg, "Functions of polyamines in mammals," *Journal of Biological Chemistry*, vol. 291, no. 29, pp. 14904–14912, 2016.

[94] A. E. Pegg, "Mammalian polyamine metabolism and function," *IUBMB Life*, vol. 61, no. 9, pp. 880–894, 2009.

[95] R. A. Casero Jr., T. Murray Stewart, and A. E. Pegg, "Polyamine metabolism and cancer: treatments, challenges and opportunities," *Nature Reviews Cancer*, vol. 18, no. 11, pp. 681–695, 2018.

[96] N. Seiler, "Polyamine metabolism," *Digestion*, vol. 46, no. 2, pp. 319–330, 1990.

[97] A. E. Pegg, "Toxicity of polyamines and their metabolic products," *Chemical Research in Toxicology*, vol. 26, no. 12, pp. 1782–1800, 2013.

[98] H. Xu, R. Chaturvedi, Y. Cheng et al., "Spermine oxidation induced by *Helicobacter pylori* results in apoptosis and DNA damage: implications for gastric carcinogenesis," *Cancer Research*, vol. 64, no. 23, pp. 8521–8525, 2004.

[99] R. Chaturvedi, T. de Sablet, R. M. Peek Jr., and K. T. Wilson, "Spermine oxidase, a polyamine catabolic enzyme that links *Helicobacter pylori* CagA and gastric cancer risk," *Gut Microbes*, vol. 3, no. 1, pp. 48–56, 2012.

[100] R. Chaturvedi, T. de Sablet, M. Asim et al., "Increased *Helicobacter* pylori-associated gastric cancer risk in the Andean region of Colombia is mediated by spermine oxidase," *Oncogene*, vol. 34, no. 26, pp. 3429–3440, 2015.

[101] R. Chaturvedi, M. Asim, M. B. Piazuelo et al., "Activation of EGFR and ERBB2 by *Helicobacter pylori* results in survival of gastric epithelial cells with DNA damage," *Gastroenterology*, vol. 146, no. 7, pp. 1739–1751.e14, 2014.

[102] R. V. Purcell, J. Pearson, A. Aitchison, L. Dixon, F. A. Frizelle, and J. I. Keenan, "Colonization with enterotoxigenic *Bacteroides fragilis* is associated with early-stage colorectal neoplasia," *PLoS One*, vol. 12, no. 2, article e0171602, 2017.

[103] A. C. Goodwin, C. E. D. Shields, S. Wu et al., "Polyamine catabolism contributes to enterotoxigenic *Bacteroides fragilis*-induced colon tumorigenesis," *Proceedings of the National Academy of Sciences of the United States of America*, vol. 108, no. 37, pp. 15354–15359, 2011.

[104] A. V. Snezhkina, G. S. Krasnov, A. V. Lipatova et al., "The dysregulation of polyamine metabolism in colorectal cancer is associated with overexpression of c-Myc and C/EBPβ rather than enterotoxigenic *Bacteroides fragilis* infection," *Oxidative Medicine and Cellular Longevity*, vol. 2016, Article ID 2353560, 11 pages, 2016.

[105] A. C. Goodwin, S. Jadallah, A. Toubaji et al., "Increased spermine oxidase expression in human prostate cancer and prostatic intraepithelial neoplasia tissues," *The Prostate*, vol. 68, no. 7, pp. 766–772, 2008.

[106] O. A. Smirnova, T. A. Keinanen, O. N. Ivanova et al., "Hepatitis C virus alters metabolism of biogenic polyamines by affecting expression of key enzymes of their metabolism," *Biochemical and Biophysical Research Communications*, vol. 483, no. 2, pp. 904–909, 2017.

[107] T. Hu, D. Sun, J. Zhang et al., "Spermine oxidase is upregulated and promotes tumor growth in hepatocellular

carcinoma," *Hepatology Research*, vol. 48, no. 12, pp. 967–977, 2018.

[108] O. N. Ivanova, A. V. Snezhkina, G. S. Krasnov et al., "Activation of polyamine catabolism by N^1,N^{11}-diethylnorspermine in hepatic HepaRG cells induces dedifferentiation and mesenchymal-like phenotype," *Cells*, vol. 7, no. 12, p. 275, 2018.

[109] M. Spotheim-Maurizot, S. Ruiz, R. Sabattier, and M. Charlier, "Radioprotection of DNA by polyamines," *International Journal of Radiation Biology*, vol. 68, no. 5, pp. 571–577, 1995.

[110] H. C. Ha, N. S. Sirisoma, P. Kuppusamy, J. L. Zweier, P. M. Woster, and R. A. Casero Jr., "The natural polyamine spermine functions directly as a free radical scavenger," *Proceedings of the National Academy of Sciences of the United States of America*, vol. 95, no. 19, pp. 11140–11145, 1998.

[111] R. L. Warters, G. L. Newton, P. L. Olive, and R. C. Fahey, "Radioprotection of human cell nuclear DNA by polyamines: radiosensitivity of chromatin is influenced by tightly bound spermine," *Radiation Research*, vol. 151, no. 3, pp. 354–362, 1999.

[112] T. Douki, Y. Bretonniere, and J. Cadet, "Protection against radiation-induced degradation of DNA bases by polyamines," *Radiation Research*, vol. 153, no. 1, pp. 29–35, 2000.

[113] B. G. Feuerstein, N. Pattabiraman, and L. J. Marton, "Spermine-DNA interactions: a theoretical study," *Proceedings of the National Academy of Sciences of the United States of America*, vol. 83, no. 16, pp. 5948–5952, 1986.

[114] H. S. Basu, H. C. A. Schwietert, B. G. Feuerstein, and L. J. Marton, "Effects of variation in the structure of spermine on the association with DNA and the induction of DNA conformational changes," *Biochemical Journal*, vol. 269, no. 2, pp. 329–334, 1990.

[115] E. Pedreno, A. J. Lopez-Contreras, A. Cremades, and R. Penafiel, "Protecting or promoting effects of spermine on DNA strand breakage induced by iron or copper ions as a function of metal concentration," *Journal of Inorganic Biochemistry*, vol. 99, no. 10, pp. 2074–2080, 2005.

[116] Y. Ou, S. J. Wang, D. Li, B. Chu, and W. Gu, "Activation of SAT1 engages polyamine metabolism with p53-mediated ferroptotic responses," *Proceedings of the National Academy of Sciences of the United States of America*, vol. 113, no. 44, pp. E6806–E6812, 2016.

[117] N. Seiler, "Catabolism of polyamines," *Amino Acids*, vol. 26, no. 3, pp. 217–233, 2004.

[118] T. Bieganski, J. Kusche, W. Lorenz, R. Hesterberg, C. D. Stahlknecht, and K. D. Feussner, "Distribution and properties of human intestinal diamine oxidase and its relevance for the histamine catabolism," *Biochimica et Biophysica Acta (BBA) - General Subjects*, vol. 756, no. 2, pp. 196–203, 1983.

[119] G. Houen, "Mammalian Cu-containing amine oxidases (CAOs): new methods of analysis, structural relationships, and possible functions," *APMIS*, vol. 107, no. S96, pp. 5–46, 1999.

[120] A. Keskinege, S. Elgün, and E. Yilmaz, "Possible implications of arginase and diamine oxidase in prostatic carcinoma," *Cancer Detection and Prevention*, vol. 25, no. 1, pp. 76–79, 2001.

[121] J. Y. Lu, Y. Yang, and Y. J. Liang, "Immunohistochemical study on diamine oxidase in mammary cancer and adenosis," *Zhonghua Zhong Liu Za Zhi [Chinese journal of oncology]*, vol. 16, no. 4, pp. 288–290, 1994.

[122] R. Chanda and A. K. Ganguly, "Diamine-oxidase activity and tissue di- and poly-amine contents of human ovarian, cervical and endometrial carcinoma," *Cancer Letters*, vol. 89, no. 1-2, pp. 23–28, 1995.

[123] M. Linsalata, F. Russo, A. Cavallini, P. Berloco, and A. Di Leo, "Polyamines, diamine oxidase, and ornithine decarboxylase activity in colorectal cancer and in normal surrounding mucosa," *Diseases of the Colon and Rectum*, vol. 36, no. 7, pp. 662–667, 1993.

[124] N. E. Borglin and B. Willert, "Increased histaminolytic power of plasma in endometrial adenocarcinoma," *Cancer*, vol. 15, no. 2, pp. 271–275, 1962.

[125] S. B. Baylin, M. D. Abeloff, K. C. Wieman, J. W. Tomford, and D. S. Ettinger, "Elevated histaminase (diamine oxidase) activity in small-cell carcinoma of the lung," *The New England Journal of Medicine*, vol. 293, no. 25, pp. 1286–1290, 1975.

[126] A. C. Andersson, S. Henningsson, and J. Jarhult, "Diamine oxidase activity and γ-aminobutyric acid formation in medullary carcinoma of the thyroid," *Agents and Actions*, vol. 10, no. 4, pp. 299–301, 1980.

[127] T. Namikawa, I. Fukudome, H. Kitagawa, T. Okabayashi, M. Kobayashi, and K. Hanazaki, "Plasma diamine oxidase activity is a useful biomarker for evaluating gastrointestinal tract toxicities during chemotherapy with oral fluorouracil anti-cancer drugs in patients with gastric cancer," *Oncology*, vol. 82, no. 3, pp. 147–152, 2012.

[128] T. Tsujikawa, K. Uda, T. Ihara et al., "Changes in serum diamine oxidase activity during chemotherapy in patients with hematological malignancies," *Cancer Letters*, vol. 147, no. 1-2, pp. 195–198, 1999.

[129] E. Holtta, "Oxidation of spermidine and spermine in rat liver: purification and properties of polyamine oxidase," *Biochemistry*, vol. 16, no. 1, pp. 91–100, 1977.

[130] A. E. Pegg, "Spermidine/spermine-N^1-acetyltransferase: a key metabolic regulator," *American Journal of Physiology-Endocrinology and Metabolism*, vol. 294, no. 6, pp. E995–1010, 2008.

[131] Y. Wang and R. A. Casero Jr., "Mammalian polyamine catabolism: a therapeutic target, a pathological problem, or both?," *Journal of Biochemistry*, vol. 139, no. 1, pp. 17–25, 2006.

[132] Y. Wang, W. Devereux, P. M. Woster, T. M. Stewart, A. Hacker, and R. A. Casero Jr., "Cloning and characterization of a human polyamine oxidase that is inducible by polyamine analogue exposure," *Cancer Research*, vol. 61, no. 14, pp. 5370–5373, 2001.

[133] S. Vujcic, P. Diegelman, C. J. Bacchi, D. L. Kramer, and C. W. Porter, "Identification and characterization of a novel flavin-containing spermine oxidase of mammalian cell origin," *Biochemical Journal*, vol. 367, no. 3, pp. 665–675, 2002.

[134] T. Murray-Stewart, Y. Wang, A. Goodwin, A. Hacker, A. Meeker, and R. A. Casero Jr., "Nuclear localization of human spermine oxidase isoforms - possible implications in drug response and disease etiology," *The FEBS Journal*, vol. 275, no. 11, pp. 2795–2806, 2008.

[135] A. Pledgie, Y. Huang, A. Hacker et al., "Spermine oxidase SMO(PAOh1), Not N^1-acetylpolyamine oxidase PAO, is the primary source of cytotoxic H_2O_2 in polyamine analogue-treated human breast cancer cell lines," *Journal of Biological Chemistry*, vol. 280, no. 48, pp. 39843–39851, 2005.

[136] F. Stirpe and E. Della Corte, "The regulation of rat liver xanthine oxidase. Conversion in vitro of the enzyme activity

from dehydrogenase (type D) to oxidase (type O)," *Journal of Biological Chemistry*, vol. 244, no. 14, pp. 3855–3863, 1969.

[137] T. Nishino and T. Nishino, "The conversion from the dehydrogenase type to the oxidase type of rat liver xanthine dehydrogenase by modification of cysteine residues with fluorodinitrobenzene," *Journal of Biological Chemistry*, vol. 272, no. 47, pp. 29859–29864, 1997.

[138] T. Nishino, K. Okamoto, B. T. Eger, E. F. Pai, and T. Nishino, "Mammalian xanthine oxidoreductase - mechanism of transition from xanthine dehydrogenase to xanthine oxidase," *The FEBS Journal*, vol. 275, no. 13, pp. 3278–3289, 2008.

[139] Z. Zhang, D. R. Blake, C. R. Stevens et al., "A reappraisal of xanthine dehydrogenase and oxidase in hypoxic reperfusion injury: the role of NADH as an electron donor," *Free Radical Research*, vol. 28, no. 2, pp. 151–164, 1998.

[140] C. M. Harris and V. Massey, "The oxidative half-reaction of xanthine dehydrogenase with NAD; reaction kinetics and steady-state mechanism," *Journal of Biological Chemistry*, vol. 272, no. 45, pp. 28335–28341, 1997.

[141] T. M. Millar, C. R. Stevens, N. Benjamin, R. Eisenthal, R. Harrison, and D. R. Blake, "Xanthine oxidoreductase catalyses the reduction of nitrates and nitrite to nitric oxide under hypoxic conditions," *FEBS Letters*, vol. 427, no. 2, pp. 225–228, 1998.

[142] E. Boyland and M. E. Boyland, "Studies in tissue metabolism: lactic dehydrogenase, xanthine oxidase and nucleosidase in tumour and muscle extracts," *Biochemical Journal*, vol. 29, no. 5, pp. 1097–1101, 1935.

[143] M. G. Battelli, L. Polito, M. Bortolotti, and A. Bolognesi, "Xanthine oxidoreductase in cancer: more than a differentiation marker," *Cancer Medicine*, vol. 5, no. 3, pp. 546–557, 2016.

[144] E. Kokoglu, A. Belce, E. Ozyurt, and Z. Tepeler, "Xanthine oxidase levels in human brain tumors," *Cancer Letters*, vol. 50, no. 3, pp. 179–181, 1990.

[145] İ. Durak, C. Ü. Işik, O. Canbolat, Ö. Akyol, and M. Kavutçu, "Adenosine deaminase, 5′ nucleotidase, xanthine oxidase, superoxide dismutase, and catalase activities in cancerous and noncancerous human laryngeal tissues," *Free Radical Biology & Medicine*, vol. 15, no. 6, pp. 681–684, 1993.

[146] H. S. Oztürk, M. Karaayvaz, M. Kacmaz, M. Kavutcu, H. Akgül, and I. Durak, "Activities of the enzymes participating in purine and free-radical metabolism in cancerous human colorectal tissues," *Cancer Biochemistry Biophysics*, vol. 16, no. 1-2, pp. 157–168, 1998.

[147] D. W. Nebert and D. W. Russell, "Clinical importance of the cytochromes P450," *The Lancet*, vol. 360, no. 9340, pp. 1155–1162, 2002.

[148] E. G. Hrycay and S. M. Bandiera, "Monooxygenase, peroxidase and peroxygenase properties and reaction mechanisms of cytochrome P450 enzymes," *Advances in Experimental Medicine and Biology*, vol. 851, pp. 1–61, 2015.

[149] D. Werck-Reichhart and R. Feyereisen, "Cytochromes P450: a success story," *Genome Biology*, vol. 1, no. 6, article reviews3003.1, 2000.

[150] E. G. Hrycay and S. M. Bandiera, "Involvement of cytochrome P450 in reactive oxygen species formation and cancer," *Advances in Pharmacology*, vol. 74, pp. 35–84, 2015.

[151] M. Seliskar and D. Rozman, "Mammalian cytochromes P450—importance of tissue specificity," *Biochimica et Biophysica Acta (BBA) - General Subjects*, vol. 1770, no. 3, pp. 458–466, 2007.

[152] Y. S. Bae, H. Oh, S. G. Rhee, and Y. D. Yoo, "Regulation of reactive oxygen species generation in cell signaling," *Molecules and Cells*, vol. 32, no. 6, pp. 491–509, 2011.

[153] R. C. Zangar, D. R. Davydov, and S. Verma, "Mechanisms that regulate production of reactive oxygen species by cytochrome P450," *Toxicology and Applied Pharmacology*, vol. 199, no. 3, pp. 316–331, 2004.

[154] A. A. Caro and A. I. Cederbaum, "Oxidative stress, toxicology, and pharmacology of CYP2E1," *Annual Review of Pharmacology and Toxicology*, vol. 44, no. 1, pp. 27–42, 2004.

[155] W. D. Landry and T. G. Cotter, "ROS signalling, NADPH oxidases and cancer," *Biochemical Society Transactions*, vol. 42, no. 4, pp. 934–938, 2014.

[156] K. Bedard and K. H. Krause, "The NOX family of ROS-generating NADPH oxidases: physiology and pathophysiology," *Physiological Reviews*, vol. 87, no. 1, pp. 245–313, 2007.

[157] K. Block and Y. Gorin, "Aiding and abetting roles of NOX oxidases in cellular transformation," *Nature Reviews Cancer*, vol. 12, no. 9, pp. 627–637, 2012.

[158] J. N. Moloney, J. Stanicka, and T. G. Cotter, "Subcellular localization of the FLT3-ITD oncogene plays a significant role in the production of NOX- and p22^{phox}-derived reactive oxygen species in acute myeloid leukemia," *Leukemia Research*, vol. 52, pp. 34–42, 2017.

[159] C. T. Tang, X. L. Lin, S. Wu et al., "NOX4-driven ROS formation regulates proliferation and apoptosis of gastric cancer cells through the GLI1 pathway," *Cellular Signalling*, vol. 46, pp. 52–63, 2018.

[160] S. A. Castaldo, A. P. da Silva, A. Matos et al., "The role of CYBA (p22*phox*) and catalase genetic polymorphisms and their possible epistatic interaction in cervical cancer," *Tumour Biology*, vol. 36, no. 2, pp. 909–914, 2015.

[161] H. S. Eun, S. Y. Cho, J. S. Joo et al., "Gene expression of NOX family members and their clinical significance in hepatocellular carcinoma," *Scientific Reports*, vol. 7, no. 1, p. 11060, 2017.

[162] A. Panday, M. K. Sahoo, D. Osorio, and S. Batra, "NADPH oxidases: an overview from structure to innate immunity-associated pathologies," *Cellular & Molecular Immunology*, vol. 12, no. 1, pp. 5–23, 2015.

[163] H. S. Park, H. Y. Jung, E. Y. Park, J. Kim, W. J. Lee, and Y. S. Bae, "Cutting edge: direct interaction of TLR4 with NAD(P)H oxidase 4 isozyme is essential for lipopolysaccharide-induced production of reactive oxygen species and activation of NF-κB," *The Journal of Immunology*, vol. 173, no. 6, pp. 3589–3593, 2004.

[164] J. H. Joo, J. H. Ryu, C. H. Kim et al., "Dual oxidase 2 is essential for the Toll-like receptor 5-mediated inflammatory response in airway mucosa," *Antioxidants & Redox Signaling*, vol. 16, no. 1, pp. 57–70, 2012.

[165] C. S. Yang, D. M. Shin, K. H. Kim et al., "NADPH oxidase 2 interaction with TLR2 is required for efficient innate immune responses to mycobacteria via cathelicidin expression," *The Journal of Immunology*, vol. 182, no. 6, pp. 3696–3705, 2009.

[166] F. Martinon and J. Tschopp, "Inflammatory caspases and inflammasomes: master switches of inflammation," *Cell Death & Differentiation*, vol. 14, no. 1, pp. 10–22, 2007.

[167] F. Bauernfeind, E. Bartok, A. Rieger, L. Franchi, G. Nunez, and V. Hornung, "Cutting edge: reactive oxygen species inhibitors block priming, but not activation, of the NLRP3

inflammasome," *The Journal of Immunology*, vol. 187, no. 2, pp. 613–617, 2011.

[168] S. Lipinski, A. Till, C. Sina et al., "DUOX2-derived reactive oxygen species are effectors of NOD2-mediated antibacterial responses," *Journal of Cell Science*, vol. 122, no. 19, pp. 3522–3530, 2009.

[169] N. S. R. de Mochel, S. Seronello, S. H. Wang et al., "Hepatocyte NAD(P)H oxidases as an endogenous source of reactive oxygen species during hepatitis C virus infection," *Hepatology*, vol. 52, no. 1, pp. 47–59, 2010.

[170] H. E. Boudreau, S. U. Emerson, A. Korzeniowska, M. A. Jendrysik, and T. L. Leto, "Hepatitis C virus (HCV) proteins induce NADPH oxidase 4 expression in a transforming growth factor β-dependent manner: a new contributor to HCV-induced oxidative stress," *Journal of Virology*, vol. 83, no. 24, pp. 12934–12946, 2009.

[171] C. Bureau, J. Bernad, N. Chaouche et al., "Nonstructural 3 protein of hepatitis C virus triggers an oxidative burst in human monocytes via activation of NADPH oxidase," *Journal of Biological Chemistry*, vol. 276, no. 25, pp. 23077–23083, 2001.

[172] F. Thoren, A. Romero, M. Lindh, C. Dahlgren, and K. Hellstrand, "A hepatitis C virus-encoded, nonstructural protein (NS3) triggers dysfunction and apoptosis in lymphocytes: role of NADPH oxidase-derived oxygen radicals," *Journal of Leukocyte Biology*, vol. 76, no. 6, pp. 1180–1186, 2004.

[173] G. Fürstenberger, P. Krieg, K. Müller-Decker, and A. J. R. Habenicht, "What are cyclooxygenases and lipoxygenases doing in the driver's seat of carcinogenesis?," *International Journal of Cancer*, vol. 119, no. 10, pp. 2247–2254, 2006.

[174] C.-M. Kim, J.-Y. Kim, and J.-H. Kim, "Cytosolic phospholipase A_2, lipoxygenase metabolites, and reactive oxygen species," *BMB Reports*, vol. 41, no. 8, pp. 555–559, 2008.

[175] C. Schneider, D. A. Pratt, N. A. Porter, and A. R. Brash, "Control of oxygenation in lipoxygenase and cyclooxygenase catalysis," *Chemistry & Biology*, vol. 14, no. 5, pp. 473–488, 2007.

[176] R. N. Dubois, S. B. Abramson, L. Crofford et al., "Cyclooxygenase in biology and disease," *The FASEB Journal*, vol. 12, no. 12, pp. 1063–1073, 1998.

[177] N. V. Chandrasekharan, H. Dai, K. L. T. Roos et al., "COX-3, a cyclooxygenase-1 variant inhibited by acetaminophen and other analgesic/antipyretic drugs: cloning, structure, and expression," *Proceedings of the National Academy of Sciences of the United States of America*, vol. 99, no. 21, pp. 13926–13931, 2002.

[178] J. M. Schwab, H. J. Schluesener, R. Meyermann, and C. N. Serhan, "COX-3 the enzyme and the concept: steps towards highly specialized pathways and precision therapeutics?," *Prostaglandins, Leukotrienes, and Essential Fatty Acids*, vol. 69, no. 5, pp. 339–343, 2003.

[179] H. Parfenova, V. Levine, W. M. Gunther, M. Pourcyrous, and C. W. Leffler, "COX-1 and COX-2 contributions to basal and IL-1β-stimulated prostanoid synthesis in human neonatal cerebral microvascular endothelial cells," *Pediatric Research*, vol. 52, no. 3, pp. 342–348, 2002.

[180] T. Kuwano, S. Nakao, H. Yamamoto et al., "Cyclooxygenase 2 is a key enzyme for inflammatory cytokine-induced angiogenesis," *The FASEB Journal*, vol. 18, no. 2, pp. 300–310, 2004.

[181] E. Fosslien, "Molecular pathology of cyclooxygenase-2 in neoplasia," *Annals of Clinical and Laboratory Science*, vol. 30, no. 1, pp. 3–21, 2000.

[182] P. J. Bostrom, V. Aaltonen, K. O. Soderstrom, P. Uotila, and M. Laato, "Expression of cyclooxygenase-1 and -2 in urinary bladder carcinomas *in vivo* and *in vitro* and prostaglandin E_2 synthesis in cultured bladder cancer cells," *Pathology*, vol. 33, no. 4, pp. 469–474, 2001.

[183] S. Tomozawa, N. H. Tsuno, E. Sunami et al., "Cyclooxygenase-2 overexpression correlates with tumour recurrence, especially haematogenous metastasis, of colorectal cancer," *British Journal of Cancer*, vol. 83, no. 3, pp. 324–328, 2000.

[184] M. K. Sackett, I. Bairati, F. Meyer et al., "Prognostic significance of cyclooxygenase-2 overexpression in glottic cancer," *Clinical Cancer Research*, vol. 14, no. 1, pp. 67–73, 2008.

[185] D. Hwang, D. Scollard, J. Byrne, and E. Levine, "Expression of cyclooxygenase-1 and cyclooxygenase-2 in human breast cancer," *Journal of the National Cancer Institute*, vol. 90, no. 6, pp. 455–460, 1998.

[186] K. J. Sales, A. A. Katz, B. Howard, R. P. Soeters, R. P. Millar, and H. N. Jabbour, "Cyclooxygenase-1 is up-regulated in cervical carcinomas: autocrine/paracrine regulation of cyclooxygenase-2, prostaglandin e receptors, and angiogenic factors by cyclooxygenase-1," *Cancer Research*, vol. 62, no. 2, pp. 424–432, 2002.

[187] A. J. Wilson, O. Fadare, A. Beeghly-Fadiel et al., "Aberrant over-expression of COX-1 intersects multiple protumorigenic pathways in high-grade serous ovarian cancer," *Oncotarget*, vol. 6, no. 25, pp. 21353–21368, 2015.

[188] T. Sugimoto, T. Koizumi, T. Sudo et al., "Correlative expression of cyclooxygenase-1 (Cox-1) and human epidermal growth factor receptor type-2 (Her-2) in endometrial cancer," *The Kobe Journal of Medical Sciences*, vol. 53, no. 5, pp. 177–187, 2007.

[189] S. Sankhasard, N. Lertprasertsuk, U. Vinitketkumnuen, and R. Cressey, "Expression of cyclooxygenase-1 and -2 and clinicopathologic features of colorectal cancer in northern Thailand," *Asian Pacific Journal of Cancer Prevention*, vol. 5, no. 1, pp. 44–49, 2004.

[190] S. Chariyalertsak, V. Sirikulchayanonta, D. Mayer et al., "Aberrant cyclooxygenase isozyme expression in human intrahepatic cholangiocarcinoma," *Gut*, vol. 48, no. 1, pp. 80–86, 2001.

[191] A. W. Bach, N. C. Lan, D. L. Johnson et al., "cDNA cloning of human liver monoamine oxidase A and B: molecular basis of differences in enzymatic properties," *Proceedings of the National Academy of Sciences of the United States of America*, vol. 85, no. 13, pp. 4934–4938, 1988.

[192] D. E. Edmondson, C. Binda, J. Wang, A. K. Upadhyay, and A. Mattevi, "Molecular and mechanistic properties of the membrane-bound mitochondrial monoamine oxidases," *Biochemistry*, vol. 48, no. 20, pp. 4220–4230, 2009.

[193] R. R. Ramsay and A. Albreht, "Kinetics, mechanism, and inhibition of monoamine oxidase," *Journal of Neural Transmission*, vol. 125, no. 11, pp. 1659–1683, 2018.

[194] P. F. Fitzpatrick, "Oxidation of amines by flavoproteins," *Archives of Biochemistry and Biophysics*, vol. 493, no. 1, pp. 13–25, 2010.

[195] M. Bortolato, K. Chen, and J. C. Shih, "Monoamine oxidase inactivation: from pathophysiology to therapeutics,"

Advanced Drug Delivery Reviews, vol. 60, no. 13-14, pp. 1527–1533, 2008.

[196] D. Maggiorani, N. Manzella, D. E. Edmondson et al., "Mono-amine oxidases, oxidative stress, and altered mitochondrial dynamics in cardiac ageing," *Oxidative Medicine and Cellular Longevity*, vol. 2017, Article ID 3017947, 8 pages, 2017.

[197] J. B. Wu, C. Shao, X. Li et al., "Monoamine oxidase A mediates prostate tumorigenesis and cancer metastasis," *The Journal of Clinical Investigation*, vol. 124, no. 7, pp. 2891–2908, 2014.

[198] F. Liu, L. Hu, Y. Ma et al., "Increased expression of mono-amine oxidase A is associated with epithelial to mesenchymal transition and clinicopathological features in non-small cell lung cancer," *Oncology Letters*, vol. 15, no. 3, pp. 3245–3251, 2018.

[199] L. True, I. Coleman, S. Hawley et al., "A molecular correlate to the Gleason grading system for prostate adenocarcinoma," *Proceedings of the National Academy of Sciences of the United States of America*, vol. 103, no. 29, pp. 10991–10996, 2006.

[200] W. Y. Sun, J. Choi, Y. J. Cha, and J. S. Koo, "Evaluation of the expression of amine oxidase proteins in breast cancer," *International Journal of Molecular Sciences*, vol. 18, no. 12, p. 2775, 2017.

[201] D. M. Peehl, M. Coram, H. Khine, S. Reese, R. Nolley, and H. Zhao, "The significance of monoamine oxidase-A expression in high grade prostate cancer," *The Journal of Urology*, vol. 180, no. 5, pp. 2206–2211, 2008.

[202] J. Li, X. M. Yang, Y. H. Wang et al., "Monoamine oxidase A suppresses hepatocellular carcinoma metastasis by inhibiting the adrenergic system and its transactivation of EGFR signaling," *Journal of Hepatology*, vol. 60, no. 6, pp. 1225–1234, 2014.

[203] L. Huang, G. Frampton, A. Rao et al., "Monoamine oxidase A expression is suppressed in human cholangiocarcinoma via coordinated epigenetic and IL-6-driven events," *Laboratory Investigation*, vol. 92, no. 10, pp. 1451–1460, 2012.

[204] L. A. Rybaczyk, M. J. Bashaw, D. R. Pathak, and K. Huang, "An indicator of cancer: downregulation of monoamine oxidase-A in multiple organs and species," *BMC Genomics*, vol. 9, no. 1, p. 134, 2008.

[205] A. K. Sood, R. Bhatty, A. A. Kamat et al., "Stress hormone-mediated invasion of ovarian cancer cells," *Clinical Cancer Research*, vol. 12, no. 2, pp. 369–375, 2006.

[206] K. S. R. Sastry, Y. Karpova, S. Prokopovich et al., "Epineph-rine protects cancer cells from apoptosis via activation of cAMP-dependent protein kinase and BAD phosphorylation," *Journal of Biological Chemistry*, vol. 282, no. 19, pp. 14094–14100, 2007.

[207] X. Grau-Bove, I. Ruiz-Trillo, and F. Rodriguez-Pascual, "Ori-gin and evolution of lysyl oxidases," *Scientific Reports*, vol. 5, no. 1, article 10568, 2015.

[208] J. Xu, D. Li, X. Li et al., "67 laminin receptor promotes the malignant potential of tumour cells up-regulating lysyl oxidase-like 2 expression in cholangiocarcinoma," *Digestive and Liver Disease*, vol. 46, no. 8, pp. 750–757, 2014.

[209] J. S. Park, J. H. Lee, Y. S. Lee, J. K. Kim, S. M. Dong, and D. S. Yoon, "Emerging role of LOXL2 in the promotion of pan-creas cancer metastasis," *Oncotarget*, vol. 7, no. 27, pp. 42539–42552, 2016.

[210] Y. H. Shih, K. W. Chang, M. Y. Chen et al., "Lysyl oxidase and enhancement of cell proliferation and angiogenesis in oral

[211] A. Albinger-Hegyi, S. J. Stoeckli, S. Schmid et al., "Lysyl oxi-dase expression is an independent marker of prognosis and a predictor of lymph node metastasis in oral and oropharyn-geal squamous cell carcinoma (OSCC)," *International Journal of Cancer*, vol. 126, no. 11, pp. 2653–2662, 2010.

[212] L. Peng, Y. L. Ran, H. Hu et al., "Secreted LOXL2 is a novel therapeutic target that promotes gastric cancer metastasis via the Src/FAK pathway," *Carcinogenesis*, vol. 30, no. 10, pp. 1660–1669, 2009.

[213] N. Scola and T. Gorogh, "LOXL4 as a selective molecular marker in primary and metastatic head/neck carcinoma," *Anticancer Research*, vol. 30, no. 11, pp. 4567–4571, 2010.

[214] C. Leo, C. Cotic, V. Pomp, D. Fink, and Z. Varga, "Overex-pression of Lox in triple-negative breast cancer," *Annals of Diagnostic Pathology*, vol. 34, pp. 98–102, 2018.

[215] A. Nakanishi, Y. Wada, Y. Kitagishi, and S. Matsuda, "Link between PI3K/AKT/PTEN Pathway and NOX Proteinin Dis-eases," *Aging and Disease*, vol. 5, no. 3, pp. 203–211, 2014.

[216] V. Alvarez-Garcia, Y. Tawil, H. M. Wise, and N. R. Leslie, "Mechanisms of PTEN loss in cancer: it's all about diversity," *Seminars in Cancer Biology*, 2019.

[217] N. Chalhoub and S. J. Baker, "PTEN and the PI3-kinase path-way in cancer," *Annual Review of Pathology*, vol. 4, no. 1, pp. 127–150, 2009.

[218] J. El-Benna, P. M. C. Dang, M. A. Gougerot-Pocidalo, J. C. Marie, and F. Braut-Boucher, "p47phox, the phagocyte NADPH oxidase/NOX2 organizer: structure, phosphoryla-tion and implication in diseases," *Experimental & Molecular Medicine*, vol. 41, no. 4, pp. 217–225, 2009.

[219] N. R. Leslie, D. Bennett, Y. E. Lindsay, H. Stewart, A. Gray, and C. P. Downes, "Redox regulation of PI 3-kinase signalling via inactivation of PTEN," *The EMBO Journal*, vol. 22, no. 20, pp. 5501–5510, 2003.

[220] R. Rastogi, X. Geng, F. Li, and Y. Ding, "NOX activation by subunit interaction and underlying mechanisms in disease," *Frontiers in Cellular Neuroscience*, vol. 10, p. 301, 2017.

[221] K. K. Haagenson and G. S. Wu, "Mitogen activated protein kinase phosphatases and cancer," *Cancer Biology & Therapy*, vol. 9, no. 5, pp. 337–340, 2010.

[222] A. Caretta and C. Mucignat-Caretta, "Protein kinase a in cancer," *Cancers*, vol. 3, no. 1, pp. 913–926, 2011.

[223] R. Kumar, A. E. Gururaj, and C. J. Barnes, "p21-activated kinases in cancer," *Nature Reviews Cancer*, vol. 6, no. 6, pp. 459–471, 2006.

[224] B. Vurusaner, G. Poli, and H. Basaga, "Tumor suppressor genes and ROS: complex networks of interactions," *Free Radical Biology & Medicine*, vol. 52, no. 1, pp. 7–18, 2012.

[225] S. P. Hussain, P. Amstad, P. He et al., "p53-induced up-regulation of MnSOD and GPx but not catalase increases oxidative stress and apoptosis," *Cancer Research*, vol. 64, no. 7, pp. 2350–2356, 2004.

[226] M. Tan, S. Li, M. Swaroop, K. Guan, L. W. Oberley, and Y. Sun, "Transcriptional activation of the human glutathione peroxidase promoter by p53," *Journal of Biological Chemistry*, vol. 274, no. 17, pp. 12061–12066, 1999.

[227] A. V. Budanov, A. A. Sablina, E. Feinstein, E. V. Koonin, and P. M. Chumakov, "Regeneration of peroxiredoxins by p53-regulated sestrins, homologs of bacterial AhpD," *Science*, vol. 304, no. 5670, pp. 596–600, 2004.

[228] S. Suzuki, T. Tanaka, M. V. Poyurovsky et al., "Phosphate-activated glutaminase (GLS2), a p53-inducible regulator of glutamine metabolism and reactive oxygen species," *Proceedings of the National Academy of Sciences of the United States of America*, vol. 107, no. 16, pp. 7461–7466, 2010.

[229] K. Bensaad, A. Tsuruta, M. A. Selak et al., "TIGAR, a p53-inducible regulator of glycolysis and apoptosis," *Cell*, vol. 126, no. 1, pp. 107–120, 2006.

[230] C. A. Hu, W. W. Lin, and D. Valle, "Cloning, characterization, and expression of cDNAs encoding human Δ_1-pyrroline-5-carboxylate dehydrogenase," *Journal of Biological Chemistry*, vol. 271, no. 16, pp. 9795–9800, 1996.

[231] K. A. Yoon, Y. Nakamura, and H. Arakawa, "Identification of ALDH4 as a p53-inducible gene and its protective role in cellular stresses," *Journal of Human Genetics*, vol. 49, no. 3, pp. 134–140, 2004.

[232] Z. Liu, H. Lu, H. Shi et al., "PUMA overexpression induces reactive oxygen species generation and proteasome-mediated stathmin degradation in colorectal cancer cells," *Cancer Research*, vol. 65, no. 5, pp. 1647–1654, 2005.

[233] M. Giorgio, E. Migliaccio, F. Orsini et al., "Electron transfer between cytochrome c and p66^Shc generates reactive oxygen species that trigger mitochondrial apoptosis," *Cell*, vol. 122, no. 2, pp. 221–233, 2005.

[234] K. Polyak, Y. Xia, J. L. Zweier, K. W. Kinzler, and B. Vogelstein, "A model for p53-induced apoptosis," *Nature*, vol. 389, no. 6648, pp. 300–305, 1997.

[235] A. A. Sablina, A. V. Budanov, G. V. Ilyinskaya, L. S. Agapova, J. E. Kravchenko, and P. M. Chumakov, "The antioxidant function of the p53 tumor suppressor," *Nature Medicine*, vol. 11, no. 12, pp. 1306–1313, 2005.

[236] M. G. Vander Heiden, L. C. Cantley, and C. B. Thompson, "Understanding the Warburg effect: the metabolic requirements of cell proliferation," *Science*, vol. 324, no. 5930, pp. 1029–1033, 2009.

[237] O. Warburg, "On the origin of cancer cells," *Science*, vol. 123, no. 3191, pp. 309–314, 1956.

[238] X. Tong, F. Zhao, and C. B. Thompson, "The molecular determinants of de novo nucleotide biosynthesis in cancer cells," *Current Opinion in Genetics & Development*, vol. 19, no. 1, pp. 32–37, 2009.

[239] C. M. Labak, P. Y. Wang, R. Arora et al., "Glucose transport: meeting the metabolic demands of cancer, and applications in glioblastoma treatment," *American Journal of Cancer Research*, vol. 6, no. 8, pp. 1599–1608, 2016.

[240] E. A. Pudova, A. V. Kudryavtseva, M. S. Fedorova et al., "HK3 overexpression associated with epithelial-mesenchymal transition in colorectal cancer," *BMC Genomics*, vol. 19, Supplement 3, p. 113, 2018.

[241] G. S. Krasnov, A. A. Dmitriev, A. F. Sadtritdinova et al., "Evaluation of gene expression of hexokinases in colorectal cancer with the use of bioinformatics methods," *Biofizika*, vol. 60, no. 6, pp. 1050–1056, 2015.

[242] N. Y. Oparina, A. V. Snezhkina, A. F. Sadritdinova et al., "Differential expression of genes that encode glycolysis enzymes in kidney and lung cancer in humans," *Russian Journal of Genetics*, vol. 49, no. 7, pp. 707–716, 2013.

[243] G. S. Krasnov, A. A. Dmitriev, A. V. Snezhkina, and A. V. Kudryavtseva, "Deregulation of glycolysis in cancer: glyceraldehyde-3-phosphate dehydrogenase as a therapeutic target," *Expert Opinion on Therapeutic Targets*, vol. 17, no. 6, pp. 681–693, 2013.

[244] A. V. Snezhkina, G. S. Krasnov, S. O. Zhikrivetskaya et al., "Overexpression of microRNAs miR-9,-98, and-199 correlates with the downregulation of HK2 expression in colorectal cancer," *Molecular Biology*, vol. 52, no. 2, pp. 190–199, 2018.

[245] A. V. Snezhkina, G. S. Krasnov, A. R. Zaretsky et al., "Differential expression of alternatively spliced transcripts related to energy metabolism in colorectal cancer," *BMC Genomics*, vol. 17, Supplement 14, p. 1011, 2016.

[246] M. S. Fedorova, A. V. Kudryavtseva, V. A. Lakunina et al., "Downregulation of OGDHL expression is associated with promoter hypermethylation in colorectal cancer," *Molecular Biology*, vol. 49, no. 4, pp. 608–617, 2015.

[247] M. Lee and J. H. Yoon, "Metabolic interplay between glycolysis and mitochondrial oxidation: the reverse Warburg effect and its therapeutic implication," *World Journal of Biological Chemistry*, vol. 6, no. 3, pp. 148–161, 2015.

[248] P. J. Fernandez-Marcos and S. Nobrega-Pereira, "NADPH: new oxygen for the ROS theory of aging," *Oncotarget*, vol. 7, no. 32, pp. 50814-50815, 2016.

[249] R. C. Stanton, "Glucose-6-phosphate dehydrogenase, NADPH, and cell survival," *IUBMB Life*, vol. 64, no. 5, pp. 362–369, 2012.

[250] D. Holten, D. Procsal, and H. L. Chang, "Regulation of pentose phosphate pathway dehydrogenases by NADP^+/-NADPH ratios," *Biochemical and Biophysical Research Communications*, vol. 68, no. 2, pp. 436–441, 1976.

[251] E. Mullarky and L. C. Cantley, "Diverting glycolysis to combat oxidative stress," in *Innovative Medicine: Basic Research and Development*, K. Nakao, N. Minato, and S. Uemoto, Eds., pp. 3–23, Springer, Tokyo, 2015.

[252] Z. Ghanbari Movahed, M. Rastegari-Pouyani, M. H. Mohammadi, and K. Mansouri, "Cancer cells change their glucose metabolism to overcome increased ROS: One step from cancer cell to cancer stem cell?," *Biomedicine & Pharmacotherapy*, vol. 112, article 108690, 2019.

[253] X. Chen, M. Song, B. Zhang, and Y. Zhang, "Reactive oxygen species regulate T cell immune response in the tumor microenvironment," *Oxidative Medicine and Cellular Longevity*, vol. 2016, Article ID 1580967, 10 pages, 2016.

[254] T. L. Whiteside, "The tumor microenvironment and its role in promoting tumor growth," *Oncogene*, vol. 27, no. 45, pp. 5904–5912, 2008.

[255] P. Carmeliet and R. K. Jain, "Molecular mechanisms and clinical applications of angiogenesis," *Nature*, vol. 473, no. 7347, pp. 298–307, 2011.

[256] J. Frisch, A. Angenendt, M. Hoth, L. Prates Roma, and A. Lis, "STIM-Orai channels and reactive oxygen species in the tumor microenvironment," *Cancers*, vol. 11, no. 4, p. 457, 2019.

[257] R. Bhome, M. D. Bullock, H. A. Al Saihati et al., "A top-down view of the tumor microenvironment: structure, cells and signaling," *Frontiers in Cell and Developmental Biology*, vol. 3, p. 33, 2015.

[258] M. Wang, J. Zhao, L. Zhang et al., "Role of tumor microenvironment in tumorigenesis," *Journal of Cancer*, vol. 8, no. 5, pp. 761–773, 2017.

[259] Y. Sun, "Tumor microenvironment and cancer therapy resistance," *Cancer Letters*, vol. 380, no. 1, pp. 205–215, 2016.

[260] Y. Yu and J. Cui, "Present and future of cancer immunotherapy: a tumor microenvironmental perspective," *Oncology Letters*, vol. 16, no. 4, pp. 4105–4113, 2018.

[261] G. P. Bienert, J. K. Schjoerring, and T. P. Jahn, "Membrane transport of hydrogen peroxide," *Biochimica et Biophysica Acta (BBA) - Biomembranes*, vol. 1758, no. 8, pp. 994–1003, 2006.

[262] T. Henzler and E. Steudle, "Transport and metabolic degradation of hydrogen peroxide in *Chara corallina*: model calculations and measurements with the pressure probe suggest transport of H_2O_2 across water channels," *Journal of Experimental Botany*, vol. 51, no. 353, pp. 2053–2066, 2000.

[263] M. Hara-Chikuma, H. Satooka, S. Watanabe et al., "Aquaporin-3-mediated hydrogen peroxide transport is required for NF-κB signalling in keratinocytes and development of psoriasis," *Nature Communications*, vol. 6, no. 1, article 7454, 2015.

[264] M. O. Laukkanen, "Extracellular superoxide dismutase: growth promoter or tumor suppressor?," *Oxidative Medicine and Cellular Longevity*, vol. 2016, Article ID 3612589, 9 pages, 2016.

[265] W. M. Nauseef, "Detection of superoxide anion and hydrogen peroxide production by cellular NADPH oxidases," *Biochimica et Biophysica Acta (BBA) - General Subjects*, vol. 1840, no. 2, pp. 757–767, 2014.

[266] G. Bauer, "Targeting extracellular ROS signaling of tumor cells," *Anticancer Research*, vol. 34, no. 4, pp. 1467–1482, 2014.

[267] J. S. K. Chan, M. J. Tan, M. K. Sng et al., "Cancer-associated fibroblasts enact field cancerization by promoting extratumoral oxidative stress," *Cell Death & Disease*, vol. 8, no. 1, article e2562, 2018.

[268] L. M. Paardekooper, W. Vos, and G. Bogaart, "Oxygen in the tumor microenvironment: effects on dendritic cell function," *Oncotarget*, vol. 10, no. 8, pp. 883–896, 2019.

[269] E. Birben, U. M. Sahiner, C. Sackesen, S. Erzurum, and O. Kalayci, "Oxidative stress and antioxidant defense," *The World Allergy Organization Journal*, vol. 5, no. 1, pp. 9–19, 2012.

[270] A. N. Onyango, "Endogenous generation of singlet oxygen and ozone in human and animal tissues: mechanisms, biological significance, and influence of dietary components," *Oxidative Medicine and Cellular Longevity*, vol. 2016, Article ID 2398573, 22 pages, 2016.

Research Article

Therapeutic Effect of the Mitochondria-Targeted Antioxidant SkQ1 on the Culture Model of Multiple Sclerosis

Elena K. Fetisova, Maria S. Muntyan ⓘ **, Konstantin G. Lyamzaev, and Boris V. Chernyak** ⓘ

A.N. Belozersky Institute of Physico-Chemical Biology, Lomonosov Moscow State University, Moscow, Russia

Correspondence should be addressed to Maria S. Muntyan; muntyan@genebee.msu.ru

Multiple sclerosis (MS) is a heterogeneous autoimmune disease of unknown etiology characterized by inflammation, demyelination, and axonal degeneration that affects both the white and gray matter of CNS. Recent large-scale epidemiological and genomic studies identified several genetic and environmental risk factors for the disease. Among them are environmental factors of infectious origin, possibly causing MS, which include Epstein-Barr virus infection, reactivation of some endogenous retrovirus groups, and infection by pathogenic bacteria (mycobacteria, *Chlamydia pneumoniae*, and *Helicobacter pylori*). However, the nature of the events leading to the activation of immune cells in MS is mostly unknown and there is no effective therapy against the disease. Amazingly, whatever the cause of the disease, signs of damage to the nerve tissue with MS lesions were the same as with infectious leprosy, while in the latter case nitrozooxidative stress was suggested as the main cause of the nerve damage. With this in mind and following the hypothesis that excessive production of mitochondrial reactive oxygen species critically contributes to MS pathogenesis, we studied the effect of mitochondria-targeted antioxidant SkQ1 in an *in vitro* MS model of the primary oligodendrocyte culture of the cerebellum, challenged with lipopolysaccharide (LPS). SkQ1 was found to accumulate in the mitochondria of oligodendrocytes and microglial cells, and it was also found to prevent LPS-induced inhibition of myelin production in oligodendrocytes. The results implicate that mitochondria-targeted antioxidants could be promising candidates as components of a combined therapy for MS and related neurological disorders.

1. Introduction

Typical multiple sclerosis (MS) is a widespread chronic inflammatory demyelinating disease of the central nervous system (CNS), a hallmark of which is considered the demyelination of cerebral white matter and a consequent progressive neuronal loss and neurological disability. The etiology of MS is multifactorial and usually associated with autoimmune processes, but it remains not clear as of now [1]. During the last decades, a significant body of data indicated a critical contribution of mitochondria and oxidative stress to both inflammatory and neurodegenerative aspects of MS pathogenesis [2]. The recent observation of the sharp appearance of the free mitochondrial DNA in the serum of patients with MS at the onset of the disease also supports this view [3].

In this context, it should be noted that myelin-producing glial cells called oligodendrocytes are particularly susceptible to oxidative stress and inflammatory mediators [4–6] and are one of the main targets of MS. All of these led us to suggest that mitochondria-targeted antioxidants (mtAO), detoxifying mitochondrial reactive oxygen species (mtROS), could be promising components of combined programs for MS therapy. Among mtAO, the most widely used is MitoQ 10-(6′-ubiquinonyl) decyltriphenylphosphonium bromide, which has been shown to inhibit oxidative stress in nervous tissue in various animal models of neurological diseases, including Alzheimer's [7] and Parkinson's [8] diseases, as well as amyotrophic lateral sclerosis [9]. Application of MitoQ to experimental autoimmune encephalomyelitis (EAE), a mouse model of MS, demonstrated an increase

in myelin basic protein (MBP) production and attenuation of neurodegeneration [10]. Developed in 2008, mtAO compounds of the SkQ family (conjugates of plastoquinol with various penetrating cations [11, 12]) were found to be more effective than MitoQ in various in vitro models of diseases. The pronounced protective effects of SkQ1 (10-(6′-plastoquinonyl) decyltriphenylphosphonium) and its analogs were observed in the model of open focal trauma of the sensorimotor cortex [13] and in the model of brain ischemia/reperfusion injury [14]. SkQ1 significantly improved neurological deficits in the senescence-accelerated OXYS rats, which in various aspects resembled symptoms of Alzheimer's disease. The long-term treatment with SkQ1 slowed down the pathological accumulation of beta-amyloid and the hyperphosphorylation of tau protein (markers of Alzheimer's disease pathogenesis) in the cortex and hippocampus of OXYS rats [15, 16].

In MS therapy, the protection of oligodendrocytes from oxidative stress could be a key strategy that can ensure the maturation of immature oligodendrocytes and their remyelinization, as well as increase the chances of improving the neurological state of patients [17]. In the present study, we made the first step to test the effect of SkQ1 on oligodendrocytes in vitro and used for this purpose the primary oligodendrocyte culture that migrated from cerebellar explants, which was challenged with lipopolysaccharide (LPS). This culture also contains microglia [18], in which the effects of LPS are mediated in at least two ways: (i) at low LPS concentrations (1 ng/ml) by specific toll-like receptor TLR4, which is not expressed in oligodendrocytes [19, 20], and (ii) at LPS concentrations two or three orders of magnitude higher by a TLR4-independent pathway [21]. An important advantage of the used culture model is the preservation of conditions for the survival (and maturation) of oligodendrocyte progenitor cells, as well as mature myelinating oligodendrocytes. The challenge of the culture with LPS recapitulates various features of brain inflammation including oxidative stress, demyelination, and axonal damage [22, 23]. These features of the used primary oligodendrocyte culture of cerebellar explants make it suitable for the examination of various agents affecting the myelination/demyelination of oligodendrocytes. In the present study, we demonstrated that SkQ1 in as low as nanomolar concentrations significantly inhibited an LPS-induced decrease in myelin content in oligodendrocytes.

2. Materials and Methods

2.1. Reagents.
LPS from *E. coli* (# 055:B5) was purchased from Sigma-Aldrich (USA). Mitochondria-targeted antioxidant SkQ1 (10-(6′-plastoquinonyl) decyltriphenylphosphonium bromide) was synthesized as described earlier [11] and kindly provided by the Institute of Mitoengineering, Lomonosov Moscow State University. For immunostaining, the following antibodies were used: rabbit polyclonal anti-beta III tubulin antibody (Abcam, ab76287), a neuronal marker; mouse anti-Oligo1 monoclonal antibody (# MAB5540; Millipore, USA) against oligodendrocyte transcription factor; antibody against myelin basic protein (MBP) (# M3821

Sigma-Aldrich); anti-iNOS antibody against inducible NO-synthase (Abcam, ab3523), and Alexa Fluor 488-conjugated anti-IgG (Invitrogen, USA).

2.2. Preparation of the Primary Oligodendrocyte Cell Cultures.
The primary oligodendrocyte cell cultures were formed by the cells that migrated from the cerebellar explants which were prepared from the brains of newborn rats (1–2 days old) and cultivated according to the method of Viktorov and Kernarskaya [24]. Cerebellum fragments (1×1 mm) were plated upon poly-D-lysine-coated, 5 μg/ml (Sigma-Aldrich) coverslips placed inside Petri dishes filled with nutrient medium where the cultivation was performed at 37°C in an air atmosphere containing 5% CO_2. The nutrient medium was composed of DMEM containing glucose 4.5 g/l (Dulbecco's Modified Eagle's Medium) and F12 (Ham's Medium) at a ratio of 1:1 (v/v), supplemented with 24% fetal bovine sera, 9% embrional chicken extract, and 5 mM glutamine, where all reagents and solutions were from PanEco, Russia. Additionally, the nutrient medium was supplemented with 10 μM acetylsalicylic acid (Sigma-Aldrich), 0.5 μg/ml insulin (Sigma-Aldrich), streptomycin (100 U/ml), and penicillin (100 U/ml). Every 2-3 days, the medium was replaced for a fresh one.

2.3. Investigation of the Primary Oligodendrocyte Cell Cultures.
Myelin synthesis by oligodendrocytes was analyzed by probing the cultures with rabbit antibody to MBP. Cultures were treated with 5 nM SkQ1 solution for 10 days and with 10 nM SkQ1 solution for the last 2 days of cultivation. LPS (5 μg/ml) was added from the third day of cultivation for 10 days and removed for the last 2 days of cultivation.

2.4. Immunostaining.
Before immunostaining, cells grown on glass coverslips were fixed with 1% formaldehyde in phosphate-buffered saline solution (PBS) for 1.5 hours at room temperature to ensure thorough fixation essential for preventing the fragments from being detached. Thereafter, these preparations were rinsed with PBS and initially stained with the following antibodies: anti-Oligo1 antibody for oligodendrocytes, anti-beta III tubulin antibody for neurons, antibody against MBP, and antibody against iNOS. Alexa-Fluor-488-conjugated secondary antibodies were used after processing with the primary antibodies. Immunofluorescence was observed and analyzed with an LSM 510 confocal microscope (Carl Zeiss, Germany) using optical filters "555 nm" (red) and "488 nm" (green).

2.5. Statistical Analysis.
For statistical analyses, one-way ANOVA followed by Bonferroni's test was performed using GraphPad Prism version 6.01 for Windows (GraphPad Software, La Jolla California USA, http://www.graphpad.com). A p value of <0.05 was considered statistically significant.

3. Results and Discussion

In the present study, we used the explant culture of newborn rat cerebellum (1) for the preparation the primary culture of oligodendrocytes (2), both cultures, (1) and (2), being formed on the same glass coverslip (Figure 1(a)). The primary

(a)

(b)

Anti-oligo1

(c)

Anti-beta III tubulin


(d)

Merge

(e)

(f)
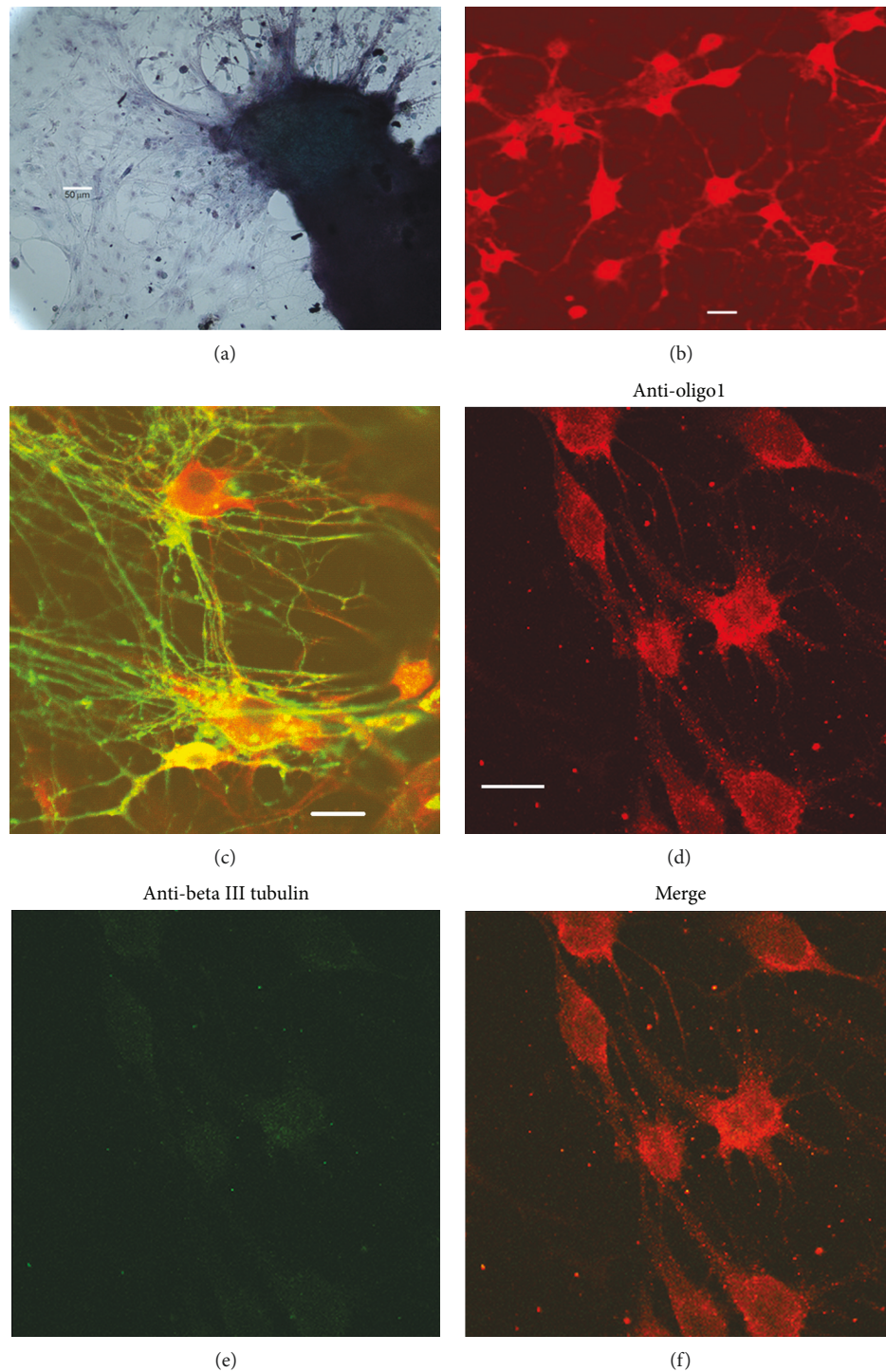
FIGURE 1: Determination of the cell types forming the migration zone in the primary oligodendrocyte culture of cerebellar explants upon 10 days of cultivation. (a) Cultured oligodendrocytes of a newborn rat: general view of the culture. The cells radially migrate from the explant of the cerebellum (dark-gray fragment on the right side) *in vitro*. Bar, 50 μm; transmitted-light microscopy; objective—10x. (b) The field of view within the formed migration zone. The cells were probed with anti-Oligo1 antibody. (c) Myelin synthesis by oligodendrocytes; merged image; probing with both antibody types, anti-Oligo1 to mark oligodendrocytes (red) and antibodies to MBP to mark myelin (green). (d–f) The cells were probed with both types of antibodies, anti-Oligo1 antibody for oligodendrocytes (positive result, red) and anti-beta III tubulin antibody for neurons (negative result, green). (b–f) Bar, 10 μm; confocal microscope, Carl Zeiss LSM 510.

culture of oligodendrocytes in this case is formed in the process of emigration of cells from the explant for 10-14 days, which leads to the formation of a cell monolayer on the same coverslip as can be seen by staining the cultures with the specific antibody, the marker of oligodendrocytes, Oligo1 (Figures 1(b)–1(d) and 1(f)). Oligodendroglia is the first to

emigrate from the explant due to the mobility of oligodendrocytes and the ability of cells to change their shape and size, which was well documented by several authors [18, 25, 26]. In our study, we confirm these observations of the mentioned authors and demonstrate that the first emigrants formed the cell layer presented practically only by oligodendrocytes (Figures 1(b)–1(f)). Neither neuron cells nor other types of cells were detected in these monolayers. The positively Oligo1-stained cells of irregular shape and relatively large sizes were forming the cell-to-cell chains characteristic of oligodendrocytes, which resemble "being engaged in a tug-of-war" [26]. The barely perceptible "green" signal (Figure 1(e)) on staining with the anti-beta III tubulin antibody (marker of neurons) fully coincides with the bright "red" signal of anti-Oligo1 identifying only oligodendrocytes present in the field. Thus, the poor "green" signal is the background staining and the absence of bright "green" demonstrates the lack of neurons in the monolayer field of the migration zone in accordance with the observations made earlier [26, 27]. Moreover, the absence of the "green" background staining shows as well the lack of any other cell types in this migration zone which apparently is inhabited mainly by oligodendrocytes. However, the primary explant culture of oligodendrocytes is formed on the same surface as the cerebellar explant itself. Note that although cultures (1) and (2) are spatially separated as they are located on the different parts of the coverslip, the layer of the emigrated cells and the parent explant are covered by the common thin layer of the liquid nutrient medium. Consequently, all the cell types that inhabit the coverslip can exchange metabolites among themselves. This means that oxidative stress factors are common to all cells of each coverslip, each of which, accordingly, in general, contains a total set of neuroglial cells represented in the cerebellum: neurons, astrocytes, oligodendrocytes, and microglia. In such tissue type, on average, the number of neuroglia is 8-10 times more than that of neuron cells [28, 29]. As shown in Figure 1(c), upon 10 days of cultivation, a regular myelin synthesis (green) was observed in the processes of cultured oligodendrocytes (red). Within the 10–14-day period, when oligodendrocytes and their processes were visualized as a dense green network due to abundantly synthesized myelin (anti-MBP staining; see Figure 2(a) and Supplementary Figures 1(a) and 1(c)), investigation of oligodendrocyte demyelination/remyelination was carried out.

Prior to investigating demyelination/remyelination, we studied the antioxidant penetration in the cultured cells. To analyze localization of SkQ1 in oligodendrocytes, we used the fluorescent SkQ1 analog, SkQR1, in which the cationic constituent, triphenylphoshonium, was replaced by cation rhodamine-19. According to their antioxidant protective properties, both analogs are among the most effective in the SkQ family and are of the same level of penetrating ability for model lipid membranes [11, 30] and mitochondria of both various cell types *in vitro* [11] and some tissues *in vivo* [31]. As to their antioxidant property, the protective antioxidant effect of SkQR1 compared to SkQ1 was slightly higher in some of the models *in vitro* [11] and *in vivo* [31, 32]. Mitochondrial localization of SkQR1 was earlier demonstrated in various cell types, such as HeLa cells [11], endothelial cells of

the EaHy926 cell line [33], and human neutrophils [34], as well as human skin fibroblasts [35] and myofibroblasts [36]. Like in the other cell types, in oligodendrocytes migrating from cerebellar explants, SkQR1 selectively accumulated in mitochondria that formed the well-recognized mitochondrial network, shown both during this study (Figure 3(a)) and in previous examinations (Figure 1 in ref. [2]).

Due to natural causes, some cells inside the explant died during the cultivation and microglial cells were visible in the space adjacent to the cerebellar explant. Figure 3(b) shows a dense mitochondrial network (orange) that pierces microglial cells visible in the explant cerebellar cultures stained with anti-iNOS antibody (green) and mitochondria-targeted antioxidant SkQR1.

To initiate neuroinflammation in the explant culture, we used LPS in high concentration (5 μg/ml) in the presence of serum which was a component of the cultivation medium. A strong LPS-induced decrease in the myelin content in oligodendrocytes was observed (Figure 2(c) and Supplementary Figures 1(b) and 1(d)). Under these conditions, the effect of LPS on microglia is mediated by both TLR4-dependent and TLR4-independent pathways as described earlier [21]. The direct effects of LPS on oligodendrocytes also cannot be excluded [37, 38]. The pretreatment of the culture with SkQ1 in nanomolar concentrations significantly protected oligodendrocytes (Figure 2(d)). The decrease and disappearance of staining for myelin were not the result of cell death in the culture, because in all experiments the number of cells in the samples remained constant (Figure 2(f)).

This result indicates an important contribution of glial mitochondria to the total oxidative burst caused by LPS, if we take into account the experimental data on the mechanism of SkQ1 action [39]. SkQ1 is a lipophilic antioxidant molecule, and its primary targets in the inner mitochondrial membrane are lipid radicals formed there, one of the main sources of which is cardiolipin, the phospholipid most sensitive to peroxidation. Cardiolipin is an important structural component of various enzyme complexes, and its oxidation leads to the deterioration of the functioning of mitochondria. Being the only negatively charged phospholipid in the mitochondrial membrane, cardiolipin is considered as a primary partner for the interaction with cationic SkQ1, which thus performs its protective antioxidant function. Moreover, SkQ1 and other derivatives of this family were also shown to protect various cells from death induced by exogenous H_2O_2, and this protective effect correlated with the decrease in intracellular ROS accumulation [11, 40]. Since in the cited studies SkQ1 selectively accumulated in mitochondria, it was suggested that mtROS were the primary target of SkQ1 antioxidant action. The accumulation of cytoplasmic ROS was observed only as a secondary event after a significant lag-phase as a result of mitochondrial dysfunction and excess ROS production. The SkQ1-dependent decrease in mtROS was proved using the H_2O_2-sensitive fluorescent protein HyPer expressed in mitochondria [41] and using a novel mitochondria-targeted dye sensitive to lipid peroxidation [42].

(a)

(b)

(c)

(d)

(e)

(f)
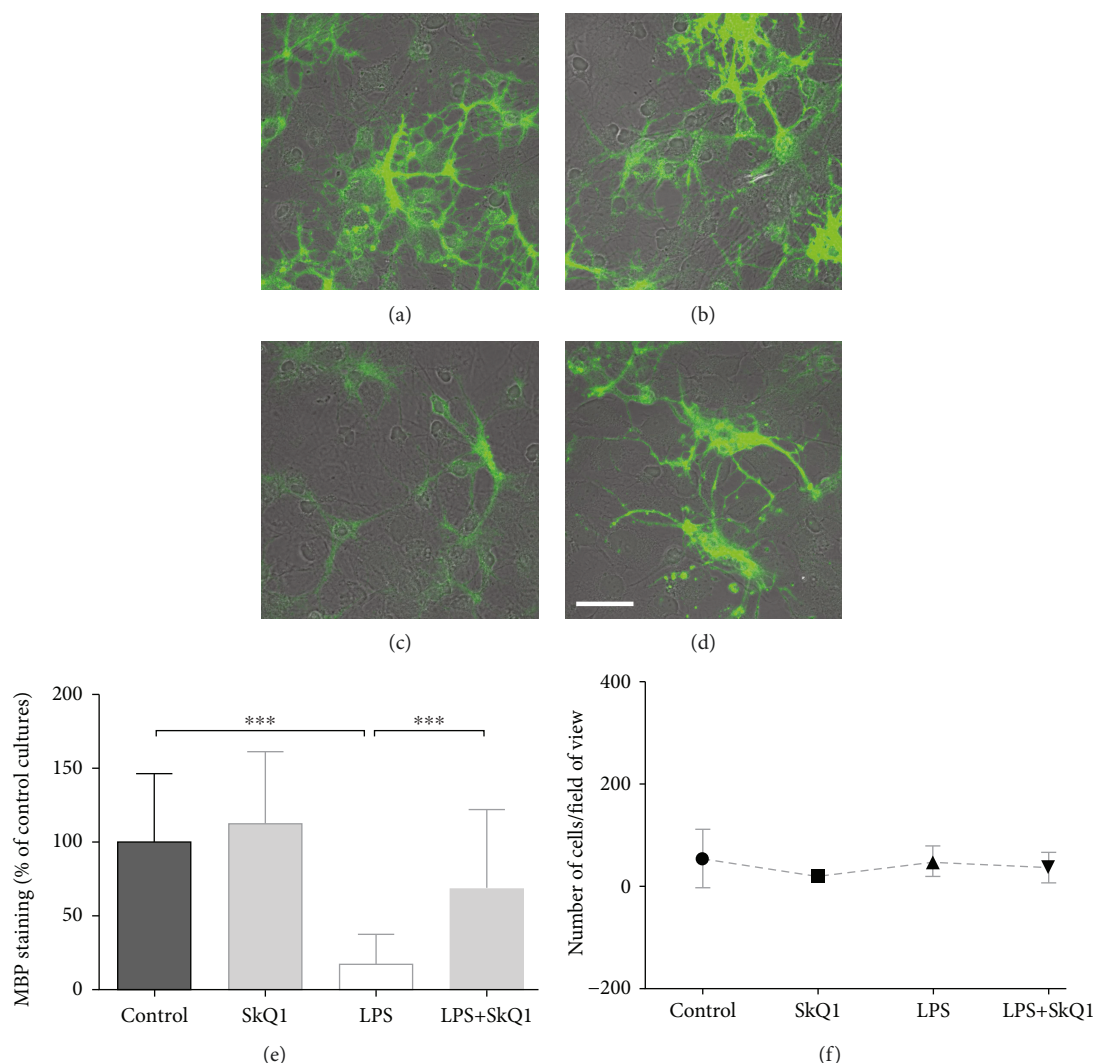
FIGURE 2: SkQ1 protects against the LPS-induced decrease in myelin content in oligodendrocytes. (a–d) Representative images of immunostaining for MBP: (a) control and treatment with the reagents (b) SkQ1, (c) LPS, and (d) LPS+SkQ1. (e) MBP staining was quantified, measuring 7-60 fields of view per treatment and expressed as the stained area percentage of untreated control cultures. (f) The number of cells in the field of view. Samples were prepared from the brain of eight newborn rats in seven independent experiments. Data are expressed as mean ± SD (***$p < 0.0003$; one-way ANOVA, Bonferroni's post hoc test). Scale bar, 20 μm.

Since in the present study mtAO accumulates in mitochondria of both oligodendrocytes and microglia, as shown in Figures 3(a) and 3(b), it can be assumed that mtAO deactivates mtROS in these cell types. Inasmuch as it has been evidenced that it is peroxynitrite that has a detrimental effect on myelin production by oligodendrocytes [43], it is an important result that mitochondria were abundantly present in the same microglial cells as iNOS molecules and in the myelin-filled oligodendrocytes. This observation points out in favor of the assumption that peroxynitrite can be generated also due to mtROS under pathological conditions; therefore, we cannot exclude the direct effect of mtAO on oligodendrocytes where mtAO scavenges ROS and consequently reduces the possibility of peroxynitrite formation. What else needs attention is that, due to its lipophilic nature, mtAOs are more soluble in the lipid phase and, in particular, SkQ1 concentration can be up to four orders of magnitude higher in lipid structures compared to the aqueous phase in accordance with the membrane/water distribution coefficient [44]. In addition, the plasma membrane is charged and maintains $\Delta\psi$ of about 60 mV across itself with a negative cell interior, which allows electrophoretic accumulation of a monovalent SkQ1 cation in the cytoplasm by a factor of 10. Therefore, it is reasonable to assume that SkQ1, although accumulating in fatty myelin at concentrations of about 3-4 orders lower than that in mitochondria (in the latter, the magnification of SkQ1 concentration reaches 10^8 [12]), can also provide antioxidant defense there, as in the case with cardiolipin (see the preceding paragraph). This effect is especially likely in the presence of a reductant or in close vicinity of mitochondria, where mtAO can be constantly recharged into an effectively working, reduced form.

(a)   (b)
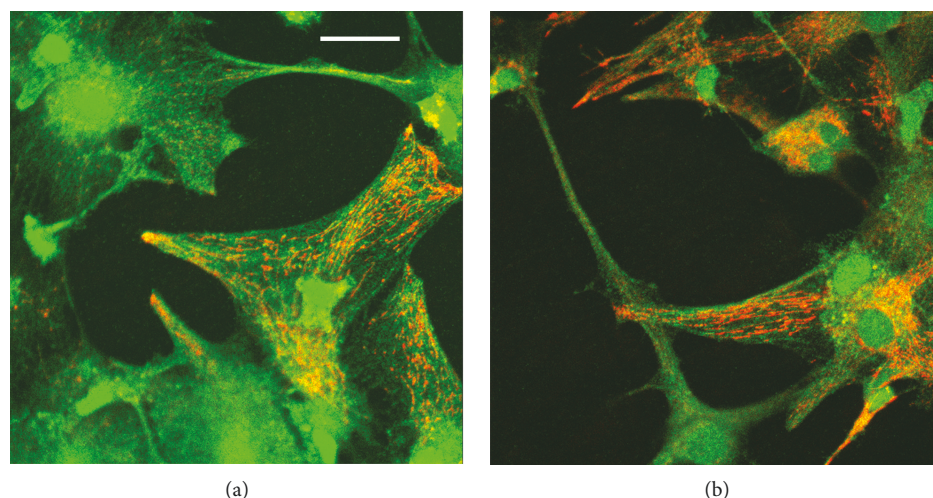
FIGURE 3: Mitochondria-targeted antioxidant SkQR1, a red-colored fluorescent SkQ derivative, selectively accumulates in mitochondria (orange) of glial cells: (a) oligodendrocytes and (b) microglial cells. The primary oligodendrocyte culture of cerebellar explants was preincubated with both (a, b) 50 nM SkQR1 for 2 h and (a) anti-Oligo1 antibody for staining oligodendrocytes (green) or (b) anti-iNOS antibody (green). Images are the merge of views with "red" and "green" optical filters. Scale bar, 5 μm. Confocal microscope, Carl Zeiss LSM 510.

Within the framework of the in vitro MS model used by us, a hypothetic scheme of the events induced by LPS in the primary oligodendrocyte culture of the cerebellum, containing microglia, is presented in Figure 4.

This chain of events, typical of oxidative stress, includes NF-κB stimulation leading to the induction of proinflammatory cytokines, chemokines, and other mediators [46, 47]. Oxidative stress is implicated in many neurological diseases, including MS [48]. In this context, it is interesting to note that along with neuroprotective action [2, 13–16], SkQ1 and its mtAO analogs demonstrated a pronounced anti-inflammatory effect in the models of local acute inflammation [49] and systemic inflammatory response syndrome (SIRS) [50]. Recently, it was demonstrated that SkQ1 suppressed NF-κB-dependent gene expression in the aortas of old mice [51] and SIRS mice [50]. SkQ1 also inhibited activation of NF-κB, which was induced by tumor necrosis factor in endothelial cells in vitro [51]. These findings indicate that the inhibition of NF-κB by SkQ1 in the LPS-stimulated microglia could contribute to oligodendrocyte protection against demyelination shown by us in the present study.

NADPH oxidase (NOX2) is another participant of the oxidative stress events that produces significant amounts of extracellular ROS, which could play a critical role in the neuroinflammation accompanying MS [52, 53]. Regarding our results, the protective effect of SkQ1 in relation to myelin content in oligodendrocytes (Figure 2) could be explained by the anti-inflammatory action of SkQ1 in microglia, just as SkQ1 prevented NOX2 activation (oxidative burst) recently observed in neutrophils [34].

Also, it is obvious that a decrease in mtROS in activated microglia in the presence of NO produced by iNOS [20] should result in the reduction of RNS generation and thus provide protection to oligodendrocytes in MS [20, 54–56]. Our findings cross-talk with a recent report that RNS pro-

duction by activated macrophages plays a crucial role in axon demyelination and peripheral neuropathy in leprosy [57]. The demyelination in this mycobacterial disease is analogous to that in MS, and RNS-dependent destruction of mitochondria was suggested to contribute to demyelination in both cases [57]. If this is the case, the mitochondria-targeted antioxidants such as SkQ1, which proved to be effective in the MS model in our experiments, could be considered as a potential medicine against mycobacterial pathogens. The obtained results on the protective effect of the SkQ1 antioxidant are especially relevant in light of the latest data on the accumulation pressure of proinflammatory stimuli on the statistical manifestation of MS [58]. As demonstrated, such incentives include heterogeneous factors leading to inflammatory reactions: smoking, working with organic solvents, and the presence of leukocyte antigen genes in the human genotype. All this means that taking antioxidants that lower the level of ROS, RNS, and inflammation should reduce the risk of MS.

In the context of intractable immunoinflammatory diseases, the results of our study offer an important potentiality for using the antioxidant SkQ1 in an alternative therapy when immunotherapy is not applicable. Recently, a number of immunomodulating, disease-modifying therapies have been introduced, which are aimed at reducing the inflammatory response in MS. Such treatments in varying degrees weaken immune surveillance and may predispose patients to the development of various opportunistic infections that are rarely seen in neurological practice [59]. Among the immunosuppressive drugs, natalizumab, an FDA-approved humanized monoclonal antibody against α4-integrin, is considered one of the most effective ways to prevent relapse. Its effect is based on the suppression of both the adhesion of leukocytes (except neutrophils) to the endothelium and their penetration through the blood-brain barrier. However, the high risk of progressive multifocal leukoencephalopathy
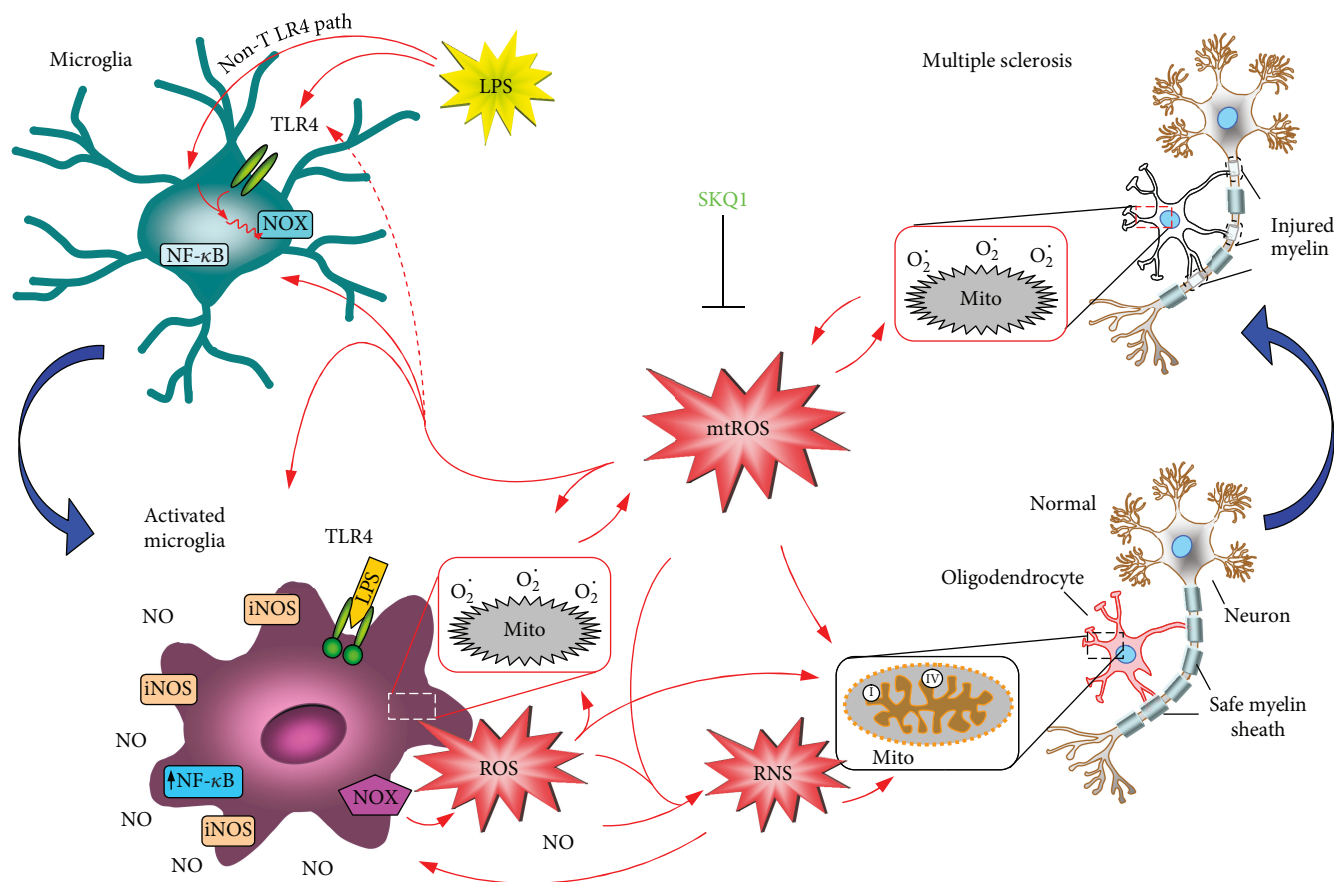
FIGURE 4: The hypothetic scheme of events induced by LPS in the primary oligodendrocyte culture of cerebellar explants considering the published data. Shown are oligodendrocytes in normal (pink) and pathological (white) states, LPS-initiated microglia (olive) transformed into activated microglia (dark lilac), and the expressed iNOS enzyme producing NO that activates the NOX enzyme (magenta pentagon) making the initial burst of ROS. The appearance of NO and ROS results in generating RNS; mitochondria (framed) with the indicated respiratory complexes I and IV, which mainly produce ROS in them after being toxified by RNS [45]. Blue arrows show transitions from normal to pathological states. Antioxidant SkQ1 (light-green) scavenges ROS and thus decreases the microglia activation, earlier identified as a critical factor contributing to multiple neurodegenerative diseases. For details, see the text.

(PML) limits the long-term treatment with natalizumab. PML can be induced by the John Cunningham virus (JCV), a type of polyomavirus that becomes pathogenic only in cases of immunodeficiency (as in AIDS) or drug-induced immunosuppression [60]. Another immunosuppressive drug, fingolimod, is considered mainly for the postnatalizumab therapy for MS, but its use may increase the incidence of varicella-zoster virus infection [61]. In contrast to immunomodulatory drugs, mitochondria-targeted antioxidants did not cause any signs of immunosuppression in various studies in animal models [12–16]; therefore, their use for MS therapy would presumably be free from the described complications.

4. Conclusion

Our study is the first demonstration of the protective effect of the mtAO SkQ1 on oligodendrocytes affected by MS at the level of the culture model of the disease. The pronounced protective action of SkQ1 clearly demonstrates that mtROS participate in the suppression of myelin pro-

duction in oligodendrocytes. Supporting recent studies [58], we assume that people at risk should take antioxidants to reduce the probability of MS from rising. Also, our results implicate that mtAO could be promising components of a combined therapy for MS, especially in patients with various opportunistic infections accompanying MS, as well as in some disastrous diseases involving neurological disorders.

Abbreviations

MS: Multiple sclerosis
mtROS: Reactive oxygen species produced in mitochondria
mtAO: Mitochondria-targeted antioxidants
SkQ1: 10-(6′-Plastoquinonyl) decyltriphenylphosphonium
SkQR1: 10-(6′-Plastoquinonyl) decylrhodamine-19
LPS: Lipopolysaccharide
MBP: Myelin basic protein
NF-κB: Proinflammatory nuclear factor-κB
RNS: Reactive nitrogen species.

Data Availability

The experimental data used to support the findings of this study are included within the article.

Conflicts of Interest

The authors declare no financial or other conflicts of interest regarding the publication of this article.

Acknowledgments

Supplementary Materials

Figure S1: myelin content diminished in the cultures after incubation with LPS. The primary oligodendrocyte culture of cerebellar explants of newborn rats upon 14 days of cultivation. Representative images of immunostaining for MBP: (a, c) control and (b, d) treatment with LPS. Number of cells in the field views: (a) 44, (b) 45, (c) 34, and (d) 36. The cells were incubated with rabbit antibodies to MBP and Alexa Fluor 488-conjugated anti-IgG to mark myelin (green). Scale bar, 20 μm. Confocal microscope, Carl Zeiss LSM 510. (Supplementary Materials)

References

[1] A. J. Thompson, S. E. Baranzini, J. Geurts, B. Hemmer, and O. Ciccarelli, "Multiple sclerosis," *Lancet*, vol. 391, no. 10130, pp. 1622–1636, 2018.

[2] E. Fetisova, B. Chernyak, G. Korshunova, M. Muntyan, and V. Skulachev, "Mitochondria-targeted antioxidants as a prospective therapeutic strategy for multiple sclerosis," *Current Medicinal Chemistry*, vol. 24, no. 19, pp. 2086–2114, 2017.

[3] K. N. Varhaug, C. A. Vedeler, K. M. Myhr, J. H. Aarseth, C. Tzoulis, and L. A. Bindoff, "Increased levels of cell-free mitochondrial DNA in the cerebrospinal fluid of patients with multiple sclerosis," *Mitochondrion*, vol. 34, pp. 32–35, 2017.

[4] J. van Horssen, G. Schreibelt, J. Drexhage et al., "Severe oxidative damage in multiple sclerosis lesions coincides with enhanced antioxidant enzyme expression," *Free Radical Biology and Medicine*, vol. 45, no. 12, pp. 1729–1737, 2008.

[5] H. M. French, M. Reid, P. Mamontov, R. A. Simmons, and J. B. Grinspan, "Oxidative stress disrupts oligodendrocyte maturation," *Journal of Neuroscience Research*, vol. 87, no. 14, pp. 3076–3087, 2009.

[6] A. Nonneman, W. Robberecht, and L. V. Van Den Bosch, "The role of oligodendroglial dysfunction in amyotrophic lateral sclerosis," *Neurodegenerative Disease Management*, vol. 4, no. 3, pp. 223–239, 2014.

[7] M. J. McManus, M. P. Murphy, and J. L. Franklin, "The mitochondria-targeted antioxidant MitoQ prevents loss of spatial memory retention and early neuropathology in a transgenic mouse model of Alzheimer's disease," *Journal of Neuroscience*, vol. 31, no. 44, pp. 15703–15715, 2011.

[8] A. Ghosh, K. Chandran, S. V. Kalivendi et al., "Neuroprotection by a mitochondria-targeted drug in a Parkinson's disease model," *Free Radical Biology and Medicine*, vol. 49, no. 11, pp. 1674–1684, 2010.

[9] E. Miquel, A. Cassina, L. Martínez-Palma, J. M. Souza, C. Bolatto, and S. Rodríguez-Bottero, "Neuroprotective effects of the mitochondria-targeted antioxidant MitoQ in a model of inherited amyotrophic lateral sclerosis," *Free Radical Biology and Medicine*, vol. 70, pp. 204–213, 2014.

[10] P. Mao, M. Manczak, U. P. Shirendeb, and P. H. Reddy, "MitoQ, a mitochondria-targeted antioxidant, delays disease progression and alleviates pathogenesis in an experimental autoimmune encephalomyelitis mouse model of multiple sclerosis," *Biochimica et Biophysica Acta (BBA) - Molecular Basis of Disease*, vol. 1832, no. 12, pp. 2322–2331, 2013.

[11] Y. N. Antonenko, A. V. Avetisyan, L. E. Bakeeva et al., "Mitochondria-targeted plastoquinone derivatives as tools to interrupt execution of the aging program. 1. Cationic plastoquinone derivatives: synthesis and in vitro studies," *Biochemistry (Moscow)*, vol. 73, no. 12, pp. 1273–1287, 2008.

[12] V. P. Skulachev, "Cationic antioxidants as a powerful tool against mitochondrial oxidative stress," *Biochemical and Biophysical Research Communications*, vol. 441, no. 2, pp. 275–279, 2013.

[13] N. K. Isaev, S. V. Novikova, E. V. Stelmashook et al., "Mitochondria-targeted plastoquinone antioxidant SkQR1 decreases trauma-induced neurological deficit in rat," *Biochemistry (Moscow)*, vol. 77, no. 9, pp. 996–999, 2012.

[14] D. Silachev, E. Plotnikov, L. Zorova et al., "Neuroprotective effects of mitochondria-targeted plastoquinone and thymoquinone in a rat model of brain ischemia/reperfusion injury," *Molecules*, vol. 20, no. 8, pp. 14487–14503, 2015.

[15] A. V. Avetisyan, A. N. Samokhin, I. Y. Alexandrova, R. A. Zinovkin, R. A. Simonyan, and N. V. Bobkova, "Mitochondrial dysfunction in neocortex and hippocampus of olfactory bulbectomized mice, a model of Alzheimer's disease," *Biochemistry (Moscow)*, vol. 81, no. 6, pp. 615–623, 2016.

[16] N. G. Kolosova, M. A. Tyumentsev, N. A. Muraleva, E. Kiseleva, A. O. Vitovtov, and N. A. Stefanova, "Antioxidant SkQ1 alleviates signs of Alzheimer's disease-like pathology in old OXYS rats by reversing mitochondrial deterioration," *Current Alzheimer Research*, vol. 14, no. 12, pp. 1283–1292, 2017.

[17] J. van Horssen, M. E. Witte, G. Schreibelt, and H. E. de Vries, "Radical changes in multiple sclerosis pathogenesis," *Biochimica et Biophysica Acta (BBA) - Molecular Basis of Disease*, vol. 1812, no. 2, pp. 141–150, 2011.

[18] A. S. Khalansky, "Neuroglia and subsidiary cells in culture," in *Guide Culturing Neural Tissue. Methods. Equipment. Problems*, Veprintsev, Victorov, and Vil'ner, Eds., Nauka, Moscow, 2nd Ed. edition, 1988, (In Russ.).

[19] S. Lehnardt, C. Lachance, S. Patrizi et al., "The Toll-like receptor TLR4 is necessary for lipopolysaccharide-induced oligodendrocyte injury in the CNS," *Journal of Neurochemistry*, vol. 22, no. 7, pp. 2478–2486, 2002.

[20] J. Li, O. Baud, T. Vartanian, J. J. Volpe, and P. A. Rosenberg, "Peroxynitrite generated by inducible nitric oxide synthase and NADPH oxidase mediates microglial toxicity to oligodendrocytes," *Proceedings of the National Academy of Sciences of the United States of America*, vol. 102, no. 28, pp. 9936–9941, 2005.

[21] L. Qin, G. Li, X. Qian et al., "Interactive role of the toll-like receptor 4 and reactive oxygen species in LPS-induced microglia activation," *Glia*, vol. 52, no. 1, pp. 78–84, 2005.

[22] J. Y. Kim, S. Shen, K. Dietz et al., "HDAC1 nuclear export induced by pathological conditions is essential for the onset of axonal damage," *Nature Neuroscience*, vol. 13, no. 2, pp. 180–189, 2010.

[23] A. di Penta, B. Moreno, S. Reix et al., "Oxidative stress and proinflammatory cytokines contribute to demyelination and axonal damage in a cerebellar culture model of neuroinflammation," *PLoS One*, vol. 8, no. 2, p. e54722, 2013.

[24] I. V. Viktorov and E. M. Kenarskaya, "A device for nerve tissue cultivation," *Bulletin of Experimental Biology and Medicine*, vol. 80, no. 2, pp. 991-992, 1975.

[25] M. R. Murray, "Nervous tissues isolated in culture," in *Metabolic Turnover in the Nervous System*, Springer, Boston, MA, 1971.

[26] O. Berg and B. Källén, "Studies on rat neuroglia cells in tissue culture," *Journal of Neuropathology and Experimental Neurology*, vol. 18, no. 3, pp. 458–467, 1959.

[27] I. V. Victorov, L. G. Khaspekov, and N. A. Shashkova, "Cultivation of tissue and cells of the central nervous system," in *Guide Culturing Neural Tissue. Methods. Equipment. Problems*, Veprintsev, Victorov, and Vil'ner, Eds., Nauka, Moscow, 2nd Ed. edition, 1988, (In Russ.).

[28] R. Galambos, "A glia-neural theory of brain function," *Proceedings of the National Academy of Sciences of the United States of America*, vol. 47, no. 1, pp. 129–136, 1961.

[29] R. Bahizs and J. E. Cremer, Eds., "The neuroglial compartments at light microscopic and electron microscopic levels," in *In Metabolic Compartmentation in the Brain*, pp. 209–231, The Macmillan Press LTD, Palgrave, London, 1973.

[30] T. I. Rokitskaya, S. S. Klishin, I. I. Severina, V. P. Skulachev, and Y. N. Antonenko, "Kinetic analysis of permeation of mitochondria-targeted antioxidants across bilayer lipid membranes," *Journal of Membrane Biology*, vol. 224, no. 1-3, pp. 9–19, 2008.

[31] L. E. Bakeeva, I. V. Barskov, M. V. Egorov et al., "Mitochondria-targeted plastoquinone derivatives as tools to interrupt execution of the aging program. 2. Treatment of some ROS- and age-related diseases (heart arrhythmia, heart infarctions, kidney ischemia, and stroke)," *Biochemistry (Moscow)*, vol. 73, no. 12, pp. 1288–1299, 2008.

[32] E. Y. Plotnikov, D. N. Silachev, A. A. Chupyrkina et al., "New-generation Skulachev ions exhibiting nephroprotective and neuroprotective properties," *Biochemistry (Moscow)*, vol. 75, no. 2, pp. 145–150, 2010.

[33] I. I. Galkin, O. Y. Pletjushkina, R. A. Zinovkin et al., "Mitochondria-targeted antioxidants prevent TNFα-induced endothelial cell damage," *Biochemistry (Moscow)*, vol. 79, no. 2, pp. 124–130, 2014.

[34] N. Vorobjeva, A. Prikhodko, I. Galkin et al., "Mitochondrial reactive oxygen species are involved in chemoattractant-induced oxidative burst and degranulation of human neutrophils in vitro," *European Journal of Cell Biology*, vol. 96, no. 3, pp. 254–265, 2017.

[35] D. S. Izyumov, L. V. Domnina, O. K. Nepryakhina et al., "Mitochondria as source of reactive oxygen species under oxidative stress. Study with novel mitochondria-targeted antioxidants—the "Skulachev-ion" derivatives," *Biochemistry (Moscow)*, vol. 75, no. 2, pp. 123–129, 2010.

[36] E. N. Popova, O. Y. Pletjushkina, V. B. Dugina et al., "Scavenging of reactive oxygen species in mitochondria induces myofibroblast differentiation," *Antioxidants and Redox Signaling*, vol. 13, no. 9, pp. 1297–1307, 2010.

[37] M. Bsibsi, R. Ravid, D. Gveric, and J. M. van Noort, "Broad expression of Toll-like receptors in the human central nervous system," *Journal of Neuropathology and Experimental Neurology*, vol. 61, no. 11, pp. 1013–1021, 2002.

[38] S. Yao, P. Pandey, A. Ljunggren-Rose, and S. Sriram, "LPS mediated injury to oligodendrocytes is mediated by the activation of nNOS: relevance to human demyelinating disease," *Nitric Oxide*, vol. 22, no. 3, pp. 197–204, 2010.

[39] V. P. Skulachev, Y. N. Antonenko, D. A. Cherepanov et al., "Prevention of cardiolipin oxidation and fatty acid cycling as two antioxidant mechanisms of cationic derivatives of plastoquinone (SkQs)," *Biochimica et Biophysica Acta*, vol. 1797, no. 6-7, pp. 878–889, 2010.

[40] B. V. Chernyak, D. S. Izyumov, K. G. Lyamzaev et al., "Production of reactive oxygen species in mitochondria of HeLa cells under oxidative stress," *Biochimica et Biophysica Acta*, vol. 1757, no. 5-6, pp. 525–534, 2006.

[41] E. R. Galimov, B. V. Chernyak, A. S. Sidorenko, A. V. Tereshkova, and P. M. Chumakov, "Prooxidant properties of p66shc are mediated by mitochondria in human cells," *PLoS One*, vol. 9, no. 3, p. e86521, 2014.

[42] A. M. Nesterenko, E. G. Kholina, K. G. Lyamzaev, A. Y. Mulkidjanian, and B. V. Chernyak, "Molecular dynamics modeling of the interaction of cationic fluorescent lipid peroxidation-sensitive probes with the mitochondrial membrane," *Doklady Biochemistry and Biophysics*, vol. 486, no. 4, 2019.

[43] R. C. Van der Veen and L. J. Roberts, "Contrasting roles for nitric oxide and peroxynitrite in the peroxidation of myelin lipids," *Journal of Neuroimmunology*, vol. 95, no. 1-2, pp. 1–7, 1999.

[44] M. V. Skulachev, Y. N. Antonenko, V. N. Anisimov et al., "Mitochondrial-Targeted Plastoquinone Derivatives. Effect on Senescence and Acute Age-Related Pathologies," *Current Drug Targets*, vol. 12, no. 6, pp. 800–826, 2011.

[45] J. Ye, Z. Jiang, X. Chen, M. Liu, J. Li, and N. Liu, "Electron transport chain inhibitors induce microglia activation through enhancing mitochondrial reactive oxygen species production," *Experimental Cell Research*, vol. 340, no. 2, pp. 315–326, 2016.

[46] G. W. Konat, T. Kielian, and I. Marriott, "The role of Toll-like receptors in CNS response to microbial challenge," *Journal of Neurochemistry*, vol. 99, no. 1, pp. 1–12, 2006.

[47] M. K. Jha, W. H. Lee, and K. Suk, "Functional polarization of neuroglia: implications in neuroinflammation and neurological disorders," *Biochemical Pharmacology*, vol. 103, pp. 1–16, 2016.

[48] C. Mc Guire, M. Prinz, R. Beyaert, and G. van Loo, "Nuclear factor kappa B (NF-κB) in multiple sclerosis pathology," *Trends in Molecular Medicine*, vol. 19, no. 10, pp. 604–613, 2013.

[49] I. A. Demyanenko, E. N. Popova, V. V. Zakharova et al., "Mitochondria-targeted antioxidant SkQ1 improves impaired dermal wound healing in old mice," *Aging (Albany NY)*, vol. 7, no. 7, pp. 475–485, 2015.

[50] V. V. Zakharova, O. Y. Pletjushkina, I. I. Galkin et al., "Low concentration of uncouplers of oxidative phosphorylation decreases the TNF-induced endothelial permeability and lethality in mice," *Biochimica et Biophysica Acta (BBA) - Molecular Basis of Disease*, vol. 1863, no. 4, pp. 968–977, 2017.

[51] R. A. Zinovkin, V. P. Romaschenko, I. I. Galkin et al., "Role of mitochondrial reactive oxygen species in age-related inflammatory activation of endothelium," *Aging (Albany NY)*, vol. 6, no. 8, pp. 661–674, 2014.

[52] C. A. Colton and D. L. Gilbert, "Microglia, an in vivo source of reactive oxygen species in the brain," *Advances in Neurology*, vol. 59, pp. 321–326, 1993.

[53] S. Sorce and K. H. Krause, "NOX enzymes in the central nervous system: from signaling to disease," *Antioxidants and Redox Signaling*, vol. 11, no. 10, pp. 2481–2504, 2009.

[54] X. Qi, A. S. Lewin, L. Sun, W. W. Hauswirth, and J. Guy, "Mitochondrial protein nitration primes neurodegeneration in experimental autoimmune encephalomyelitis," *Journal of Biological Chemistry*, vol. 281, no. 42, pp. 31950–31962, 2006.

[55] C. Jack, J. Antel, W. Bruck, and T. Kuhlmann, "Contrasting potential of nitric oxide and peroxynitrite to mediate oligodendrocyte injury in multiple sclerosis," *Glia*, vol. 55, no. 9, pp. 926–934, 2007.

[56] M. Jana and K. Pahan, "Down-regulation of myelin gene expression in human oligodendrocytes by nitric oxide: implications for demyelination in multiple sclerosis," *Journal of Clinical and Cellular Immunology*, vol. 04, no. 04, 2013.

[57] C. A. Madigan, C. J. Cambier, K. M. Kelly-Scumpia et al., "A macrophage response to *Mycobacterium leprae* phenolic glycolipid initiates nerve damage in leprosy," *Cell*, vol. 170, no. 5, pp. 973–985.e10, 2017.

[58] A. K. Hedström, O. Hössjer, M. Katsoulis, I. Kockum, T. Olsson, and L. Alfredsson, "Organic solvents and MS susceptibility. Interaction with MS risk HLA genes," *Neurology*, vol. 91, no. 5, pp. e455–e462, 2018.

[59] E. Grebenciucova and A. Pruitt, "Infections in patients receiving multiple sclerosis disease-modifying therapies," *Current Neurology and Neuroscience Reports*, vol. 17, no. 11, 2017.

[60] C. Warnke, T. Olsson, and H. P. Hartung, "PML: the dark side of immunotherapy in multiple sclerosis," *Trends in Pharmacological Sciences*, vol. 36, no. 12, pp. 799–801, 2015.

[61] R. A. Khouy, S. Karampoor, H. Keyvani et al., "The frequency of varicella-zoster virus infection in patients with multiple sclerosis receiving fingolimod," *Journal of Neuroimmunology*, vol. 328, pp. 94–97, 2019.

Research Article

TRPV1 Contributes to Cerebral Malaria Severity and Mortality by Regulating Brain Inflammation

Domingos Magno Santos Pereira,[1] **Simone Aparecida Teixeira** [iD],[2] **Oscar Murillo** [iD],[3]
Erika Paula Machado Peixoto,[3] **Mizael Calácio Araújo,**[1] **Nágila Caroline Fialho Sousa,**[1]
Valério Monteiro-Neto [iD],[1,4] **João Batista Calixto,**[5] **Thiago Mattar Cunha,**[6]
Cláudio Romero Farias Marinho [iD],[3] **Marcelo Nicolás Muscará,**[2]
and Elizabeth Soares Fernandes [iD][1]

[1]*Programa de Pós-Graduação, Universidade CEUMA, São Luís, MA, Brazil*
[2]*Departamento de Farmacologia, Instituto de Ciências Biomédicas, Universidade de São Paulo, São Paulo, SP, Brazil*
[3]*Departamento de Parasitologia, Instituto de Ciências Biomédicas, Universidade de São Paulo, São Paulo, SP, Brazil*
[4]*Centro de Ciências da Saúde, Universidade Federal do Maranhão, São Luís, MA, Brazil*
[5]*Centro de Inovação e Ensaios Pré-Clínicos (CIEnP), Florianópolis, SC, Brazil*
[6]*Departamento de Farmacologia, Faculdade de Medicina de Ribeirão Preto, Universidade de São Paulo, São Paulo, SP, Brazil*

Correspondence should be addressed to Elizabeth Soares Fernandes; elizabeth.soares@ceuma.br

Transient receptor potential vanilloid 1 (TRPV1) is a Ca^{+2}-permeable channel expressed on neuronal and nonneuronal cells, known as an oxidative stress sensor. It plays a protective role in bacterial infection, and recent findings indicate that this receptor modulates monocyte populations in mice with malaria; however, its role in cerebral malaria progression and outcome is unclear. By using TRPV1 wild-type (WT) and knockout (KO) mice, the importance of TRPV1 to this cerebral syndrome was investigated. Infection with *Plasmodium berghei* ANKA decreased TRPV1 expression in the brain. Mice lacking TRPV1 were protected against *Plasmodium*-induced mortality and morbidity, a response that was associated with less cerebral swelling, modulation of the brain expression of endothelial tight-junction markers (junctional adhesion molecule A and claudin-5), increased oxidative stress (via inhibition of catalase activity and increased levels of H_2O_2, nitrotyrosine, and carbonyl residues), and diminished production of cytokines. *Plasmodium* load was not significantly affected by TRPV1 ablation. Repeated subcutaneous administration of the selective TRPV1 antagonist SB366791 after malaria induction increased TRPV1 expression in the brain tissue and enhanced mouse survival. These data indicate that TRPV1 channels contribute to the development and outcome of cerebral malaria.

1. Introduction

Malaria is an infectious disease of great morbidity and mortality, which claimed the lives of more than 400 thousand people worldwide in 2015 [1]. Cerebral malaria is a clinical syndrome of the severe form of the disease and is characterized by neurological complications (coma and convulsions) associated with brain inflammation (for review, see [2]) which can be lethal or cause irreversible neurological and/or cognitive sequelae in surviving patients (for review, see [3]).

Several mechanisms were found to contribute to cerebral malaria including alterations in nitric oxide availability, unbalanced oxidative stress responses, changes in the pattern of expression of inflammatory molecules, vascular leakage, and blood brain barrier disruption, amongst others [4–10]. However, its treatment has proven to be difficult and of low efficacy depending on timing and parasite resistance [3, 11],

with nearly 50% of the infected patients presenting this syndrome [3]. Importantly, 10-40% of the children with cerebral malaria die and a significant percentage develop sequelae [3, 12, 13]. In this context, the host response to infection plays a decisive role in the clinical evolution of malaria and therefore influences disease outcome.

The transient receptor potential vanilloid 1 (TRPV1) is a Ca^{+2}-permeable channel expressed on neuronal and non-neuronal cells such as brain endothelial and immune cells [14–18], which plays a role in the inflammatory response of different pathologies (for review, see [16, 19]) and an emerging role in neuroinflammation (for review, see [20]). It was found that TRPV1 is protective against bacterial infection [21–24] and modulates the innate immune response to malaria [25]. These studies also indicate that TRPV1 is detrimental to macrophage/monocyte-mediated responses, including their ability to produce inflammatory mediators, especially those related to oxidative stress [23, 26–30], in addition to regulating body temperature [21, 23]. However, the relevance of TRPV1 to the brain inflammation and symptoms of cerebral malaria has never been investigated.

Here, we used TRPV1 wild-type (WT) and knockout (KO) mice to evaluate the role of TRPV1 in cerebral malaria. Disease progression and brain inflammation were assessed in mice infected with *Plasmodium berghei* ANKA. It was found that TRPV1 contributes to disease severity and mortality, by mediating brain inflammation.

2. Methods

2.1. Mice. Nonfasted male C57BL/6 wild-type (WT) and TRPV1 knockout (TRPV1KO) mice (2-3 months of age; 22-28 g) were used. Animals were obtained from the animal's facility of the Faculdade de Medicina de Ribeirão Preto, Universidade de São Paulo (USP). Mice ($n = 3$-4/cage) were housed in a climatically controlled environment (room temperature of $22 \pm 2°C$) and humidity of around 60%, on a 12-12 h light/dark cycle (lights on at 07:00), with free access to water and food. All experiments were conducted in accordance with the Brazilian Society for Animal Welfare (SBCAL), following approval by the Ethics Committee of USP. Animals were randomly assigned into groups, and the experimenter was blinded towards the genetic background of animals during the experiment. In some cases, C57BL/6 mice received the selective TRPV1 antagonist SB366791 (0.5 mg/kg, twice a day; Sigma-Aldrich, Brazil) or vehicle (10% DMSO in saline) for up to 14 days, starting at 24 h postmalaria induction. All assays were conducted in a blinded manner.

A total of 16 infected TRPV1 WT and 14 KO mice were used for analysis of survival rates, disease stage, and severity score; these data were obtained from two independent experiments. For performing the different biochemical, qPCR, and cytokine measurement experiments, samples were collected from 12 TRPV1 WT (5 noninfected and 07 infected) and 16 TRPV1 KO (5 noninfected and 11 infected) mice with stage III/IV malaria, in three independent experiments.

In two separate experiments, 20 WTs were used for assessment of mortality rates with the TRPV1 antagonist (10 vehicle-treated and 10 SB366791-treated). Disease stage and severity score experiments included 17 WT mice (8 vehicle-treated and 9 SB366791-treated), in two independent experiments. For experiments in animals with stage III/IV malaria, 11 TRPV1 WTs were used (5 vehicle-treated and 6 SB366791-treated) in two independent experiments.

2.2. Induction of Cerebral Malaria. Malaria was induced by a single intraperitoneal (i.p.) injection of 10^6 red blood cells infected with *P. berghei* ANKA$^{GFP/HSP7}$ as previously described [31, 32]. Parasitaemia and disease progression were evaluated from day 1 postinfection, by daily recording of parasitaemia and clinical neurological signs of cerebral malaria.

2.3. Blood Parasitaemia. The percentage of parasitaemia was determined by flow cytometry. For this, a drop of blood from the tail was collected directly into 2 ml of PBS for flow cytometry analysis. Each sample was run on a FACSCalibur (Becton Dickinson, San Jose, CA, USA) flow cytometer with a 488 nm argon laser and BD CellQuest™ Pro software version 6.0.1 (Becton Dickinson, San Jose, CA, USA). Erythrocytes were identified on the basis of their specific forward (FSC) and side (SSC) light-scattering properties, and a total of 100,000 events were counted for each sample.

2.4. Analysis of the Clinical Neurological Signs of Cerebral Malaria and Mortality Rates. The neurological signs were evaluated as described by Linares et al. [33], in order to determine disease progression (stages I-IV) as follows: stage I—presence of parasitaemia and absence of neurological symptoms; stage II—presence of head deviation or hemi- or paraplegia, in the absence or presence of piloerection, altered gait or ambulation, muscle weakness, tremor, rollover response, and/or anaemia; stage III—presence of significant neurological symptoms, including head deviation, paraplegia/hemiparaplegia, immobility, muscle weakness, piloerection, anaemia, pelvic elevation, lack of responses to external stimuli, tremor, and swollen eyes; and stage IV—presence of exacerbated neurological symptoms in comparison to those observed at stage III.

Disease severity was analysed by using the Rapid Murine Coma and Behavior Scale as previously described by Carroll et al. [34], with minor modifications. Briefly, a score from 0 (normal) to 2 (severe alteration) was attributed to each one of the following parameters as follows: (i) coordination (gait and balance), (ii) exploratory behavior (motor performance), (iii) strength and tone (body position and limb strength), (iv) reflexes and self-preservation (touch escape, pinna reflex, toe pinch, and aggression), and (v) hygiene-related behavior (grooming). The summation of the scores attributed to each of the parameters for each animal was taken as severity score index, with the highest scores corresponding to the worst outcome of disease.

The animals were observed for up to 14 days postinfection and were culled by anaesthetic overdose (90 mg/kg ketamine + 2 mg/kg xylazine; i.p.) as soon as they reached stage III/IV (premortality end point). Blood samples were collected, and the plasma was obtained. Brain samples were also

collected and weighted. Collected plasma and brain tissue samples were immediately frozen and stored at -80°C until further processing for analysis of different parameters, except those used for qRT-PCR to which RNAlater was added according with the manufacturer's instructions (Sigma-Aldrich, Brazil).

Also, body weight and temperature were registered before (baseline) and at stage III/IV postinfection. All those which did not reach stage III/IV during the observation period were culled, and their measurements and samples were collected at the 14th day postinfection. Noninfected mice were used as controls.

In a separate series of experiments, mortality rates were evaluated over 14 days following induction of cerebral malaria, in independent groups of mice.

2.5. Brain Parasite Load. Tissue parasite load was evaluated in brain samples (left hemisphere) collected from infected TRPV1 WT and KO mice, as previously described [33], and modified. Tissue parasite loads were determined by quantitative PCR and expressed as copy numbers of *P. berghei* ANKA 18S DNA per milligram of host tissue. For this, RNA was extracted in RNeasy Microarray Tissue Mini Kit, according to the manufacturer's instructions (Qiagen, Brazil). Then, the cDNA was prepared by reverse transcription of 2 μg of RNA with ImProm-II Reverse Transcriptase (Promega, USA). The cDNA was assayed by qRT-PCR using the Taq-Man® system (Applied Biosystems, USA) with *P. berghei* probes (AI 38261, PN 4332079). GAPDH levels were assessed by TaqMan Mouse GAPDH System (TaqMan®, Applied Biosystems, USA) and were used as housekeeping gene controls.

2.6. TRPV1, Junctional Adhesion Molecule-A (JAM-A), and Claudin-5 Gene Expression by Real-Time qPCR. qRT-PCR was performed using GoTaq qPCR Master Mix (Promega, USA) and a Rotor-Gene 6000 real-time PCR machine (Corbett Life Science, Australia) in a final volume of 12 μl (hold: 2 min at 95°C; cycling: 40 cycles: 15 s at 95°C and 30 s at 60°C; melt: 68-90°C). The following primers were used: TRPV1 (forward 5'-GCGACCATCCCTCAAGAGT-3', reverse 5'-CTTGCGATGGCTGAAGTACA-3'; 109 bp; accession number NM_001001445.2), JAM-A (forward 5'-GGTCAGCATCCACCTCACTGT-3', reverse 5'-AGGT CAGCACTGCCCTGTTC-3'; 94 bp; accession number NM_172647), claudin-5 (forward 5'-GTGCCGGTGTC ACAGAAGTA-3', reverse 5'-GTACTTGACCGGGAAG CTGA-3'; 147 bp; accession number NM_013805), and GAPDH (forward 5'-AAGGTCATCCCAGAGCTGAA-3', reverse 5'-CTGCTTCACCACCTTCTTGA-3'; 138 bp; accession number NM_008084.2). For each gene in each sample, $2^{-efficiency \times Ct}$ values were calculated and divided by the corresponding value of $2^{-efficiency \times Ct}$ obtained for GAPDH. In order to normalize the data, all the individual results were divided by the average value obtained for the control group (noninfected WT mice). Efficiencies were of 0.47, 0.59, 0.68, and 0.8 for TRPV1, claudin-5, JAM-A, and GAPDH primers, respectively.

2.7. Cytokine Measurements. Brain samples (right hemisphere) were prepared, and the supernatant was obtained as previously described [35] and used in the assays. The tissue and plasma levels of TNFα, IFNγ, and IL-6 were evaluated by using mouse cytometric bead array (CBA) cytokine kits according to the manufacturer's instructions (BD Biosciences, Brazil). Data analysis was performed on a FACSCalibur flow cytometer (BD Biosciences Immunocytometry Systems). Results were calculated in FCAP Array Software version 3.0.1 (BD Biosciences, Brazil) and expressed as picograms of cytokine per mg of tissue protein (pg/mg of protein) or picograms per milliliter of plasma (pg/ml).

2.8. Tissue Sample Preparation for Biochemical Analysis of Oxidative Stress Pathways. Brain samples (100 mg; right hemisphere) were homogenized in 1000 μl of 0.05 M NaPO$_4$ (pH 7.4) containing ethylenediaminetetraacetic acid (EDTA, 1 mM) and centrifuged at 10,000g, for 10 min, at 4°C, and then the supernatant was collected and stored at -80°C for analysis of enzyme activities.

2.9. Superoxide Dismutase (SOD). SOD activity was measured as described by Abreu et al. [36]. Briefly, 10 μl of each sample was incubated with 260 μl of sodium carbonate buffer (50 mM; pH 9.4 containing 3 mM EDTA), 10 μl of 3 mM xanthine, 10 μl of 153 mU/ml of 2,3-bis-(2-methoxy-4-nitro-5-sulfophenyl)-2H-tetrazolium-5-carboxanilide (XTT), and 10 μl of 1.87 mU/ml xanthine oxidase. Then, 200 μl of the mixture was added per well in 96-well plates and the absorbance was read at 470 nm for 20 min. Blank reactions were prepared for each sample by boiling them for 5 min in order to inactivate SOD. Results are expressed as milliunits (mU) of SOD/mg of protein. Enzyme activity was defined as the ability of one unit of SOD to dismutate 1 μmol of O_2^-/min.

2.10. Catalase. Catalase activity was measured as previously described [36], by incubating 30 μl of brain homogenates or plasma samples with 500 μl of hydrogen peroxide (H$_2$O$_2$, 10 mmol/l) for 20 min, at 25°C. Reactions were stopped with 500 μl of sodium azide (1 mmol/l), and the concentration of the remaining H$_2$O$_2$ was determined by the oxidation of o-dianisidine. For this, 20 μl of each reaction was incubated with 200 μl of phosphate buffer (5 mM; pH 6.0) containing 0.167 mg/ml o-dianisidine and 0.095 mg/ml horseradish peroxidase (HRP). The absorbance was immediately read at 460 nm (SpectraMax Plus 384, Molecular Devices Inc., Sunnyvale, EUA) for 10 min. The remaining reactions were incubated at 60°C for 2 h, in order to inactivate catalase, and used as controls. A standard curve of H$_2$O$_2$ (11.3-8820 μM) was used for comparison. Results are expressed as international units (IU) of catalase per milligram (mg) of protein. One IU of catalase was defined as the amount of H$_2$O$_2$ (in μmol) degraded per minute.

2.11. Glutathione Peroxidase (GPx) and Reductase (GR). GR activity was assessed by measuring the consumption of nicotinamide adenine dinucleotide phosphate (NADPH) as a cofactor in the reduction of oxidized glutathione (GSSG) to reduced GSH [36]. For this, 10 μl of the sample was

incubated with 190 μl of a solution containing 2 mg/ml GSSG and 0.4 mg/ml NADPH, at 37°C. Absorbances were then recorded for 30 min (incubation period), at 340 nm. The results are expressed as μmol of NADPH per min normalized per mg of protein (μmol of NADPH/min/mg of protein).

GPx activity was determined as previously [36]. For this, 30 μl of sample per well (diluted 1:3) was incubated for 5 min at 37°C, with 145 μl per well of 0.05 M phosphate buffer (pH 7.4) containing 0.1 M EDTA, 5 μl of glutathione (GSH, 80 mM), and 5 μl glutathione reductase (0.0096 U/μl). After incubation, 5 μl of 0.46 % tert-butyl hydroperoxide solution and 10 μl of 1.2 mM NADPH were added to each well. Absorbances were monitored at 340 nm for 10 min. The results are expressed as μmol of GSH/min/mg of protein.

2.12. Thioredoxin Reductase (TrxR).

TrxR activity was determined by incubating 20 μl of the sample with 140 μl of assay buffer (0.05 M phosphate buffer (pH 7.4) containing 0.1 M EDTA, 50 mM potassium chloride, and 0.2 mg/ml bovine serum albumin), 20 μl of 2 mM NADPH, and 20 μl of 5 mM 5,5'-dithiobis(2-nitrobenzoic acid) (DTNB), in the presence and absence of a TrxR inhibitor (sodium aurothiomalate; 20 μM) [37]. Absorbances were read at 412 nm for 5 min. The results are expressed in IU of TrxR per mg of protein (IU/mg of protein). Enzyme activity was defined as the NADPH-dependent production of 2 μmol of 2-nitro-5-thiobenzoate per min at 22°C.

2.13. Protein Nitrotyrosine and Carbonyl Levels.

For analysis of protein nitrotyrosine and carbonyl levels, 2.5 μg of each sample was assayed by slot blotting. The presence of proteins containing 3-nitrotyrosine residues was analysed in the samples as previously described [38]. After sample derivatization by addition of Laemmli buffer (0.125 M Trizma, pH 6.8; 4% SDS and 20% glycerol; 20 min at room temperature and boiling for 2 min), the membrane was incubated with mouse monoclonal anti-nitrotyrosine primary antibody (1:2,000; Merck Millipore Co., Germany) overnight at 18°C.

Carbonylated proteins were determined according to the method described by Robinson et al. [39]. After the derivatization reaction by addition of 2,4-dinitrophenylhydrazine (DNPH) solution (0.1 mg/ml in 2N HCl, 5 min), the membrane was incubated with anti-DNP primary antibody (1:25,000 in blocking buffer, Abcam, UK) overnight at 18°C.

Immunoreactive bands were detected by chemiluminescence, and their intensities were estimated by densitometric analysis (ChemiDoc Image Systems, Bio-Rad, USA). Results were normalized by the band intensity values obtained after staining with Ponceau red.

2.14. Plasma and Tissue Hydrogen Peroxide Measurements.

The levels of H_2O_2 were measured in brain homogenates and plasma samples by using a H_2O_2/peroxidase assay kit (Amplex Red H_2O_2/peroxidase assay kit; Molecular Probes, Invitrogen, Brazil) according to the manufacturer's instructions. Results were obtained by comparison of each sample with a H_2O_2 (0–10 μM) standard curve and are expressed as H_2O_2 levels in μM (plasma) and in picomoles of H_2O_2 per mg of protein (brain samples).

2.15. Statistical Analysis.

The results are presented as mean ± standard error (SE). The percentage of inhibition is reported as the mean for each individual experiment. For multiple statistical comparisons between groups, data were analysed by repeated-measures analysis of variance (ANOVA) or one-way ANOVA followed by the Bonferroni test with FDR correction. Paired and unpaired t tests were used when appropriate. Survival curves were analysed by the nonparametric Mantel-Cox test. All data were analysed in GraphPad Prism 5.0. $p < 0.05$ was considered significant. All n numbers are indicated on the graphs.

3. Results

3.1. P. berghei Infection Reduces TRPV1 mRNA Expression in the Mouse Brain, a Response Attenuated by TRPV1 Antagonism.

We initially investigated whether infection with P. berghei ANKA, a plasmodium strain known to cause cerebral malaria in mice, influences TRPV1 expression in the mouse brain. Infected WT mice expressed lower TRPV1 mRNA levels (56%) in their brain tissue than non-infected controls did (Figure 1(a)). On the other hand, the systemic administration of SB366791 in C57BL/6 mice with malaria increased TRPV1 expression (2.1-fold increase) in comparison with vehicle controls (Supplementary Material Figure S1a).

3.2. Loss of TRPV1 Signaling Protects against Cerebral Malaria.

We next assessed whether the ablation of TRPV1 influences cerebral malaria progression and mortality. Data depicted in Figure 1(b) show that infected TRPV1KO mice exhibit attenuated disease in comparison with WT controls. Of note, TRPV1KOs only presented parasitaemia without any other sign or symptom of cerebral malaria, suggesting they do not develop this syndrome. Accordingly, malaria was less severe and remained at stage I in these mice whilst it progressed into stages III and IV in the majority of the WT animals over the 14-day observation period (Figures 1(b) and 1(c)). Mortality was markedly prevented by TRPV1 ablation as 90% of the TRPV1KO mice survived infection in contrast with WT animals (19% survival; Figure 1(d)). Mice treated with SB366791 presented similar disease severity and course to those receiving vehicle until day 6 postinfection, improving their condition over the 14-day observation period (Supplementary Material Figures S1b and S1c). Twenty percent of those receiving the TRPV1 antagonist survived (Supplementary Material Figure S1d). As lack of TRPV1 was previously shown to exacerbate hypothermia in mice with bacterial infection [23], mouse body temperatures were registered. At baseline conditions, both genotypes exhibited similar body temperatures; however, hypothermia was only observed in stage III/IV WT but not TRPV1KO mice (Figure 1(e)). A similar response was registered in those receiving SB366791 (Supplementary Material Figure S1e).

Blood parasitaemia was similar in both genotypes, although WT mice exhibited higher parasitaemia than TRPV1KOs did at days 6 and 7 postinfection (Figure 2(a)). On the other hand, P. berghei ANKA 18S levels were elevated
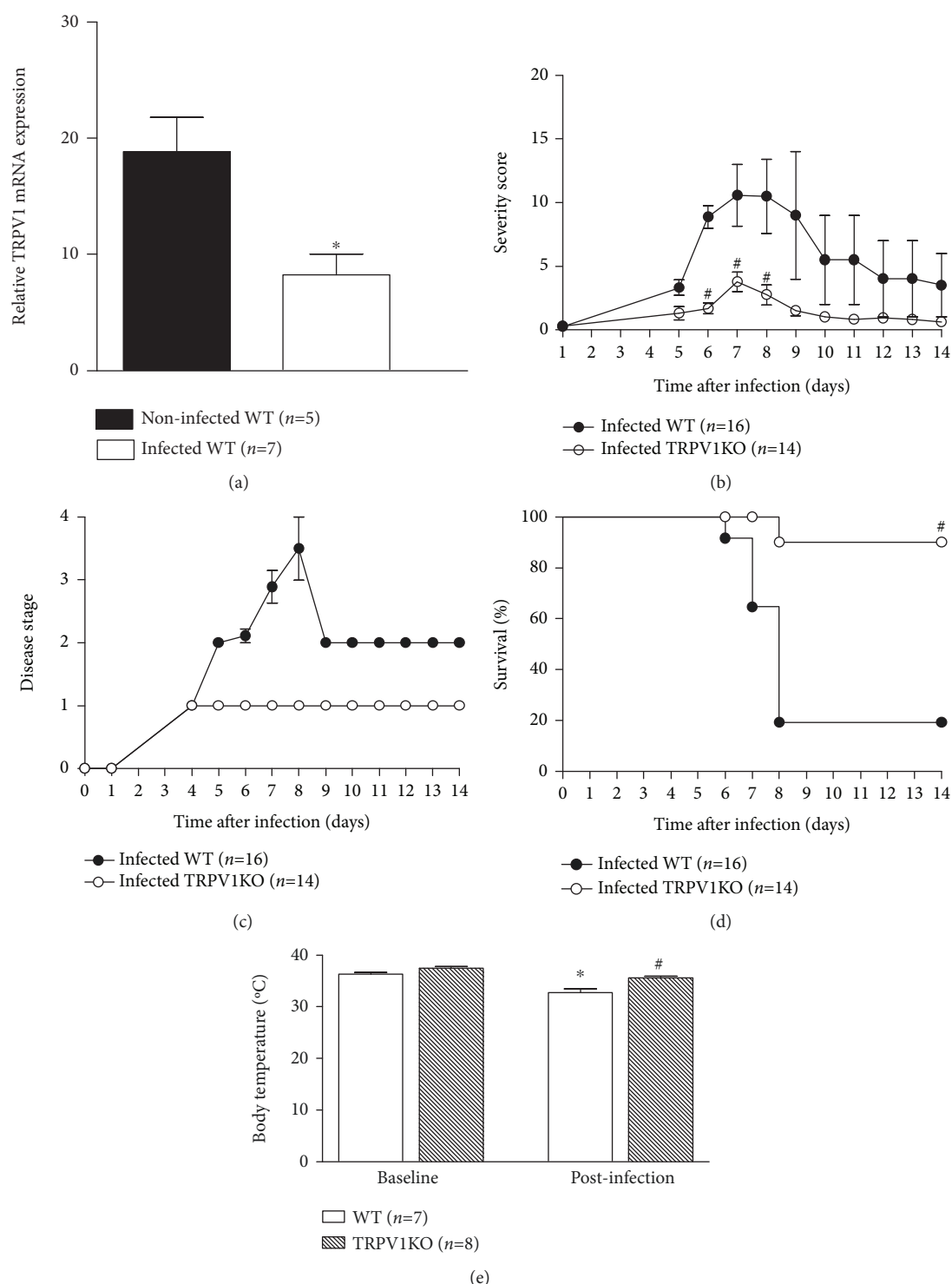
Figure 1: Brain TRPV1 mRNA expression and cerebral malaria progression. (a) TRPV1 mRNA expression in brain samples of noninfected and infected (at stage III/IV) TRPV1 wild-type (WT) mice. Disease progression (b) and stage (c); survival rates (d) and body temperature (e) recordings from TRPV1 WT and knockout (KO) mice infected with *P. berghei* ANKA. Disease progression, stage, and survival rates were registered over 14 days postinfection. Mouse body temperatures were evaluated at baseline and postmalaria induction (at stage III/IV or at day 14 for those that survived the observation period). Results represent the mean ± SEM of all mice per group, obtained from two-three independent experiments. n is indicated on each graph. Data were analysed by repeated-measures analysis of variance (ANOVA) followed by the Bonferroni test with FDR correction (panels b and c). Paired and unpaired t tests were used when appropriate (panels a and e). Survival curves were analysed by the nonparametric Mantel-Cox test (panel d). *$p < 0.05$ differs from noninfected WTs or baseline readings; #$p < 0.05$ differs from infected WT mice.
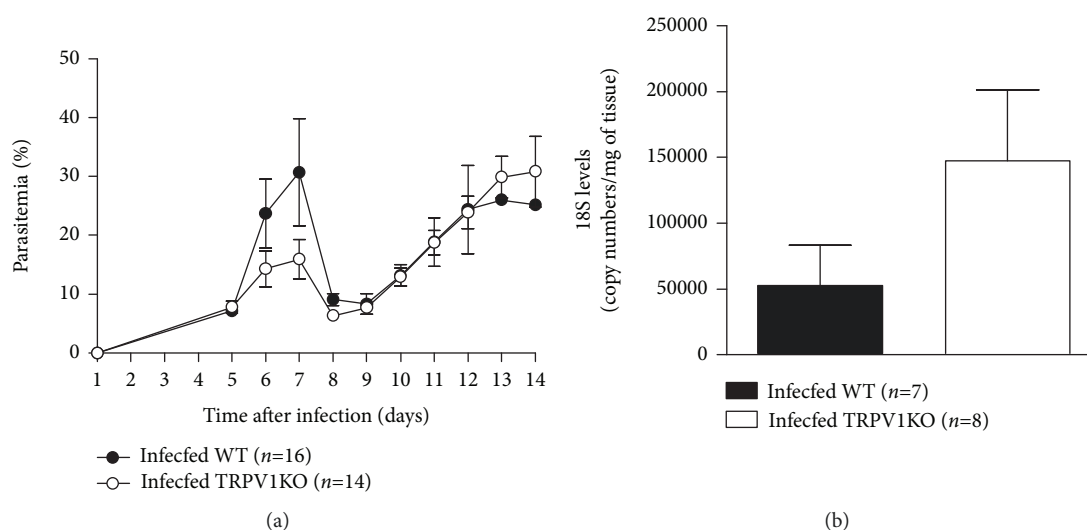
FIGURE 2: Blood and brain parasitaemia. (a) Blood parasitaemia and (b) brain 18S levels in TRPV1 wild-type (WT) and knockout (KO) mice infected with *P. berghei* ANKA. Blood parasitaemia data was collected over 14 days postinfection; brain samples were collected at stage III/IV or at day 14 for those that survived the observation period. Results represent the mean ± SEM of all mice per group, obtained from two-three independent experiments. *n* is indicated on each graph. Data were analysed by repeated-measures analysis of variance (ANOVA) followed by the Bonferroni test with FDR correction (panel a). Unpaired *t* test was used when appropriate (panel b).

in the brain samples of TRPV1KO (2.8-fold) in comparison with those obtained from WT mice (Figure 2(b)).

3.3. Lack of TRPV1 Increases the mRNA Expression of Blood Brain Barrier Integrity Markers and Attenuates Oedema Formation in the Brains of Infected Mice. Loss of integrity of the blood brain barrier is a hallmark of cerebral malaria, contributing to increased oedema formation and neuronal damage as disease progresses [40, 41]. Possible effects of TRPV1 ablation in brain oedema formation and in the gene expression of the tight junction components claudin-5 and JAM-A [41, 42] were then, investigated. Data depicted in Figure 3(a) demonstrates that infection with *P. berghei* ANKA promotes brain swelling in WT (1.7-fold) and TRPV1KO (1.2-fold) mice in comparison with their respective noninfected controls; however, this response was reduced by 25% in those lacking TRPV1. Additionally, analysis of claudin-5 and JAM-A mRNA levels revealed that infected WT mice express diminished levels of both genes (49% and 80%, respectively), in comparison with noninfected controls, a response that was attenuated in infected TRPV1KO mice (Figures 3(b) and 3(c)). Genotype did not affect brain weight/body weight ratios or claudin-5 mRNA expression in noninfected mice (Figures 3(a) and 3(b)). However, noninfected TRPV1KOs presented with lower expression of JAM-A (47%) in comparison with their WT counterparts (Figure 3(c)).

3.4. H_2O_2, Protein Nitrotyrosine and Carbonyl Residues Are Raised in Infected TRPV1KO Animals. Oxidative stress normally occurs as part of the host response to malaria [5, 43]. TRPV1 is an oxidative stress sensor [28], which not only does modulate oxidative stress [23, 27] but also can have its expression regulated by endogenous oxidant molecules [26]. Therefore, the impact of TRPV1 ablation in malaria-

associated oxidative stress was investigated. Higher levels of H_2O_2 and protein nitrotyrosine residues (indicative of NO-dependent oxidative stress; [44]) were detected in infected mice of both genotypes in comparison with their noninfected controls (Figures 4(a) and 4(b)). WT mice presented 4.8-fold and 3.7-fold increases and TRPV1KOs 6.0-fold and 2.7-fold increases for tissue H_2O_2 and protein nitrotyrosine residue levels, respectively. Protein carbonyl residues (indicative of lipid peroxidation-dependent oxidative stress; [45]) were only increased (1.9-fold) in brain samples of infected mice lacking TRPV1 (Figure 4(c)). Analysis of plasma H_2O_2 levels, and protein nitrotyrosine and carbonyl levels indicated these were raised in TRPV1KO but not WT mice infected with *P. berghei* ANKA (Figures 4(d)–4(f)). TRPV1KOs presented greater levels of plasma H_2O_2 (13.9-fold increase), protein nitrotyrosine (1.5-fold increase), and carbonyl (1.4-fold increase) residues in comparison with those observed for WT animals with cerebral malaria (Figures 4(d)–4(f)).

As TRPV1KO mice presented with an exacerbated production of oxidants, the activity of antioxidant enzymes was then, investigated. The tissue activity levels of SOD, GPx, and GR were attenuated (by ~35%, ~20%, and ~34% of reduction, respectively) in infected mice irrespective of genotype when compared to noninfected controls (Figures 5(a), 5(d), and 5(e)). Also, TrxR activity was enhanced in both infected genotypes (1.5-fold increase; Figure 5(f)). On the other hand, brain catalase activity was markedly diminished (49%) in infected TRPV1KO but not WT mice (Figure 5(b)). Infected TRPV1KO mice also displayed lower levels of catalase activity (70% less) in their plasma in comparison with WT controls (Figure 5(c)).

3.5. Diminished Cytokine Production Is Detected in Infected TRPV1KO Mice. Cytokines are involved in neuronal survival [46, 47] and therefore may affect cerebral malaria

(a)

(b)

(c)
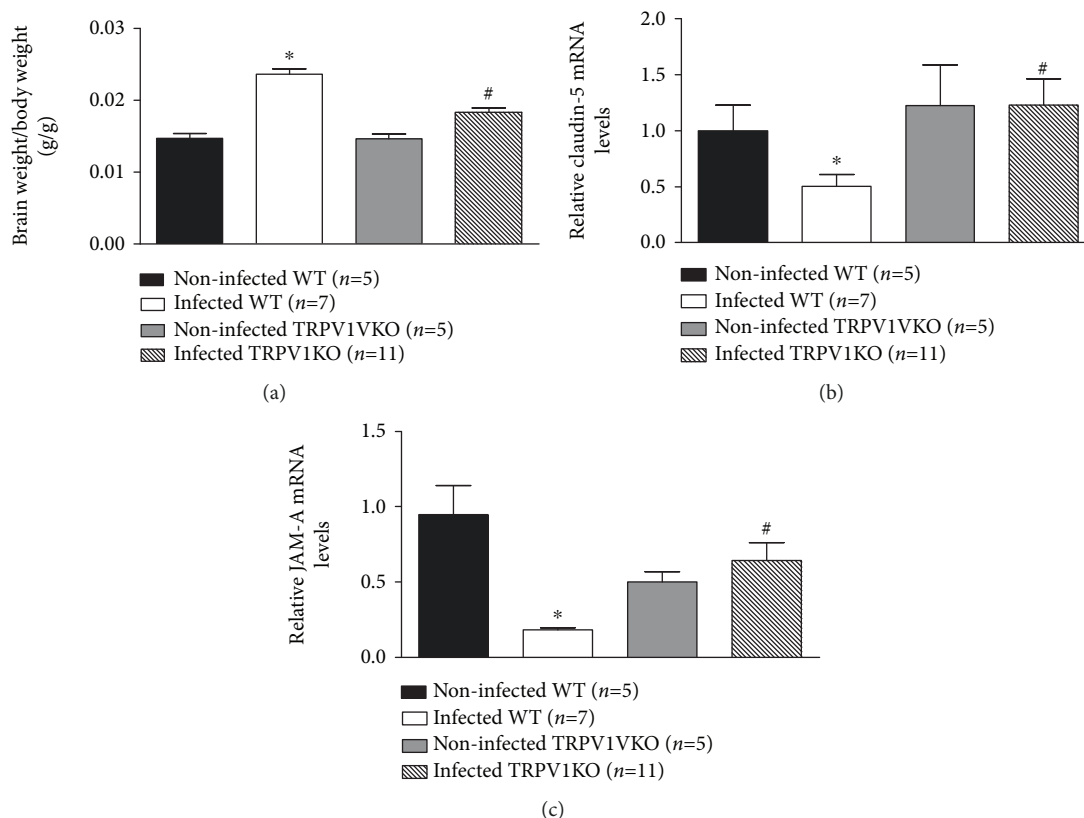
FIGURE 3: Brain swelling and expression of blood brain barrier integrity markers. (a) Brain weight/body weight ratios and mRNA expression levels of claudin-5 (b) and JAM-A (c) in brain samples of TRPV1 wild-type (WT) and knockout (KO) mice infected with *P. berghei* ANKA. Brain samples were collected at stage III/IV or at day 14 for those that survived the observation period. Samples from noninfected mice were used as controls. Results represent the mean ± SEM of all mice per group, obtained from three independent experiments. n is indicated on each graph. Data were analysed by one-way analysis of variance (ANOVA) followed by the Bonferroni test with FDR correction. $^*p < 0.05$ differs from noninfected WTs; $^\#p < 0.05$ differs from infected WT mice.

progression. Thus, the levels of both tissue and plasma IFNγ, TNFα, and IL-6 were assessed in WT and TRPV1KO mice with malaria. Tissue and plasma TNFα production was markedly reduced (52% and 64%, respectively; Figures 6(a) and 6(d)) in TRPV1KO in comparison with WT controls. A similar profile was observed for IL-6 as mice lacking TRPV1 exhibited significant lower levels of this cytokine at both tissue (65% reduction) and plasma (86% reduction) levels (Figures 6(b) and 6(d)). Genotype did not affect IFNγ levels in a significant manner (Figures 6(c) and 6(f)).

4. Discussion

Since its discovery, the TRPV1 channel has been pointed out as an essential receptor in a variety of physiological and pathological responses. This is due to its wide expression and ability to transduce signals in both neuronal and nonneuronal cells, therefore participating in responses that range from cell differentiation to death [16, 23, 48–50]. Novel and recent findings on its role indicate that the endogenous activation of TRPV1 protects mammals from bacterial infections [21–24]. More recently, a nonselective TRPV1 antagonist (capsazepine) was found to modulate

the peripheral immune response to malaria [25], but no studies have reported to date, a role for TRPV1 in cerebral malaria development and outcome. Here, we show for the first time that in the absence of TRPV1, *P. berghei* ANKA infection does not progress into cerebral malaria in the majority of the infected mice, protecting them from death and from the development of any disease symptoms and signals apart from blood parasitaemia. Protection was also observed in mice receiving the TRPV1 antagonist SB366791 repeatedly after malaria was induced. Of note, this effect was more pronounced in TRPV1KOs than in mice treated with SB366791. Although these results suggest that an intervention with a TRPV1 antagonist may be an alternative to avoid malaria progression, its use should be carefully considered as it may increase mortality upon bacterial infection [23]. Interestingly, although TRPV1 ablation exacerbates hypothermia in bacterial infection [21, 23], it was found herein that TRPV1KO mice and WTs treated with the selective TRPV1 antagonist SB366791 are protected from this condition in comparison with infected WTs.

P. berghei ANKA-infected mice treated with capsazepine were previously demonstrated to present similar blood parasitaemia to those treated with vehicle [25]. Here, we show

(a)

(b)

(c)

(d)

(e)

(f)
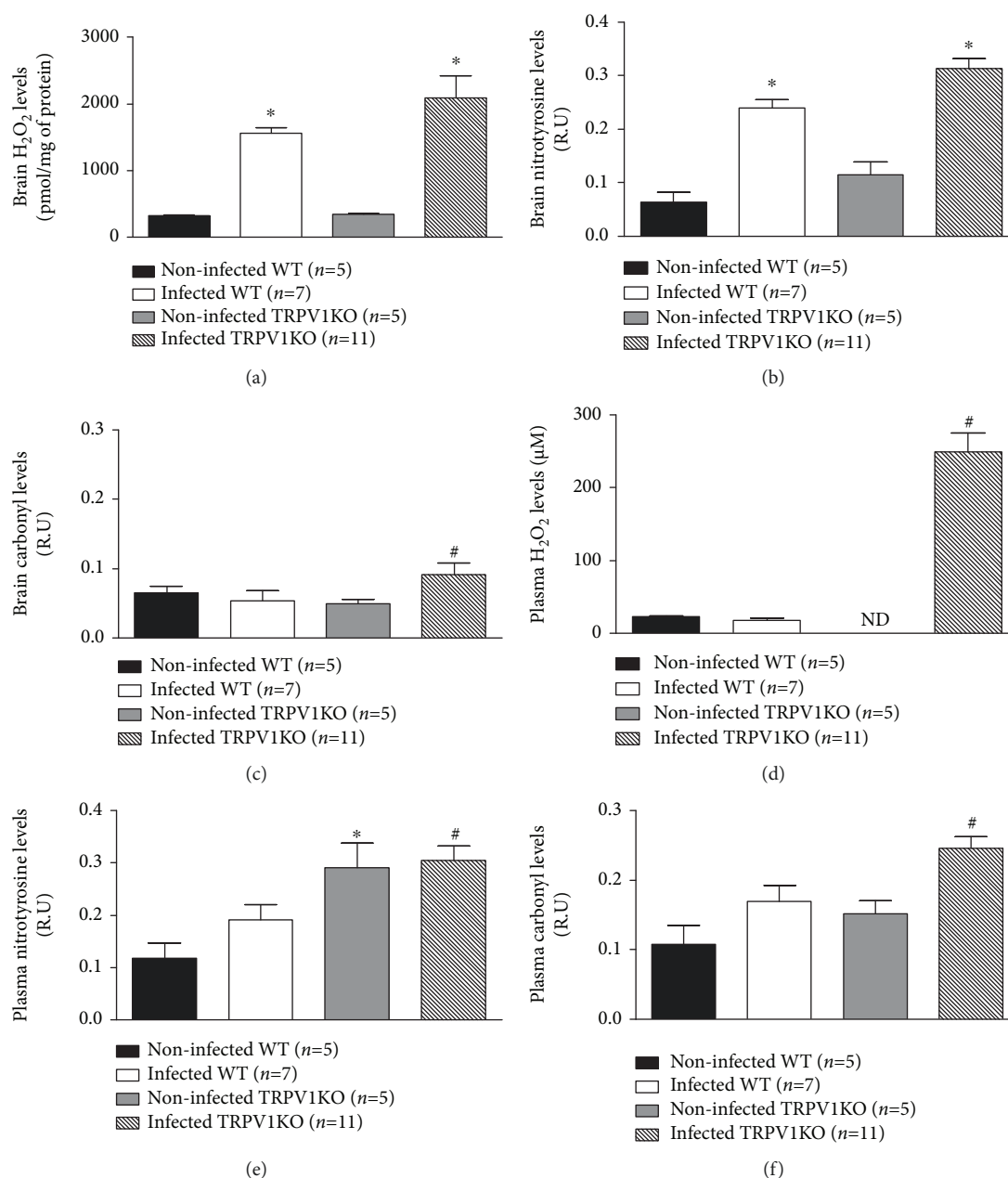
FIGURE 4: Levels of H_2O_2, protein nitrotyrosine, and carbonyl residues. (a) H_2O_2 concentrations, protein (b) nitrotyrosine and (c) carbonyl residues in brain samples obtained from TRPV1 wild-type (WT) and knockout (KO) mice infected or not with *P. berghei* ANKA. (d) H_2O_2 concentrations, protein (e) nitrotyrosine, and (f) carbonyl residues in plasma samples obtained from TRPV1 wild-type (WT) and knockout (KO) mice infected or not with *P. berghei* ANKA. Samples were collected at stage III/IV or at day 14 for those that survived the observation period. Results represent the mean ± SEM of all mice per group, obtained from three independent experiments. *n* is indicated on each graph. Data were analysed by one-way analysis of variance (ANOVA) followed by the Bonferroni test with FDR correction. *$p < 0.05$ differs from noninfected WTs; #$p < 0.05$ differs from infected WT mice.

that infected mice lacking TRPV1 present with similar blood parasitaemia to those expressing this receptor. On the other hand, at days 6 and 7 postinfection, infected WTs presented higher parasitaemia than TRPV1KOs did. Despite that, surviving TRPV1KO mice exhibited higher levels of plasmodium 18S in their brain samples than WTs did with cerebral malaria at stage III/IV. Of note, the techniques used to measure blood parasitaemia and brain parasite load are different as peripheral parasitaemia comprises the detection

of live parasites whilst brain 18S expression does not discriminate between live and dead plasmodium. However, it is possible that TRPV1KO mice are able to kill the parasites that reach the brain more efficiently than WTs are, therefore protecting those lacking TRPV1 from death.

Brain oedema formation in patients with cerebral malaria is indicative of a bad disease prognosis, especially in children [3, 51]. In adults, brain oedema is not as usual but affects 25% of these patients [52]. Brain swelling results from increased
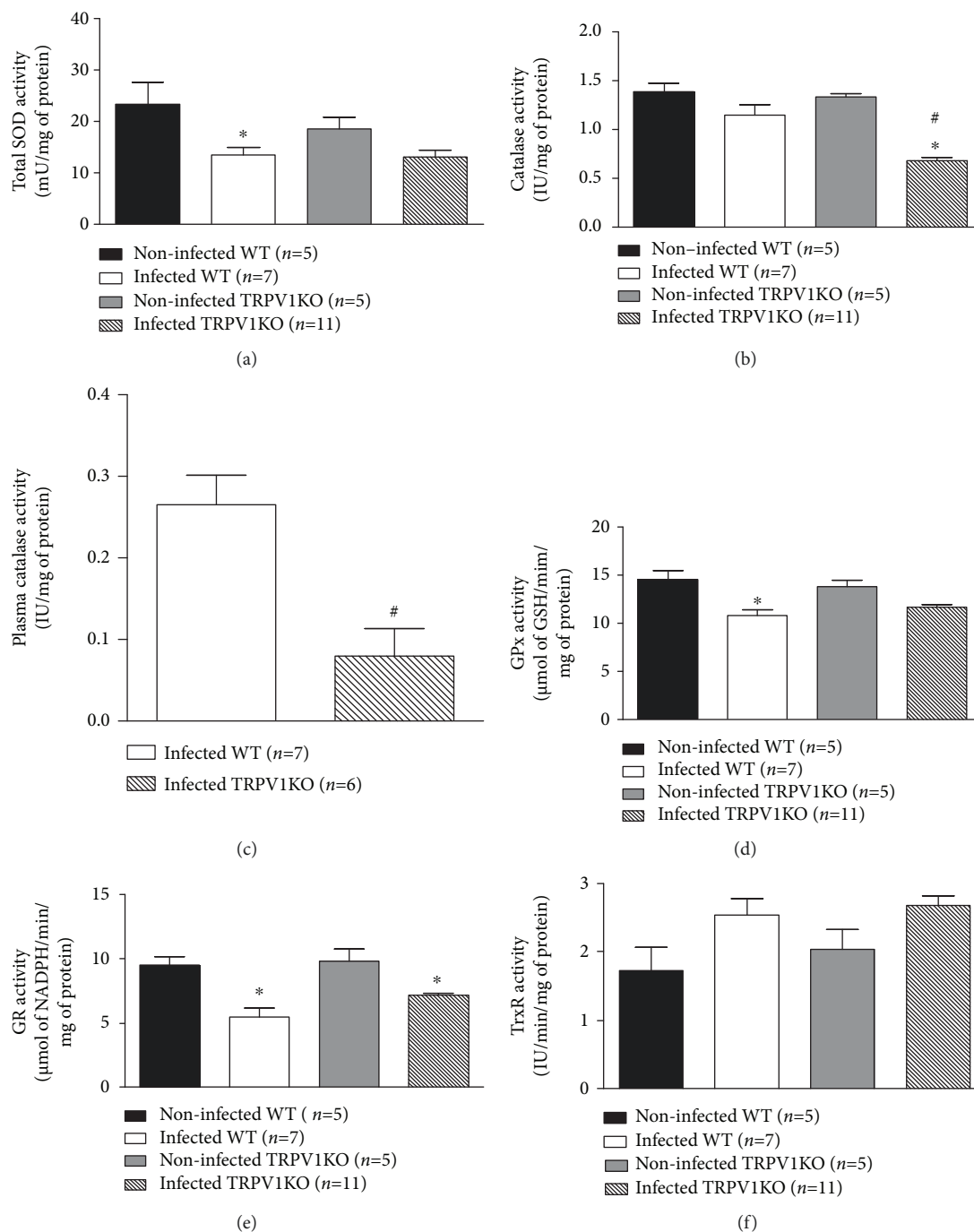
FIGURE 5: Activity levels of antioxidant enzymes. (a) Superoxide dismutase (SOD), (b) catalase, (d) glutathione peroxidase (GPx), (e) glutathione reductase (GR), and (f) thioredoxin reductase (TrxR) activity levels in brain samples obtained from TRPV1 wild-type (WT) and knockout (KO) mice infected or not with *P. berghei* ANKA. (c) Activity levels of catalase in plasma samples of infected TRPV1 WT and KO mice. Samples were collected at stage III/IV or at day 14 for those that survived the observation period. Results represent the mean ± SEM of all mice per group, obtained from three independent experiments. *n* is indicated on each graph. Data were analysed by one-way analysis of variance (ANOVA) followed by the Bonferroni test with FDR correction (panels a, b, d, e, and f). Unpaired *t* test was used when appropriate (panel c). $^*p < 0.05$ differs from noninfected WTs; $^\#p < 0.05$ differs from infected WT mice.

vascular leakage and disruption of the blood brain barrier [8, 9]. TRPV1 activation promotes vasodilation and oedema formation [53, 54]. Then, the contribution of TRPV1 to brain oedema formation was assessed in infected mice. Infected WT mice exhibited brain swelling and decreased mRNA

expression of the markers of blood brain barrier integrity JAM-A and claudin-5 [41, 42]. However, in the absence of TRPV1, there was higher JAM-A and claudin-5 mRNA expression. This response was associated with less brain oedema formation, suggesting that mice lacking TRPV1 are
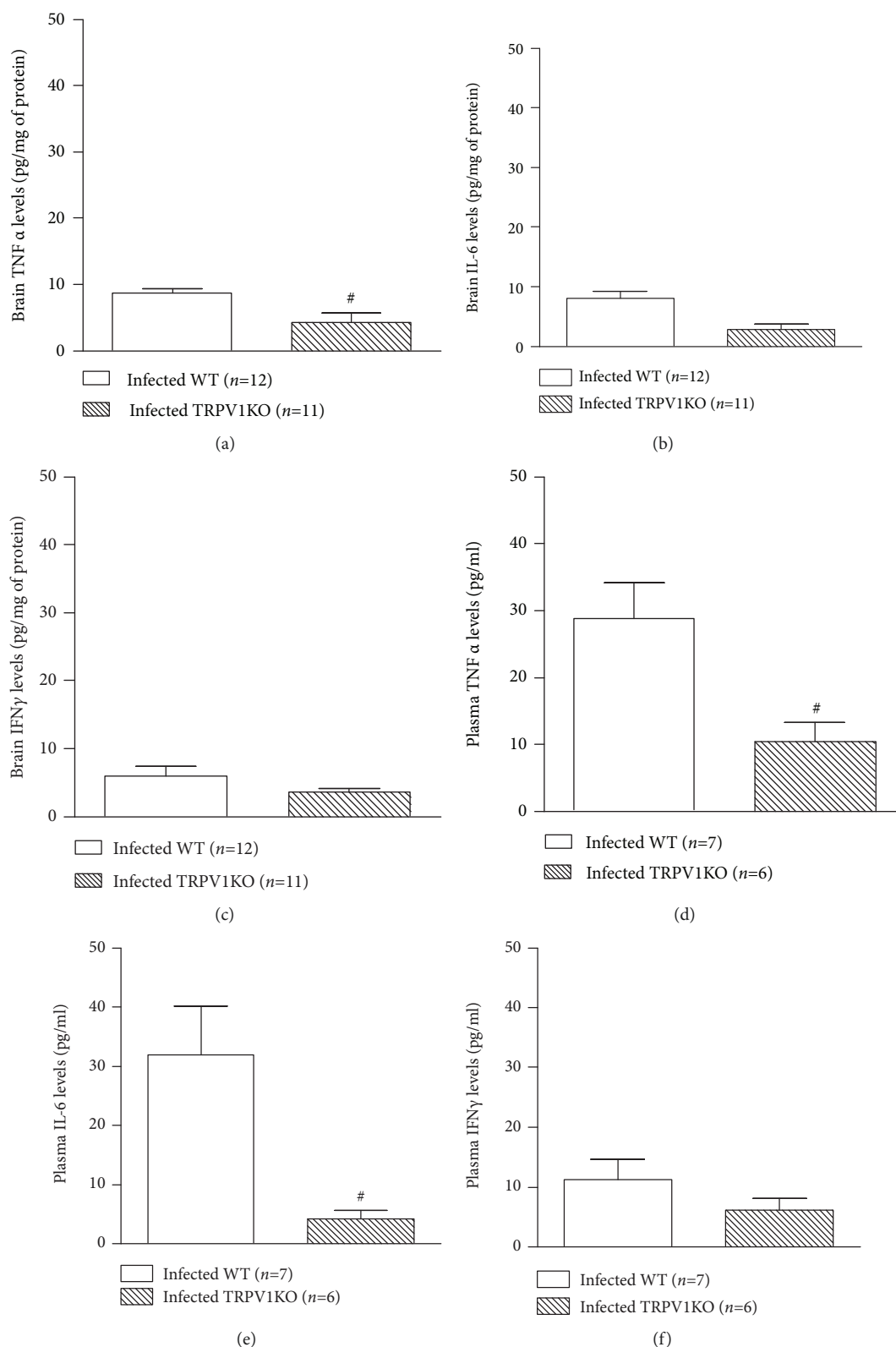
FIGURE 6: Brain and circulating levels of cytokines. Brain levels of (a) tumor necrosis α (TNFα), (b) interleukin-6 (IL-6), and (c) interferon γ (IFNγ) and plasma concentrations of (d) TNFα, (e) IL-6, and IFNγ (f) in TRPV1 wild-type (WT) and knockout (KO) mice infected with *P. berghei* ANKA. Samples were collected at stage III/IV or at day 14 for those that survived the observation period. Results represent the mean $\pm$ SEM of all mice per group, obtained from three independent experiments. n is indicated on each graph. Data were analysed by unpaired t test. $^{\#}p < 0.05$ differs from infected WT mice.
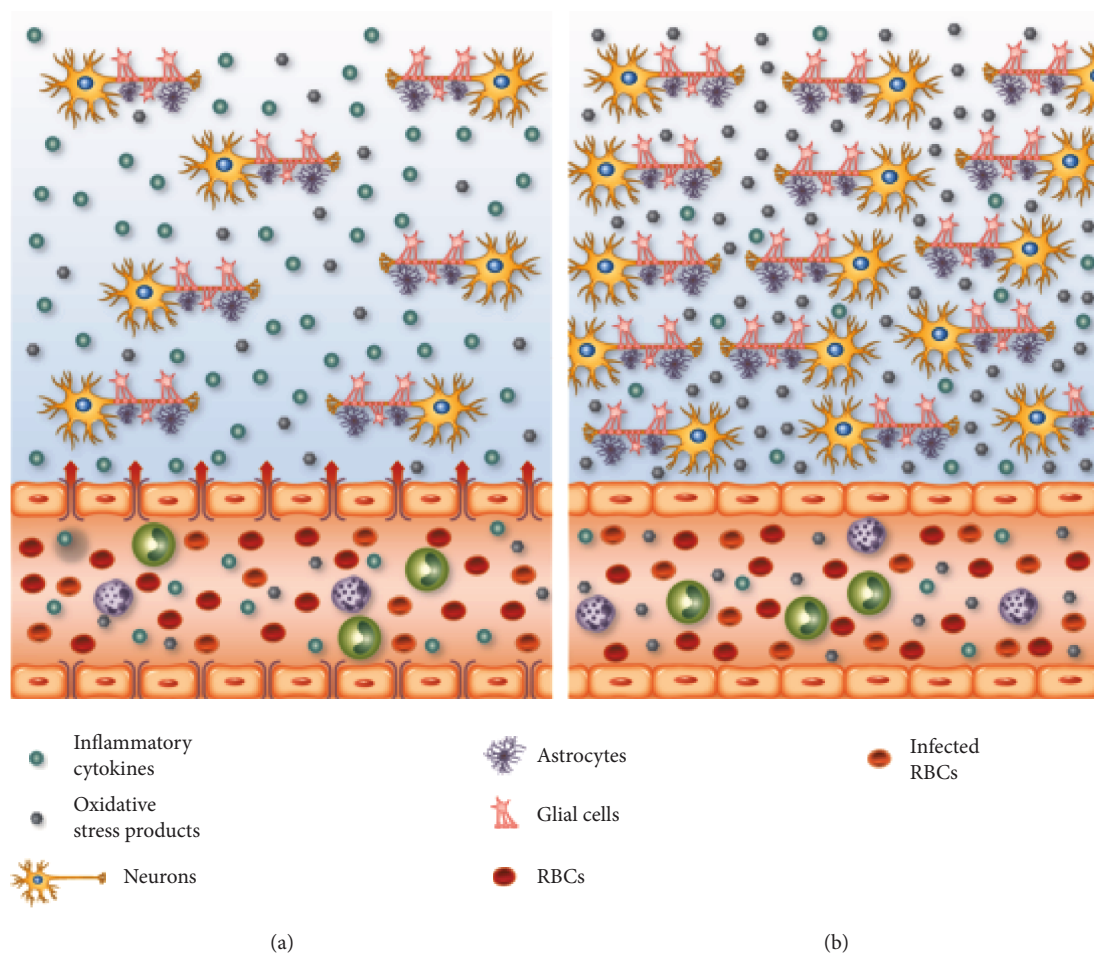
FIGURE 7: Brain and vascular changes in cerebral malaria in TRPV1 WT and KO mice. (a) Several alterations occur in the brain tissue and vasculature during cerebral malaria. Wild-type (WT) red blood cells (RBC) infected with *Plasmodium berghei* ANKA reach the brain vasculature and trigger the accumulation of leukocytes in the vascular space. As a result of this close interaction between infected RBC, leukocytes, and the endothelium, oxidative stress products (H_2O_2, nitrosylated and carbonylated proteins) and cytokines (TNFα, IL-6, and IFNγ) are detected in the circulation and in the brain tissue; H_2O_2 levels are a lot higher in the brain tissue in comparison with the circulation. Plasma extravazation is increased in the brain and this is associated with reduced mRNA expression of the tight-junction endothelial markers claudin-5 and JAM-A. These alterations may culminate with neuronal death, thus, contributing to the increased morbidity and mortality observed in WT mice following infection with *P. berghei* ANKA. (b) Infected mice lacking TRPV1 (TRPV1KO) present increased levels of H_2O_2 and nitrosylated and carbonylated proteins than WT animals at both brain tissue and circulation. TRPV1KOs also exhibit lower concentrations of plasma and brain cytokines, especially TNFα and IL-6, and less plasma extravazation than WT mice, a response that is accompanied by higher expression of claudin-5 and JAM-A in their brain vasculature. The inflammatory response profile observed in TRPV1KO mice may reflect in less neuronal damage, as these animals are protected from *P. berghei* ANKA-induced death and symptoms.

protected from the brain damage, coma, and death associated with protein leakage into the brain tissue secondary to plasmodium infection.

Intravascular oxidative stress is a common phenomenon in malaria which has been associated with alterations in the endothelium that in turn, facilitate the parasite accumulation into the brain tissue and/or vasculature [55, 56]. Additionally, decreased NO availability was recently linked to increased cerebral-vascular dysfunction in cerebral malaria [6]. A feedback between TRPV1 expression/activation and oxidative stress pathways has been previously demonstrated [23, 26–28]. Of note, the activity of oxidative stress enzymes has been investigated

in neurons under inflammatory conditions and may influence neuronal survival [57–61]. Therefore, the influence of TRPV1 on brain oxidative stress was evaluated.

Our data show that infected WTs present higher levels of H_2O_2 and protein nitrotyrosine residues (indicative of excessive NO- or peroxynitrite-dependent oxidation; [44]) in their brain tissue than noninfected mice do. Interestingly, these markers were present at even higher concentrations in mice lacking TRPV1. Of note, the elevated production of these oxidant products was observed not only in the brain tissue but also systemically. In comparison with infected WTs, TRPV1KO mice injected with *P. berghei* also exhibited increased protein carbonylation

(indicative of lipid peroxidation-dependent oxidative stress; [45]) in brain and plasma samples. The higher levels of H_2O_2 in infected TRPV1KO were accompanied by a significantly lower catalase activity in comparison with WT animals. These results reinforce the idea that TRPV1KO mice may be able to deal with the parasite load more efficiently than WTs. This is supported by data showing that TRPV1KO mice present higher H_2O_2 and NO production which may lead to increased parasite killing.

High levels of cytokines have been linked to severe malaria in both humans and mice as their production contributes to cerebral-vascular dysfunction and even neuronal death [46, 47, 62–65]. Of note, lipid peroxidation is suggested to cause suppression of NF-κB activation (for review, see [66]), a key molecule in the generation of proinflammatory cytokines. Here, plasma and cerebral TNFα and IL-6 production was markedly diminished by TRPV1 ablation, thus evidencing, once more, that TRPV1 signaling is involved in the tissue damage associated with cerebral malaria. Although not significant, a similar profile was observed for IFNγ in the same mice. Interestingly, IFNγ and TNFα have been linked to cerebral malaria progression by acting on brain endothelial cells, thus promoting their activation and/or apoptosis [67, 68]. Recently, the TRPV1 antagonist AMG9810 was found to confer neuroprotection by attenuating TNFα production in a rodent model of stroke [54]. These evidences and the gathered data allow us to suggest that the diminished cytokine generation by TRPV1KO mice contributes to the diminished brain swelling and damage observed in *P. berghei* ANKA-infected mice, a response that is associated with a greater ability of these mice to produce higher amounts of oxygen/nitrogen-derived oxidant species which in turn may enhance their capacity of killing this parasite.

Figure 7 summarizes the inflammatory events that occur in the brain of TRPV1 WT and KO mice during cerebral malaria. Overall, the data presented here, indicate that TRPV1 channels contribute to the development and outcome of cerebral malaria. Although antagonists targeting this receptor may be useful to preventing the development of the cerebral syndrome caused by *Plasmodium* sp., their clinical use may be limited as they worsen sepsis outcome.

Data Availability

The datasets used to support this study will be made available upon request. Requests should be sent to the corresponding author.

Conflicts of Interest

The authors declare no conflicts of interest.

Authors' Contributions

D.M.S. Pereira, S.A. Teixeira, O. Murillo, E.P.M. Peixoto, M.C. Araújo, and N.C.F. Sousa performed the experiments and data analysis; C.R.F. Marinho, M.N. Muscará, and E.S. Fernandes designed the experiments and supervised the study; E.S. Fernandes secured the funding support and originally drafted the manuscript; V. Monteiro-Neto, J.B. Calixto, T.M. Cunha, C.R.F. Marinho, M.N. Muscará, and E.S. Fernandes critically revised the manuscript.

Acknowledgments

Supplementary Materials

Figure S1: Effect of the selective TRPV1 antagonist SB366791 in the brain expression of TRPV1 mRNA and in cerebral malaria progression. (a) TRPV1 mRNA expression in brain samples of infected (at stage III/IV) TRPV1 wild-type (WT) mice. Disease progression (b) and stage (c); survival rates (d) and body temperature (e) recordings from TRPV1 WT mice infected with P. berghei ANKA. Disease progression, stage, and survival rates were registered over 14 days postinfection. Mouse body temperatures were evaluated at baseline and postmalaria induction (at stage III/IV or at day 14 for those that survived the observation period). Mice received the TRPV1 antagonist SB366791 (0.5 mg/kg, s.c., twice a day) or vehicle (10% DMSO in saline), from 24 h postinduction of malaria. Results represent the mean + SEM of all mice per group, obtained from three independent experiments. n is indicated on each graph. $^*p < 0.05$ differs from baseline readings; $^\#p < 0.05$ differs from infected WT mice treated with vehicle. (*Supplementary Materials*)

References

[1] World Health Organization, *World Malaria Report 2016*, World Health Organization, 2016.

[2] H. J. Shikani, B. D. Freeman, M. P. Lisanti, L. M. Weiss, H. B. Tanowitz, and M. S. Desruisseaux, "Cerebral malaria: we have come a long way," *The American Journal of Pathology*, vol. 181, no. 5, pp. 1484–1492, 2012.

[3] World Health Organization, "Severe Malaria," *Tropical Medicine & International Health*, vol. 19, pp. 7–131, 2014.

[4] I. Gramaglia, P. Sobolewski, D. Meays et al., "Low nitric oxide bioavailability contributes to the genesis of experimental cerebral malaria," *Nature Medicine*, vol. 12, no. 12, pp. 1417–1422, 2006.

[5] N. Narsaria, C. Mohanty, B. K. Das, S. P. Mishra, and R. Prasad, "Oxidative stress in children with severe malaria," *Journal of Tropical Pediatrics*, vol. 58, no. 2, pp. 147–150, 2012.

[6] P. K. Ong, B. Melchior, Y. C. Martins et al., "Nitric oxide synthase dysfunction contributes to impaired cerebroarteriolar reactivity in experimental cerebral malaria," *PLoS Pathogens*, vol. 9, no. 6, article e1003444, 2013.

[7] M. Hernandez-Valladares, P. Rihet, and F. A. Iraqi, "Host susceptibility to malaria in human and mice: compatible approaches to identify potential resistant genes," *Physiological Genomics*, vol. 46, no. 1, pp. 1–16, 2014.

[8] M. J. Hackett, J. B. Aitken, F. el-Assaad et al., "Mechanisms of murine cerebral malaria: multimodal imaging of altered cerebral metabolism and protein oxidation at hemorrhage sites," *Science Advances*, vol. 1, no. 11, p. e1500911, 2015.

[9] J. Dunst, F. Kamena, and K. Matuschewski, "Cytokines and chemokines in cerebral malaria pathogenesis," *Frontiers in Cellular and Infection Microbiology*, vol. 7, article 324, 2017.

[10] P. Strangward, M. J. Haley, T. N. Shaw et al., "A quantitative brain map of experimental cerebral malaria pathology," *PLoS Pathogens*, vol. 13, no. 3, article e1006267, 2017.

[11] M. Marks, A. Gupta-Wright, J. F. Doherty, M. Singer, and D. Walker, "Managing malaria in the intensive care unit," *British Journal of Anaesthesia*, vol. 113, no. 6, pp. 910–921, 2014.

[12] A. Dondorp, F. Nosten, K. Stepniewska, N. Day, and N. White, "Artesunate versus quinine for treatment of severe falciparum malaria: a randomised trial," *The Lancet*, vol. 366, no. 9487, pp. 717–725, 2005.

[13] A. M. Dondorp, C. I. Fanello, I. C. Hendriksen et al., "Artesunate versus quinine in the treatment of severe falciparum malaria in African children (AQUAMAT): an open-label, randomised trial," *The Lancet*, vol. 376, no. 9753, pp. 1647–1657, 2010.

[14] S. A. Golech, R. M. McCarron, Y. Chen et al., "Human brain endothelium: coexpression and function of vanilloid and endocannabinoid receptors," *Molecular Brain Research*, vol. 132, no. 1, pp. 87–92, 2004.

[15] A. Tóth, J. Boczán, N. Kedei et al., "Expression and distribution of vanilloid receptor 1 (TRPV1) in the adult rat brain," *Molecular Brain Research*, vol. 135, no. 1-2, pp. 162–168, 2005.

[16] E. S. Fernandes, M. A. Fernandes, and J. E. Keeble, "The functions of TRPA1 and TRPV1: moving away from sensory nerves," *British Journal of Pharmacology*, vol. 166, no. 2, pp. 510–521, 2012.

[17] D. Martins, I. Tavares, and C. Morgado, ""Hotheaded": the role of TRPV1 in brain functions," *Neuropharmacology*, vol. 85, pp. 151–157, 2014.

[18] B. M. Assas, W. H. Abdulaal, M. H. Wakid, H. A. Zakai, J. Miyan, and J. L. Pennock, "The use of flow cytometry to examine calcium signalling by TRPV1 in mixed cell populations," *Analytical Biochemistry*, vol. 527, pp. 13–19, 2017.

[19] I. Vetter, P. R. Kym, and A. Szallasi, "Feeling hot, feeling cold: TRP channels-a great story unfolds," *Temperature*, vol. 2, no. 2, pp. 150-151, 2015.

[20] W. L. Kong, Y. Y. Peng, and B. W. Peng, "Modulation of neuroinflammation: Role and therapeutic potential of TRPV1 in the neuro-immune axis," *Brain, Behavior, and Immunity*, vol. 64, pp. 354–366, 2017.

[21] N. Clark, J. Keeble, E. S. Fernandes et al., "The transient receptor potential vanilloid 1 (TRPV1) receptor protects against the onset of sepsis after endotoxin," *The FASEB Journal*, vol. 21, no. 13, pp. 3747–3755, 2007.

[22] V. Guptill, X. Cui, A. Khaibullina et al., "Disruption of the transient receptor potential vanilloid 1 can affect survival, bacterial clearance, and cytokine gene expression during murine sepsis," *Anesthesiology*, vol. 114, no. 5, pp. 1190–1199, 2011.

[23] E. S. Fernandes, L. Liang, S. J. Smillie et al., "TRPV1 deletion enhances local inflammation and accelerates the onset of systemic inflammatory response syndrome," *Journal of Immunology*, vol. 188, no. 11, pp. 5741–5751, 2012.

[24] S. P. Wanner, A. Garami, E. Pakai et al., "Aging reverses the role of the transient receptor potential vanilloid-1 channel in systemic inflammation from anti-inflammatory to proinflammatory," *Cell Cycle*, vol. 11, no. 2, pp. 343–349, 2012.

[25] E. S. Fernandes, C. X. L. Brito, S. A. Teixeira et al., "TRPV1 antagonism by capsazepine modulates innate immune response in mice infected with *Plasmodium berghei* ANKA," *Mediators of Inflammation*, vol. 2014, Article ID 506450, 12 pages, 2014.

[26] P. Puntambekar, D. Mukherjea, S. Jajoo, and V. Ramkumar, "Essential role of Rac1/NADPH oxidase in nerve growth factor induction of TRPV1 expression," *Journal of Neurochemistry*, vol. 95, no. 6, pp. 1689–1703, 2005.

[27] A. Starr, R. Graepel, J. Keeble et al., "A reactive oxygen species-mediated component in neurogenic vasodilatation," *Cardiovascular Research*, vol. 78, no. 1, pp. 139–147, 2008.

[28] J. E. Keeble, J. V. Bodkin, L. Liang et al., "Hydrogen peroxide is a novel mediator of inflammatory hyperalgesia, acting via transient receptor potential vanilloid 1-dependent and independent mechanisms," *Pain*, vol. 141, no. 1, pp. 135–142, 2009.

[29] T. Schilling and C. Eder, "Importance of the non-selective cation channel TRPV1 for microglial reactive oxygen species generation," *Journal of Neuroimmunology*, vol. 216, no. 1-2, pp. 118–121, 2009.

[30] T. Schilling and C. Eder, "Stimulus-dependent requirement of ion channels for microglial NADPH oxidase-mediated production of reactive oxygen species," *Journal of Neuroimmunology*, vol. 225, no. 1-2, pp. 190–194, 2010.

[31] R. M. Elias, M. Correa-Costa, C. R. Barreto et al., "Oxidative stress and modification of renal vascular permeability are associated with acute kidney injury during *P. berghei* ANKA infection," *PLoS One*, vol. 7, no. 8, p. e44004, 2012.

[32] A. S. Miranda, F. Brant, N. P. Rocha et al., "Further evidence for an anti-inflammatory role of artesunate in experimental cerebral malaria," *Malaria Journal*, vol. 12, no. 1, 2013.

[33] M. Linares, P. Marín-García, S. Pérez-Benavente et al., "Brain-derived neurotrophic factor and the course of experimental cerebral malaria," *Brain Research*, vol. 1490, pp. 210–224, 2013.

[34] R. W. Carroll, M. S. Wainwright, K. Y. Kim et al., "A rapid murine coma and behavior scale for quantitative assessment of murine cerebral malaria," *PLoS One*, vol. 5, no. 10, article e13124, 2010.

[35] E. S. Fernandes, G. F. Passos, M. M. Campos et al., "Cytokines and neutrophils as important mediators of platelet-activating factor-induced kinin B_1 receptor expression," *British Journal of Pharmacology*, vol. 146, no. 2, pp. 209–216, 2005.

[36] F. F. Abreu, A. C. A. Souza, S. A. Teixeira et al., "Elucidating the role of oxidative stress in the therapeutic effect of

rutin on experimental acute pancreatitis," *Free Radical Research*, vol. 50, no. 12, pp. 1350–1360, 2016.

[37] K. E. Hill, G. W. McCollum, and R. F. Burk, "Determination of thioredoxin reductase activity in rat liver supernatant," *Analytical Biochemistry*, vol. 253, no. 1, pp. 123–125, 1997.

[38] R. Sultana and D. A. Butterfield, "Slot-blot analysis of 3-nitrotyrosine-modified brain proteins," *Methods in Enzymology*, vol. 440, pp. 309–316, 2008.

[39] C. E. Robinson, A. Keshavarzian, D. S. Pasco, T. O. Frommel, D. H. Winship, and E. W. Holmes, "Determination of protein carbonyl groups by immunoblotting," *Analytical Biochemistry*, vol. 266, no. 1, pp. 48–57, 1999.

[40] L. Rénia, S. W. Howland, C. Claser et al., "Cerebral malaria: mysteries at the blood-brain barrier," *Virulence*, vol. 3, no. 2, pp. 193–201, 2012.

[41] A. Nacer, A. Movila, F. Sohet et al., "Experimental cerebral malaria pathogenesis–hemodynamics at the blood brain barrier," *PLoS Pathogens*, vol. 10, no. 12, article e1004528, 2014.

[42] S. M. Stamatovic, N. Sladojevic, R. F. Keep, and A. V. Andjelkovic, "Relocalization of junctional adhesion molecule A during inflammatory stimulation of brain endothelial cells," *Molecular and Cellular Biology*, vol. 32, no. 17, pp. 3414–3427, 2012.

[43] S. Percário, D. R. Moreira, B. A. Gomes et al., "Oxidative stress in malaria," *International Journal of Molecular Sciences*, vol. 13, no. 12, pp. 16346–16372, 2012.

[44] R. Kissner, T. Nauser, C. Kurz, and W. H. Koppenol, "Peroxynitrous acid - where is the hydroxyl radical?," *IUBMB Life*, vol. 55, no. 10, pp. 567–572, 2004.

[45] Y. J. Suzuki, M. Carini, and D. A. Butterfield, "Protein carbonylation," *Antioxidants & Redox Signaling*, vol. 12, no. 3, pp. 323–325, 2010.

[46] L. Wiese, C. Hempel, M. Penkowa, N. Kirkby, and J. A. L. Kurtzhals, "Recombinant human erythropoietin increases survival and reduces neuronal apoptosis in a murine model of cerebral malaria," *Malaria Journal*, vol. 7, no. 1, 2008.

[47] T. Rodney, N. Osier, and J. Gill, "Pro- and anti-inflammatory biomarkers and traumatic brain injury outcomes: a review," *Cytokine*, vol. 110, pp. 248–256, 2018.

[48] K. Stock, A. Garthe, F. de Almeida Sassi, R. Glass, S. A. Wolf, and H. Kettenmann, "The capsaicin receptor TRPV1 as a novel modulator of neural precursor cell proliferation," *Stem Cells*, vol. 32, no. 12, pp. 3183–3195, 2014.

[49] R. Ramírez-Barrantes, C. Cordova, H. Poblete et al., "Perspectives of TRPV1 function on the neurogenesis and neural plasticity," *Neural Plasticity*, vol. 2016, Article ID 1568145, 12 pages, 2016.

[50] C. Amantini, V. Farfariello, C. Cardinali et al., "The TRPV1 ion channel regulates thymocyte differentiation by modulating autophagy and proteasome activity," *Oncotarget*, vol. 8, no. 53, pp. 90766–90780, 2017.

[51] M. J. Potchen, S. D. Kampondeni, K. B. Seydel et al., "Acute brain MRI findings in 120 Malawian children with cerebral malaria: new insights into an ancient disease," *American Journal of Neuroradiology*, vol. 33, no. 9, pp. 1740–1746, 2012.

[52] Y. S. Cordoliani, J. L. Sarrazin, D. Felten, E. Caumes, C. Lévêque, and A. Fisch, "MR of cerebral malaria," *American Journal of Neuroradiology*, vol. 19, pp. 871–874, 1998.

[53] J. Keeble, F. Russell, B. Curtis, A. Starr, E. Pinter, and S. D. Brain, "Involvement of transient receptor potential vanilloid 1 in the vascular and hyperalgesic components of joint inflammation," *Arthritis and Rheumatism*, vol. 52, no. 10, pp. 3248–3256, 2005.

[54] E. Hakimizadeh, A. Shamsizadeh, A. Roohbakhsh et al., "Inhibition of transient receptor potential vanilloid-1 confers neuroprotection, reduces tumor necrosis factor-alpha, and increases IL-10 in a rat stroke model," *Fundamental & Clinical Pharmacology*, vol. 31, no. 4, pp. 420–428, 2017.

[55] S. Kumar and U. Bandyopadhyay, "Free heme toxicity and its detoxification systems in human," *Toxicology Letters*, vol. 157, no. 3, pp. 175–188, 2005.

[56] H. Phiri, J. Montgomery, M. Molyneux, and A. Craig, "Competitive endothelial adhesion between *Plasmodium falciparum* isolates under physiological flow conditions," *Malaria Journal*, vol. 8, no. 1, 2009.

[57] L. L. Guo, Z. Z. Guan, Y. Huang, Y. L. Wang, and J. S. Shi, "The neurotoxicity of β-amyloid peptide toward rat brain is associated with enhanced oxidative stress, inflammation and apoptosis, all of which can be attenuated by scutellarin," *Experimental and Toxicologic Pathology*, vol. 65, no. 5, pp. 579–584, 2013.

[58] J. Wei, W. Fang, L. Sha et al., "XQ-1H suppresses neutrophils infiltration and oxidative stress induced by cerebral ischemia injury both in vivo and in vitro," *Neurochemical Research*, vol. 38, no. 12, pp. 2542–2549, 2013.

[59] H. Y. Jung, D. W. Kim, H. S. Yim et al., "Heme oxygenase-1 protects neurons from ischemic damage by upregulating expression of Cu,Zn-superoxide dismutase, catalase, and brain-derived neurotrophic factor in the rabbit spinal cord," *Neurochemical Research*, vol. 41, no. 4, pp. 869–879, 2016.

[60] S. J. Yang, E. A. Kim, M. J. Chang et al., "*N*-Adamantyl-4-methylthiazol-2-amine attenuates glutamate-induced oxidative stress and inflammation in the brain," *Neurotoxicity Research*, vol. 32, no. 1, pp. 107–120, 2017.

[61] M. Cohen-Kutner, L. Khomsky, M. Trus et al., "Thioredoxin-mimetic peptide CB3 lowers MAPKinase activity in the Zucker rat brain," *Redox Biology*, vol. 2, pp. 447–456, 2014.

[62] H. B. Armah, N. O. Wilson, B. Y. Sarfo et al., "Cerebrospinal fluid and serum biomarkers of cerebral malaria mortality in Ghanaian children," *Malaria Journal*, vol. 6, no. 1, p. 147, 2007.

[63] C. C. John, A. Panoskaltsis-Mortari, R. O. Opoka et al., "Cerebrospinal fluid cytokine levels and cognitive impairment in cerebral malaria," *The American Journal of Tropical Medicine and Hygiene*, vol. 78, no. 2, pp. 198–205, 2008.

[64] M. Krupka, K. Seydel, C. M. Feintuch et al., "Mild Plasmodium falciparum malaria following an episode of severe malaria is associated with induction of the interferon pathway in Malawian children," *Infection and Immunity*, vol. 80, no. 3, pp. 1150–1155, 2012.

[65] W. L. Mandala, C. L. Msefula, E. N. Gondwe, M. T. Drayson, M. E. Molyneux, and C. A. MacLennan, "Cytokine profiles in Malawian children presenting with uncomplicated malaria, severe malarial anemia, and cerebral malaria," *Clinical and Vaccine Immunology*, vol. 24, no. 4, 2017.

[66] E. Schwarzer, P. Arese, and O. A. Skorokhod, "Role of the lipoperoxidation product 4-hydroxynonenal in the pathogenesis of severe malaria anemia and malaria immunodepression," *Oxidative Medicine and Cellular Longevity*, vol. 2015, Article ID 638416, 11 pages, 2015.

[67] N. H. Hunt, H. J. Ball, A. M. Hansen et al., "Cerebral malaria: gamma-interferon redux," *Frontiers in Cellular and Infection Microbiology*, vol. 4, 2014.

[68] A. Villegas-Mendez, P. Strangward, T. N. Shaw et al., "Gamma interferon mediates experimental cerebral malaria by signaling within both the hematopoietic and nonhematopoietic compartments," *Infection and Immunity*, vol. 85, no. 11, 2017.